Republic of Iraq

Ministry of Higher Education and Scientific Research

University of Misan/College of Engineering

Civil Engineering Department

SEISMIC PERFORMANCE OF CLAY BRICKS CONSTRUCTION IN IRAQ

A THESIS

SUBMITTED TO THE COLLEGE OF ENGINEERING OF MISAN UNIVERSITY IN PARTIAL FULFILLMENT OF THE REQUIREMENTS FOR THE DEGREE OF MASTER OF SCIENCE IN CIVIL ENGINEERING

(STRUCTURES)

BY

JABBAR ABDALAALI KADHIM

B.Sc. in Civil Engineering, 2003

Supervised by

Assist. Prof. Dr. Abbas Oda Dawood

September 2019 **Muharram 1441**

بسم الله الرحمن الرحيم

خَلَقَ ٱلسَّمَٰوَٰتِ بِغَيۡرِ عَمَدٖ تَرَوۡنَهَاۖ وَأَلۡقَىٰ فِي ٱلۡأَرۡضِ رَوَٰسِيَ أَن
تَمِيدَ بِكُمۡ وَبَثَّ فِيهَا مِن كُلِّ دَآبَّةٖۚ وَأَنزَلۡنَا مِنَ ٱلسَّمَآءِ مَآءٗ فَأَنۢبَتۡنَا فِيهَا
مِن كُلِّ زَوۡجٖ كَرِيمٍ

صدق الله العلي العظيم

لقمان:10

Dedication

I dedicate this work to

my parents and my cousin, Ali

to my teachers

to my family

to my colleagues

Certification of the supervisor

*I certify that this thesis entitled "**Seismic Performance of Clay bricks construction in Iraq**", which is being submitted by **JabbarAbdalaali Kadhim**, was made under my supervision at University of Misan/College of Engineering, in partial fulfillment of the requirements for the Degree of Master of Science in Civil Engineering.*

(Structures).

Signature:

Name: Assist.Pof. Dr. Abbas Oda Dawood

(Supervisor)

Date: / /2020

In view of the available recommendations, I forward this thesis for debate by the examining committee.

Signature:

Name: Dr.Samir Mohammed Chassib

Head of the Civil Engineering Department /University of Misan

Date: 17/ 2/2020

Certification of Examination Committee

We certify that we have read this thesis entitled "**Seismic Performance of Clay Bricks Construction in Iraq**", and as an Examining Committee, we examined the student (**Jabbar Abdalaali Kadhim**) in its content and in what is connected with it and that in our opinion it meets standard of a thesis for the degree of Master of Science in Civil Engineering (Structures).

Signature:

Name: Prof. Dr. Ali L. Abbas

(Chairman)

Date: / / 2020

Signature:

Name: Assist. Prof. Dr. Saad F. Resan

(member)

Date: / / 2020

Signature:

Name: Dr. Fatin I. Mussa

(Member)

Date: / / 2020

Signature:

Name: Assist. Prof .Dr. Abbas O. Dawood

(Supervisor)

Date: / / 2020

Approved by the Dean of the College of Engineering

Signature:

Name: Assist. Prof. Dr. Abbas Oda Dawood

Acting Dean, College of Engineering / University of Misan

Date: 17 / 2 / 2020

Acknowledgements

First of all, I would like to thank ALLAH “His Majesty”, who created me and gave me all I have. Next, I would like to thank and express my respects to my supervisor, Assist Prof. Dr. Abbas O. Dawood, for his motivating encouragement, influential directions, and all things he did to complete this project.

I would like to express my great appreciation to the dean of the college of engineering, Prof. Dr. Ahmad K. Al-Sharaa, and I would also like to thank all the lecturers and engineering college members in Misan University for their invaluable support and help throughout my MS.C. study.

I should not forget the great help presented by Dr. Alaa Hassan Abid and my friends Aqeel Ali Abid and engineer Laith Nasir Hussein. Also, I am grateful to the geologist, Ali Ramthan, for his essential aids. Great appreciations are for the employees of the structural lab in Al-Shatra technical institute who approved and helped to achieve some tests required within the study.

Abstract

Masonry is the oldest building type. It is still widely used in Iraq and throughout the world. It has a low tensile strength making it the most vulnerable construction under the effect of lateral loading such as seismic loading. The considerable seismic hazard in Iraq requires extent verifications of the seismic performance of masonry buildings. This study aims to evaluate the mechanical properties of masonry and to investigate the nonlinear seismic response of masonry buildings. The compressive strength, tensile strength, and modulus of elasticity of masonry have been evaluated and found as 5.5 MPa, 0.15 MPa, and 2723 MPa, respectively. Also, the mechanical properties of masonry constituents (bricks and mortar) have been investigated.

ANSYS 18.2 release was used to perform the nonlinear time-history analyses for the studied models. Two experimentally studied walls were simulated to verify the validity of the aimed simulations, and the results have good acceptance compared to the experimental results. The study accomplished the simulation of the prism test with both micro and macro models. The micro-modeling gives more accurate results, but it is not simple to use for large models. The solution terminated at 98% of the average experimental result in the micro-modeling and at 83.6% in the macro-modeling. Consequently, the analysis with the macro-modeling approach is more conservative compared to the analysis with micro-modeling. However, masonry models were simulated with the macro-modeling using Willam-Warnke failure criterion, which predicts the failure of concrete materials.

The seismic data were downloaded from the PEER (Pacific Earthquake Engineering Research) site to be as representative as possible to the seismic characteristics of the area of the study. The PGAs (Peak Ground Accelerations) of the selected records range between 0.1 g and 0.324 g. Also, the seismosignal software was used to obtain the velocity and displacement time-histories from

the acceleration time-histories of the 7.3 Mw (moment magnitude) earthquake that hit the Iraq-Iran border on 12 November 2017.

The results of the nonlinear time-history analysis reveal the poor seismic performance of URM (unreinforced masonry) buildings as severe damages occur in walls under the effect of earthquakes having the probable PGAs. It was observed that increasing the compressive strength of masonry do not enhance in-plane load capacity and then do not enhance the seismic response if the low tensile strength is still unchanged. On the other hand, increasing the tensile strength obviously enhances the seismic response and in-plane load capacity. For the URM wall that analyzed statically, when the tensile strength was increased from 0.15 MPa to 0.3 MPa, the in-plane load capacity increased 41%.

The study investigated the effect of retrofitting of walls by plaster layers reinforced with steel wire meshes. The model of the retrofitted single-room overrode a 0.324 PGA with an ultimate drift of 1.036% in z-direction and 1.289% in x-direction . The dense cracks indicate the ability of the retrofitting layers to prevent the disintegration of damaged walls during an earthquake. Also, the increases in natural frequencies of retrofitted models indicate the stiffness enhancement due to the existence of retrofitting. The structural enhancement of this retrofitting was investigated by analyzing a retrofitted wall statically. It was found that it increased the out-of-plane load capacity 494% and the in-plane load capacity 319.5%, and it increased the out-of-plane displacement 11.4%.

List of Contents

Item No.	*Title*	*Page No.*
Acknowledgement		i
Abstract		ii
List of contents		iv
List of figures		vii
List of plates		xiv
List of tables		xv
Abbreviations and Symbols		xvi
Chapter One: Introduction		
1.1	Introduction	1
1.2	Earthquakes	2
1.2.1	Earthquake Definition and Basic Nomenclature	2
1.2.2	Earthquake Forces on Structures	3
1.2.3	Vertical Ground Acceleration	3
1.2.4	Causes of Earthquakes	4
1.2.5	Seismic Waves	4
1.2.6	Global Seismic Hazard	5
1.2.7	Seismic hazard in Iraq	6
1.3	Masonry	8
1.3.1	Usage of Clay Bricks Masonry in Iraq	8
1.3.2	Mechanical Characteristics of Masonry	8
1.3.3	Masonry Failure Modes	9
1.3.4	Retrofitting Techniques for Masonry	10
1.4	Analysis Procedures	10
1.5	Objectives of The Study	10
1.6	Layout of The Study	11

Chapter Two: Literature Review		
2.1	Introduction	12
2.2	Previous Theoretical and Experimental Studies	12
2.3	Remarks	27
Chapter Three: Experimental Work for Mechanical Properties		
3.1	Introduction	28
3.2	Compressive Strength of Masonry	28
3.3	Tensile Strength of Masonry	29
3.4	Modulus of Elasticity of Masonry	30
3.5	Mechanical Properties of Clay Bricks	32
3.6	Mechanical Properties of Cement-Sand Mortar	33
3.7	Cohesion Stress Between Units and Mortar (f_{v°)	37
Chapter Four: Numerical Formulation of The Problem		
4.1	Introduction	38
4.2	Solid65 Element	39
4.3	Modeling Strategies of Masonry	39
4.3.1	Micro-modeling of Masonry	39
4.3.2	Macro-modeling of Masonry	40
4.3.3	Equivalent Frame Model	40
4.4	ANSYS Multilinear Stress-Strain Relationship	41
4.5	Willam-Warnke Plasticity model	41
4.6	Analysis Types	42
4.7	Damping	44
4.8	Newton-Raphson Procedure	45
4.9	Convergence Criteria	45
4.10	Seismic Loading for Transient Analysis	46
4.11	Selection of Acceleration Time-Histories	46
4.12	Seismosignal Software	48

4.13	Micro-modeling of The Prism Test	49
4.14	Contact Problems	49
4.15	ANSYS Simulation of CM Models	49
4.16	Retrofitting Simulation	50
Chapter Five: FE Simulations, Results, and Discussions		
5.1	Introduction	51
5.2	Verification Model No.1	51
5.3	Verification Model No. 2	54
5.4	Verification Model No. 3	57
5.5	Verification model No.4	61
5.6	Boundary Conditions	62
5.7	Model No. 1	63
5.8	Model No. 2	77
5.9	Model No. 3	85
5.10	Model No. 4	92
5.11	Model No.5	97
5.12	Model No.6	105
5.13	Model No.7	108
5.14	Model No.8	110
5.15	General Discussion	112
Chapter Six: Conclusions and Recommendations		
6.1	Conclusions	116
6.2	Recommendations	117
6.2.1	Recommendations for Practice	117
6.2.2	Recommendations for Future Studies	118
References		119

List of Figures

Fig. No.	*Figure*	*Page No.*
1.1	Earthquake nomenclature	2
1.2	Effects of vertical acceleration	4
1.3	Tectonic setting of Iraq and surrounding territories	6
1.4	Catalogue of instrumental seismicity in Iraq	7
1.5	Failure Modes of In-Plane Loaded URM walls	9
2.1	Idealized bilinear load-displacement relationship of the pier F1 tested by Franklin et al.	13
2.2	Geometry and Instrumental Case for the wall tested by Naseer	18
2.3	Lateral displacement subjected to the wall tested by Naseer	18
2.4	The hysteresis envelope and idealized curve of load-displacement relationship of the wall tested by Naseer	19
3.1	Stress-Strain curve for masonry specimen 1	31
3.2	Stress-Strain curve for masonry specimen 2	31
3.3	Stress-Strain curve for masonry specimen 3	31
3.4	Modulus of Elasticity for Masonry According to MSJC Code	32
4.1	Geometry of Solid65 Element	39
4.2	Strategies for modeling of masonry	40
4.3	Stress-Strain or Force-Displacement relationship with the part not involved into ANSYS simulations	41
4.4	Parameters of concrete failure criterion	42
4.5	Peak Ground Acceleration Map for Iraq	47
4.6	Distribution of projects used by Mohammed and Abdulrassol	47
5.1	FE model for the wall tested by Naseer	51

5.2	Experimental and numerical load-displacement relationships for the wall tested by Naseer	52
5.3	Displacement in x-direction for verification model No.1 (mm)	52
5.4	Aspect ratio and predominant stiffness of masonry walls according to MSJC code	53
5.5	Crack pattern for FE model of the wall tested by Naseer	53
5.6	3rd principal stress in the model of the wall tested by Naseer	54
5.7	The FE model for Pier (F1) tested by Franklin	55
5.8	Displacement in x-direction for verification model No.2	55
5.9	ANSYS load-displacement curve for Pier F1 tested by Franklin	56
5.10	Cracks in the FE model of Pier F1 tested by Franklin	56
5.11	FE micro model for masonry prism	58
5.12	Reaction in y-direction in prism micro model	59
5.13	The stress in y-direction (σ_y) (micro model)	60
5.14	Crack pattern in prism failure state (micro model)	60
5.15	Stress in x-direction (σ_x) in joint mortar (MPa)	60
5.16	1st principal stress in bed joint mortar (MPa)	61
5.17	Masonry multi-linear stress-strain curve	61
5.18	Cracks in the macro model of prism test	62
5.19	Stress in y-direction (σ_y) for macro model (MPa)	62
5.20	Single room plan	63
5.21	FE model No.1	64
5.22	1st mode of Model No.1	65
5.23	2nd mode of Model No.1	65
5.24	3rd mode of Model No.1	65
5.25	The first three natural frequencies of Model No.1	66

5.26	ANSYS report for modal analysis of Model No.1	66
5.27	Horizontal-1 component of $\ddot{u}_g$ of Northwest Calif., 1938 event	66
5.28	Horizontal-2 component of $\ddot{u}_g$ of Northwest Calif., 1938 event	67
5.29	Vertical component of $\ddot{u}_g$of Northwest Calif., 1938 event	67
5.30	Horizontal-1 component of $\dot{u}_g$ of Northwest Calif., 1938 event.	67
5.31	Horizontal-2 component of $\dot{u}_g$ of Northwest Calif., 1938 event.	68
5.32	Vertical component of $\dot{u}_g$ of Northwest Calif., 1938 event.	68
5.33	Horizontal-1 component of u_g of Northwest Calif., 1938 event	68
5.34	Horizontal-2 component of u_g of Northwest Calif., 1938 event	69
5.35	Vertical component of u_g of Northwest Calif., 1938 event	69
5.36	u_z^t at base level of Model No. 1 (mm).	69
5.37	u_z^t at roof level of Model No. 1 (mm).	70
5.38	Displacement nomenclature	71
5.39	u_z at roof level of Model No.1	71
5.40	u_x at roof level in Model No.1.	72
5.41	cracks in Model No. 1	72
5.42	H1-acceleration for Abadan records during the 7.3 event	73
5.43	H1-ground displacement for Abadan records during the 7.3 event	74
5.44	Response in z-direction for Model No.1 under the seismic wave recorded at Abadan station for the 7.3 M_w event.	74
5.45	ANSYS acceleration at base level of Model No.1 (mm/sec^2) for Model No.1 subjected to the seismic wave of Abadan station	74
5.46	H1-acceleration for Abadan records during the 7.3 event	75

	(mm/s^2)	
5.47	Damped free vibration of Model No.1	76
5.48	u_z of Model No.1 with the modeling of damping	76
5.49	Plan of the one-story house	77
5.50	FE Model No. 2	77
5.51	ANSYS. report for modal analysis of Model No.2	78
5.52	1^{st} mode of Model No.2	78
5.53	2^{nd} mode of Model No.2	78
5.54	3^{rd} mode of Model No.2	79
5.55	H-1 component of $\ddot{u}_g$ of the November 7.3 M_w earthquake recorded at Ravansar station	79
5.56	H-2 component of $\ddot{u}_g$ of the November 7.3 M_w earthquake recorded at Ravansar station	80
5.57	Vertical component of $\ddot{u}_g$ of the November 7.3 M_w earthquake recorded at Ravansar station	80
5.58	Response at roof level in z-direction for Model No. 2	81
5.59	Response at roof level in x-direction for Model No. 2	81
5.60	Crack pattern in Model No.2	81
5.61	1^{st} principal stress in walls of Model No.2	82
5.62	3^{rd} principal stress in walls of Model No. 2	82
5.63	Cracks in concrete slab of Model No. 2	83
5.64	1^{st} principal stress in concrete slab of Model No.2	83
5.65	Responses at roof level in z-direction before and after mesh refinement for Model. 2	84
5.66	Damped response (u_x) of Model No.2	85
5.67	Plan of Model No. 3	86
5.68	FE Model No. 3	86
5.69	ANSYS. report for Model No.3	87

5.70	1^{st} mode of Model No.3	87
5.71	2^{nd} mode of Model No.3	87
5.72	3^{rd} mode of Model No.3	88
5.73	u_z at first level of Model No. 3	88
5.74	u_z at second level of Model No. 3	89
5.75	u_x at first level of Model No. 3	89
5.76	u_x at second level of Model No. 3	89
5.77	First cracks in Model No. 3	90
5.78	Crack pattern in Model No. 3	90
5.79	1^{st} principal stress in walls of Model No.3	91
5.80	Von misses stress in concrete slabs and lintels	91
5.81	FE Model No.4	92
5.82	FE simulation of columns reinforcement in Model No.4	93
5.83	ANSYS. report for modal analysis of Model No.4	93
5.84	1^{st} mode of Model No.4	94
5.85	2^{nd} mode of Model No.4	94
5. 86	3^{rd} mode of Model No.4	94
5.87	u_z at roof level of Model No.4.	95
5.88	u_x at roof level of Model No.4	95
5.89	Crack pattern in masonry walls of Model No.4	96
5.90	Crack pattern in concrete frame of Model No.4	96
5.91	Stress in steel reinforcement of columns in Model No.4	97
5.92	FE Model No.5	98
5.93	ANSYS. report for modal analysis of Model No.5	98
5.94	1^{st} mode of Model No.5	99
5.95	2^{nd} mode of Model No.5	99
5.96	3^{rd} mode of Model No.5.	99
5.97	Horizontal -1 component of $\ddot{u}_g$ of Mammoth, 1980 event	100

5.98	Horizontal -2 component of $\ddot{u}_g$ of Mammoth, 1980 event	100
5.99	Vertical component of $\ddot{u}_g$ of Mammoth, 1980 event	101
5.100	u_z^t at base level of Model No.5 (mm).	101
5.101	H -1 component of u_g of Mammoth, 1980 event	102
5.102	Response u_z at roof level of Mode No.5	102
5.103	Response u_x at roof level of Mode No.5	102
5.104	Crack pattern in masonry walls of Model No.5.	103
5.105	Crack pattern in concrete frame of Model No.5	103
5.106	Crack pattern in retrofitting layers of Model No.5	104
5.107	Stress in steel reinforcement of Model No.5	104
5.108	FE Model No.6	105
5.109	1st mode of Model No.6	105
5.110	2nd mode of Model No.6	106
5.111	3rd mode of Model No.6	106
5.112	ANSYS. report for modal analysis of Model No.6	106
5.113	Crack pattern in masonry walls of Model No.6	107
5.114	Crack pattern in retrofitting layers of Model No.6	107
5.115	FE Model No.7	108
5.116	Deflected shape of Model No.7	108
5.117	Reaction in z-direction for Model No.7	109
5.118	Ultimate in-plane load for Model No.7 having f_t= 0.15 MPa	109
5.119	Ultimate in-plane load for Model No.7 having f_t= 0.3 MPa	110
5.120	FE Model No.8	111
5.121	Deflected shape of Model No.8	111
5.122	The out-of-plane load at end of solution for Model No.8	111
5.123	The in-plane load at end of solution for Model No.8	112
5.124	Effect of overburden pressure on the in-plane load capacity of URM walls	114

5.125	Effect of tensile strength on the in-plane load capacity of URM walls.	115

List of Plates

No.	***Plate***	***Page No.***
1.1	Main forms of masonry usage in Iraq	8
2.1	Diagonal shear failure in post-earthquake observed buildings	16
2.2	A damage Observed after (2009 L'Aquila earthquake, Italy)	23
3.1	Prism test	29
3.2	Tensile Strength Test	29
3.3	A masonry specimen under testing for the modulus of elasticity	30
3.4	A brick under compression test	33
3.5	Prepared brick specimens after tensile test	33
3.6	Tensile test for a brick specimen	34
3.7	A mortar cube under compression test	35
3.8	A mortar specimen under tension test	35
3.9	A mortar specimen after tensile failure	35
3.10	A Cylindrical Mortar Specimen under Compression	36
3.11	Cohesion test of masonry specimen	37
5.1	Initial cracks in Pier F1 at a 0.1% drift	57
5.2	Rotation about toe in Pier F1 at 2% drift	57

List of Tables

Table No.	*Description*	*Page No.*
2.1	Mechanical Properties Pier (F1) tested by Franklin.	13
2.2	Mechanical Properties of the wall tested by Naseer	17
3.1	Different Formulae for Evaluating $E_{\acute{m}}$	30
3.2	Moduli of Elasticity of Masonry Specimens	32
3.3	Tensile Strength of Mortar Specimens	36
3.4	strains and corresponding stresses for mortar	37
4.1	Site classification	48
5.1	Mechanical properties of bricks and mortar	58
5.2	Mechanical properties of masonry	61
5.3	Description of the seismic records applied to model No. 1	64
5.4	Description of the seismic records applied to Model No. 2	79
5.5	Mechanical properties of concrete and reinforcement steel	92
5.6	Description of the seismic records applied to Model No. 5	100

Abbreviations and Symbols

Abbreviation/Symbol	Description
a	Acceleration
[C]	Damping matrix
CS	Compressive strength
e	The natural exponent
$E_{\acute{m}}$	Modulus of elasticity of masonry in MPa
F	Force
f_b	Compressive strength of bricks in MPa
FE	Finite Element
FEMA	Federal Emergency Management Agency
$\{F_i\}$	Load vector at the load step i
f_m	Compressive strength of mortar in MPa
$f_{\acute{m}}$	Compressive strength of masonry in MPa
f_t	Tensile strength of masonry in MPa
f_{v°	Mortar- bricks Cohesion in MPa
f_y	Yield stress of steel reinforcement in MPa
IBC	International Building Code
$[K_e]$	Element stiffness matrix
$[K_i^T]$	Tangential stiffness matrix
L	Length of the masonry wall in m
m	mass
[M]	Mass matrix
N	Vertical load applied to the wall
p	Overburden pressure
PEER	Pacific Earthquake Engineering Reasearch

PGA	Peak ground acceleration
PI	Plasticity index
PSHA	Probabilistic seismic hazard assessment
SPT	Standard penetration test
S_u	Undreined shear strength of soil of the site
u	Relative displacement
$\{\dot{u}\}$	Velocity vector
$\{\ddot{u}\}$	Acceleration vector
u_g	Ground displacements
u^t	Total displacement
V	The in-plane loading applied to the wall
V_{s30}	Shear wave velocity of the upper 30 m of the site
w	Water content
W	Gravity load
α	Mass matrix multiplier of Rayleigh damping form
β	Stiffness matrix multiplier Rayleigh damping form
δ_y	Yield displacement of the unreinforced masonry wall
ζ	Damping ratio
λ	Aspect ratio of the wall (height/length)
ν	Poisson's ratio
τ	Shear stress
ω_i	The natural circular frequency at the mode i
ω_j	The natural circular frequency at the mode j

Chapter One

Introduction

CHAPTER ONE
INTRODUCTION

1.1 Introduction

Masonry is the oldest building type that used throughout the world. It was used in Mesopotamia about 5000 B.C.[1]. Masonry is a construction built up of bricks or stones using a binding material[2]. The IBC (International Building Code) defines it as “a built-up construction or combination of building units or materials of clay, shale, concrete, glass, gypsum, stone or other approved units bonded together with or without mortar or grout or other accepted methods of joining.”[3].

In Iraq, stones besides other building types are used in the northern and western portions of the country[4]. In the middle and southern areas, clay bricks and concrete blocks are the general construction. However, unreinforced clay bricks masonry is mostly used, especially in residential buildings. Masonry has advantageous characteristics; it is economical and easy to be constructed. The primary materials and skills needed to erect it are available, and it has an adequate fire resistance that is a 215 mm thick wall without finishing can resist fire for about 6 hours [4]. On the other hand, it has disadvantageous properties; it is a brittle material having low tensile strength. Consequently, URM (Unreinforced Masonry) structures are the most vulnerable under the effect of lateral loadings, such as seismic forces. The weakness in tensile strength is attributed to the weakness in bond stress between mortar and brick units, which makes contact surfaces represent potential failure planes [5].

The non-instrumentally recorded and recent earthquakes denote the seismic hazard in Iraq. Therefore, structures should be designed to resist earthquakes as required by the seismic codes, such as the preliminary draft of the Iraqi seismic code. Under the seismic loading, structures can be analyzed with linear dynamic, nonlinear dynamic, linear static (equivalent static), and nonlinear static (pushover) analysis. Since masonry structures are widely spread in Iraq, extensive studies are required to assess their seismic performance, and to propose adequate retrofitting techniques that can enhance the structural behavior and mitigate losses in life and properties.

1.2 Earthquakes

1.2.1 Earthquake Definition and Basic Nomenclature

An earthquake is the shaking of the Earth's crust caused by a sudden energy release within the lithosphere due to rock rupture at a point known as the hypocenter or focus, as shown in Fig. (1.1). The break happens at that portion of the crust when it is subjected to a stress exceeding its breaking strength. The point on the Earth's surface that locates directly above the hypocenter is known as the epicenter. The distance measured from the hypocenter to the epicenter is the hypocenter depth or focal depth. The distance measured from any point on the Earth's surface (maybe an observing station) to the epicenter is known as the epicentral distance. Depending on the focal depth, earthquakes are divided into three categories: shallow, intermediate, and deep earthquakes. Shallow earthquakes have focal depths less than 60 Km. Earthquakes with hypocentral depths between 60 and 300 Km are intermediate, while hypocentral depths exceeding 300 Km characterize earthquakes as deep ones[6].

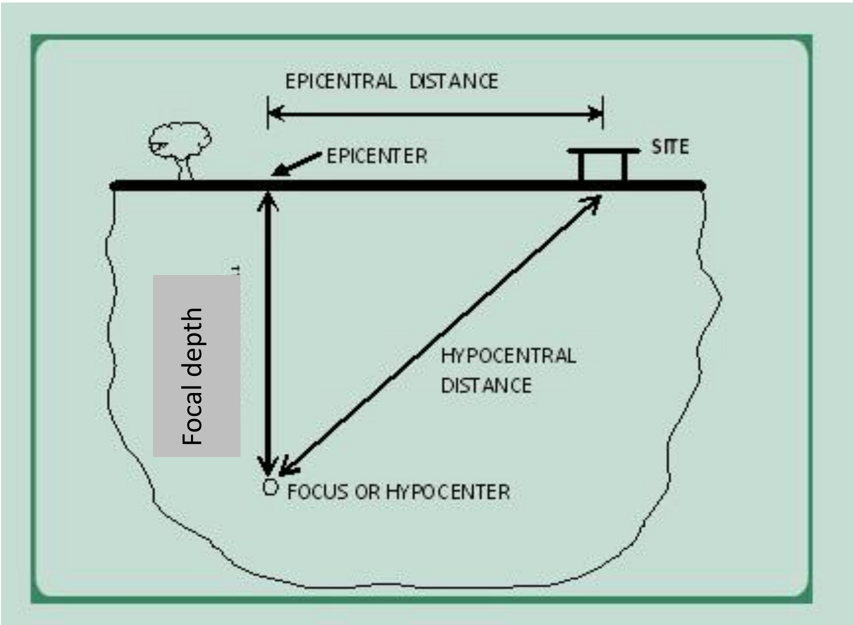

Figure (1.1) Earthquake Nomenclature [6].

1.2.2 Earthquake Forces on Structures

Earthquakes produce inertial forces in the elements of structural systems. The inertial forces are related to the masses of the structural components, according to Newton's second law, as illustrated in Eq. (1.1). They act at centers of masses.

$$F = m \cdot a \tag{1.1}$$

Where: F: force, m: mass, and a: acceleration.

The ground motion during an earthquake has three components. Two ones are horizontal, and the third is vertical. The stability of the structure subjected to lateral movements is disturbed; it may have local or global damaging. Therefore, the Structural damages during earthquakes are mainly caused by the horizontal components of ground motion[7]. Since the structures are designed to resist seismic forces in two orthogonal horizontal directions, they can withstand an oblique earthquake. Typically, the major and minor axes of the structure are considered in the seismic analysis [6].

1.2.3 Vertical Ground Acceleration

The vertical ground acceleration, whose peak value is commonly one-third of the peak value of the horizontal one, reduces gravity effects when the ground is accelerated downward. In contrast, an upward vertical acceleration increases the effects of vertical loads. So, it may cause severe effects on cantilevers and long-span horizontal elements [8]. This effect is clearly felt as an apparent weight increase by those inside an upward accelerating elevator or a taking off plane. Fig. (1.2) illustrates this physical action. In Fig. (1.2.a), the body (the blue colored block) is accelerated upward with a constant acceleration of a. It is easy to find the vertical reaction (R) from equilibrium in the vertical direction by applying Newton's second law as follows:

$$R - W = m \cdot a \tag{1.2}$$

Where W: gravity load, and m: mass of the body.

Eq. (1.2) can be written as $P = W + m \cdot a$, which means that when the base of the structure is accelerated upward, the effect of the dead load (R)increases with a magnitude of the dead load multiplied by the value of vertical acceleration. For the downward acceleration shown in Fig. (1.2.b), the value of base reaction (R) can be found as follows:

$$R = W - m\,.a \tag{1.3}$$

Eq.(1.3) demonstrates how R decreases due to downward acceleration.

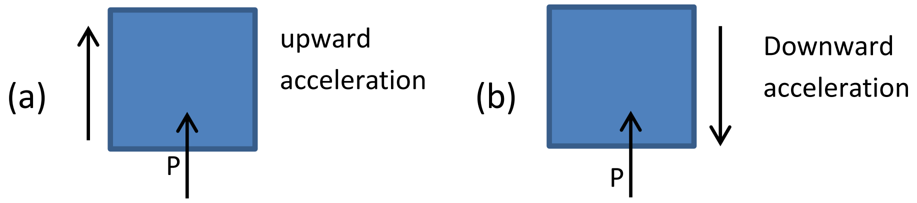

Figure (1.2) Effect of vertical acceleration

1.2.4 Causes of Earthquakes

The lithosphere, the Earth’s crust with the uppermost mantle, is formed of colossal rock shells called the plates. The plates are in permanent relative motion. Consequently, crust dislocations happen between adjacent plates resulting in rock elastic straining and then in releasing the elastic strain energy after the rupturing of rocks. This natural phenomenon is the source of most earthquakes. The academic field that is dedicated to study the plate motion is called plate tectonics[6]. Volcanic eruptions cause some earthquakes. Also, earthquakes can occur because of human-made activities. Explosions due to mining or nuclear experiments, impounding vast reservoirs behind high dams, removal of substantial amounts of rock during surface digging, extracting fluids like petroleum extraction, and injection of fluids are examples of such activities. The seismicity caused by human activities is known as induced seismicity [8].

1.2.5 Seismic Waves

The energy released from a tectonic rupture is partially dissipated as seismic waves (about 10% of the total energy). Two kinds of waves cause medium motion during earthquakes: body waves which spread through the interior of the Earth and surface waves which propagate only within the surface of the Earth. The body waves comprise primary or longitudinal waves (termed P-waves) and secondary or transverse waves (termed ‘S-waves’). P-waves displace the particles of their traveling medium back and forth in the same direction of wave propagation, exhibiting similar behavior to sound waves. Therefore, they are compression waves, and thus they can propagate in fluids. Differently, S-waves propagation makes their medium particles move in side-to-side motion vertically and horizontally. Therefore, they cause shear stresses in their traveling medium, and thus can not travel in fluids. S-waves go slower than P-waves, and this property is utilized to determine the epicentral distance by a simple mathematical relationship combining the distance with the difference in the arrival time between P and S-waves and their velocities. S-waves diffuse more energy causing the majority of structural damages[6] [9].

Surface waves, which include Love waves and Rayleigh waves, propagate just in the surface layer of the Earth’s crust. They are formed as a result when body waves spreading parallel to the ground surface constructively interfere. Surface waves have a long duration, and they are likely to cause severe damages to structures[6] [9].

1.2.6 Global Seismic Hazard

Earthquakes are one of the most catastrophic natural hazards which cause dreadful losses of life and possessions. As an average, about 10,000 people die yearly, and the annual economic wastages are in billions of dollars. The most hazardous area through the world, nicknamed the ring of fire, includes the pacific coasts of South America, North America, the Aleutian Islands, Japan, Southeast Asia, and Australia. In the Middle East, it is estimated that about 160,000 people died because of earthquakes between the years 1900 and 1979, also in the same region, more than 500,000 people became homeless between 1953 and 1979. Earthquakes show more losses when they occur in developing countries because of poorly implemented structures. For instance, in 2003, the small Iranian city of Bam was beaten by a 6.6 earthquake (on the Richter magnitude scale), killing more than 43,000 people and leaving about 60,000 people homeless. In that area, approximately 60% of the buildings are URM buildings [6] [9] [10].

1.2.7 Seismic hazard in Iraq

Iraq is in the north of the Arabian Plate, as shown in Fig. (1.3). It has active seismicity in the north and east where the tectonic boundary between the Arabian Plate and the Eurasian Plate generates severe seismicity, while its large portion locates within the Arabian Platform. Based on the moment magnitude (Mw), the catalogue of instrumental seismicity in Iraq for the years between 1900 and 2009 is illustrated in Fig. (1.4)[11].

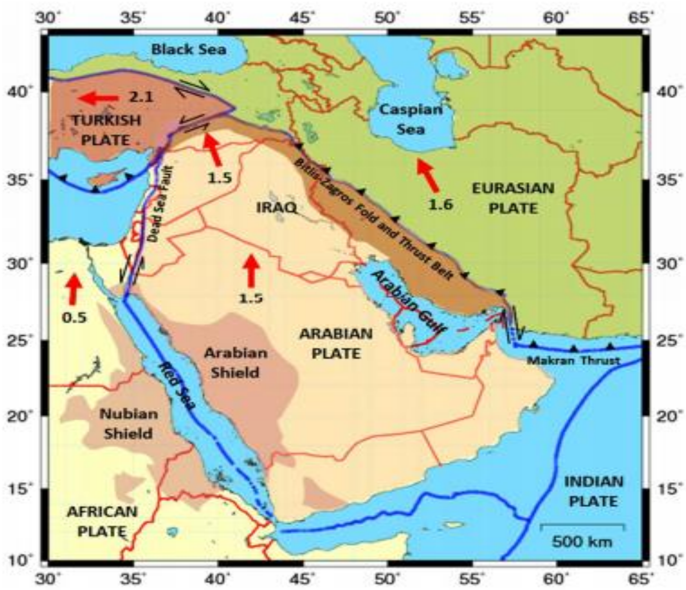

Figure (1.3) Tectonic Setting of Iraq and Surrounding territories[11].

Some earthquake examples are mentioned as follows [12]:

- In July 1940 and January 1950, earthquakes beat Baghdad, and many houses collapsed.
- On 17/10/1946, 1/12/1950, and March 1956, Baghdad was beaten by strong earthquakes that caused tremendous damages in properties.
- In 1992, an earthquake hit Kasimiyah village, 50 Km east of Erbil. It destroyed tens of houses, but no human fatalities were recorded.
- In August 2004, an earthquake beat AL-Rafaee (a town in Dhi Qar gov-

ernorate, 300 Km to the South of Baghdad), and some houses collapsed.

- In March 2013, an earthquake beat Mosul. Its main effects were obvious in many villages, including cracking of houses and other buildings.
- The deadly earthquake with MW 7.3 hit the Iraq-Iran border on 12 November 2017. Its epicenter is about 30 Km to the south of the Iraqi town of Halabja (a city in Sulaymaniyah governorate, 240 Km to the Northwest of Baghdad). It is the strongest event in the territory that instrumentally recorded[13]. At least 630 people died, and more than 8,100 were injured. Most casualties on the Iraqi side were from Halabja, while the Iranian province of Kermanshah had the majority of fatalities on the other side. Many buildings and structures were damaged.
- The 6.3 M_w earthquake hit the Iran-Iraq border on 25/11/2018, and damages were observed in masonry buildings.

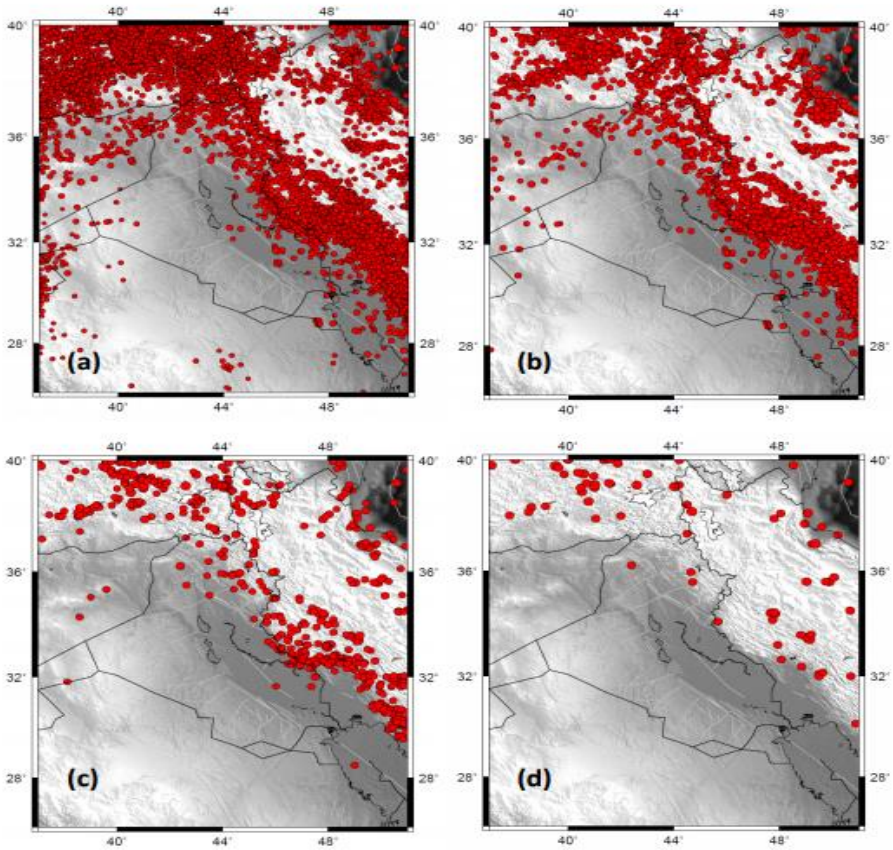

Figure (1.4) Catalogue of Instrumental Seismicity in Iraq (a) M_W>3, (b) M_W>4, (c) M_W>5, AND (d) M_W>6 [11].

1.3 Masonry

1.3.1 Usage of Clay Bricks Masonry in Iraq

Masonry is used in the form of URM, CM (confined masonry) buildings, and infill walls in RC (reinforced concrete) frames. In contrast with the masonry infill walls in RC frames, masonry walls should be built before the pouring of the confining concrete in confined masonry buildings, and the loads are mainly supported by the bearing walls[13][14]. Therefore, it can be observed in Plate (1.1-a) that the concrete of the columns interlocks with the masonry units. The main function of the masonry infill walls in RC frame structures is not structural, but their damage control during earthquake is an essential issue[15].

Plate (1.1) Main forms of masonry usage in Iraq: (a) Confined masonry, (b) Masonry infill in RC frame, and (c) URM bearing walls.

1.3.2 Mechanical Characteristics of Masonry

Masonry is a nonhomogeneous and anisotropic material since it is composed of two distinct materials: brick units and mortar. The interaction between units and mortar is complex and highly affects the load-displacement relationship of masonry. Due to this interaction, masonry walls subjected to lateral loads exhibit nonlinear load-displacement relationships even within small deformations[5]. The ductility of a structural member is defined as its ability to deform beyond its yield point before collapsing. In other words, it is the capability of the structural component to exhibit plastic deformations before collapsing[6]. The URM structures have poor ductility. Of course, reinforced masonry has higher ductility compared to the URM. Vertical and horizontal reinforcement mainly enhance the flexural and tensile strengths.

1.3.3 Masonry Failure Modes

Different parameters govern the failure mode of URM loaded walls: the wall geometry, the axial load applied to the top face of the wall, and the mechanical properties. The observed failure modes for in-plane loaded URM walls are: sliding, diagonal shear, and rocking failure mode[7]. Fig. (1.5) shows these failure modes, in which N and V are the vertical load applied to the top of the wall and the in-plane load, respectively. An out-of-plane loaded masonry wall fails in a flexural mode, in which a horizontal longitudinal crack propagates along bed joint close the base while the wall is turning about a longitudinal axis.

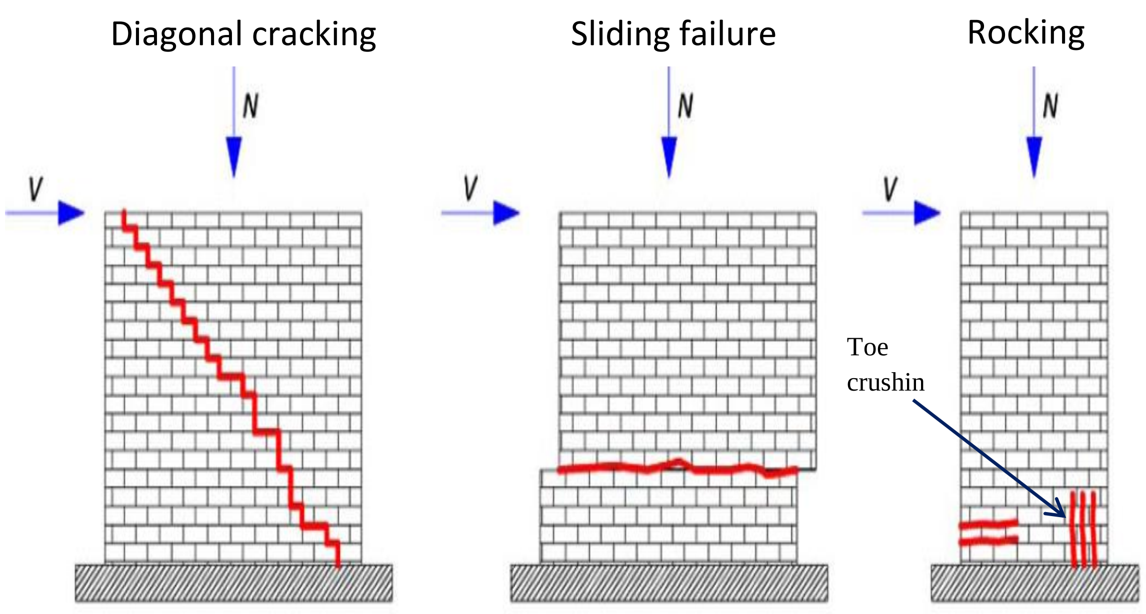

Figure (1.5) Failure Modes of In-Plane Loaded URM walls[7].

1.3.4 Retrofitting Techniques for Masonry

Surface treatment, grout and epoxy injection, etc., are used for retrofitting masonry walls to improve the seismic performance of existing or future URM structures. The surface treatment is the simple technique which has widely used [16]. One of the surface treatments is the use of reinforced plaster layers. This study comprises the simulation of masonry buildings of walls retrofitted by plaster layers reinforced with steel wire meshes.

1.4 Analysis Procedures

The determination of a structural response to a seismic load can be carried out by different procedures. The linear static or dynamic analyses are adequate if the structure is approximately capable of elastic responding under the effect of the seismic design loading. It is not economical nor practical to construct a structure that responds elastically during moderate or heavy earthquakes. Therefore, only nuclear plants are designed to react elastically due to the catastrophic effects of their damaging, while all other structures are designed to be earthquake-resistant structures. An earthquake-resistant structure has no damages during a minor earthquake and is damageable during moderate or severe shaking but without collapsing to ensure life[17].

The nonlinear (pushover) procedure is acceptable when contributions of higher modes are not significant. The nonlinear dynamic (time-history) is permitted for all structures. It is the most accurate method for analyzing structures subjected to ground shaking [18].

1.5 Objectives of The Study

This study is intended to:

1- Achieve a limited experimental work to determine the mechanical properties clay bricks masonry built with cement-sand mortar.
2- Simulate the masonry prism test with both micro- and macro-modeling, and then to compare the results of the two simulation approaches.

3- Study the nonlinear response of URM and CM buildings and their cracking patterns during earthquakes.
4- Investigate the effect of the compressive and tensile strengths on the seismic response of URM buildings and the in-plane load capacity of URM walls.
5- Assess the seismic improvement obtained for URM buildings through the use of plaster layers reinforced with steel wire meshes.

1.6 Layout of The Study

The study includes six chapters listed as follows:

- **Chapter One (Introduction)**: describes the headlines of the studied subject including earthquake characteristics, seismic hazard, masonry usage and nature, retrofitting and modeling strategies of masonry, and analysis methods.
- **Chapter Two (Literature Review)**: briefly reviews some previous experimental and theoretical studies related to the seismic performance of masonry structures.
- **Chapter Three**: discusses the mechanical properties of masonry constituents and composite, and reports the experimental work and its results.
- **Chapter Four**: describes the problem formulation by FEM and software used for the simulation of studied models.
- **Chapter Five**: includes simulations, analysis results, and discussions.
- **Chapter Six**: conclusions and recommendations

Chapter Two

Literature Review

CHAPTER TWO
LITERATURE REVIEW

2.1 Introduction

Masonry structures constitute a lot of residential and heritage buildings that lay in seismically hazardous areas, and they are the most vulnerable structures under the effect of lateral loads. Therefore, it is of great importance to evaluate their seismic performance. Many theoretical studies and experimental investigations have been dedicated for studying this important topic. This chapter briefly reviews some previous studies concerning the subject.

2.2 Previous Theoretical and Experimental Studies

In 1996, Lopes[19] assessed the seismic performance of an old building in Lisbon. Both experimental and numerical evaluations were conducted. For the numerical investigation, SAP90 software was used to perform a linear dynamic analysis. The study showed that the building has so poor strength, and it may collapse if it is subjected to a strong event, such the design seismic load prescribed by the Portuguese code. It was concluded that thousands of similar buildings within the area of the study would collapse under the same seismic action.

In 1999, Paquette and Bruneau[20] evaluated the seismic resistance of unreinforced bricks masonry buildings by analytical and experimental investigations. The URM building used in the experimental work has two load-bearing shear walls, each with two openings (a door and a window). Non-linear dynamic analyses were performed to investigate the seismic behavior of the tested building. The analyses the domination of the flexible diaphragms on the structural response, and support the chosen pseudo-dynamic experimental set-up adopted for full-scale testing of a building for which piers in end-walls behave in rocking during seismic response.

In 2001, Franklin S. et al.[21] studied the flexural behaviour of rehabilitatted URM walls under the effect of cyclic loads. Eight walls were tested in the experimental work of the study. In order to make direct comparison, three tested walls were non-rehabilitated. One of the non-rehabilitated URM piers, denoted by (F1), has a high aspect ratio (h/L=1.79) that it is 840 mm in length, 1500 mm in height, and 200 mm in thickness. The mechanical properties of the material are as given in Table (2.1). A constant overburden pressure of 0.29 MPa was applied at the top of the pier.

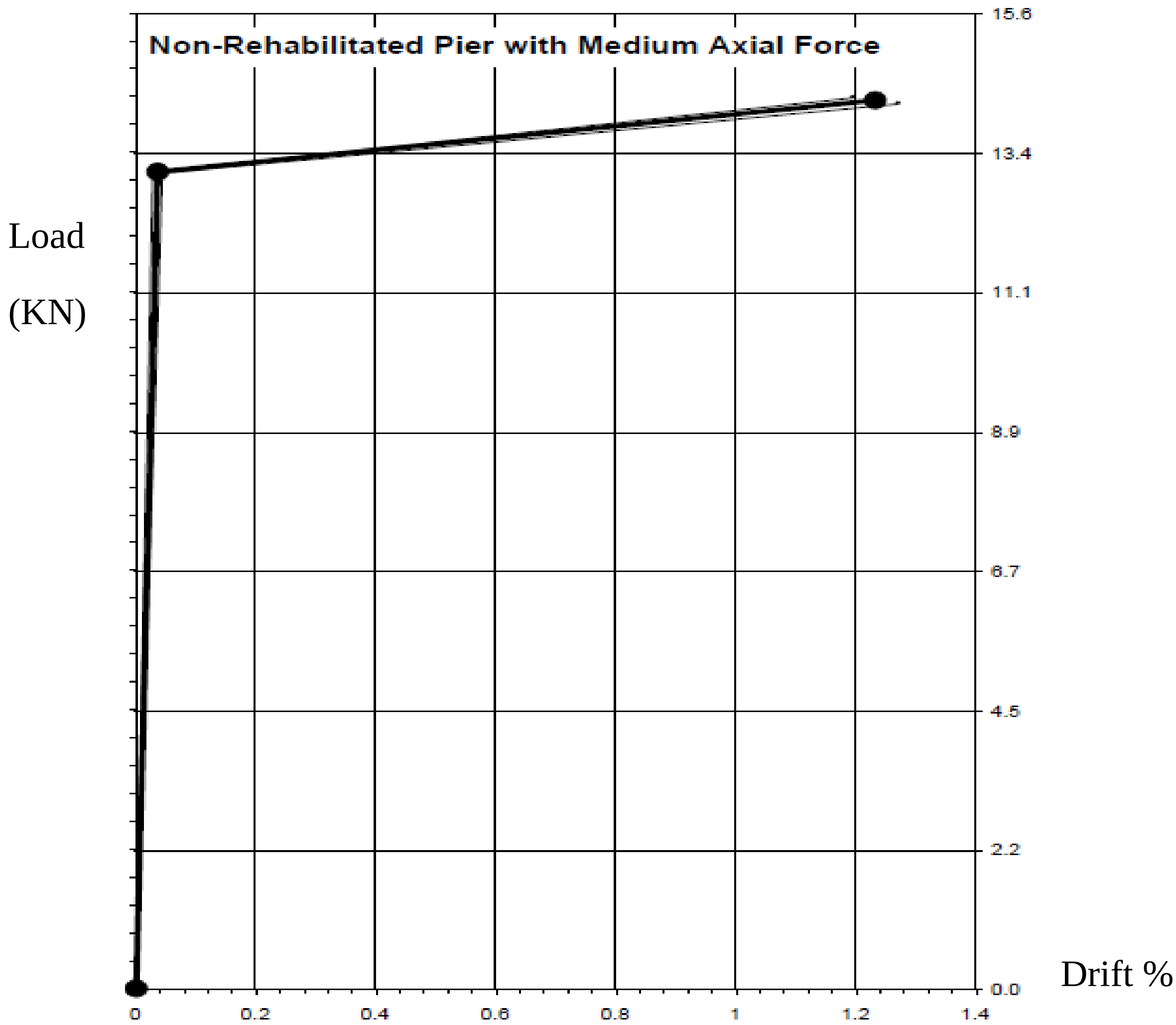

Figure (2.1) Idealized bilinear load-displacement relationship of the pier F1 tested by Franklin et al.[21]

Table (2.1) Mechanical Properties Pier (F1) tested by Franklin.

$f_{\acute{m}}$ (MPa)	f_t (MPa)	$E_{\acute{m}}$ (MPa)	ν(assumed)
7.89	0.28	4275	0.2

The bilinear idealized curve of the load-displacement relationship of the wall is as shown in Fig. (2.1), from which it can be observed that the unreinforced masonry wall yielded at a low value of lateral deformation that the drift is about 0.04% at yielding point. This behavior demonstrates the fact that the unreinforced masonry walls have a poor range for the elastic response.

In 2005, Cardoso et al.[22] studied the seismic performance of old masonry buildings taking an old masonry building from the city of Lisbon as an example. The structure of the considered building includes three-dimensional wooden members provided to contribute the seismic resistance. The timber members are enclosed in the interior walls above the first floor. For such buildings, besides the nonlinearity of masonry, the rupture of the connection between masonry and timber members is an additional source for nonlinearity. The analysis method proposed in the study is intended to deal with most nonlinearity sources. It is not applicable for regular masonry buildings. The nonlinear analysis was implemented by an iterative procedure using SAP2000 software. The exterior masonry walls were modelled with shell elements, while the timber members were modelled as bar elements that transmit only axial loads. At each step of the iterative analysis, the structure is analysed as linear with a structural state depending on the previous step which implies changing the structural stiffness as cracking or yielding occurs and vanishing the collapsed connections. The nonlinear analysis was developed by the sequence of performing linear dynamic analysis at each step by response spectrum scaled with an intensity scaling factor. Different scaling factors were used to reach the maximum scaling factor which corresponds global structural collapse. The analysis results revealed that sequential collapse occurs at relatively low seismic actions, and it initiates by the failure at the connections between the exterior masonry walls and the interior wood bracings in upper floors followed by the out-of-plane collapse of exterior masonry walls . The comparison between the analysis failure mechanisms and similar buildings failure during earthquakes confirms the reliability of the proposed analysis method.

In 2005, Bento et al.[23] proposed strengthening techniques for the same old building they had already evaluated its seismic performance as in reference[20]. The collapse mechanism of the building is the out-of-plane falling of the exterior wall (front wall) as investigated through the study in part I [20]. Therefore, the main purpose of the studied strengthening techniques is to enhance the building capacity to resist this failure mechanism. Since the failure mechanism initiates by the separation of frontal wall from the inner lateral bracing, these connections must be strengthened by steel connectors. This proposition was the first solution. The second strengthening was to construct a reinforced concrete beam (0.6×0.25) m around the perimeter of the exterior wall at the top floor only, while the third solution was providing reinforced concrete beams with the same cross-section for all floor For the three strengthening solutions, the modified building was nonlinearly analysed with the same iterative approach using SAP2000 software as in Part I study. The analysis results were compared with the results for the building performance without strengthening to assess the efficiency of strengthening techniques. It was found that the first solution is the most efficient one that increases the seismic resistance with an improvement of 140%. In addition, this solution has a positive characteristic that it is less intrusive than the other solutions. Therefore, it is more suitable to preserve the historic value of the building. The second and third solutions, as revealed by the changes in the dynamic behaviour, may reduce the seismic intensity that initiates collapse as they can develop new failure mechanisms not controlling the failure of the original building.

In 2005, Carpenteri et al.[24] introduced a nonlinear simulation and damage assessment for the eighth-century masonry tower called " Torro Sineo" in Alba(Italy). The mechanical properties of the tower were evaluated by nondestructive tools without any disturbances, and detailed survey was achieved for the geometry. In addition to mechanical properties evaluation, the nondestructive techniques are useful for investigating hidden structural members, the variety of used materials, and the presence of flaws and voids. Due to recent events in the area of the study, the investigations revealed the existence of damaged zones close to the openings, and the tower had been deflected from verticality. The numerical simulation for the tower was performed by the commercial code DIANA using twenty-node isoparametric brick element. The wooden floors were ignored in the modelling. Both material and geometrical nonlinearities were taken into account in the nonlinear analysis. The nonlinear static analysis involved the effect of dead and wind loads in addition to tilting effect. Comparing the measured stresses with the corresponding stresses obtained from analytical solution demonstrated good acceptance of the numerical model, and revealed that the structure was in elastic conditions under the effect of dead and mostly applied wind loads.

In 2008, Mahmood et al. [25] achieved an experimental investigation for the shear capacity of four URM wallets; three wallets are GFRP (Glass Fibber Reinforced Polymer) retrofitted with different configurations and the fourth one is without any retrofitting. The commonly observed failure mode of in-plane loaded URM walls during earthquakes is the diagonal shear failure, shown in Plate (2.1). Therefore, the study focused on the masonry wall capacity with this failure mode. The test results showed that the unretrofitted specimen exhibited brittle failure while a pseudo-ductility and a significant strength increase were provided by the GFRP retrofitting.

Plate (2.1) Diagonal Shear failure in post-earthquake observed buildings.[25]

In 2009, Mendes and Lourenco[26] presented a numerical analysis for the seismic performance of “Gaioleiro” masonry buildings (old masonry buildings, having a characteristic typology, mainly exist in Lisbon, Portuguese). The numerical simulation was implemented using the finite element software DIANA 2005. Shell elements were used to simulate masonry walls and wooden panel floors, while the timber joists were modelled with beam elements. Both nonlinear static (pushover) and nonlinear time-history analysis were performed, and the analysis results were calibrated with the experimental results obtained of the shaking table tests that achieved on a 1:3 reduced scale building. The study results showed that the pushover analysis is not capable of predicting the building failure under the seismic loads, and this reveals the significant contribution of higher modes in the structural response. Meanwhile, the nonlinear time-history analysis showed that the studied buildings are in their ultimate seismic load capacity.

In 2009, NASEER A.[27] studied the performance behavior of confined brick masonry buildings under seismic demand. The study has included shaking table tests on 1:4 scaled one- and two-story confined buildings. The test results indicate that the one- and two-story CM buildings can withstand with moderate damaging an earthquake with PGA (Peak Ground Acceleration) of o.4g and o.25g, respectively. Also, the study included testing masonry materials and testing URM walls subjected to cyclic loading. The dimensions of the wall are: 930 mm length, 995 mm height, and 219 mm thickness, as shown in Fig. (2.2). The mechanical properties are as in Table (2.2).

Table (2.2) Mechanical Properties of the wall tested by Naseer.

$f_{\acute{m}}$ (MPa) (Compressive strength)	f_t (MPa) (Tensile strength)	$E_{\acute{m}}$ (MPa) (Modulus of elasticity)	ν (Poisson’s ratio)
5.8	0.22	2000	0.2

The experimental cyclic lateral displacement is as shown in Fig. (2.3). The constant pressure that applied on the top area of the wall is 0.32 MPa. This value of

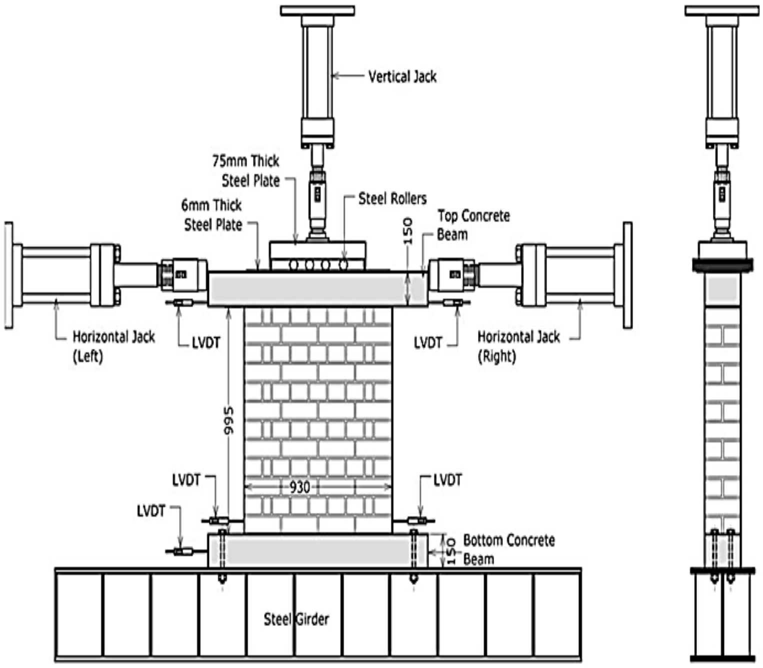

Figure (2.2) Geometry and Instrumental Case for the wall tested by Naseer[27].

the pressure is high compared to the pressure caused by gravity load applied on the top of walls of the ground level in an URM building with one or two stories. This indicates that such walls yield under the effect of in-plane loading in draft values less than the yielding draft of the wall tested by Naseer. From Fig. (2.4), the draft at yield point is (2/995), which is 0.201%.

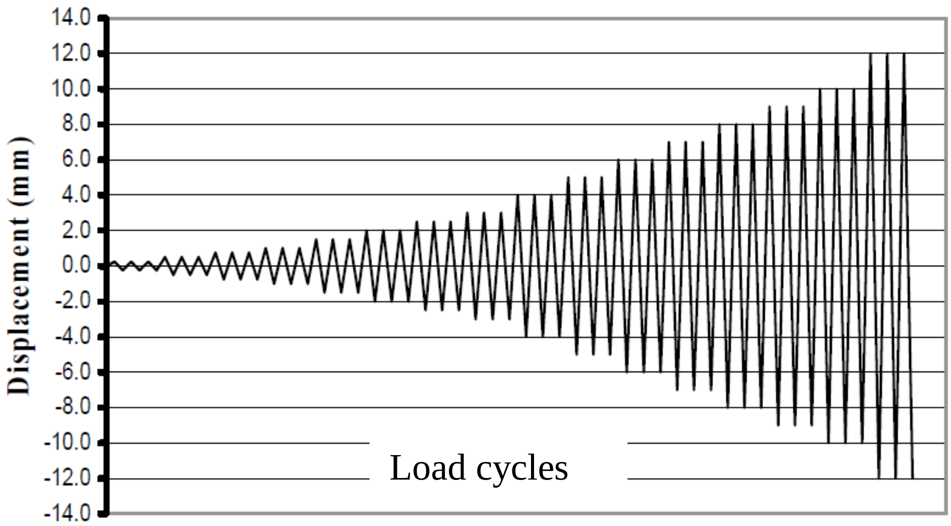

Figure (2.3) Lateral displacement subjected to the wall tested by Naseer[27].

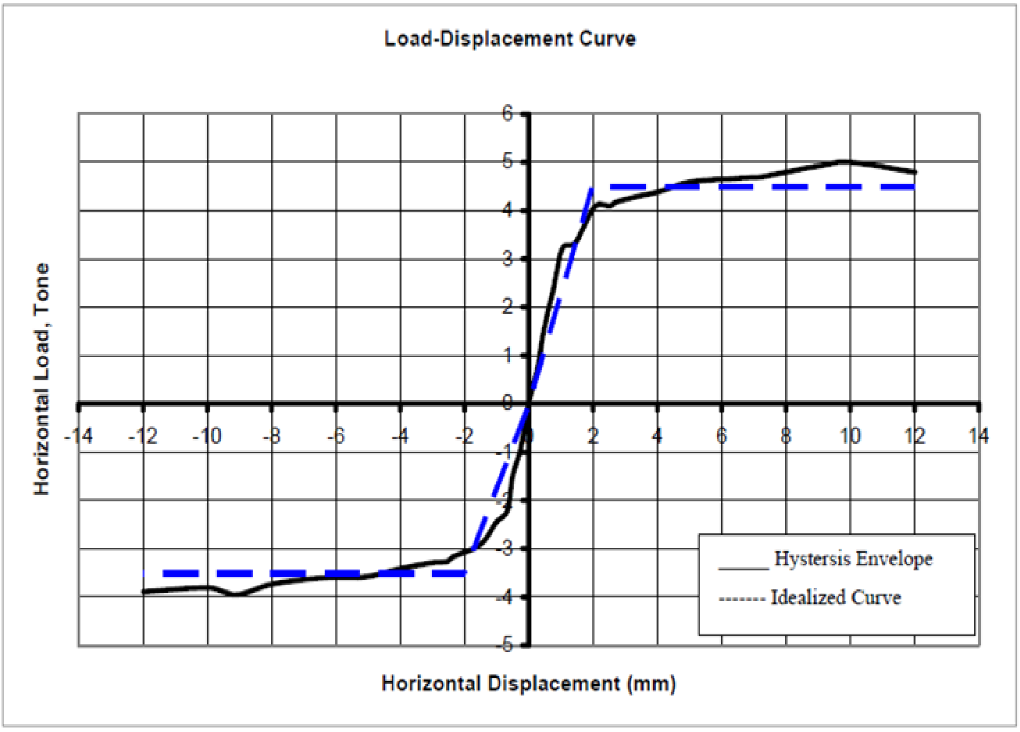

Figure (2.4) The hysteresis envelope and idealized curve of load-displacement relationship of the wall tested by Naseer[27].

In 2010, ALDEMIR A.[28] introduced an assessment for the seismic performance of brick masonry structures. The study has recommended simplified formulations to evaluate the parameters of idealized capacity curves of masonry components (piers) by using the results of the finite element analysis performed by ANSYS 11 and regression analysis through SPSS software. First, local limit states of masonry components are evaluated. Then, the combination of limit states of individual piers constructs the lateral capacity curve of the whole masonry building together with the global limit states. The method is only applicable for unreinforced masonry, and useful for a population of such structures. Walls of different aspect ratios are loaded vertically with loads equal to the weights they support and horizontally with in-plane top displacements until failure occurs. Parameters such as pressure applied at the top of wall, wall thickness, length, and height also were altered, and their effects on capacity curve were analyzed. The base shear versus top displacement were obtained for each case. Then, the effect of each individual parameter on yield and ultimate displacement was obtained. The nonlinear regression, a statistical method by which a nonlinear relation between a dependent variable and a set of independent variables can be obtained, was performed using SPSS Manual 2006. The simplified analysis methodology proposed by the study was tested on an existing building in Istanbul and the tests proved its validity for the seismic analysis of URM buildings, especially for a population of such buildings needed to be assessed quickly.

In 2010, Demirel [29] assessed the performance of the URM buildings in Turkey through a nonlinear equivalent frame model. The analysis was carried out using SAP2000 software, which is capable of simulating material nonlinearity by means of frame hinges which are defined manually. The reliability of the proposed simulation was verified by a reversed cyclic experiment implemented on a full scale, two-storey URM building. Also a shaking table test was carried out on a half scale, two-storey URM building to compare its results with the time-history response obtained by the numerical simulation. Acceptable agreement is found between experimental and numerical results. Consequently, the study results confirm the validity of the nonlinear equivalent frame model for the analysis of URM masonry buildings.

In 2012, Costa[30] evaluated the out-of-plane seismic behavior of stone masonry walls subjected to quasi-static and dynamic loads. Unreinforced and strengthened existing stone buildings were considered for the experimental evaluation of the behavior under the effect of quasi-static loads. Simplified analytical predictions were introduced to evaluate the maximum strengths of tested specimens to compare them with the corresponding experimental values. Five stone multi-leaf walls were tested under the effect of cyclic loads in order to study the out-of-plane behavior and to propose adequate strengthening techniques. The first proposed and studied technique is applying two plaster layers (one at each face of wall) reinforced with steel mesh strictly connected to the wall. The second strengthening solution is mainly aimed to prevent out-of-plane falling of frontal walls and done by restraining parallel walls through connecting them to the floor/roof with steel plates and wood beams as connecting elements. The third solution technique is pouring a reinforced concrete beam along the walls for both wall sides at the foundation level, as a complementary solution added the first solution. The main structural benefit of this beam is to provide enough anchorage for the steel meshes to make full use of their tensile contribution. The tested strengthened specimens proved the significant efficiency of strengthening techniques when compared to the unreinforced walls. It was observed that both strength and energy dissipation capacities increased twice for wall with top connection technique and three times when used together with reinforced plaster technique. Shaking table tests were performed on a full scale one-storey stone building. Numerically, the out-of-plane dynamic behavior was numerically simulated with the approach that is called “multibody dynamics” in which the structure is considered as an assemblage of substructures with nonlinear characteristics concentrated only at contact areas . The MSC Adams 2012™ software was used for the numerical simulation of the multibody dynamics simulation. The results of shaking plate tests revealed that the frontal wall mainly behaves as a rigid body and affected by the existence of multiple leaves. The energy dissipation was found to occur at the impacts between the frontal wall and perpendicular walls (interior walls), and some flexural behavior was also noticed.

In 2013, Lagomarsino et al.[31] described a nonlinear analysis for masonry buildings subjected to a seismic load by an equivalent frame model simulated through the use of TREMURI software. In the equivalent frame model, the masonry walls are idealized with equivalent frame in which the portions that expected to deform are connected by the nodes that assumed as rigid parts. The rigidness assumption for the nodes is due to post-earthquake observations which showed that the deformations in these portions are negligible. The deformable parts, where the nonlinear response is concentrated, are the parts that usually observed to have cracks and involve failure modes. They are divided into piers and spandrels. Piers are the main vertical parts that resist both vertical and lateral loads, while spandrels are the portions of the wall between two vertically aligned openings. Spandrels are considered as secondary regarding vertical loads, but they highly affect the boundary conditions of the adjacent piers in lateral loading cases. Both piers and spandrels are modeled as 2D elements with the assumption of bilinear force-displacement relation, while the nonlinear phase is modeled by stiffness decay. The whole three-dimensional model is assembled by defining a global coordinate system (x,y,z).

In 2013, Parisi and Augenti[32] investigated the seismic capacity of URM walls with openings. The main aim of the study is to introduce a simplified methodology for the assessment of the irregularity influence on the in-plane seismic capacity of the URM walls with openings. A macroelement method used for masonry walls modeling, and the method reliability was confirmed by the experimental results. The basic irregularities of URM walls with openings comprise horizontal (openings with different heights), vertical (openings with different lengths), alignment offset, or openings number irregularity. Even the peripheral walls are regular, irregularities are commonly found in the interior walls. Therefore, even a masonry building satisfies the global regularity stipulated by seismic codes, it still encompasses irregular components. An irregularity of a wall does not only cause the gravity loads to be nonuniformly distributed but also concentrates damages in some zones arising the seismic vulnerability of the wall. Plate (2.2) shows one of the post-earthquake observations that reveals the damage concentration caused by the irregularity. The methodology proposed by the study can be precisely defined as the irregularities quantifications by means of geometric indices and their influences on seismic capacity of the perforated URM masonry walls through both sensitivity and regression analysis. It was found by the study results that the in-plane seismic capacity is highly affected by a geometrical irregularity, especially the irregularity attributed to openings with unequal heights.

Plate (2.2) A damage Observed after (2009 L'Aquila earthquake, Italy)[32].

In 2015, Yaseen A. A.[33] investigated the seismic fragility of the existing URM buildings in the north of Iraq (Kurdistan region) which represent approximately 87% of all buildings in this region. The main purpose of the study is to know how such buildings respond to the expected future events in order to mitigate predicted damages and losses by performing adequate strengthening techniques. One-story (3 m high with (15×10) m plan) and two-story (with doubled height and repeated plan) buildings were studied. The macro modeling and incremental dynamic analysis were achieved using TREMURI program to perform a nonlinear time-history analysis. The mean values used for the mechanical properties of masonry are 4350 MPa for modulus of elasticity and 1740 MPa for modulus of rigidity.The compressive strength of masonry was estimated depending on strengths of its constituents according to Eq. (2.1) as follows:

$$f_{\acute{m}} = k\ f_b^{\ 0.7}\ f_m^{\ 0.3} \tag{2.1}$$

where k: factor ranging from 0.4 to 0.6.

The study results indicated that the seismic safety of the studied low-rise URM buildings in the concerned region is questionable denoting the need for strengthening such structures to mitigate the potential economic and life losses probably happen during future strong earthquakes.

In 2015, Abd A. H. [34] presented an assessment of earthquake effects on masonry structures. ANSYS 15.0 software and the isoparametric solid65 were used to carry out the nonlinear dynamic (time-history) analysis. The study demonstrated acceptance of ANSYS results compared with experimental works for a cyclically loaded wall. The earthquake data were downloaded from PEER website. The study mainly focused on mosque domes and minarets. The study results lead to conclude that yielding mostly starts at the lowest parts of the masonry structures, failure takes place quicker if the wall thickness gets smaller, and the openings in domes need to be enhanced.

In 2017, Abdulla et al. [35] described a simplified micro-model for the simulation of masonry utilizing the extended finite element method and a combination of plasticity-based models. The detailed micro-modeling gives accurate and detailed results, but it takes intensive computations and thus it is used for small masonry models. Therefore, a simplified micro-model is proposed by this study, in which the brick units are expanded to compensate the vanished mortar volume while the interaction between enlarged units is modeled by discontinuous elements. In the described method, the nonlinear compressive behavior of masonry is simulated by the Drucker-Prager model of plasticity, and the modulus of elasticity of expanded units is adjusted assuming uniform stress distribution and full bond between masonry units and mortar. The analysis was carried out through ABAQUS 6.13 software using 3D hexahedral, eight node, linear element for masonry units. The interaction between adjacent expanded units was simulated with cohesive approach by node to surface contact. The modeling permits adjacent unit surfaces to transmit pressure when they are in contact, while both tensile stress and penetration are prevented. The validation of the proposed method was verified by comparison to the results of experimentally tested masonry walls subjected to in-plane cyclic, out-of-plane monotonic, and in-plane monotonic loads; the comparison showed a good accuracy for the analysis method.

In 2017, M. H. Saeed [36] investigated the nonlinear time-history response of URM masonry buildings in Iraq. The study encompassed the test of masonry prisms to determine the compressive strength of masonry constructed of cement-sand mortar and perforated clay bricks. The compressive strength of masonry was evaluated as 5.35 MPa. The ABAQUS 6-13 software was used to perform the nonlinear analysis. In each analysis, only one acceleration component was applied to the model either in z- or x-direction. The results of the study showed that the models are more efficient when the acceleration is applied in the long direction than when applied in the short one.

In 2018, Kallioras et al. [37] presented the results of an experimental test carried out on a full-scale, single storey URM building. A unidirectional-table test was implemented on the building which is consisted of double-wythe clay brick URM walls including large openings and a floor made of timber beams and planks composing a flexible diaphragm. Its sharply inclined roof is composed of timber trusses. The parts of the perimeter walls above the floor (the gables) are the weaker when affected by an out-of-plane excitation. The mechanical properties of the building walls are 9.23 MPa compressive strength, 8123 MPa modulus of elasticity evaluated as the slope of the secant at 33% of the compressive strength, 0.23 MPa bond stress obtained by bond wrench tests, 0.15 MPa brick-mortar cohesion at zero pressure case, and 0.55 internal friction coefficient (μ). It was observed that only minor damage occurred for the excited building up to an input accelerogram with PGA of 0.23 g, while the collapse state was reached at a motion with a PGA of 0.68 g. Zones of high acceleration response, such as gables, exhibited major out-of-plane damage. As a result, the study confirmed that the most vulnerable parts of such buildings under seismic action are the gable walls. The damage caused by in-plane response was exhibited by rocking of slender piers.

In 2018, Shakarmi B. et al.[38] used the LS-DYNA software for the simulation of confined masonry walls loaded with cyclic, in-plane, lateral loads to examine the effect of aspect and reinforcement ratio on the structural behavior of the studied walls. The validity of using the micro-model has been verified by comparing it to the results of a previous test performed on a confined wall. The study showed that an aspect ratio of (height/length=1) makes the wall having better structural behavior concerning resisting mechanism, energy absorption, and deformability

In 2019, M. A. Erberik et al. [39] compared the seismic performance of URM buildings to that of confined masonry (CM) buildings. Capacity curve parameters were evaluated based on previous studies, and then capacity curves were constructed first for components of both URM and CM buildings. Secondly, the buildings composed of the assemblages of walls with the already obtained capacity curves are analyzed. The results demonstrated the superior performance of CM type over URM during seismic excitation. It is found that low rise CM buildings are suitable even high seismic intensity exists. This is attributed to the effect of confinement which prevents wall-to-wall action that propagates seismic damage and also to the enhancement of the structure capability of dissipating energy. The results demonstrated high effect of masonry compressive strength on the seismic performance of URM buildings. Whereas, it is not the case for CM building models which are notably affected by other parameters such as reinforcement and cross-section of confining concrete columns and diagonal shear strength of confined masonry walls.

In 2019, Ismail N. and N. Khattack[40] studied failure modes of the URM buildings that were damaged due to the Mw 7.5 earthquake that hit the North of Pakistan on 26 October 2015. The commonly observed failure modes encompassed toppling of minarets, local or global out-of-plane collapse of URM walls, diagonal shear cracking in piers, flexural cracking in spandrels, damage of corner, pounding damage, and damage due to ground settlement. Most fatalities were due to the collapse of URM walls and subsequent collapse of roofs.

In 2019, Sorrentino L. et al.[41] studied the structural behavior of masonry buildings during the nine earthquakes ranging from 5 to 6 of the moment magnitude that hit Central Italy during the period between August 2016 and January 2017. The unreinforced masonry buildings represent about 75% of the constructions in the affected territory. Severe damage and complete collapse were observed in URM buildings, while better structural behavior was observed in modern buildings constructed with hollow clay blocks. This better seismic performance is attributed to the adequate quality of masonry, the relatively lightweight structures due to the presence of cavities in masonry units and the configuration redundancy.

2.3 Remarks

Regarding the experimental and theoretical studies that have been previewed in this chapter, this chapter, the following remarks can be noticed:

1- Different numerical methods, which are validated by calibration with experimental results, are presented to evaluate the seismic performance of masonry structures.

2- Different techniques have been investigated and proposed to improve the seismic performance of URM structures.

3- It is not easy to build a finite element model with detailed micro-modeling. Therefore, macro-modeling is widely used for masonry simulation.

4- Few studies aimed to assess the seismic performance of masonry structures in Iraq.

5- Few studies involved an experimental work to investigate the mechanical properties of masonry in Iraq.

6- The dynamic response of URM houses in Iraq under the effect of earthquakes has scarcely been investigated.

7- The nonlinear dynamic response of CM buildings under the seismic action has rarely been presented.

Chapter Three

Experimental Work for Mechanical Properties

CHAPTER THREE
EXPERIMENTAL WORK FOR MECHANICAL PROPERTIES

3.1 Introduction

It is clear that the reliability of the numerical simulation results are pertinent to the accuracy of the mechanical properties which must be as actual as possible. Few previous experimental studies can be found regarding the mechanical properties of masonry in Iraq, such as the study presented by Al-Chaar et al.[42]. A notable variance exists in the evaluation of masonry mechanical properties referring to the relatively high uncertainty caused by the complex nature of unit-mortar assemblage and the variance in properties of its constituents through the different countries.

3.2 Compressive Strength of Masonry

The compressive strength (CS) of masonry can be considered as its fundamental characteristic because other mechanical properties can be estimated depending on it by proposed relationships. The masonry CS depends on the compressive strengths of its constituents (brick units and mortar). The difference in stiffness and Poisson's ratio between bricks and mortar makes one of the two constituent tends to expand laterally more than the other as masonry being compressed. Consequently, shear stresses develop at the contact surfaces between bricks and mortar initiating masonry failure[5]. If the bricks are stiffer than mortar, mortar will be in a triaxial compression state of stress, while mortar will be stretched outside if it is the stiffer. This behavior has been demonstrated study. To determine the CS of masonry, in the simulation with the micro-modeling of masonry prism test in the this six prisms were tested, as shown in Plate (3.1). The average compressive strength is 5.5 MPa with a standard deviation of 0.4 MPa. For all masonry and mortar specimens, the specimens were cured and tested after 28 days age.

Plate(3.1) Prism test.

3.3 Tensile Strength of Masonry

The tensile strength of each of masonry constituents is higher than the ultimate bond stress between them that is normal to the interaction surface. Therefore, the tensile strength of masonry is controlled by the value of this bond stress. In the this study, a simple method was used to test directly the tensile strength of masonry. The specimen used for the test is two bricks built together as in Plate (3.2) with cement-sand mortar of 1:3 mix proportion.

Plate (3.2) Tensile Strength Test.

The lower brick of the specimen in Plate (3.2) is loaded gradually with weights that put in the lower iron frame, which is free to fall when tensile failure occurs while the upper brick is still hanged. Then, the total suspended weight is divided by the loaded area of the unit-mortar interaction to find tensile strength.

15 specimens were tested in this study, and the average value of the tensile strength is 0.15 MPa with a standard deviation of 0.03 MPa.

3.4 Modulus of Elasticity of Masonry

The modulus of elasticity of masonry ($E_{\acute{m}}$) can be estimated depending on the compressive strength value, but the challenge is that the codes have a large extent of variation in the proposed relationships as shown in Table (3.1).

Table (3.1) Different Formulae for Evaluating $E_{\acute{m}}$

Code	Proposed Value for $E_{\acute{m}}$
Building Code Requirements and Specifications for Masonry Structures By The Masonry Standards Joint Committee (MSJC)	700 $f_{\acute{m}}$ or evaluated as the slope of the chord taken between 0.05 and 0.33 of the maximum CS of masonry in the stress-strain curve[43].
Turkish Code (TEC2007)	200 $f_{\acute{m}}$ [28].
Eurocode 6	1000 $f_{\acute{m}}$ [44]
FEMA 356	550 $f_{\acute{m}}$ [18]

In the this study, a simple steel frame was done to measure $E_{\acute{m}}$. Three prisms (three-brick prisms) were tested under uniaxial compression, as shown in Plate (3.3). The length shortening was measured with a dial gauge and the corresponding load is recorded. Only the eight screws (two from each side) are fixed to the specimen.

Plate (3.3) A masonry specimen under testing for the modulus of elasticity.

The stress-strain curves are as shown in Figures (3.1) to (3.3).

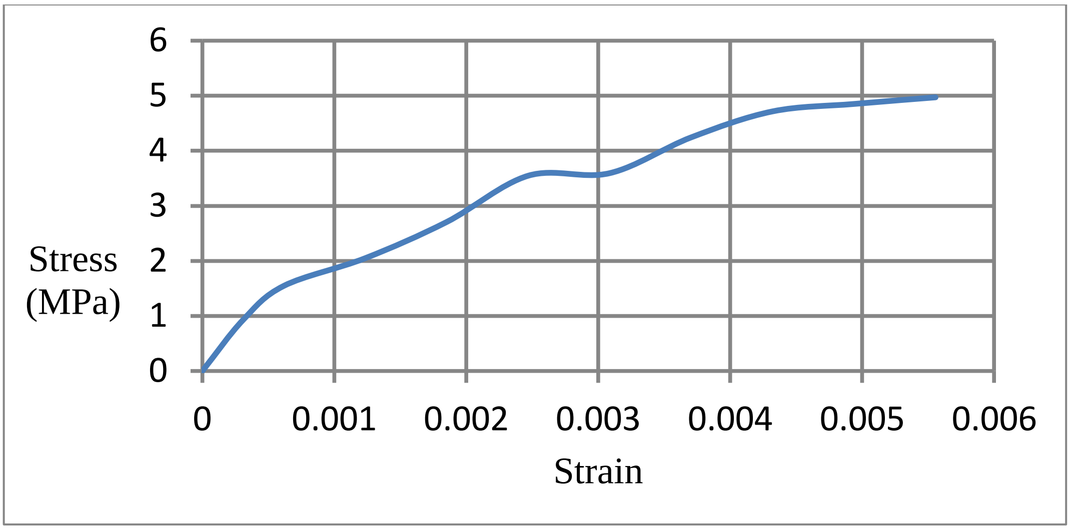

Figure (3.1) Stress-Strain curve for masonry specimen 1.

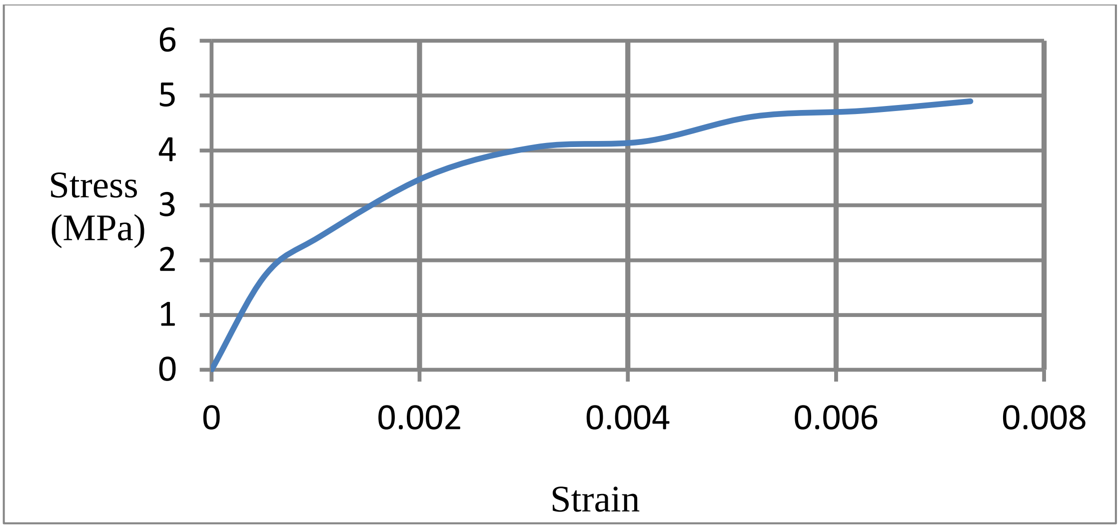

Figure (3.2) Stress-Strain curve for masonry specimen 2.

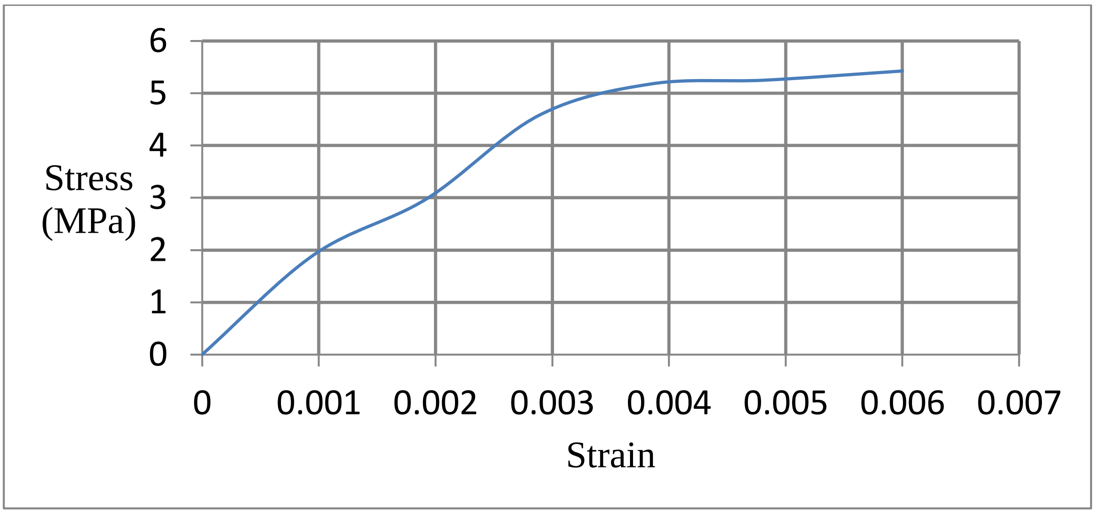

Figure (3.3) Stress-Strain curve for masonry specimen 3.

The modulus of elasticity can be obtained from the stress-strain curve according to the MSJC code as illustrated in Fig. (3.4). Consequently, the moduli of elasticity for the three specimens have been evaluated to be as in Table (3.2).

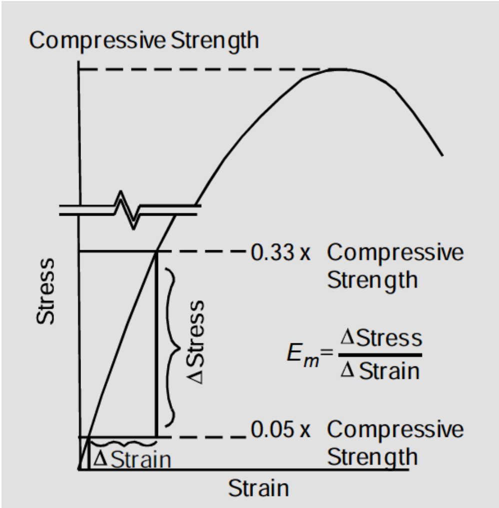

Figure (3.4) Modulus of Elasticity for Masonry According to MSJC Code [43].

Table (3.2) Moduli of Elasticity of Masonry Specimens.

specimen	1	2	3
$E_{\acute{m}}$ (MPa)	2399	3610	2160

The average value of $E_{\acute{m}}$ is 2723 MPa with a standard deviation of 777 MPa. Returning to the proposed evaluations for $E_{\acute{m}}$ in the different codes, it can be observed that the average value obtained from the test is close to the value recommended by the FEMA 356 code ($E_{\acute{m}} = 550f_{\acute{m}}$) which is equal to 3025 MPa. However, a value of 2750 MPa has been used in this study.

3.5 Mechanical Properties of Clay Bricks

The compressive strength of clay bricks (f_b) has been determined for 10 arbitrarily chosen bricks. Plate (3.4) shows a brick specimen during test. The average compressive strength is 9 MPa with a standard deviation of 0.5 MPa. The Iraqi specifications require that the minimum average compressive strength of brick units is not less than 13 MPa for bearing walls. However, the test results represent the non-engineered masonry buildings which represent the common case for houses in Iraq.

Plate (3.4) A Brick under Compression Test.

The tensile strength of clay bricks (f_{bt}) has been found using three specimens prepared to be similar to the standardized specimens of mortar. Each brick specimen is prepared by cutting and abrading a piece of a brick to be as identical as possible to the same geometry of the specimens used for measuring the tensile strength of mortar. The average tensile strength obtained is 1.17 MPa with a standard deviation of 0.04 MPa. The specimens after test are shown in Plate (3.5) and a specimen under test is shown in Plate (3.6).

Plate (3.5) Prepared Brick Specimens after Tensile Test.

3.6 Mechanical Properties of Cement-Sand Mortar

The tested cement-sand mortar has a volumetric mix proportion of 1:3 which is the commonly used in practice for masonry construction in Iraq. Twelve (70*70*70) mm cubes were tested to determine the compressive strength for joint mortar. The average strength obtained is 18 MPa with a standard deviation of .6 MPa. The water/cement ratio was used as that provides the practical workability. Plate (3.7) shows a mortar specimen under compression test. The tensile strength of mortar is also determined by testing three specimens, which are poured in a standardized mold. Plates (3.8) and (3.9) show a mortar specimen under tensile test and after tensile failure, respectively. The results of the test are in Table (3.3). The minimum CS required for the mortar according the Iraqi standards is 24 MPa. However, this value is used with a value of 18 MPa for the CS of bricks to estimate the CS of masonry according to Eq. (2.4) as follows:

$f_{\acute{m}} = 0.5\ 18^{0.7}\, 24^{0.3} = 9.811$ MPa.

This value was used in the numerical analyses to investigate the effect of the CS of masonry on its seismic response.

Plate (3.6) Tensile test for a brick specimen.

Plate (3.7) A mortar cube under compression test.

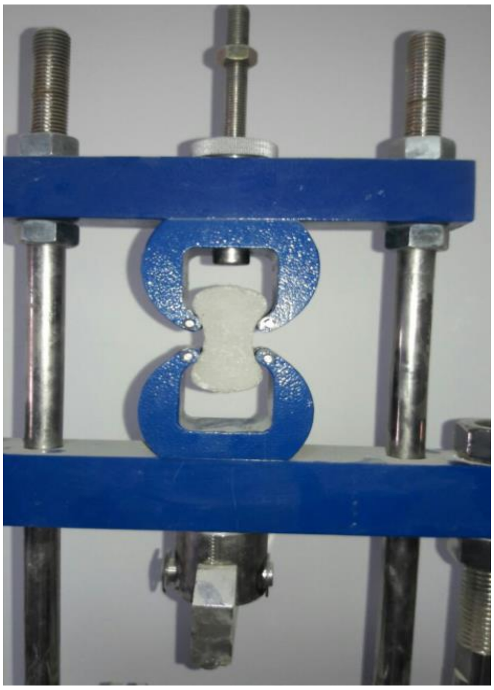

Plate (3.8) A mortar specimen under tension test.

Plate (3.9) A mortar specimen after tensile failure.

Table (3.3) Tensile Strength of Mortar Specimens.

No.	Cross-section area	Ultimate load (Kg)	Tensile strength (MPa)	Average Tensile strength (MPa)	Standard Deviation (MPa)
1	(2.54 * 2.54) cm	195	2.96	3.2	0.24
2	(2.54 * 2.54) cm	213	3.24		
3	(2.54 * 2.54) cm	227	3.45		

The modulus of elasticity of mortar (E_m) has been determined by testing three standardized specimens with diameter of 150 mm and height of 300mm, as shown in Plate (3.10). The relative longitudinal displacements between the upper and lower sets of screws are measured by a dial gage and the corresponding loads were recorded. The strains and corresponding average stresses are as in Table (3.4).

Plate (3.10) A Cylindrical Mortar Specimen under Compression.

Table (3.4) Strains and corresponding stresses for mortar specimens.

No.	Strain	Stress (MPa)	No.	Strain	Stress (MPa)
1	0.00004	0.4	7	0.0005333	10.412270
2	0.000133333	2.6596559	8	0.0006	11.430861
3	0.0002	4.8100160	9	0.0006666	11.940157
4	0.000266667	6.2247266	10	0.0008	13.920752
5	0.000333333	7.4130835	11	0.0008666	14.147106
6	0.0004	8.7146173	12	0.0009333	14.316871

The tangent modulus of elasticity is found by dividing the stress 0.4 MPa by the corresponding strain, and it is equal to 10,000 MPa.

3.7 Cohesion Stress Between Units and Mortar (f_{v^o})

The shear stress at zero pressure between mortar and units, also called cohesion[37], is needed to define friction at their interaction surfaces into ANSYS modeling when a contact pair is created in the micro-modeling. Also it is needed for the calculation of shear strength of masonry walls. In the this study, five specimens were tested, as shown in Fig. (3.11). The average value of the ultimate adhesive stress is 0.6 MPa with a standard deviation of 0.1 MPa.

Plate (3.11) Cohesion test of masonry specimen.

Chapter Four

Numerical Formulation Of The Problem

CHAPTER FOUR
NUMERICAL FORMULATION OF THE PROBLEM

4.1 Introduction

The finite element method (FEM) is a powerful numerical tool in which complicated problems can be solved through replacing them by simpler ones. Consequently, only approximate solutions can be obtained for the replaced problems. In the FEM, the solution domain is deemed as built up of assembling many small, interconnected subdomains known as finite elements. The points of interconnection are called nodes. Every element is connected to other elements by its exterior nodes. Interpolation function (commonly a polynomials) are assumed for the field variables and then shape functions are derived in terms of the nodal values of the field variables. An exterior node has the same values of the field variable for all elements at which they are connected thus the continuity of the field variable is inherited. In structural problems, the field variables are displacements, but the engineers are mainly interested with strains and stresses. The strains can be found since they are the derivatives of displacements. Consequently, the stresses can be obtained too. The number of elements for an analyzed domain (structure) is increased, which means the mesh is refined, till the variation in the results becomes negligible. Software packages based on FEM are used for the different simulations such as ANSYS, ABAQUS, ADINA, etc.

In this study, ANSYS 18.2 software was used to simulate the studied masonry models. ANSYS (ANalysis SYStem) is a software package used to solve different types of problems including structural, mechanical, thermal, fluid, electromagnetic, etc. For structural problems, the program provides a large library of different elements for the different simulations. Also different types of analyses are provided; linear and nonlinear static, linear and nonlinear dynamic analysis are applicable. Both geometric and material nonlinearities can be taken into account in the simulation. In this study, Solid65 element has been used to simulate concrete materials (masonry, brick units, and mortar), and time-history analysis was used to analyze the studied models [45][46][47].

4.2 Solid65 Element

The three-dimensions, eight node, isotropic solid element labeled solid65 has the distinguishing characteristic that it is capable of crushing in compression and cracking in tension. Hence, it can simulate brittle materials such as concrete, masonry, brick units, etc. The element can include smeared reinforcement. Also it can be used as plain concrete through setting its real constants as equal to zero values. At each node, the element has three degrees of freedom which are three translations: u_x, u_y, and u_z)[48]. Fig. (4.1) shows the geometry of the element.

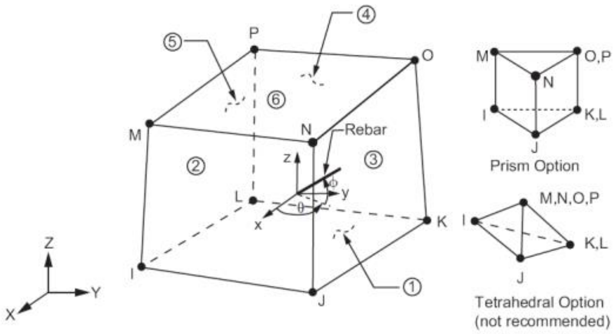

Figure (4.1) Geometry of Solid65 Element [48].

4.3 Modeling Strategies of Masonry

4.3.1 Micro-modeling of Masonry

Masonry is composed of brick units and mortar joints. Therefore, the micro-modeling is aimed to do as-built simulation for this assemblage, and it has two strategies [28]:

- Detailed micro-modeling, shown in (Fig. 4.2b), in which the bricks and mortar joints are modeled by continuum elements. Discontinuous elements are used to represent the unit-mortar interface. So, mechanical properties should be defined for each material separately, in addition to the interface properties. This approach has been used in this study for micro-modeling of the masonry prism test.
- Simplified micro-modeling, shown in (Fig. 4.2c), in which the units are

expanded and represented with continuum elements, while mortar joints volume is compensated by the expansion of units. The unit-mortar interaction properties are represented by interface elements.

The simulations with micro-modeling need a long time for both modeling and solution. Also, the solution requires a large computer memory. Therefore, this modeling approach is tedious for large models.

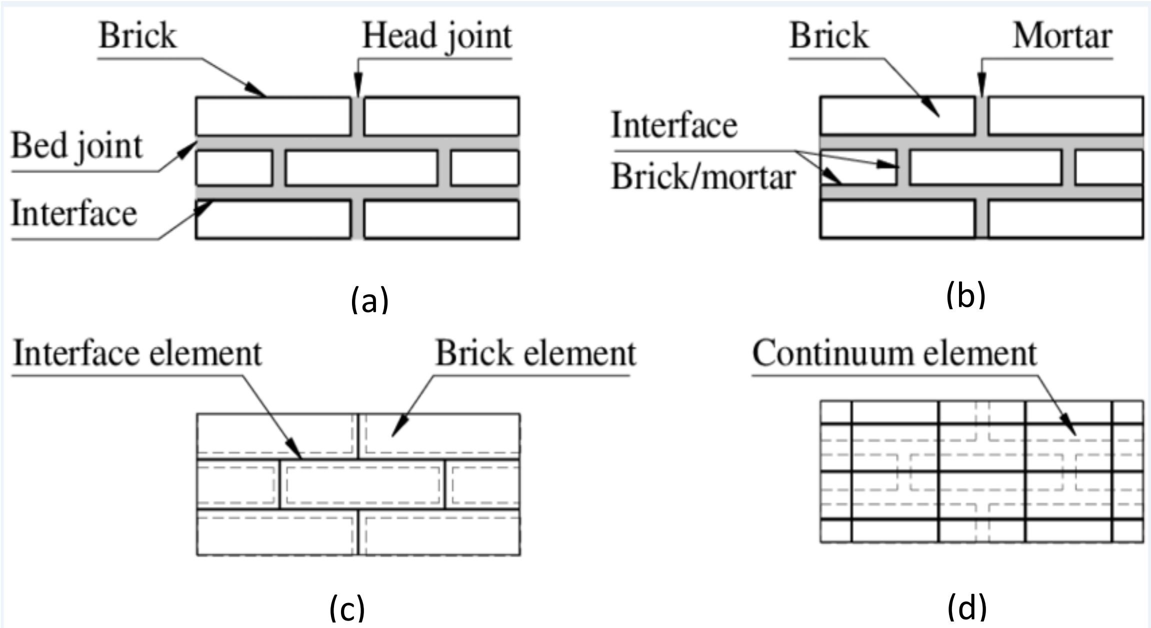

Figure (4.2) Strategies for modeling of masonry: (a) a masonry sample, (b) detailed micro-model, (c) simplified micro-model, and (d) macro model[28].

4.3.2 Macro-modeling of Masonry

It is the simplest way in which masonry is deemed as a homogeneous material, as shown in Fig.(4.2d)[28]. When the overall behaviour of the structure is aimed rather than the detailed concentration of stresses, the macro-modeling is efficient to simulate masonry structures. This approach has been used for modeling in this study.

4.3.3 Equivalent Frame Model

This simple approach is based on dealing with the masonry walls as they are composed of vertical (piers) and horizontal (spandrel) components, which are connected by rigid zones. Both piers and spandrel components are modeled with suitable elements like two-node macro elements [29].

4.4 ANSYS Multilinear Stress-Strain Relationship

The stress-strain curve for a nonlinear material model can be defined into ANSYS. through the multilinear stress-strain curve which is formed by joining a number of line segments. The slope of the first line segment must be equal to the modulus of elasticity, and no other segment can have a slope greater than it. The slopes of values less than zero can not be input. Consequently, the descending parts of the stress-strain and force-displacement curve shown in Fig. (4.3) can not be involved into ANSYS. In case of a linear analysis, the stress-strain relationship is linear and defined by inputting the linear properties. The linear properties are also required for the nonlinear analysis. In the present study, all models are considered as isotropic materials for which the linear properties are the modulus of elasticity and Poisson's ratio[49].

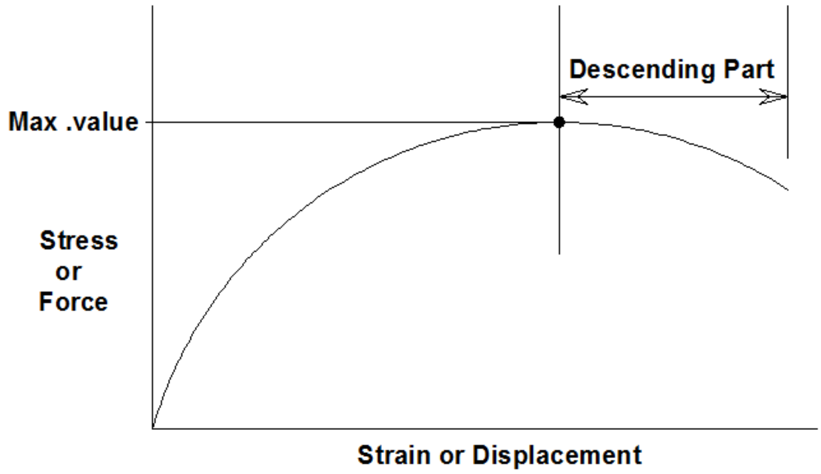

Figure (4.3) Stress-Strain or Force-Displacement relationship with the part not involved into ANSYS simulations.

4.5 Willam-Warnke Failure Criterion

According to Willam-Warnke failure criterion which predicts failure of brittle materials, the parameters shown in the ANSYS window, shown in Fig. (4.4), should be input except ones that can be taken as default by ANSYS [49]. From top to down, the first parameter whose value ranges from 0 to 1 defines the reduction in shear capacity of an open cracked surface. The second one defines the shear capacity of a closed cracked section. In this study, the first and second parameters are taken equal to 0 and 1, respectively. The third and fourth parameters are the uniaxial tensile and compressive strengths. As stated by ANSYS theory reference, the stress-strain matrix is modified for a cracked element. The program implements this modification by inserting a weakness plane perpendicular to the crack face. Also shear transfer coefficients are used into the modified matrix. For the purposes of numerical stability, the value of the last parameter is taken as 1×10^{-6}. The remaining parameters (from fifth through eighth one) are taken as default, but if any one of them is input the others should be input too [49].

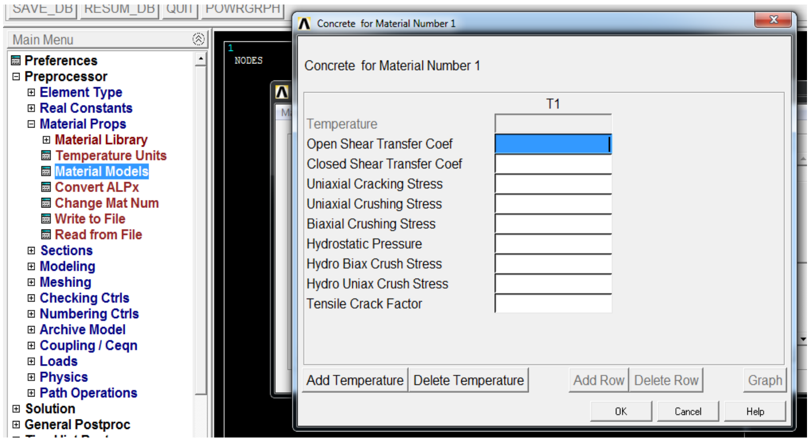

Figure (4.4) Parameters of concrete failure criterion.

4.6 Analysis Types

Different solution types are provided by ANSYS Mechanical APDL. In all these analysis types, the program forms the global stiffness matrix through the addition of element stiffness matrices. The global mass matrix is built up, where it is required, by the addition of consistent mass matrices of elements. The analysis types into ANSYS Mechanical APDL are briefly outlined as follows[50]:

1- **Static Analysis**: analyzes a structure linearly or nonlinearly under quasistatic loading. Hence, inertia and damping forces are not considered in the equilibrium status of the structure. For a linear static analysis, the program solves the overall equilibrium equations in the following form:

$[K]\{U\} = \{F\}$ (4.1)

Where:

[K]: global stiffness matrix$= \sum_{1}^{N}[K_e]$ …(N: number of elements).

: nodal displacement vector.

: force vector.

For a nonlinear system in which the stiffness matrix depends on the displacement, the Newton-Raphson iterative method is used to solve the nonlinear set of equations and the global stiffness matrix is updated at each load sub-step.

2- **Modal Analysis**: needs only the definition of density and elastic properties as well as boundary conditions of a structure to capture its natural frequencies and mode shapes. This analysis is required to perform other analyses based on mode shapes of the structure.

3- **Harmonic Analysis**: used to describe the linear behavior of a structure subjected to a sinusoidal (cyclic) load. It enables a designer to avoid resonance, fatigue, and other bad effects of forced vibrations.

4- **Spectrum Analysis**: evaluates the maximum linear response of a structure under the effect of an arbitrary time-varying load whose response spectrum for single-DOF (degree of freedom) systems is known and defined into the analysis input data. The structures are designed so that some local damages are permitted during moderate earthquakes to dissipate energy because the linear design under seismic loads is unviable. If even local damages in the structure can cause catastrophic effects it should be designed to respond linearly for seismic loads. Therefore, the spectrum analysis is used to design nuclear plants.

5- **Buckling Analysis**: used for the determination of the bucking loads which are the critical loads that make a structure unstable and buckled mode shapes (the shape associated with the response of a buckled structure).

6- **Transient Analysis**:

The transient analysis (also called time-history) is used to determine the response of a linear or nonlinear structural system subjected to any time-dependent load. Also it can be used to find the response of a freely vibrating structure with our without damping effect. In this analysis, the program solves the overall equations in the form that follows:

$$[\mathrm{M}]\{\ddot{U}\} + [\mathrm{C}]\{\dot{U}\} + [\mathrm{K}]\{\mathrm{U}\} = \{\mathrm{F_t}\} \quad (4.2)$$

Where:

[M]: global mass matrix.

$\{\ddot{U}\}$: vector of nodal accelerations.

[C] : damping matrix.

$\{\dot{U}\}$: vector of nodal velocities.

[K] : global stiffness matrix.

{U} : vector of nodal displacements.

$\{\mathrm{F_t}\}$: load vector.

At any time (t), the set of equations above can be considered as equations of static equilibrium, and the program utilizes the iterative approach to solve them. For the sequent time increments, an improved method (known as HHT) or Newmark integration method is used to perform the incremental dynamic analysis [50].

4.7 Damping

Damping can be defined as “ the process by which free vibration steadily diminishes in amplitude”[51]. In other words, it is the dissipation of the energy of an oscillating system caused by various mechanisms, such as the internal friction and thermal effect of repeated straining. In transient analysis in ANSYS, the form of Rayleigh damping can be used, in which the damping matrix is formed by summing the mass and stiffness matrices multiplied by mass matrix multiplier (Alpha) and stiffness matrix multiplier (Beta). Assuming the same damping ratio for all modes, the coefficients of Rayleigh damping (α and β) were evaluated in this study according to Eqs. (4.3) and (4.4)[50][51]:

$$\alpha = \zeta \frac{2\omega_i \omega_j}{\omega_i + \omega_j} \qquad (4.3)$$

$$\beta = \zeta \frac{2}{\omega_i + \omega_j} \qquad (4.4)$$

Where: ζ: the constant damping ratio, ω_i: the circular frequency at the mode i, and ω_j: the circular frequency at the mode j.

4.8 Newton-Raphson Procedure

The solution of nonlinear equations, in which the stiffness matrix is a function of the DOFs or their derivatives, is accomplished in ANSYS using Newton-Raphson method. The Newton-Raphson equation used for the nonlinear solution can be written as follows:

$$[K_i^T].\{\Delta U_i\} = \{F^a\} - \{F_i^{nr}\} \qquad (4.5)$$

Where:

$[K_i^T]$: Tangential stiffness matrix.

$\{F^a\}$: Applied loads vector.

$\{F_i^{nr}\}$: Vector of element internal loads (resorting loads).

In transient analysis, $\{F_i^{nr}\}$ includes the effective inertia and damping forces. The final converged solution should be in equilibrium so that the internal loads computed from current stresses be equal to the external applied loads within some tolerance. This is implemented with a step-by-step incremental analysis in which the final applied load is reached by applying it in increments and performing the Newton-Raphson method in each load step[49].

4.9 Convergence Criteria

The iterative process requires a convergence criterion to terminate when the solution satisfies the required accuracy. The nonlinear convergence criteria are used in ANSYS for the nonlinear structural solutions which is solved by Newton-Raphson method. The force, displacement, moment, and rotation criteria are provided [49]. In this study, both force and displacement criteria were used.

4.10 Seismic Loading for Transient Analysis

The seismic load can defined into ANSYS to perform a transient analysis by applying the components of both ground displacement and velocity to the base area of the structure. An accelerogram can be converted into a displacement time-history by double integration technique which is nowadays carried out by professional software packages such as Seismosignal software. In this study, the seismic data were downloaded from PEER (Pacific Earthquake Engineering Research) Berkeley site[52]. Also the seismosignal program was used to convert some accelorograms from the 7.3 M_w earthquake that hit the Iran-Iraq border on 12 November 2017. The data of the 7.3 M_w earthquake were downloaded from Iran strong motion network [53].

4.11 Selection of Acceleration Time-Histories

The ground motions that chosen for the structural analysis should be as reflective as possible for the seismic characteristics of the structures site the basic characteristics that used for the selection of the time-histories from PEER site which gives the ability to input these parameters in its search gate as well as other ones. The statistical analysis for Iraq seismicity reveals that 90.05% of events have magnitudes within the range (4−5.4), while 6.03% of the total events have magnitudes within the range (5.5−7.4). The contour map of the peak ground acceleration according to the PSHA (Probabilistic Seismic Hazard Assessment) study introduced by Onur et al.[11] is shown in Fig. (4.5). In south of Iraq, the PGA map shows that its value increases from 0.1g to more than 0.5g as the site varies towards the Iraq-Iran borderline. Therefore, the selected ground accelerations have PGAs within this range. The shear wave velocity (v_{s30}) for an area can be estimated depending on reported site investigations that performed for projects erected in it. In 2017, Mohammed Q. and Abdulrassol M.A.[54] evaluated the shear wave velocity for Iraq depending on the geotechnical reports of projects distributed as in Fig. (4.6). The main parameter used in the study is the standard penetration test (SPT) which can be used as an alternative parameter to classify sites instead of the shear wave velocity, as illustrated in Table (4.1). the study evaluated the shear wave velocity as ranging from 102 m/s to 627 m/s in South of Iraq and from 111 m/s to 420 m/s in the Eastern South. The low values of the ranges are for a soft clay soil which is obviously observed in Basra city.

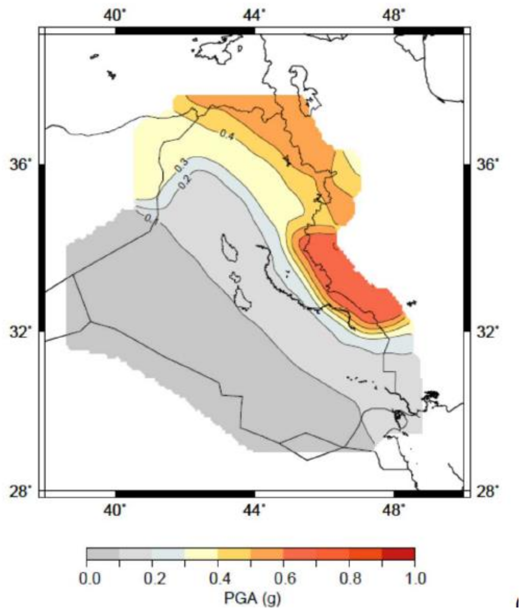

Figure (4.5) Peak Ground Acceleration Map for Iraq [11].

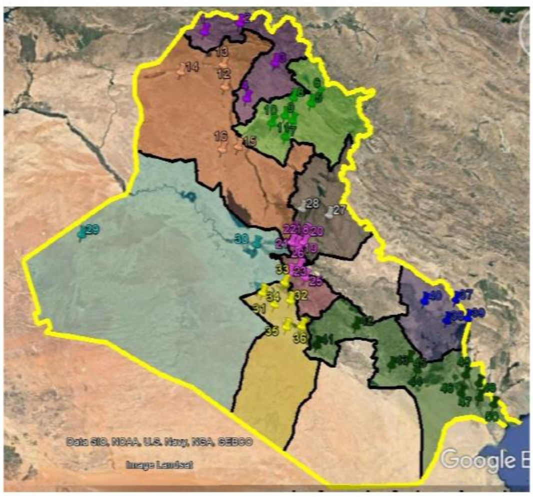

Figure (4.6) Distribution of projects used by Mohammed and Abdulrassol [54] .

Table (4.1) Site classification [55].

<table>
<tr><th>Site class</th><th>Type of soil profile</th><th>V_{s30} (m/s)</th><th>SPT, N or Nch</th><th>Undrained shear strength S_u (KPa)</th></tr>
<tr><td>A</td><td>Hard rock</td><td>>1500</td><td>NA</td><td>NA</td></tr>
<tr><td>B</td><td>Rock</td><td>760−1500</td><td>NA</td><td>NA</td></tr>
<tr><td>C</td><td>Soft rock or highly dense soil</td><td>370−760</td><td>>50</td><td>>100</td></tr>
<tr><td>D</td><td>Stiff soil</td><td>180−370</td><td>15−50</td><td>50−100</td></tr>
<tr><td rowspan="2">E</td><td rowspan="2">Soft clay</td><td><180</td><td><15</td><td><50</td></tr>
<tr><td colspan="3">Any soil profile with more than 3m depth having the following properties:
- PI (plasticity index) > 20
- Moisture content (w)$\geq$ 40%
- $S_u < 25$ KPa</td></tr>
<tr><td>F</td><td>Soils require response analysis</td><td colspan="3">- Soils that vulnerable to failure or collapse under seismic loads such as liquefiable soils.
- Highly organic clay.
- Clayey soils having very high plasticity.</td></tr>
</table>

4.12 Seismosignal Software

The accelerograms that recorded by the strong motion stations can be integrated to obtain the time histories of both ground velocity (from single integration) and ground displacement (from double integration). Seismosignal software is used for this purpose. The program has the ability to perform filtration and baseline correction for the row data. Appendix (A) explains the basic steps for using the program.

4.13 Micro-modeling of The Prism Test

This study has adopted macro-modeling for masonry models. In addition, a micro-model has been implemented for the masonry prism test that carried out in the experimental part of the study. The prism test was also simulated with the macro-modeling to compare the results of each modeling approach to the experimental results and also to compare between the results of the two methods themselves. The micro-modeling requires the simulation of contact state which causes high nonlinearity and becomes tedious for relatively large models.

4.14 Contact Problems

ANSYS provides different types of contacts to define the interaction between the distinct components of the model; volume to volume, surface to surface, and node to node contact pairs are provided. To simulate the contact between two surfaces of two bodies, at least one of the two bodies should be already meshed. One of the two surfaces is considered as a target surface, while the other is considered as a contact surface. The contact surface can move on the target one. If rigid-flexible contact status is made the contact surface is associated to the deformable body, while the target surface should be the surface of the rigid one. When flexible-flexible contact is simulated, both bodies are deformable. The target surface and the contact surface form together what is known as contact pair. In this study, Appendix (B) gives the steps of how to create a contact pair between two surfaces.

4.15 ANSYS Simulation of CM Models

The simulation of CM models includes the simulation of confining reinforced concrete members (tie-columns and beams). Solid65 element has been used to simulate both masonry and concrete, while beam element (2-node 188 beam element) which is capable of resisting only tensile stresses has been used for steel reinforcements of tie columns. Linear properties as well as yield stress were defined for the beam element. The concrete-masonry contact has been taken as tied since the two distinct materials have been modeled by meshing the divisions of one volume.

4.16 Retrofitting Simulation

The study has simulated a classical retrofitting technique for the URM buildings. It can be used for both existing and future buildings. The simulated retrofitting technique is similar to that proposed by Costa[30] which is the use of plaster layers reinforced with steel mesh. The simulated steel meshes are with openings (150*150) mm, 6 mm wire diameter, and yield stress (F_y=300 MPa). Beam element (2-node 188 beam element) is used to simulate the B.R.C, and Solid65 element is used for masonry and plaster layers. The smeared reinforcement is used for the modeling of steel mesh in some studied models. Nonlinear static analysis for out-of-plane and in-plane loaded wall models is carried out with and without retrofitting to evaluate the structural improvement provided by the retrofitting. Also a nonlinear time-history analysis is performed for retrofitted single room to study the retrofitting effects on the seismic performance

Chapter Five

FE Simulations, Results, and Discussions

CAHPTER FIVE

FE SIMULATIONS, RESULTS, And DISCUSSIONS

5.1 Introduction

Firstly, This chapter deals with some verification models to compare the results of the analyses to the experimental results in order to verify the acceptance of ANSYS simulations carried out in the study for other models. Two walls that experimentally studied have been simulated for the verification purpose. Also for the same purpose, the prism test implemented in the study has been simulated with both micro-modeling and macro-modeling. The results of the prism micro-model has been compared to both experimental and macro-model results. Then, different seismic waves are subjected to the masonry models to determine their nonlinear seismic response. Finally, the strength enhancement of the masonry walls retrofitted with reinforced plaster has been investigated.

5.2 Verification Model No.1

The URM wall tested by Naseer A.[27] has been simulated and analyzed to verify ANSYS results. The geometry and mechanical properties are mentioned in Chapter (2) from the study. The finite element model, which is meshed with 40 mm size of the element, is shown in Fig. (5.1).

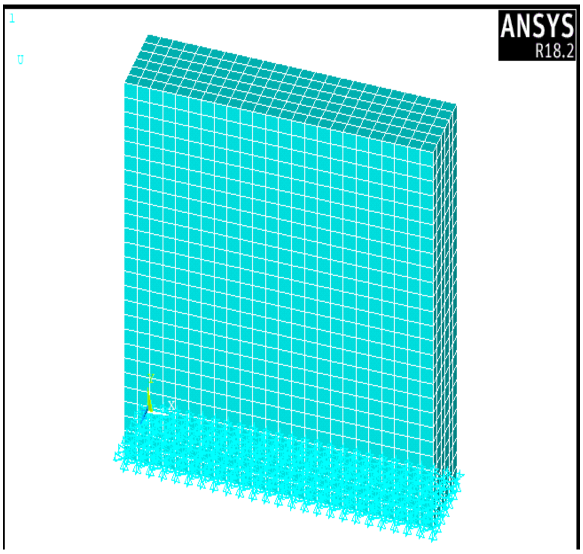

Figure (5.1) FE model for the wall tested by Naseer.

The experimental load-displacement relationship is as shown in Chapter (2). The ANSYS curve for load-displacement relationship is shown in Fig. (5.2) with the experimental and the idealized ones.

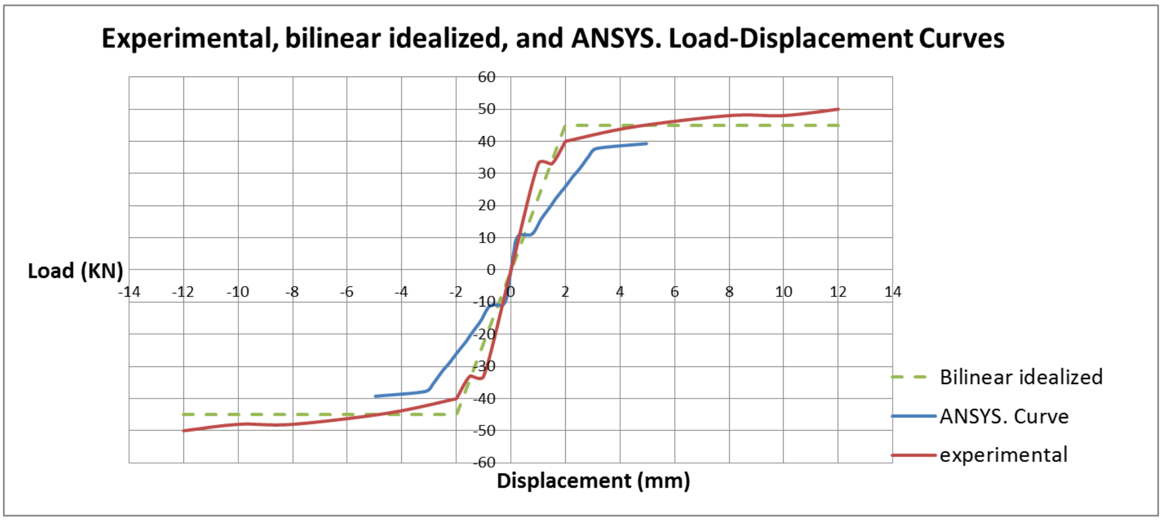

Figure (5.2) Experimental and numerical load-displacement relationships for the wall tested by Naseer.

The ultimate displacement in x-direction (u_x) is shown in Fig. (5.3) as follow:

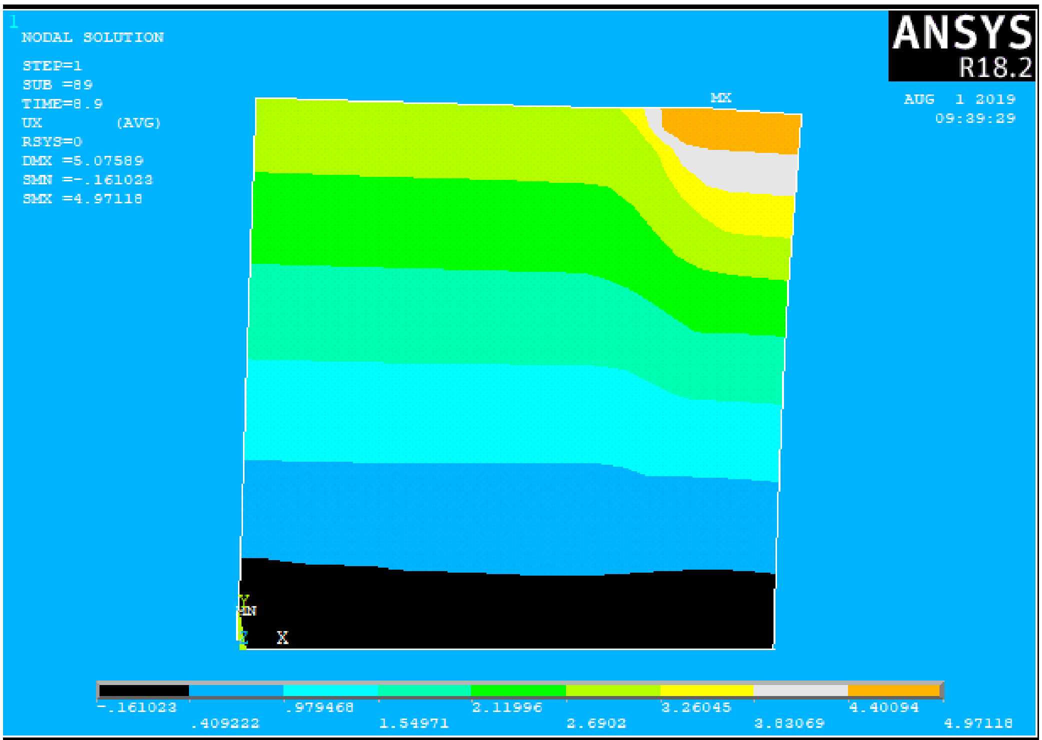

Figure (5.3) Displacement in x-direction for verification model No.1 (mm).

The numerical model exhibited less ductility compared to the experimental behavior because the numerical solution terminates due to convergence problems. The aspect ratio of the wall is approximately equal to 1, which means that both slide shear and flexural strengths are predominant according to MSJC code as illustrated in Fig. (5.4-b).

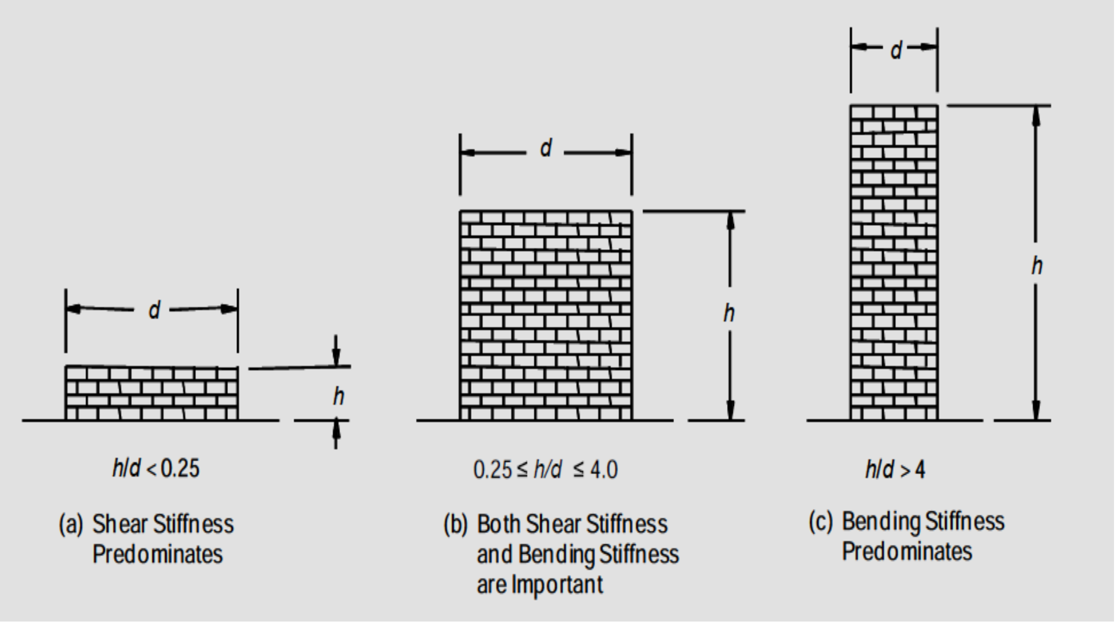

Figure (5.4) Aspect ratio and predominant stiffness of masonry walls according to MSJC code[43].

The crack pattern and the 3rd principal stress are shown in Figure (5.5) and (5.6), respectively. The two figures denote the effects of shear and flexural stiffnesses in the ANSYS mode failure.

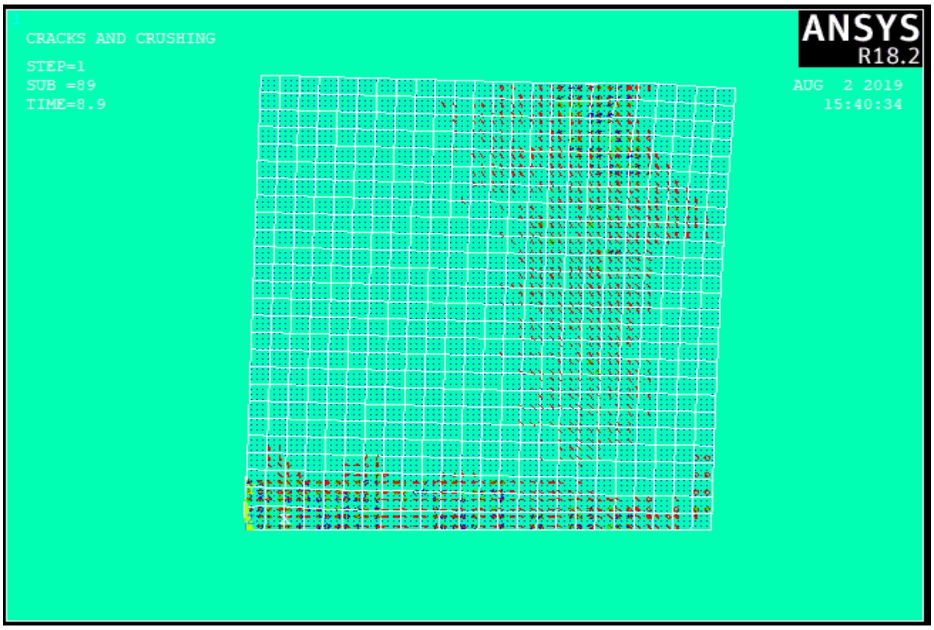

Figure (5.5) Crack pattern for FE model of the wall tested by Naseer.

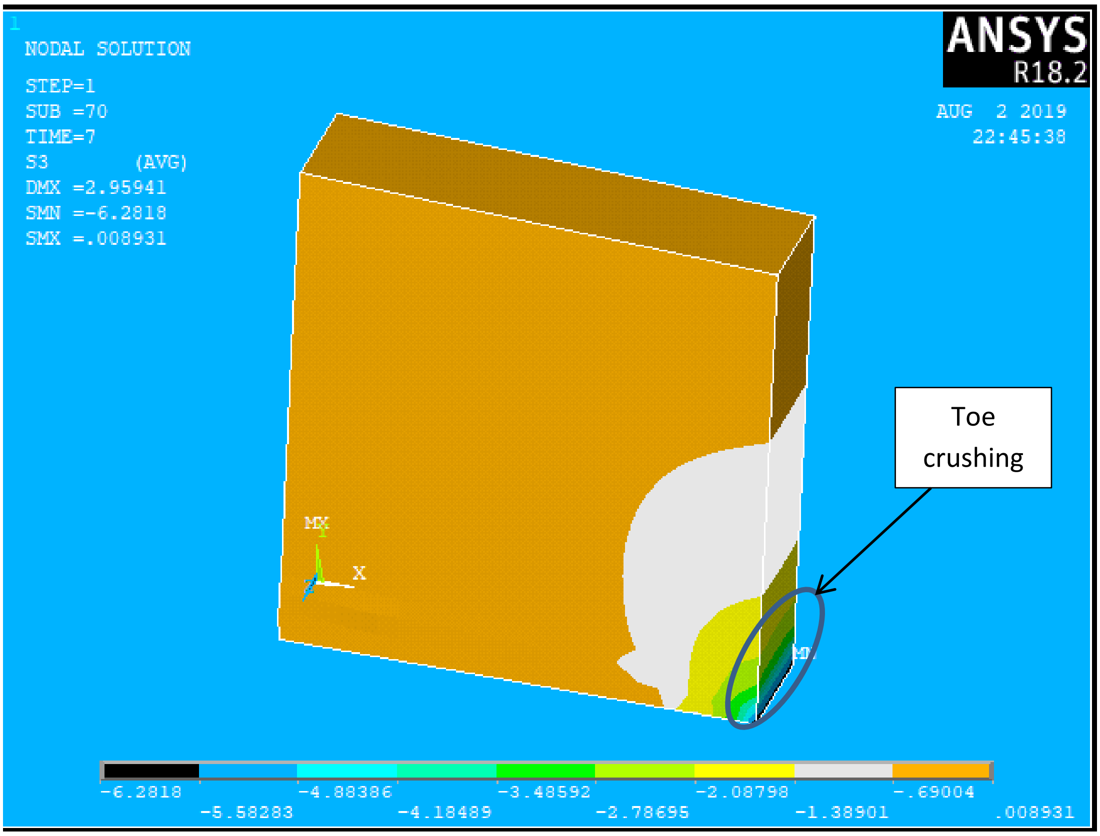

Figure (5.6) 3rd principal stress in the model of the wall tested by Naseer.

The crack propagation at the wall base along its length denotes sliding failure and the toe crushing denotes rocking failure . The two simultaneous effects mean that the wall fails in a hybrid failure mechanism. From Fig. (5.4), it can be observed that the aspect ratio of the studied wall is within the range of case (b). From Fig. (5.2), it can be observed that the experimental and numerical results are exactly the same up to slightly more than 10 KN. The comparison between the experimental and the numerical results reveals that the ANSYS simulation gives acceptable results.

5.3 Verification Model No. 2

The model is for Pier (F1) tested by Franklin et al.[21], whose details and loading are mentioned in Chapter (2) from this study. The experimental hysteresis and the bilinear idealized curves of load-displacement relationship are as shown in Chapter (2) in this study. A length of 100 mm has been used for the size of the element to mesh the FE model, which is shown in Fig. (5.7). The ultimate displacement in x-direction is shown in Fig. (5.8).

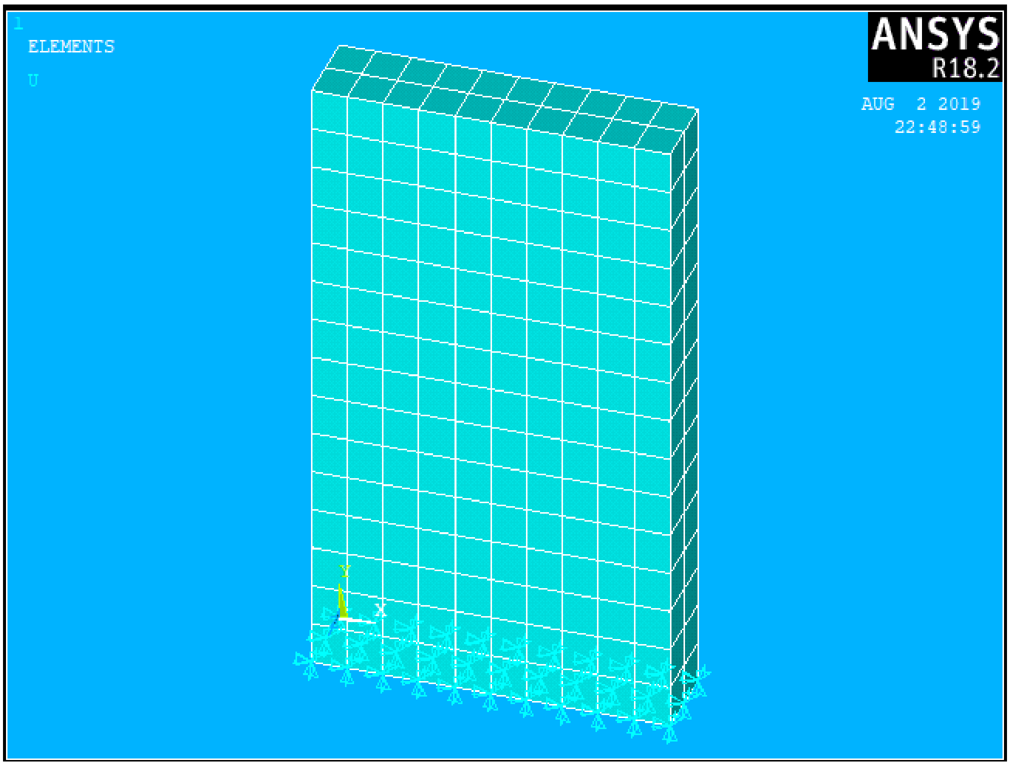

Figure (5.7) The FE model for Pier (F1) tested by Franklin.

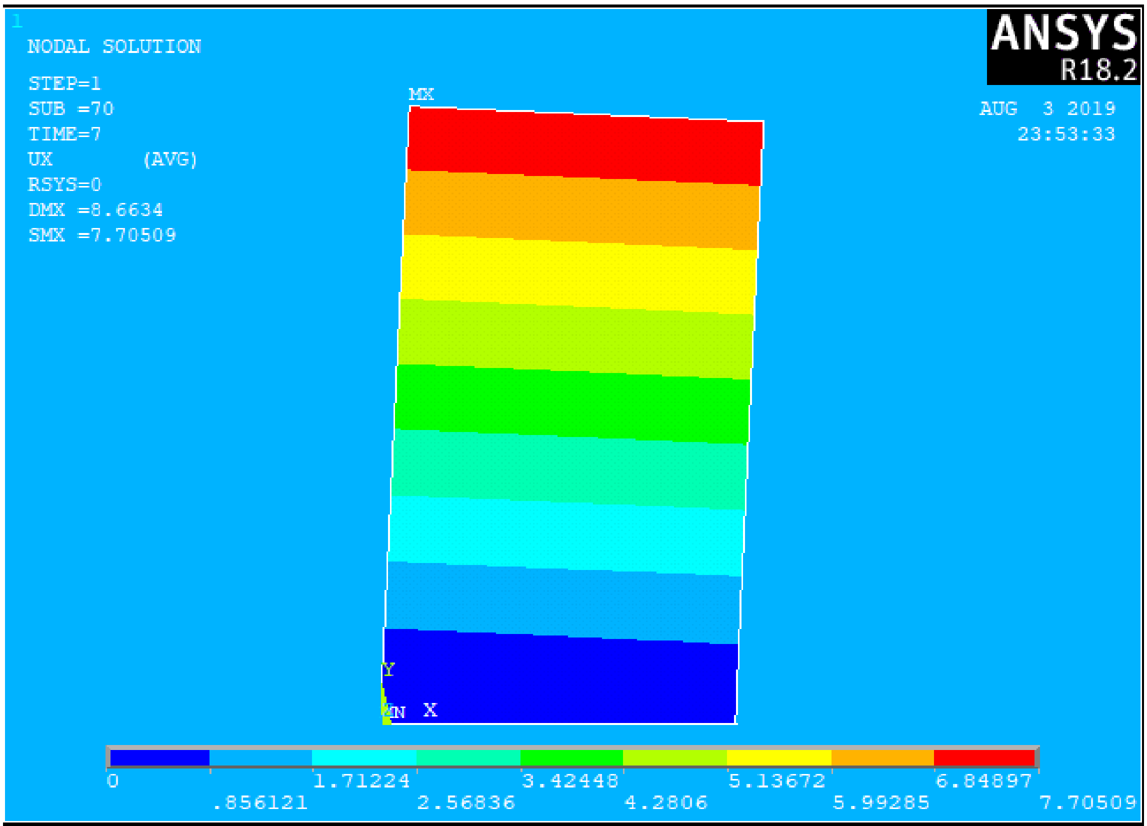

Figure (5.8) Displacement in x-direction for verification model No.2.

The load-displacement relationship obtained from ANSYS simulation is illustrated in Fig. (5.9) as follows:

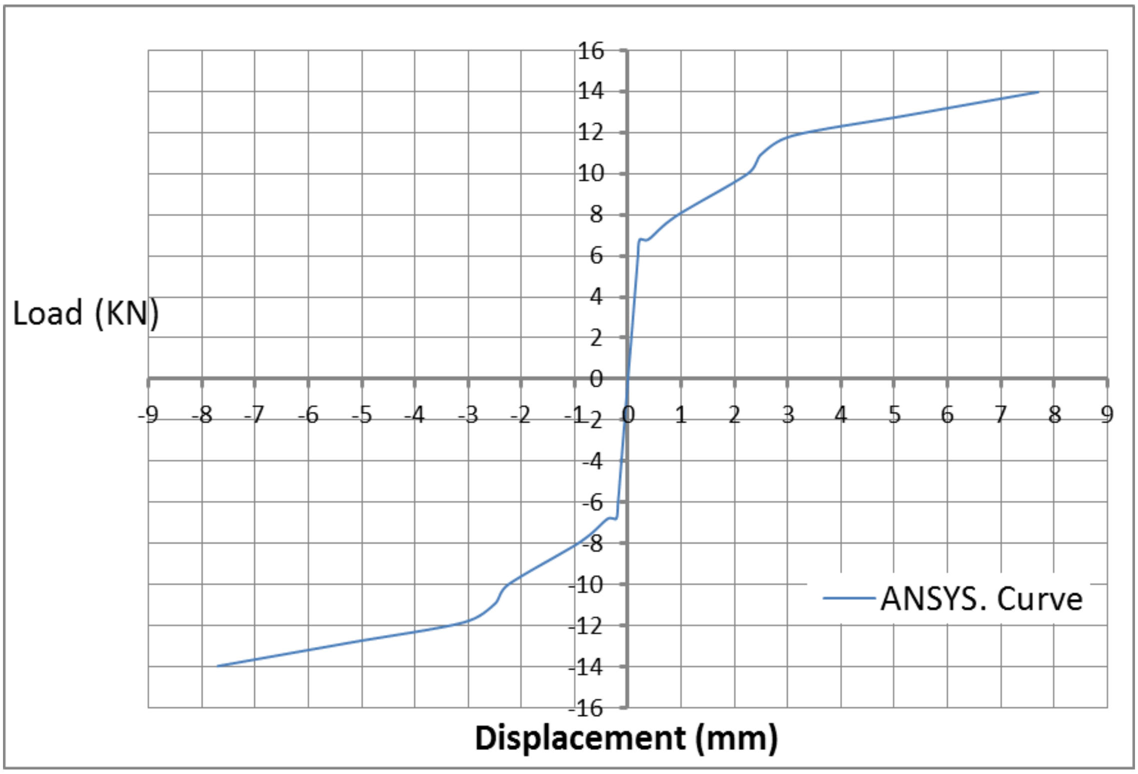

Figure (5.9) ANSYS load-displacement curve for Pier F1 tested by Franklin.

The comparison between Figures (5.9) and (2.2) reveals that the ultimate load obtained from ANSYS solution is the same as the experimental failure load. The crack pattern is as shown in Fig. (5.10).

Figure (5.10) Cracks in the FE model of Pier F1 tested by Franklin.

The initial experimental cracks at 0.1% drift and the rotation about toe at 2% draft are shown in Plates (5.1) and (5.2), respectively.

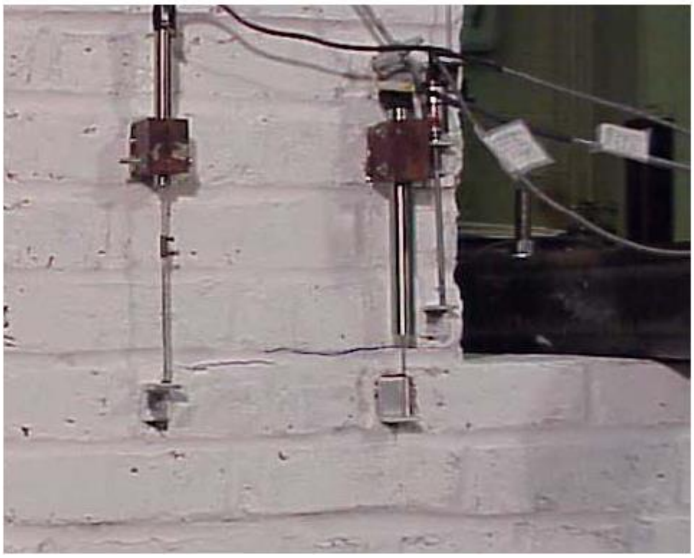

Plate (5.1) Initial cracks in Pier F1 at a 0.1% drift [21].

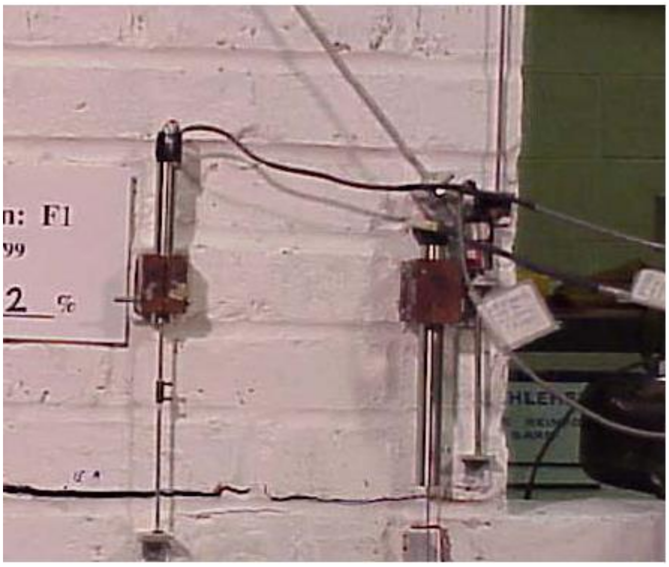

Plate (5.2) Rotation about toe in Pier F1 at 2% drift [21].

The comparison between Fig. (5.10) and Plates (5.1) and (5.2) reveals that the ANSYS simulation has well predicted the cracking pattern and failure mode. The 0.1% drift corresponds a displacement of 1.5 mm, which is relatively much less than 7.705 mm. This means that the numerical analysis went on beyond the point of initial cracking but for a limit less than the experimental one.

5.4 Verification Model No. 3

The prism test performed as a part of the current study has been simulated with a micro model as a verification for the aimed simulations, and also to compare its accuracy level to the macro-modeling results. The mechanical properties of the brick units and joint mortar are as in Table (5.1). The values of Poisson's ratio for both brick units and mortar are taken from previous studies[56]. The modulus of elasticity of bricks has been evaluated from Al-Chaar et al. study [42].

Table (5.1) Mechanical properties of bricks and mortar.

Property / Material	Modulus of elasticity (MPa)	Poisson's ratio	Compressive strength (MPa)	Tensile strength (MPa)
Brick units	2500	0.23	9	1.17
Mortar	10000	0.16	18	3.2

The FE model shown in Fig. (5.11) is built up of 9 volumes meshed and then constructed with surface-to-surface contact pairs. The joint mortar has a height of 10 mm. The mesh was fined to obtain the more accurate solution; the edge length was set to be 10 mm for the elements.

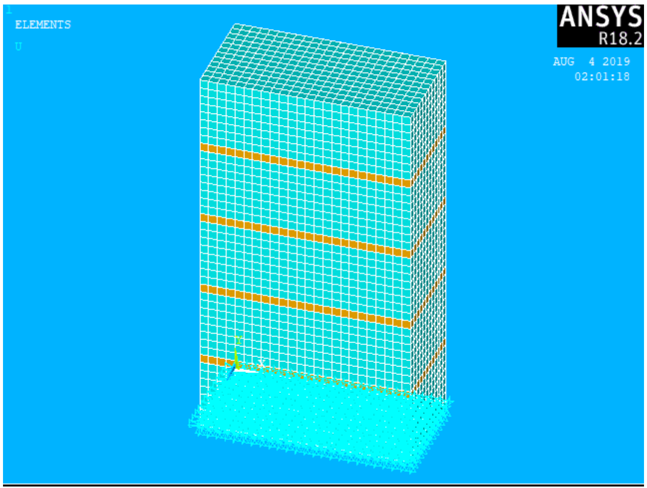

Figure (5.11) FE micro model for masonry prism.

The compressive load was applied in form of a pressure of 10 MPa at the prism top area. The time of solution was set as 10 with 100 time steps. Consequently, the ultimate load is the same as the time value at the time step that proceeds the time at which the solution terminates when it does not converge. The solution terminated at time 5.5 which means that the ultimate compressive strength from ANSYS solution is 5.4 MPa. Also it can be found from the value of the reaction in y-direction shown in Fig. (5.12) by the division of this value by the plan area of the prism as in Eq. (5.1).

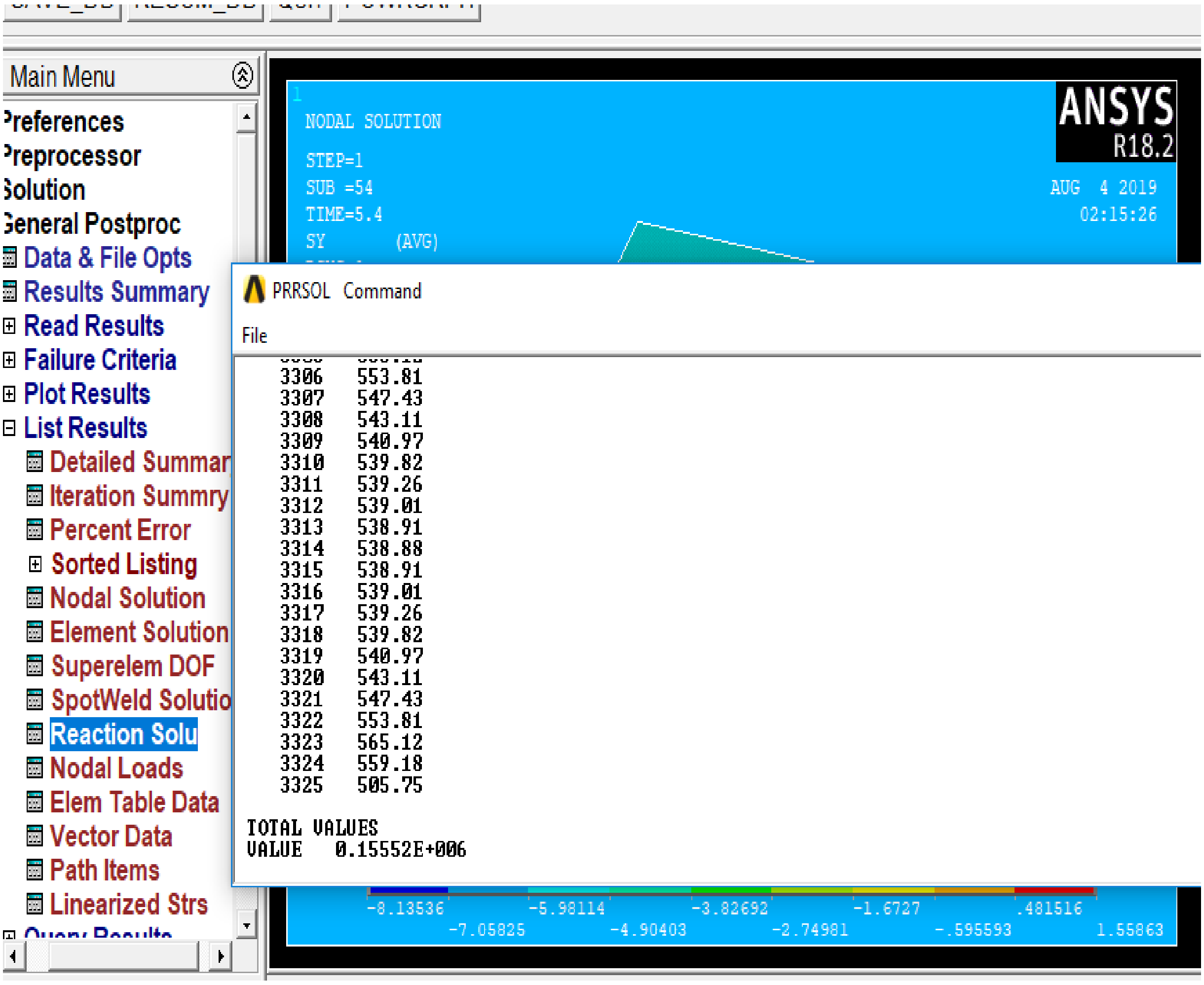

Figure (5.12) Reaction in y-direction in prism micro model.

$$f_{\acute{m}} = \frac{0.15552*10^6}{120*240} = 5.388 \approx 5.39 \text{ MPa} \tag{5.1}$$

The stress in y-direction (σ_y) is shown in Fig. (5.13), and the crack pattern is shown in Fig. (5.14). As mentioned in Chapter 3, the difference in stiffness and Poisson's ratio between bricks and joint mortar cause shear stresses and initiate failure state, and the bed joint mortar is stretched laterally if the bricks tend to expand laterally more than the mortar. This behavior has been demonstrated by the ANSYS simulation as shown in Figures (5.15) and (5.16).

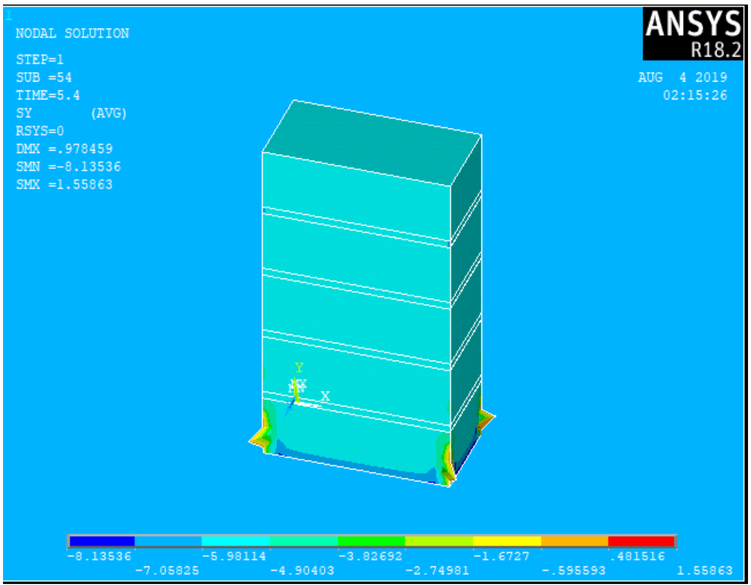

Figure (5.13) The stress in y-direction (σ_y) (micro model).

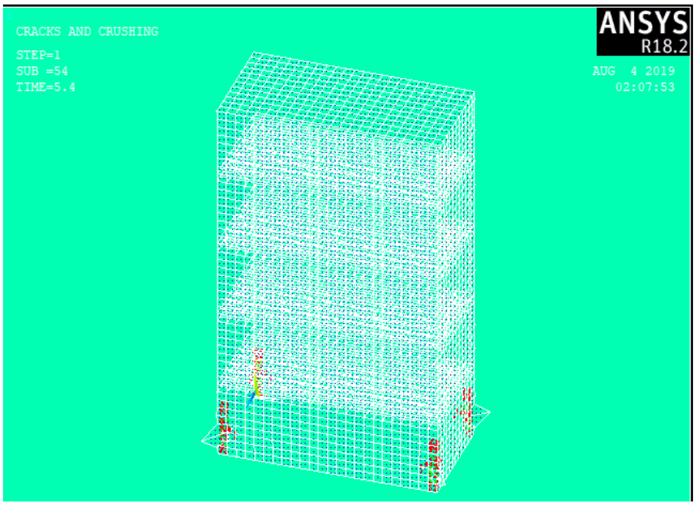

Figure (5.14) Crack pattern in prism failure state (micro model).

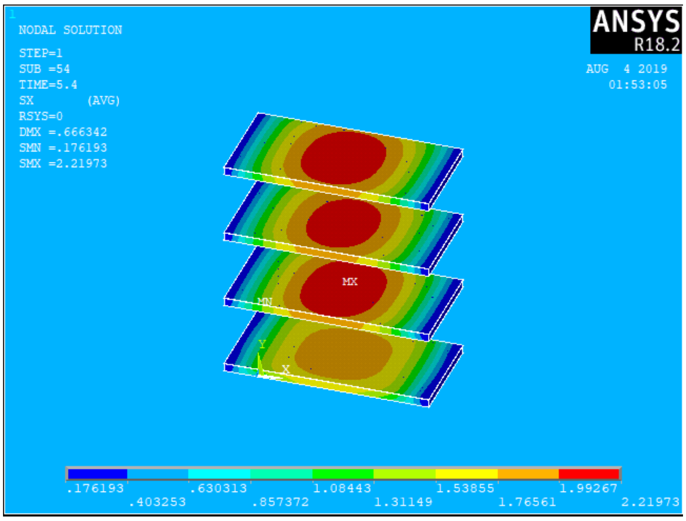

Figure (5.15) Stress in x-direction (σ_x) in joint mortar (MPa).

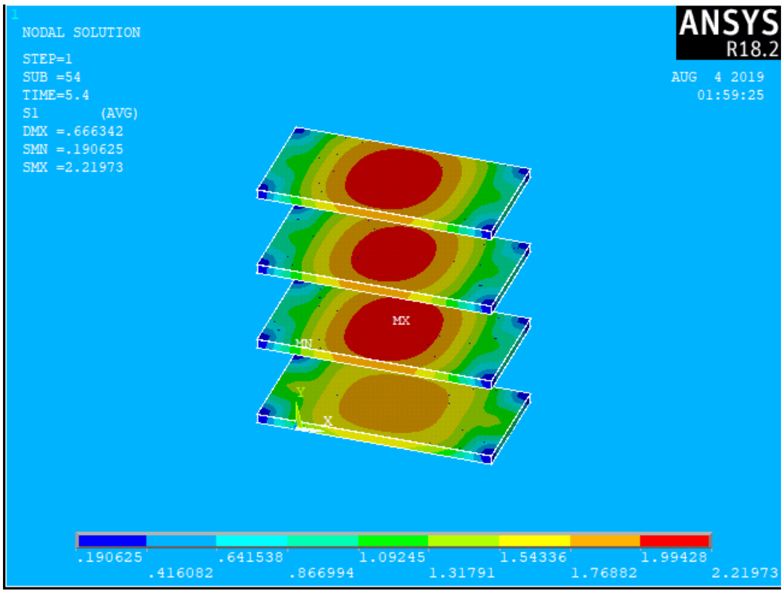

Figure (5.16) 1st principal stress in bed joint mortar (MPa).

5.5 Verification model No.4

The prism test has been simulated with a macro model having mechanical properties as given in Table (5.2), and an idealized stress-strain curve shown in Fig. (5.17). The edge length of the element was set to be 20 mm.

Table (5.2) Mechanical properties of masonry

$f_{\acute{m}}$ (MPa)	f_t (MPa)	$E_{\acute{m}}$ (MPa)	Poisson's ratio
5.5	0.15	2750	0.2

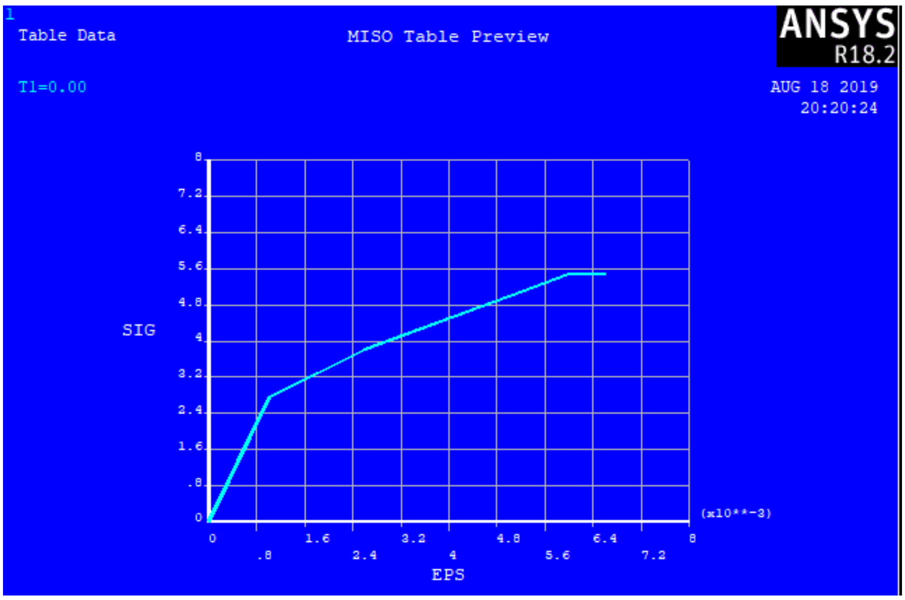

Figure (5.17) Masonry multi-linear stress-strain curve.

The applied pressure, solution time, and number of substeps were set to be 10 MPa, 10, and 100, respectively. The solution did not converge and terminated at time 4.7 which means that the last converged solution is at an axial load of 4.6 MPa. The cracked model is shown in Fig. (5.18).

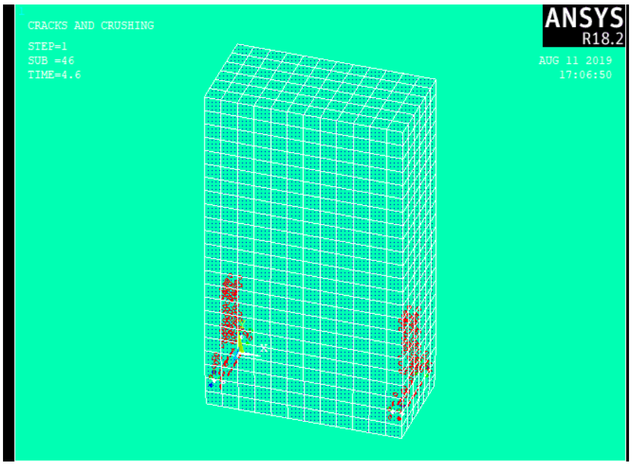

Figure (5.18) Cracks in the macro model of prism test.

The stress in y-direction are shown in Fig. (5.19) that follows:

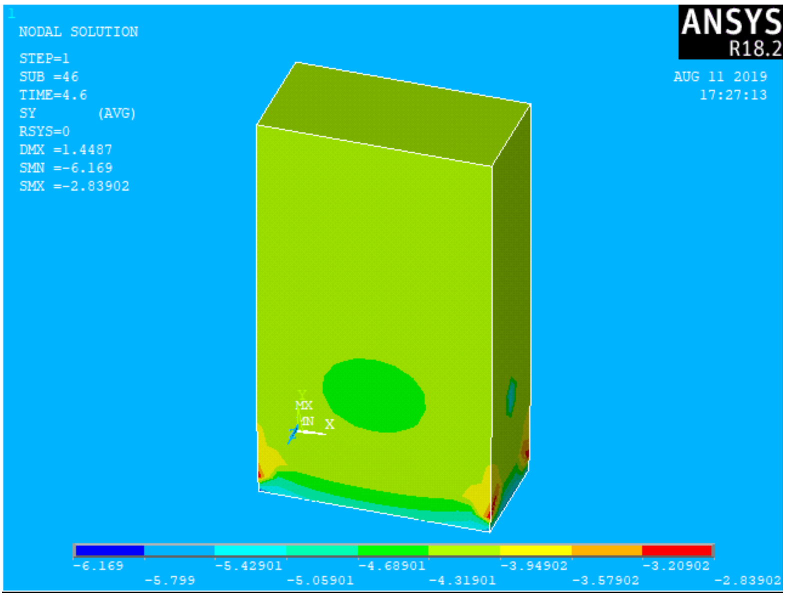

Figure (5.19) Stress in y-direction (σ_y) for macro model (MPa).

The result of the simulation with micro-modeling, which is 5,39 MPa, is very close to the experimental result which is 5.5 MPa. This reveals the acceptance of ANSYS simulations performed in this study. The comparison between the results of micro- and macro-modeling reveals that micro-modeling is conservative when the simulated structure fails under compressive stresses.

5.6 Boundary Conditions

All models analyzed in the study are fixed at the bottom. For models that statically analyzed, the fixed support is simulated by applying zero displacement for the base of the model. The models analyzed under the seismic loading are assumed in full integrity with the soil at their bases since the soil-structure interaction is out of the objectives of the study. This implies that the supports are fixed to the sub-ground and move the same as the ground motion during earthquakes.

5.7 Model No. 1

The model is a one-storey, single room with a plan shown in Fig. (5.20) and a clear height of 3 m. It has two openings: the (1*2.1) m door and the (1*1.5) window. The slab is concrete with 0.2 m thickness. The wall thickness is 0.24 m. The lintels over openings are concrete. The coordinate system in Fig. (5.20) is the same as the global coordinate system in the program in which the y-axis is perpendicular to the paper (parallel to the room height). The FE model is shown in Fig. (5.21). The edge length of the element was set to be 100 mm. Thus, the model is built up of 16164 elements with 22548 nodes.

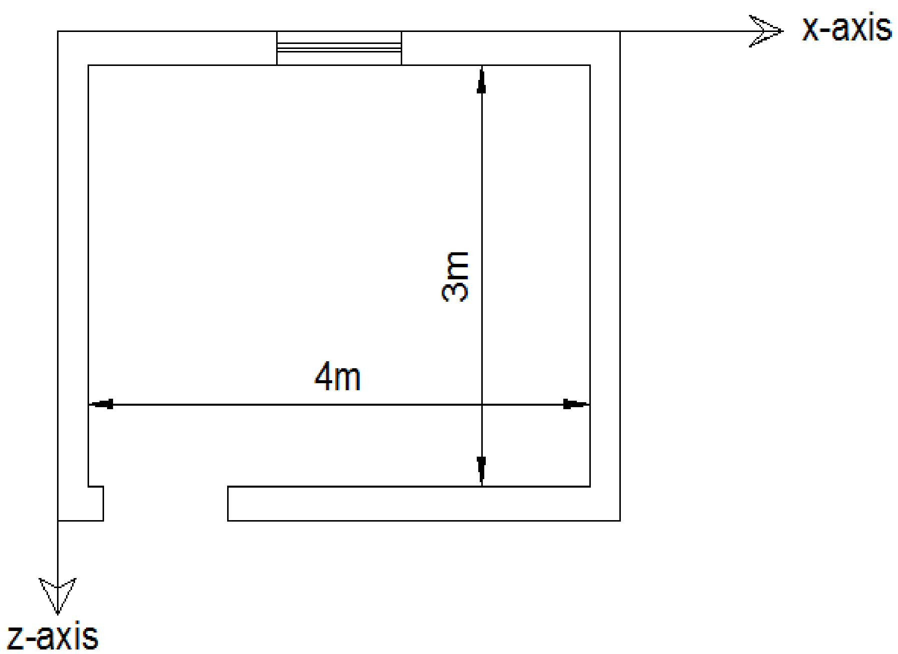

Figure (5.20) Single room plan.

The first three modes of the model are shown in Figures (5.22) to (5.24). It is important to note that the natural frequency calculated in ANSYS is in units of Hertz (cycle per second), and it is not the circular frequency as can be observed in Fig. (5.25) and also known by the natural periods in Fig. (5.26).

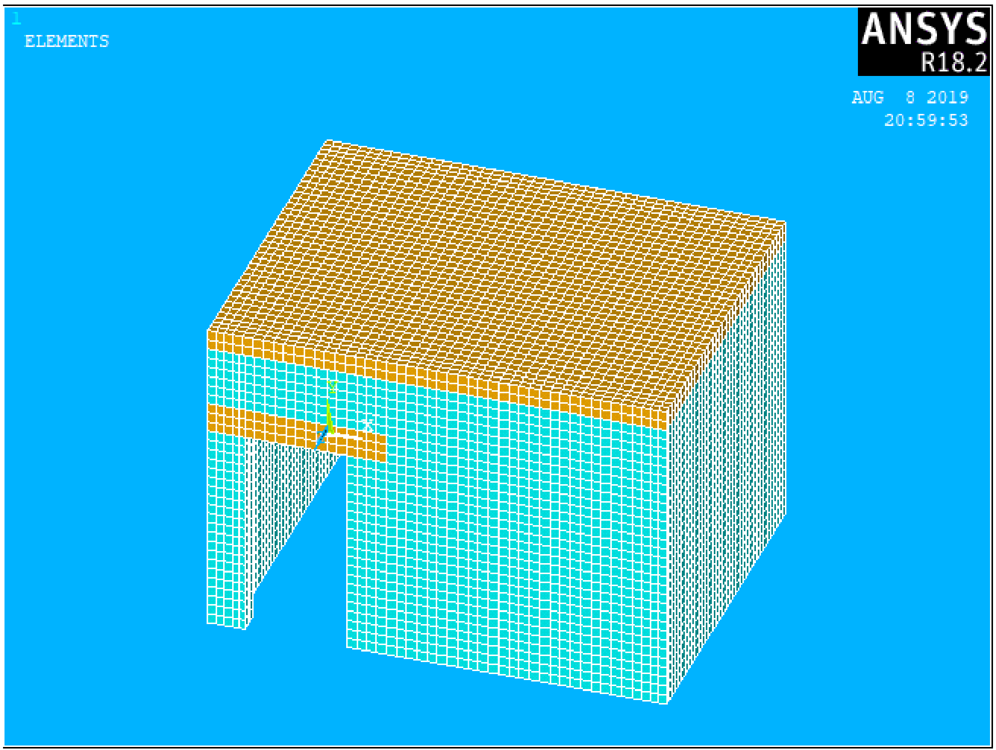

Figure (5.21) FE model No.1.

The characteristics of the seismic records applied to the model are as in Table (5.3) that follows:

Table (5.3) Description of the seismic records applied to model No.1.

Earthquake name	Station name	Date	Magnitude M_w	PGA g	V_{s30} m/s
Northwest California	Ferndale city hall	12/9/1938	5.5	0.15	219.31

The time-histories of the three components of ground acceleration, velocity, and displacement for the earthquake mentioned above are shown in Figures (5.27) to (5.35). The horizontal-1 components of both ground velocity and displacement were applied in z-direction, while horizontal-2 components were applied in x-direction. Of course, the vertical components were applied in y-direction. The solution did not converge and terminated at time 0.7 second.

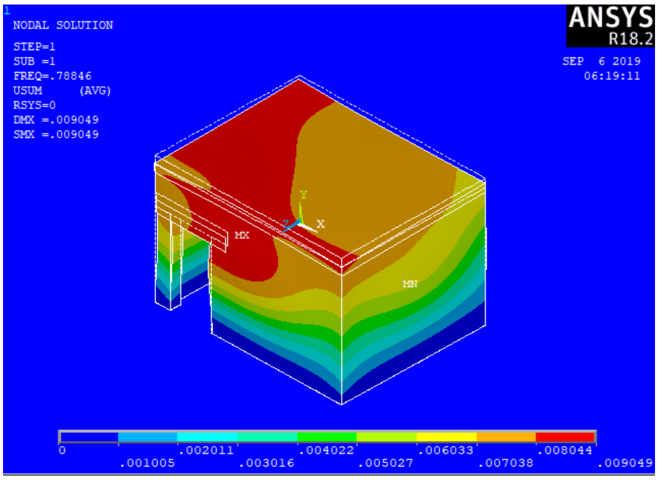

Figure (5.22) 1st mode of Model No.1.

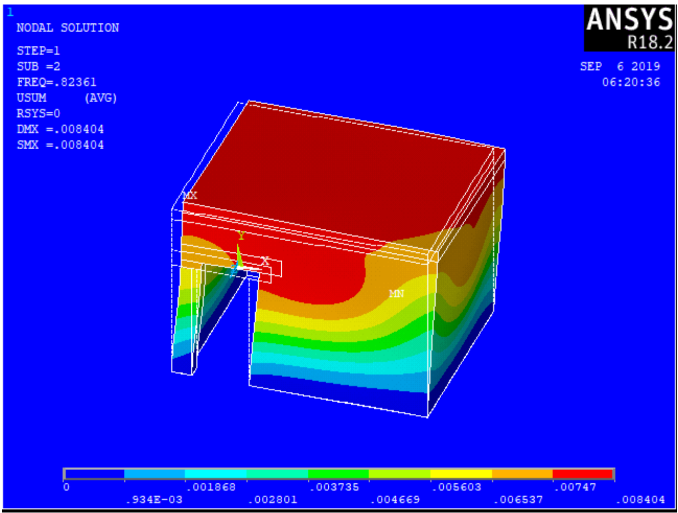

Figure (5.23) 2nd mode of Model No.1.

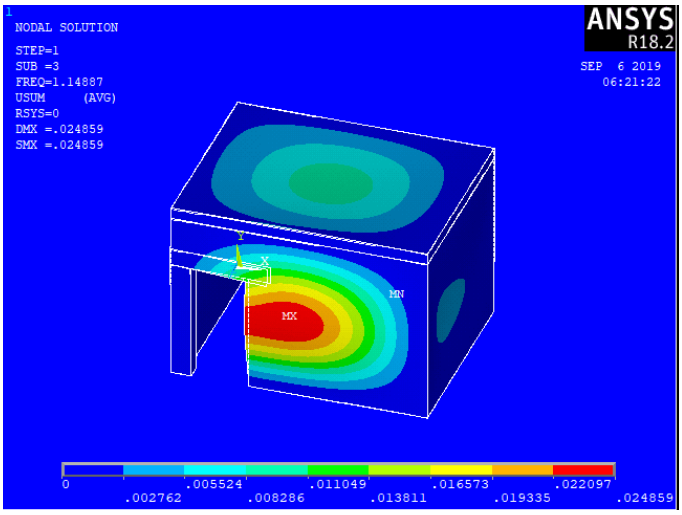

Figure (5.24) 3rd mode of Model No.1.

Mechanical APDL 18.2 Output Window

```
*** FREQUENCIES FROM BLOCK LANCZOS ITERATION ***

 MODE     FREQUENCY (HERTZ)

   1       0.7884597013942
   2       0.8236099067454
   3        1.148868752397
```

Figure (5.25) The first three natural frequencies of Model No.1.

Mechanical APDL 18.2 Output Window

***** PARTICIPATION FACTOR CALCULATION ***** X DIRECTION

MODE	FREQUENCY	PERIOD	PARTIC.FACTOR	RATIO	EFFECTIVE MASS	CUMULATIVE MASS FRACTION	RATIO EFF.MASS TO TOTAL MASS
1	0.788460	1.2683	96.283	0.922188	9270.49	0.459446	0.364061
2	0.823610	1.2142	104.41	1.000000	10900.9	0.999697	0.428090
3	1.14887	0.87042	2.4725	0.023681	6.11334	1.00000	0.240077E-03
sum					20177.5		0.792392

***** PARTICIPATION FACTOR CALCULATION ***** Y DIRECTION

MODE	FREQUENCY	PERIOD	PARTIC.FACTOR	RATIO	EFFECTIVE MASS	CUMULATIVE MASS FRACTION	RATIO EFF.MASS TO TOTAL MASS
1	0.788460	1.2683	1.8824	0.055447	3.54335	0.303258E-02	0.139151E-03
2	0.823610	1.2142	3.5126	0.103465	12.3381	0.135922E-01	0.484530E-03
3	1.14887	0.87042	-33.949	1.000000	1152.55	1.00000	0.452617E-01
sum					1168.43		0.458854E-01

***** PARTICIPATION FACTOR CALCULATION ***** Z DIRECTION

MODE	FREQUENCY	PERIOD	PARTIC.FACTOR	RATIO	EFFECTIVE MASS	CUMULATIVE MASS FRACTION	RATIO EFF.MASS TO TOTAL MASS
1	0.788460	1.2683	102.84	1.000000	10575.2	0.539859	0.415299
2	0.823610	1.2142	-94.887	0.922703	9003.53	0.999484	0.353577
3	1.14887	0.87042	-3.1793	0.030916	10.1080	1.00000	0.396952E-03
sum					19588.9		0.769273

Figure (5.26) ANSYS report for modal analysis of Model No.1.

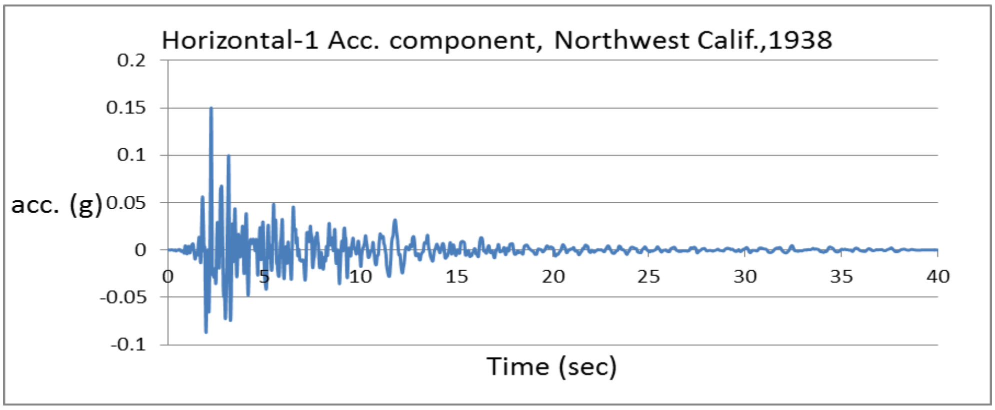

Figure (5.27) Horizontal-1 component of $\ddot{u}_g$ of Northwest Calif., 1938 event.

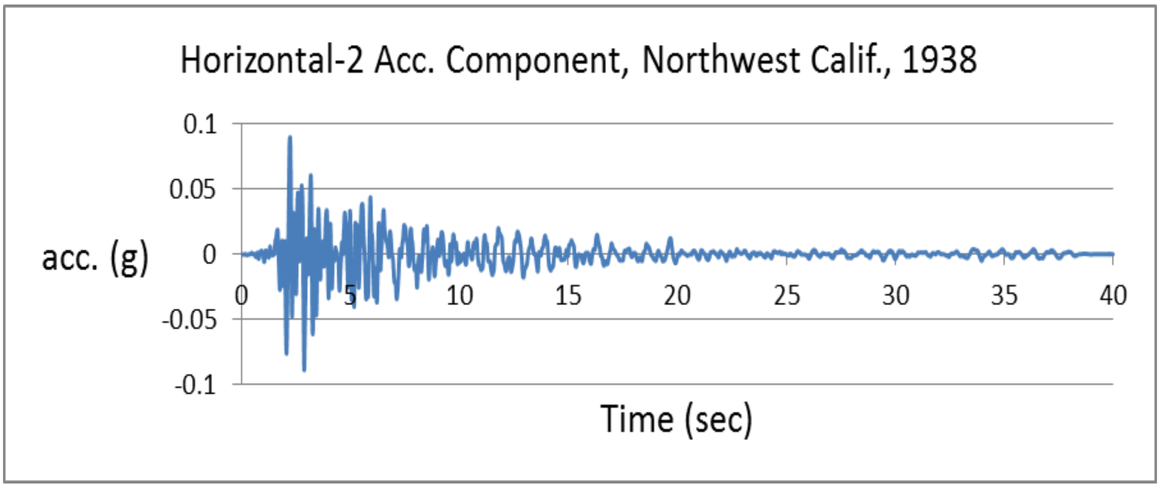

Figure (5.28) Horizontal-2 component of $\ddot{u}_g$ of Northwest Calif., 1938 event.

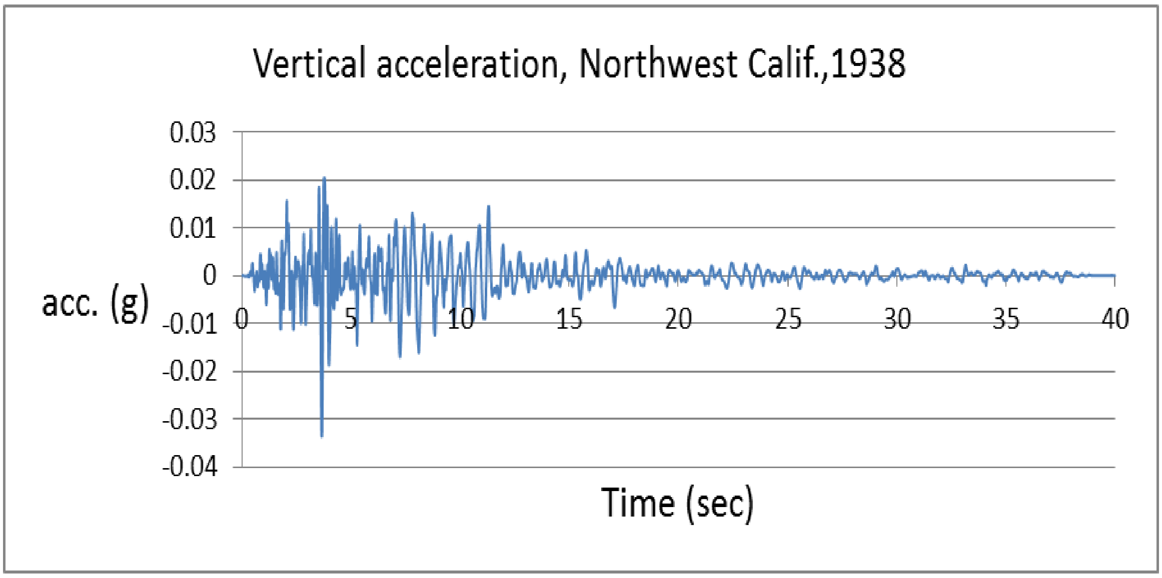

Figure (5.29) Vertical component of $\ddot{u}_g$of Northwest Calif., 1938 event.

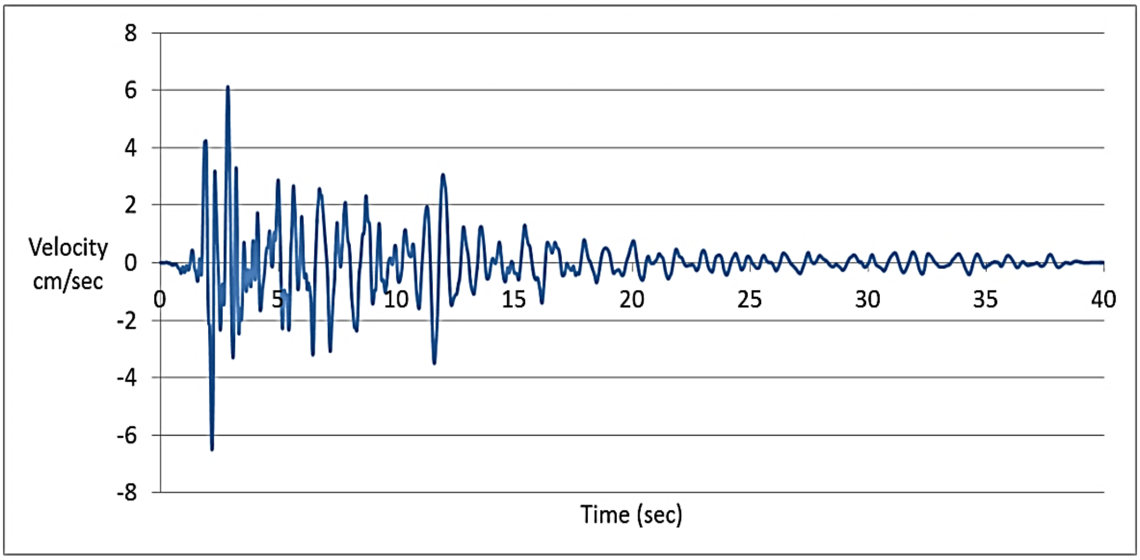

Figure (5.30) Horizontal-1 component of $\dot{u}_g$ of Northwest Calif., 1938 event.

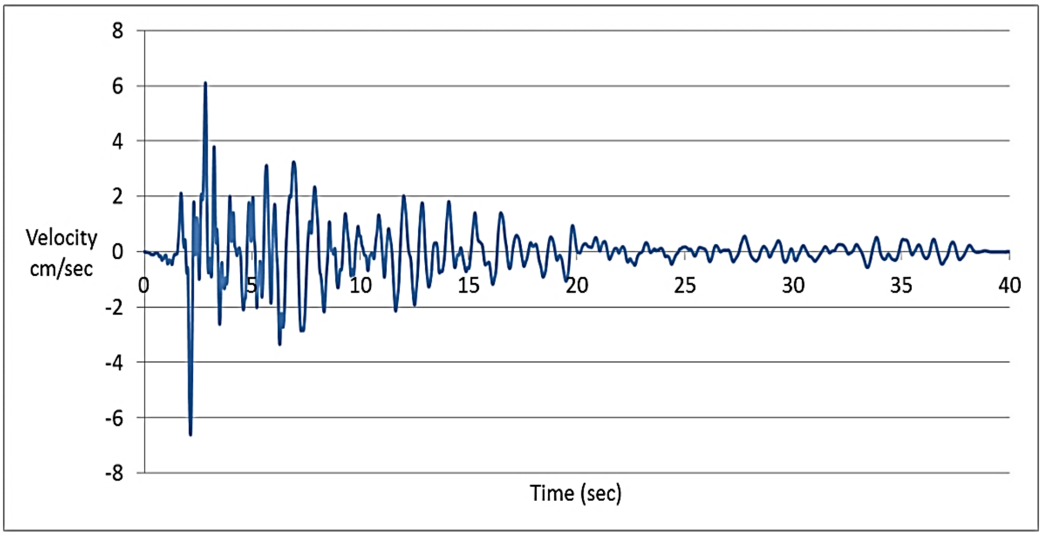

Figure (5.31) Horizontal-2 component of $\dot{u}_g$ of Northwest Calif., 1938 event.

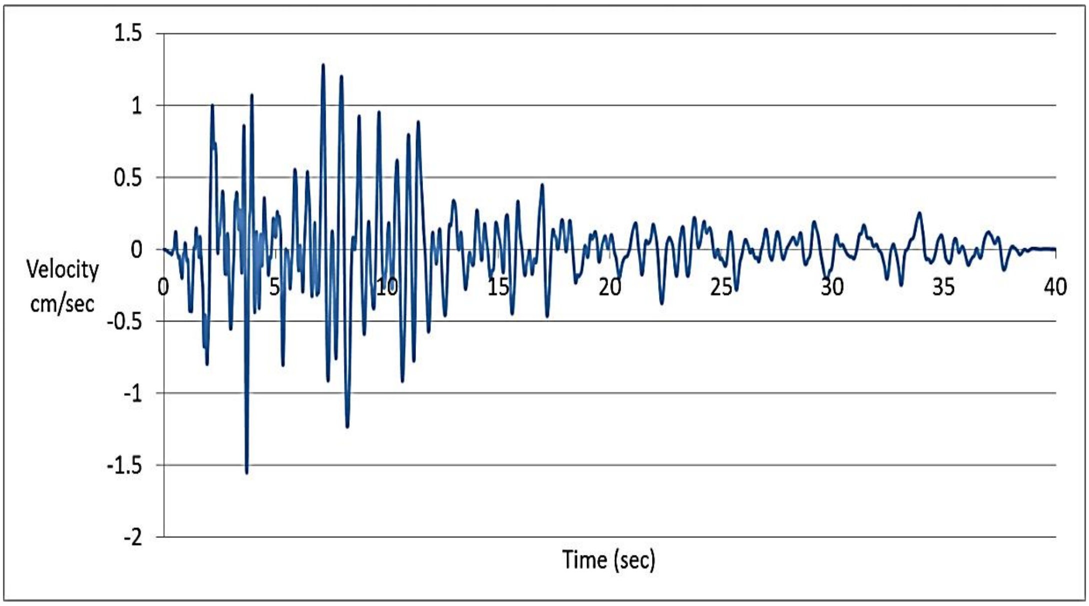

Figure (5.32) Vertical component of $\dot{u}_g$ of Northwest Calif., 1938 event.

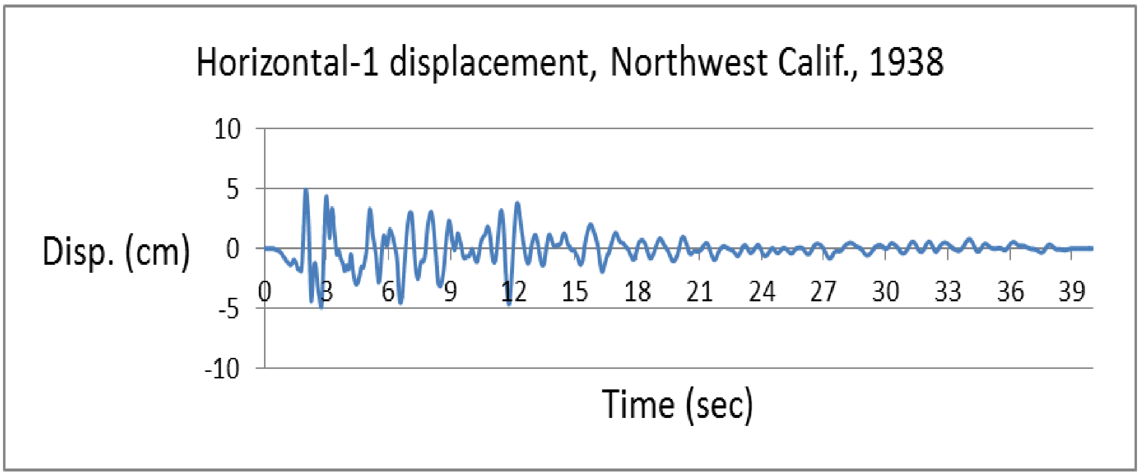

Figure (5.33) Horizontal-1 component of u_g of Northwest Calif., 1938 event.

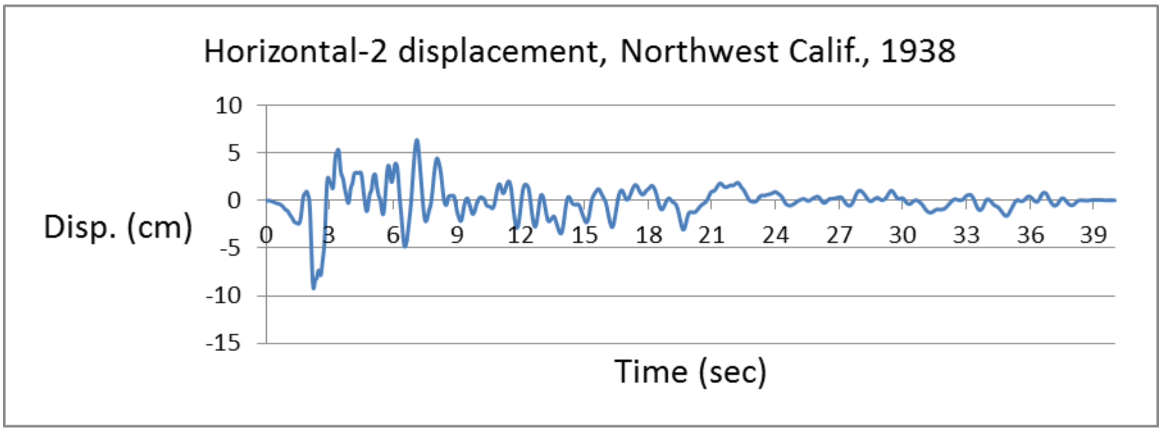

Figure (5.34) Horizontal-2 component of u_g of Northwest Calif., 1938 event.

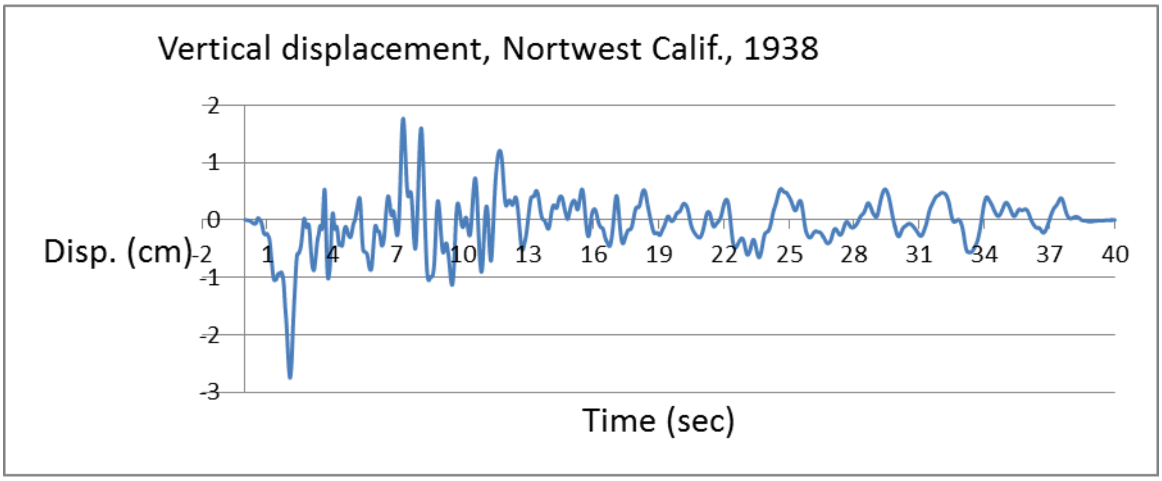

Figure (5.35) Vertical component of u_g of Northwest Calif., 1938 event.

The displacements u_z^t at base and roof levels are shown in Figures (5.36), and Fig. (5.37), respectively.

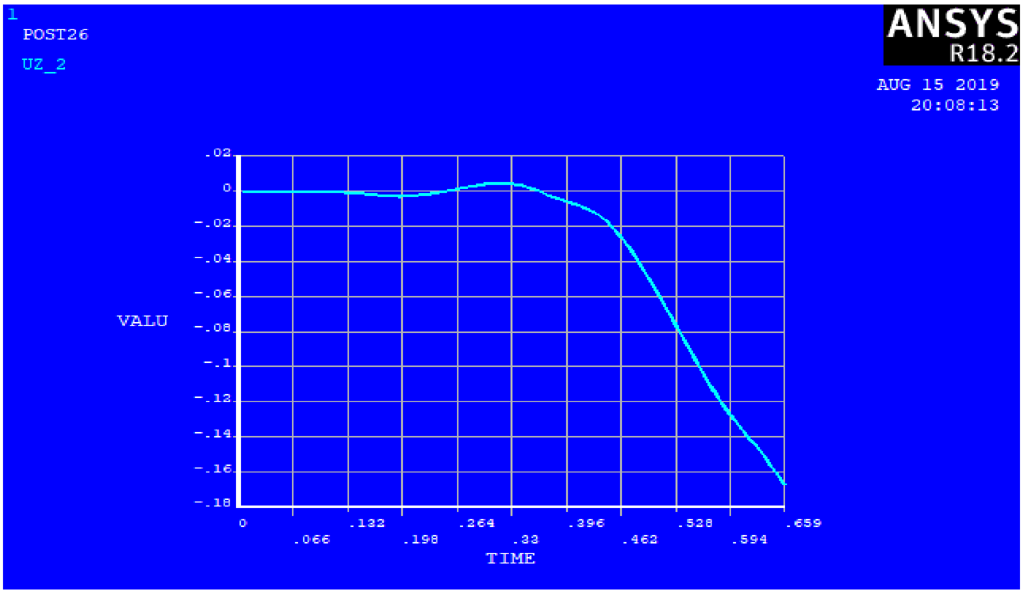

Figure (5.36) u_z^t at base level of Model No. 1 (mm).

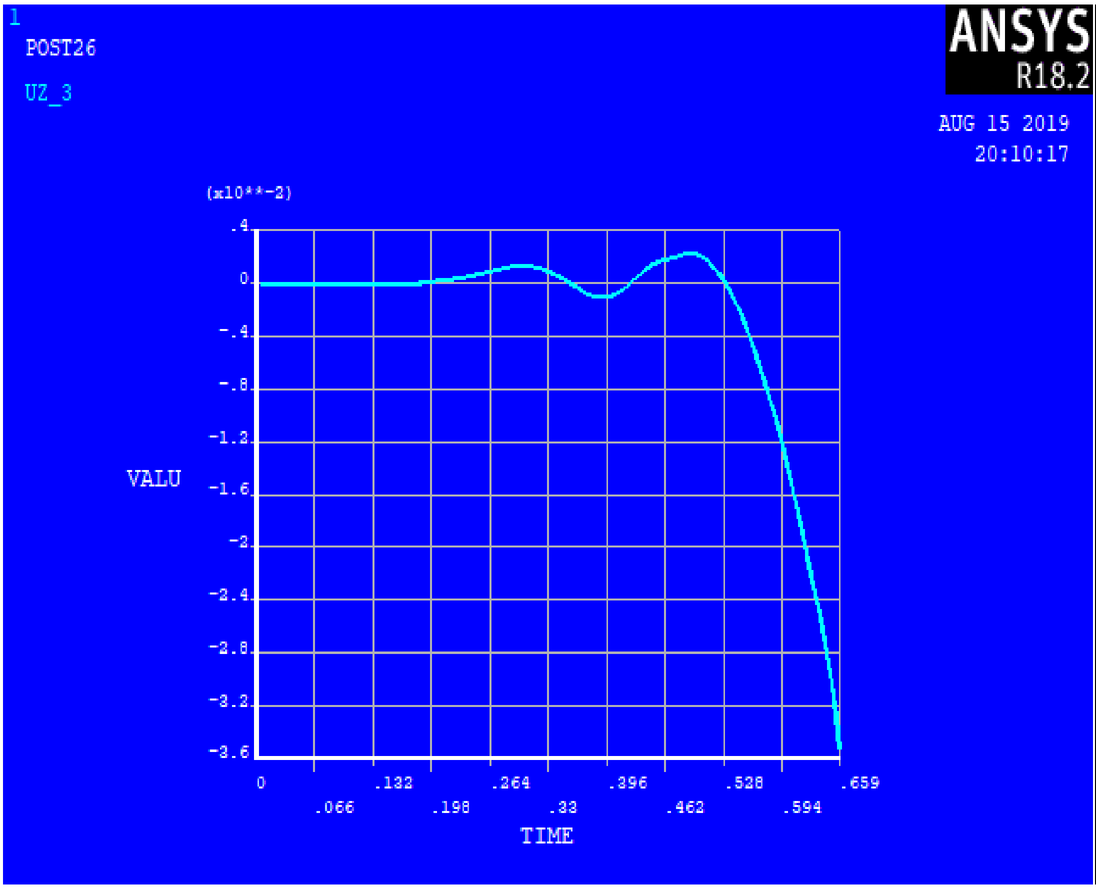

Figure (5.37) u_z^t at roof level of Model No.1 (mm).

The displacement given in ANSYS postprocessor at any node is the total displacement (u^t) at that node. Therefore, the differential (deformation) displacement (u) between any two nodes (positions) is found from subtracting ANSYS displacements for the two nodes one from the other. It is well-known that the stresses in the structure subjected to a ground motion are due to the relative displacement. Therefore, it is the main aim for the engineer. The total displacement (u^t) is given by the Eq. (5.3) as follows:

$$u^t = u + u_g \qquad (5.3)$$

where:

u^t: total displacement

u: relative displacement (deformation)

u_g : ground displacement.

The total displacement, differential displacement, and ground displacement are as in the sketch shown in Fig. (5.38).

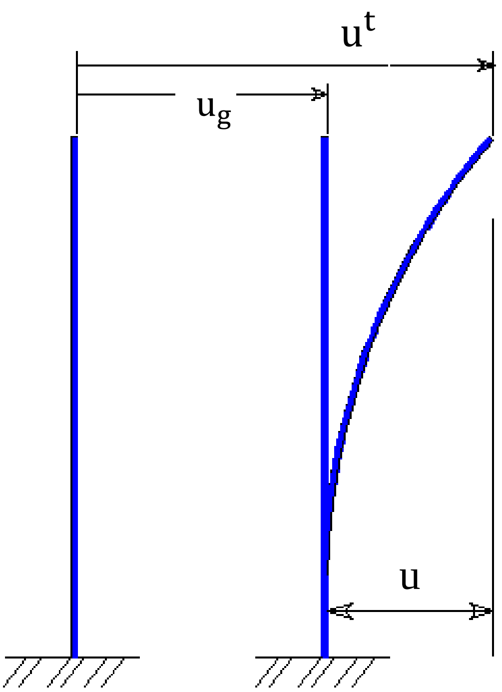

Figure (5.38) Displacement nomenclature.

As mentioned above, subtracting u_z^t at base level from u_z^t at roof level results in the response at roof level (u_z), as in Fig. (5.39) that follows:

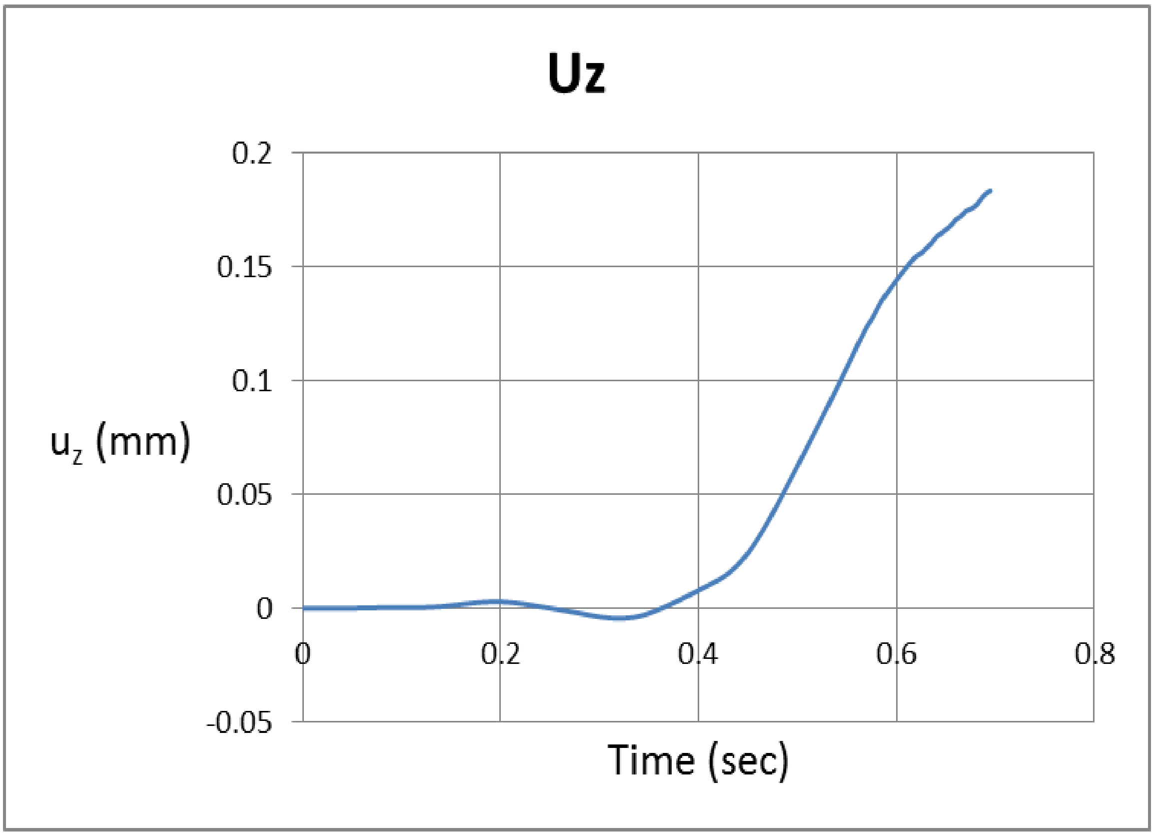

Figure (5.39) u_z at roof level of Model No. 1.

Similarly, subtracting u_x^t at base level from u_x^t at roof level results in the response (u_x), as in Fig. (5.40) that follows:

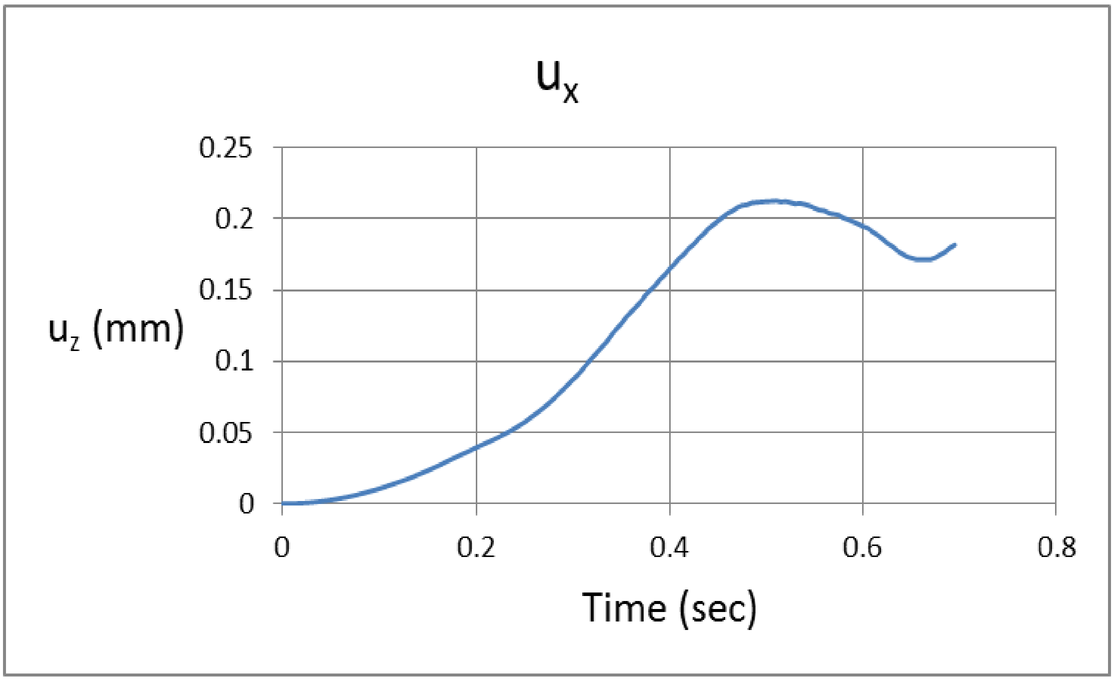

Figure (5.40) u_x at roof level in model No.1.

Fig. (5.41) shows the crack pattern at the last converged solution as follows:

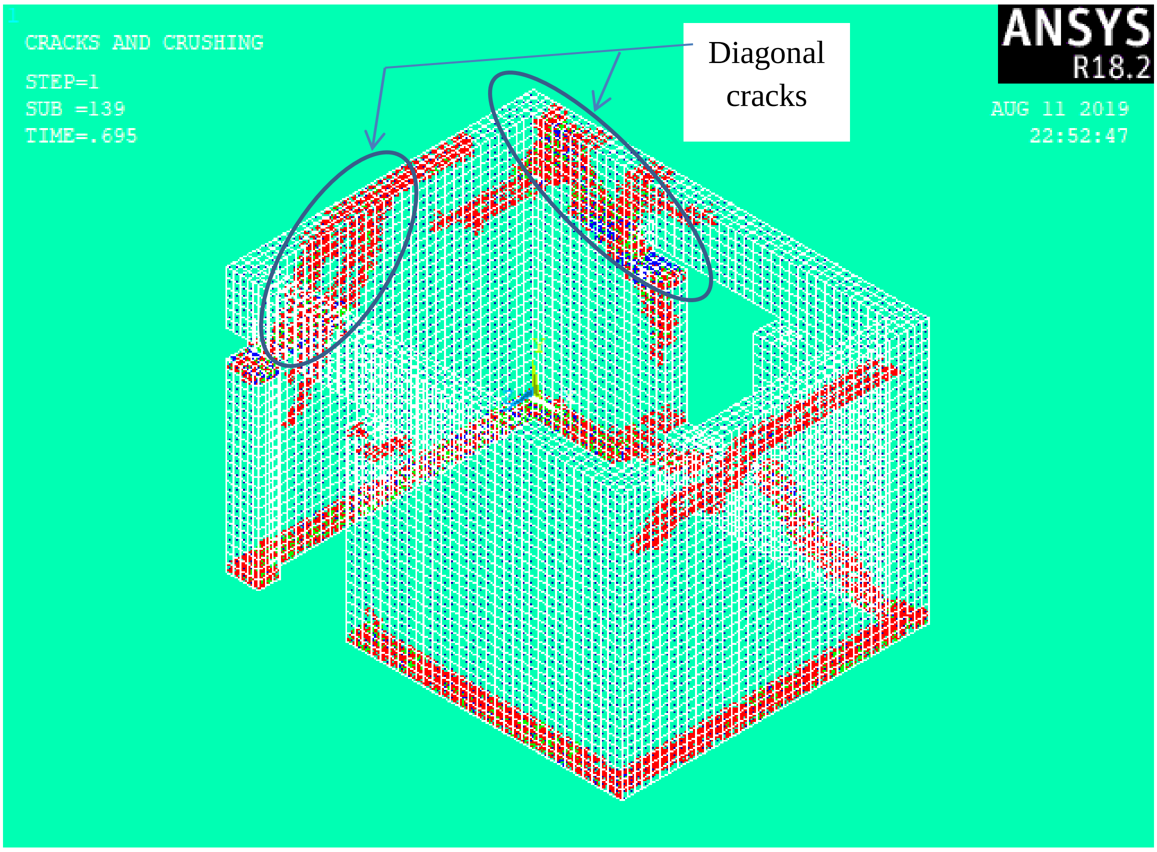

Figure (5.41) cracks in model No.1.

In Figure (5.41), the diagonal cracks can be obviously observed as well as the cracks parallel to bed joints at base of building. These two patterns of cracks are commonly observed in masonry damages due to earthquakes. The cracks denote severe local damages in the building. The model was reanalyzed under the effect of the seismic waves recorded in Abadan station during the M_w 7.3 earthquake that hit Iran-Iraq border on 12 November 2017.

In this analysis, the damping was taken into consideration, and it was modeled using Rayleigh damping. The mass matrix multiplier (α) and the stiffness matrix multiplier (β) were evaluated as described in Chapter four from this study. The H1-horizontal components of ground acceleration and displacement are shown in Figures (5.42) and (5.43). The structural response at the level of the roof in z-direction, in which the H-1 component was applied, is shown in Fig. (5.44). The ANSYS result of the acceleration in z-direction at the base level is shown in Fig. (5.45). To verify that the seismic loading is correctly applied in ANSYS modeling, it can be done by comparing the ANSYS acceleration at the base level to ground
Acceleration shown in Fig. (5.46).

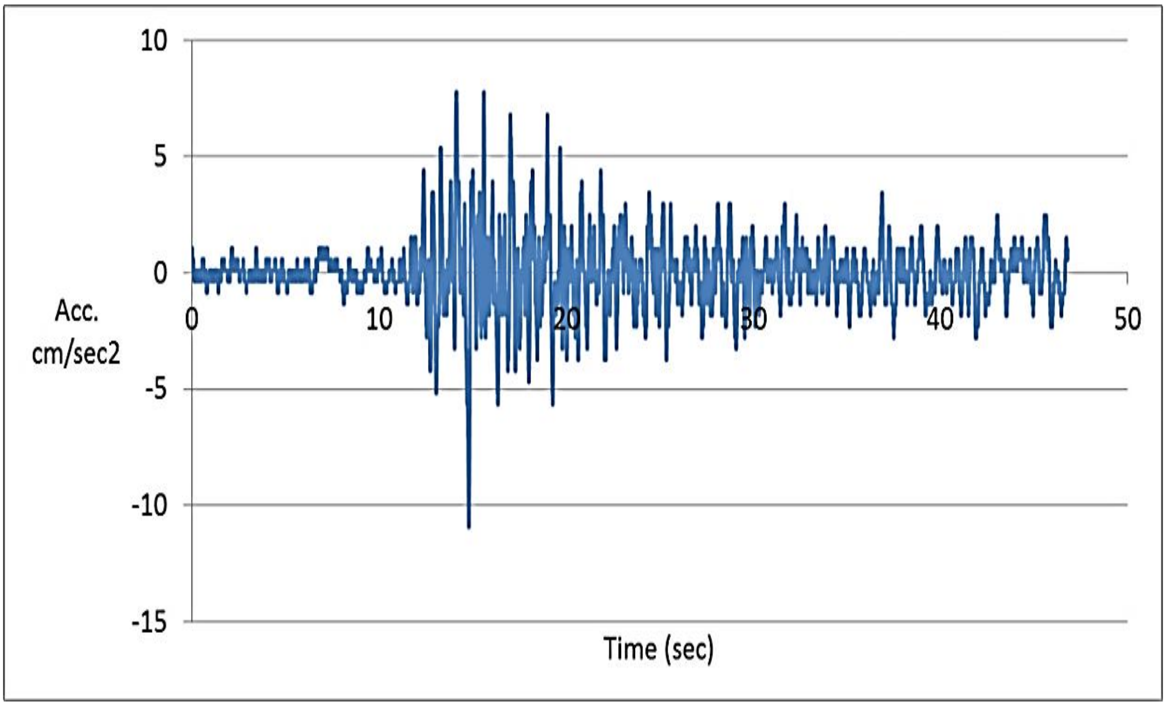

Figure (5.42) H1-acceleration for Abadan records during the 7.3 event (cm/s^2).

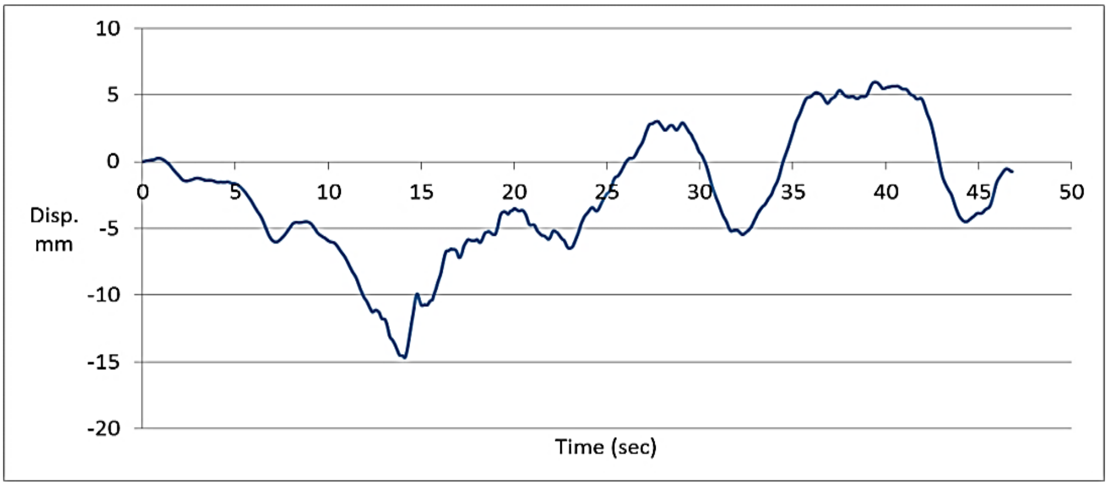

Figure (5.43) H1-ground displacement for Abadan records during the 7.3 event

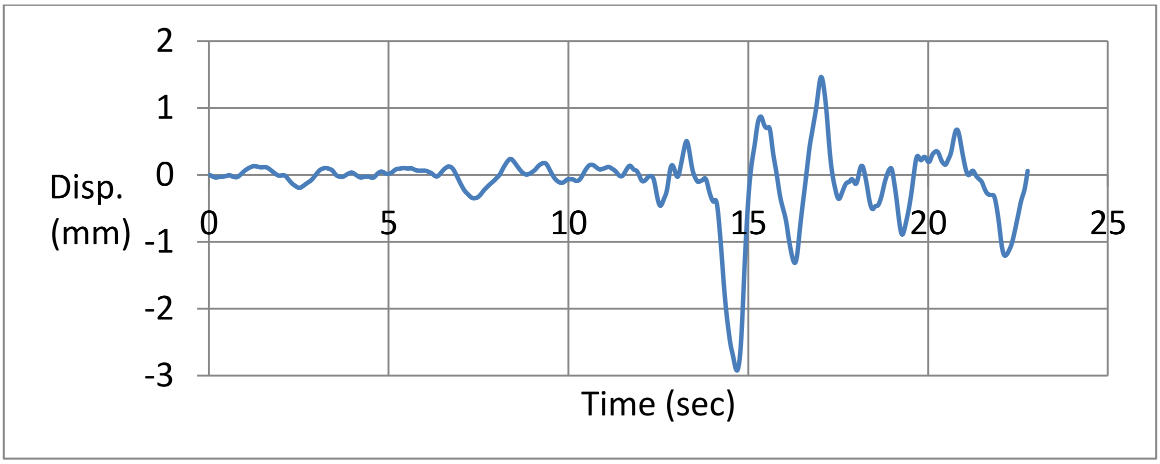

Figure (5.44) Response in z-direction for Model No.1 under the seismic wave recorded at Abadan station for the 7.3 M_w event.

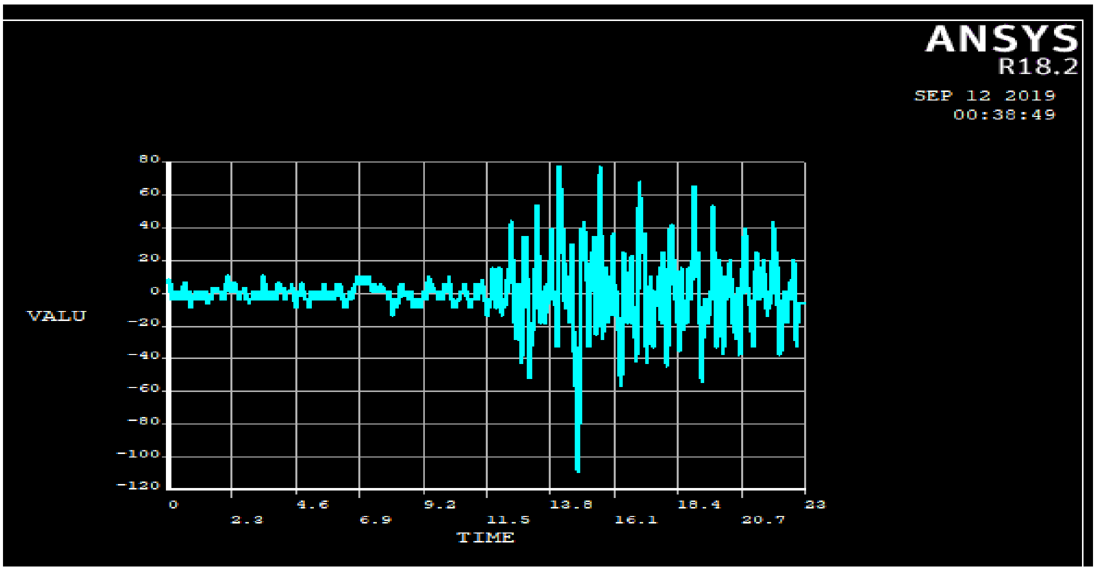

Figure (5.45) ANSYS acceleration at base level of Model No.1 (mm/sec^2) for Model No.1 subjected to the seismic wave of Abadan station.

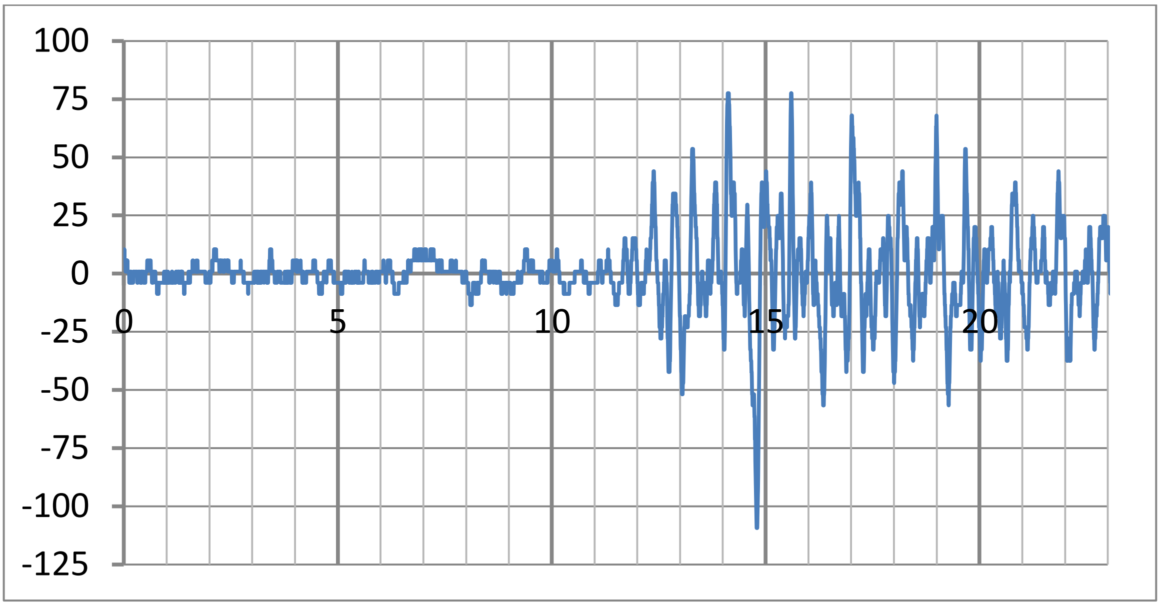

Figure (5.46) H1-acceleration for Abadan records during the 7.3 event (mm/s^2).

In Fig. (5.46), the units of acceleration have been converted to mm/s^2 and only the portion corresponding to ANSYS result has been taken in order to do the comparison strictly. As it can be seen, the seismic loading was applied correctly.

An analysis of free damped vibration was performed to investigate the damping ratio by the decay in amplitude, according to Eq. (5.2) [46]:

$$\zeta = \frac{1}{2\pi j} ln(\frac{u_i}{u_{i+j}}) \quad (5.2)$$

Where:

ζ: the constant damping ratio

ln: the natural logarithm

u_i: the amplitude at the peak (i)

u_{i+j}: the amplitude at the peak (i+j)

The structural response at the level of the roof for the damped free vibration is shown in Fig. (5.47). According to Eq. (5.2). To substitute into Eq. (5.2), the data file of the response can be imported from ANSYS to Excel. It has been found that the constant damping is 3.4%, which is so close to 3% that is taken as recommended by Anil K. Chopra [51]. The free vibration analysis was performed by applying initial conditions of zero initial velocity and initial displacements for all nodes in z-direction. The base of the model was fixed.

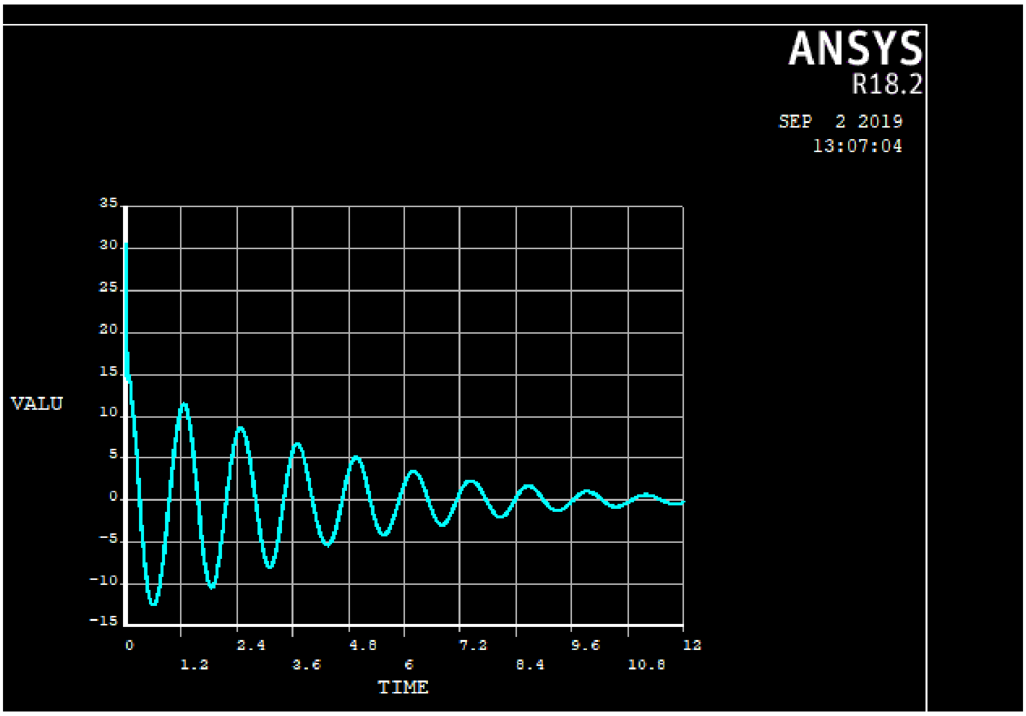

Figure (5.47) Damped free vibration of Model No.1.

The model was analyzed twice under the effect of the Northwest California earthquake but with taking the damping into consideration. Firstly, the tensile strength was 0.15 MPa, and secondly, it was 0.3 MPa. The structural responses are as shown in Fig. (5.48). The CS of masonry was increased from 5.5 MPa to 9.811 MPa and the model was analysed keeping the 0.15 MPa unchanged. It was found that the response is not affected.

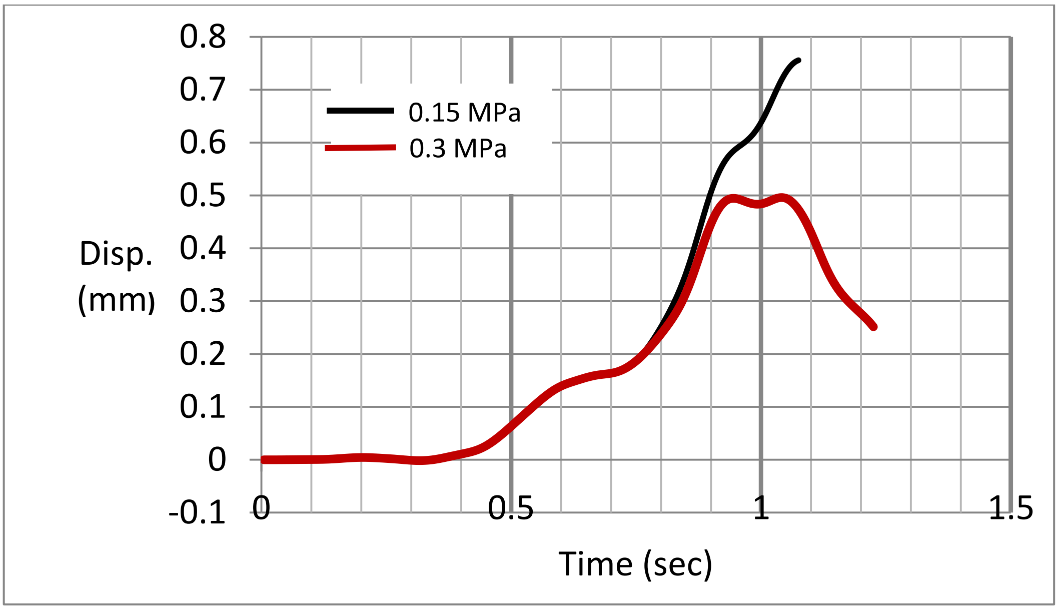

Figure (5.48) u_z of Model No.1 with the modeling of damping.

5.8 Model No. 2

The model is a one-story house with a clear height of 3 m and a plan shown in Figure (5.49) as follows:

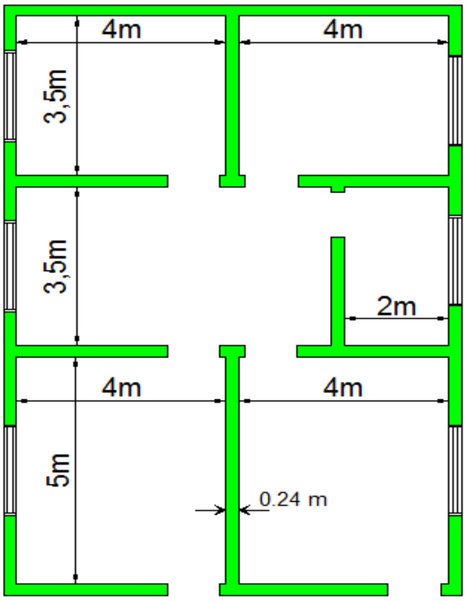

Figure (5.49) Plan of the one-story house.

The roof is a concrete slab with 0.2 m thickness. The FE model is shown in Fig. (5.50) in which the edge length of the element was set to be 200mm, thus the model is built up of 4289 elements with 8868 nodes.

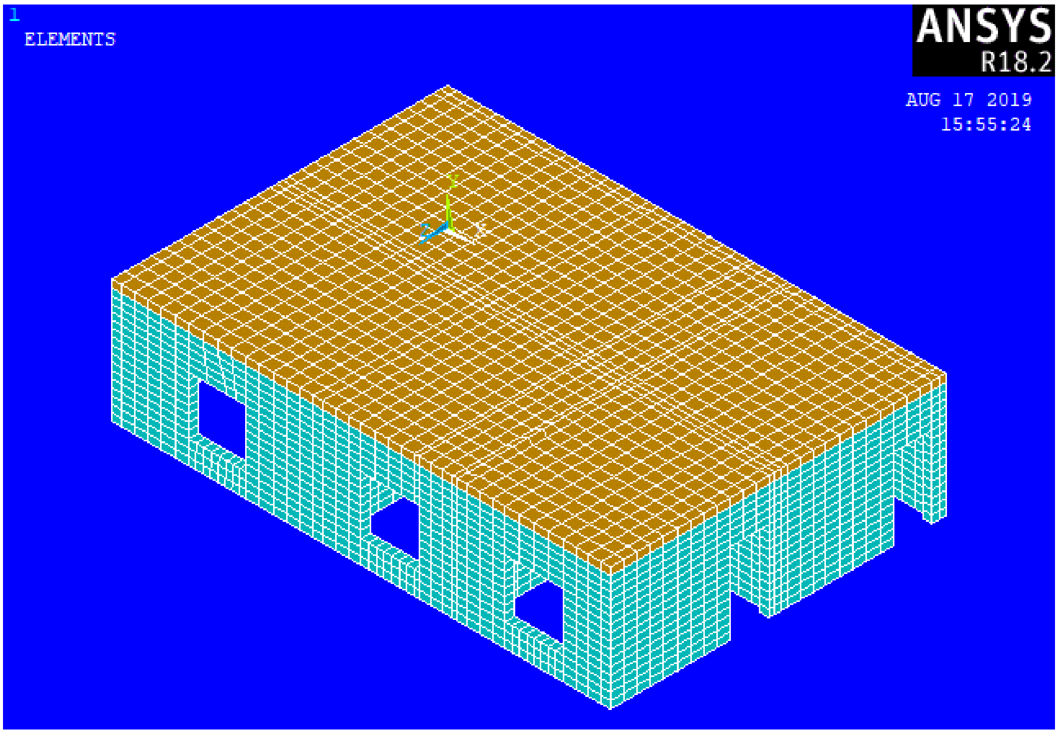

Figure (5.50) FE Model No. 2.

The modal analysis report and the first three modes are shown in Figures (5.51) to (5.54).

Mechanical APDL 18.2 Output Window

***** PARTICIPATION FACTOR CALCULATION ***** X DIRECTION

MODE	FREQUENCY	PERIOD	PARTIC.FACTOR	RATIO	EFFECTIVE MASS	CUMULATIVE MASS FRACTION	RATIO EFF.MASS TO TOTAL MASS
1	0.634553	1.5759	309.54	1.000000	95817.4	0.869225	0.710650
2	0.651364	1.5352	-117.62	0.379967	13833.7	0.994719	0.102600
3	0.807042	1.2391	24.127	0.077943	582.094	1.00000	0.431723E-02
sum					110233.		0.817568

***** PARTICIPATION FACTOR CALCULATION ***** Y DIRECTION

MODE	FREQUENCY	PERIOD	PARTIC.FACTOR	RATIO	EFFECTIVE MASS	CUMULATIVE MASS FRACTION	RATIO EFF.MASS TO TOTAL MASS
1	0.634553	1.5759	-2.6536	1.000000	7.04144	0.548506	0.522244E-04
2	0.651364	1.5352	1.0231	0.385538	1.04664	0.630036	0.776262E-05
3	0.807042	1.2391	-2.1793	0.821275	4.74940	1.00000	0.352249E-04
sum					12.8375		0.952119E-04

***** PARTICIPATION FACTOR CALCULATION ***** Z DIRECTION

MODE	FREQUENCY	PERIOD	PARTIC.FACTOR	RATIO	EFFECTIVE MASS	CUMULATIVE MASS FRACTION	RATIO EFF.MASS TO TOTAL MASS
1	0.634553	1.5759	114.10	0.369256	13018.2	0.118467	0.965524E-01
2	0.651364	1.5352	308.99	1.000000	95476.4	0.987310	0.708121
3	0.807042	1.2391	37.343	0.120855	1394.53	1.00000	0.103428E-01
sum					109889.		0.815016

Figure (5.51) ANSYS report for modal analysis of Model No.2.

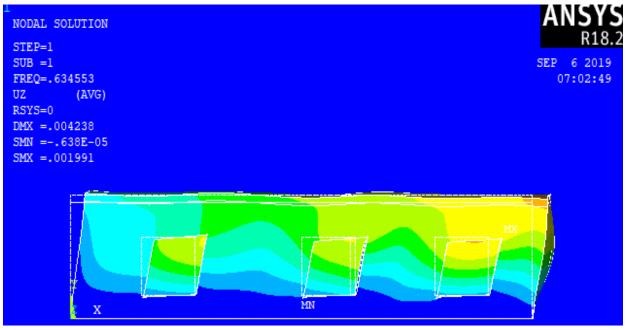

Figure (5.52) 1st mode of Model No.2.

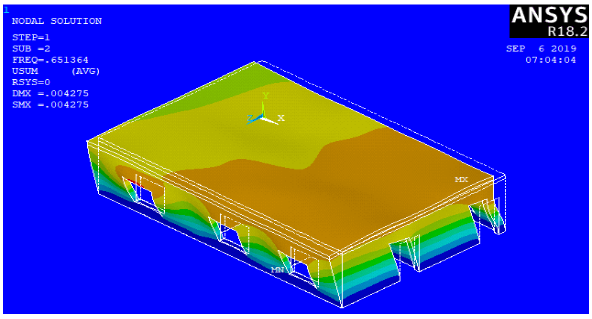

Figure (5.53) 2nd mode of Model No.2.

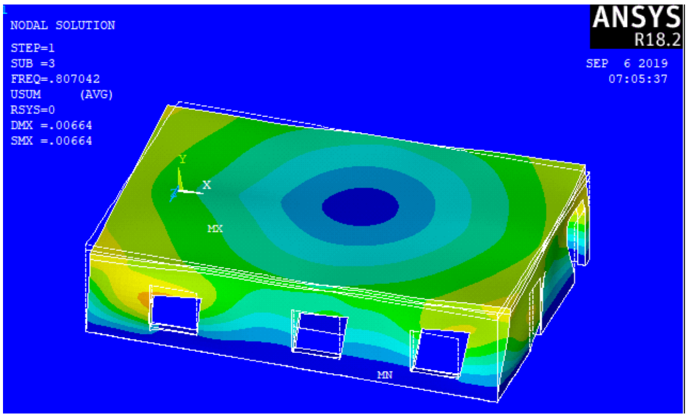

Figure (5.54) 3rd mode of Model No.2.

The displacement-time histories used for the analysis were obtained from converting the accelerograms recorded in Ravansar station (Iranian station) during the 7.3 earthquake that hit the Iraq-Iran border on 12 November 2017. The accelorigrams were converted to displacement time-histories by the use of seismosignal software. Table (5.4) demonstrates the characteristics of the seismic records applied to Model No.2. The accelreograms are shown in Figures (5.55) to (5.57).

Table (5.4) Description of the seismic records applied to Model No.2.

Earthquake name	Station name	Date	Magnitude M_w	PGA g	V_{s30} m/s
The 7.3 M_w, November 2017	Ravansar	12/11/2017	7.3	0.122	267

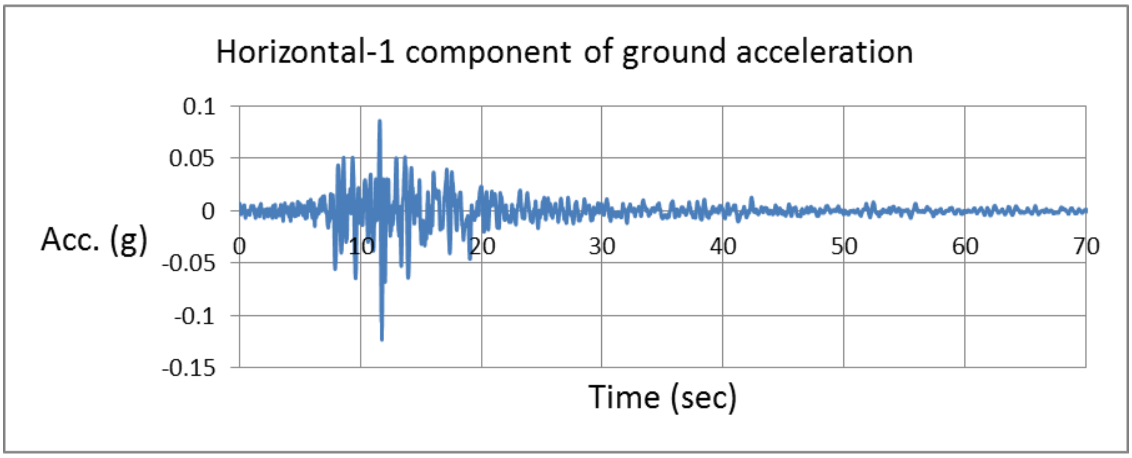

Figure (5.55) H-1 component of $\ddot{u}_g$ of the November 7.3 M_w event (Ravansar).

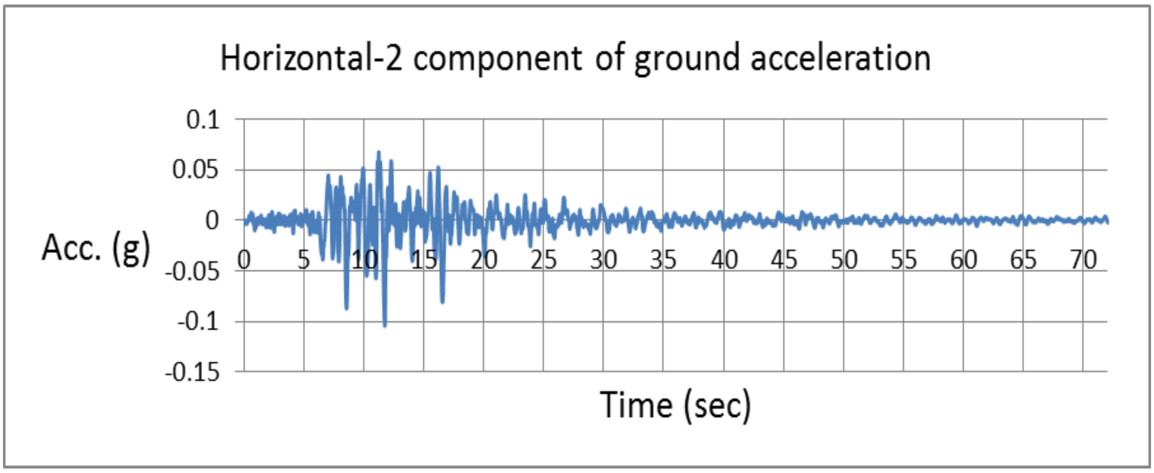

Figure (5.56) H-2 component of $\ddot{u}_g$ of the November 7.3 M_w event (Ravansar).

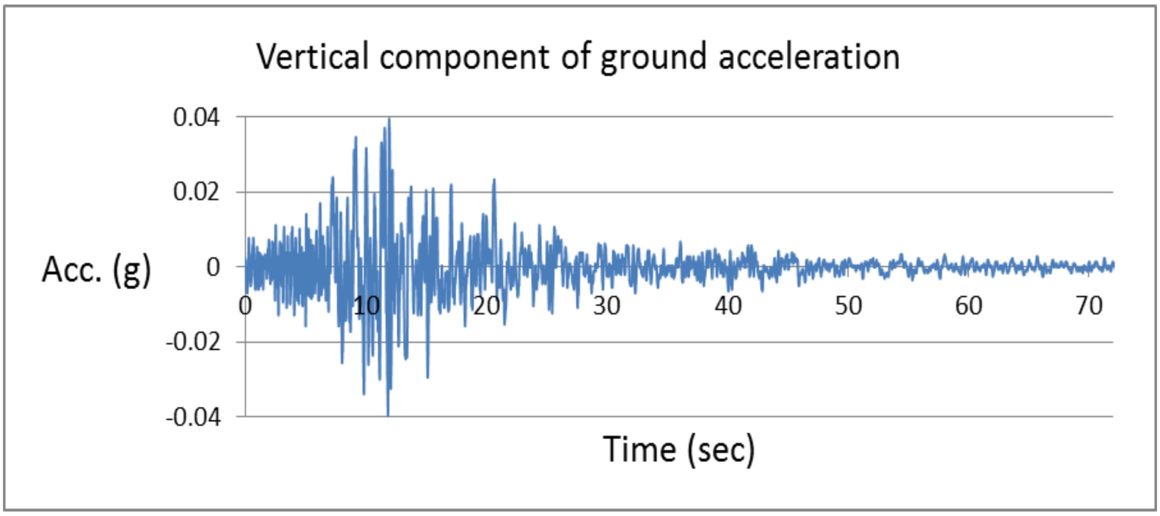

Figure (5.57) Vertical component of $\ddot{u}_g$ of the November 7.3 M_w event (Ravansar station).

The horizontal-1 component was applied in z-direction, while the second horizontal component was applied in x-direction. The vertical component of ground displacement was applied in gravity direction (y-direction). Firstly, the model was analyzed taking the tensile strength of masonry 0.15 MPa and neglecting the damping effect. The structure responses at roof level in z- and y-direction are shown in Figures (5.58) and (5.59), respectively. The crack pattern, $1^{st.}$ principal stress, and 3^{rd} principal stress in walls are shown in Figures (5.60) to (5.62). While dense cracks have been observed in masonry walls at the end of the solution, no cracks appeared in the concrete slab, as shown in Fig. (5.63). The first principal stresses in the concrete slab are shown in Fig. (5.64).

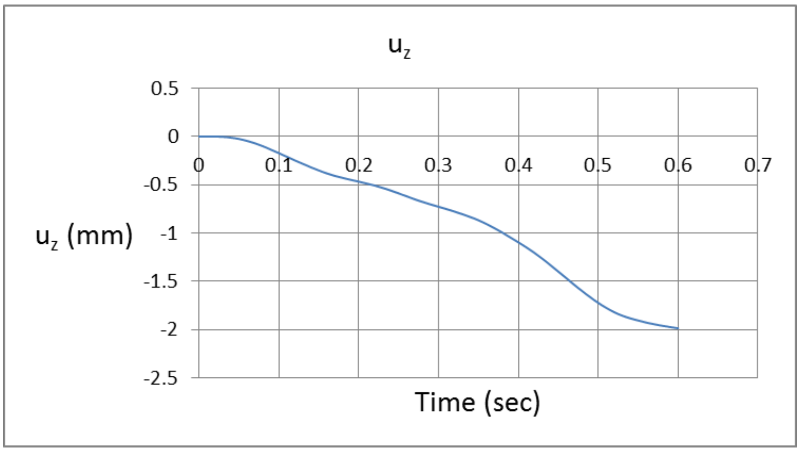

Figure (5.58) Response at roof level in z-direction for Model No. 2.

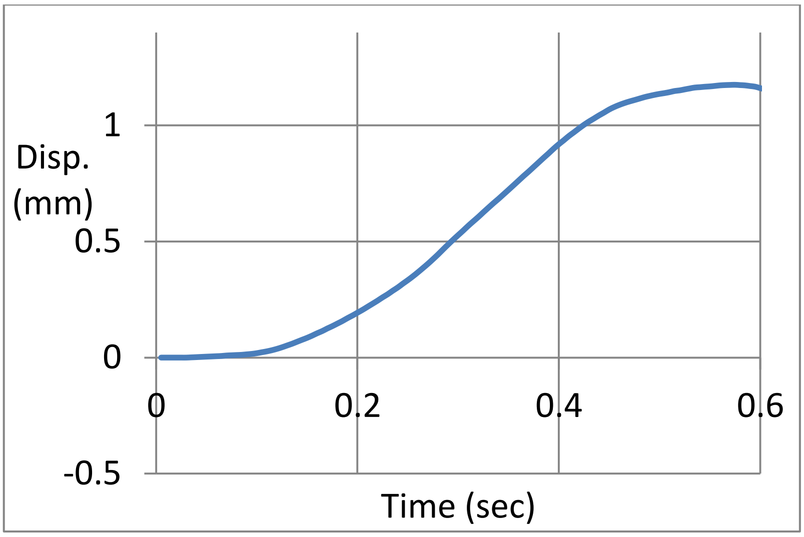

Figure (5.59) Response at roof level in x-direction for Model No. 2.

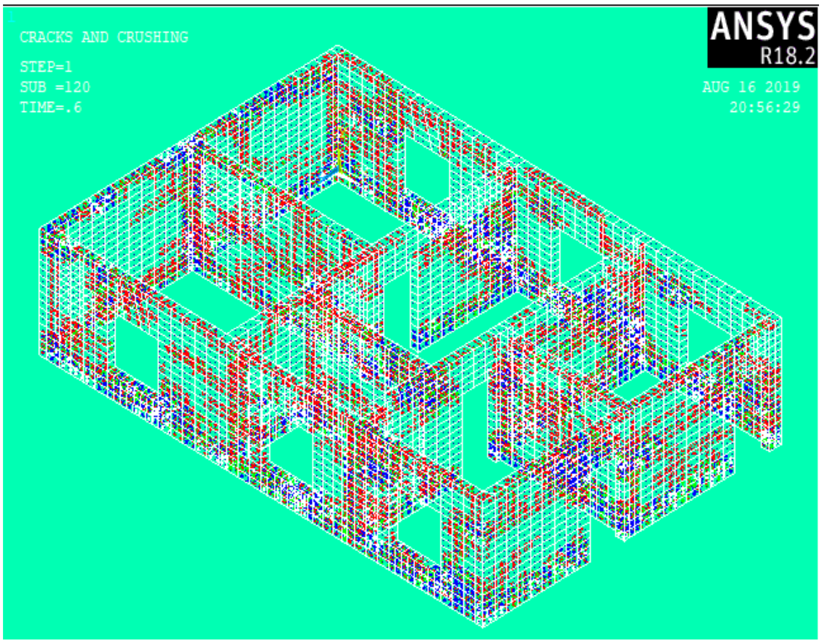

Figure (5.60) Crack pattern in Model No.2.

From figures (5.58) and (5.59), it can be seen that that the analysis terminated in so early time during the earthquake. This means that the structure is not capable of responding to the applied seismic load, but the analysis was performed without modeling the damping, which notably affects the structural response. Another essential cause of terminating the solution is the low tensile strength of masonry which is highly effects the in-plane load capacity of the masonry walls, as showed by the parametric investigation in the simulation of of Model No.7.

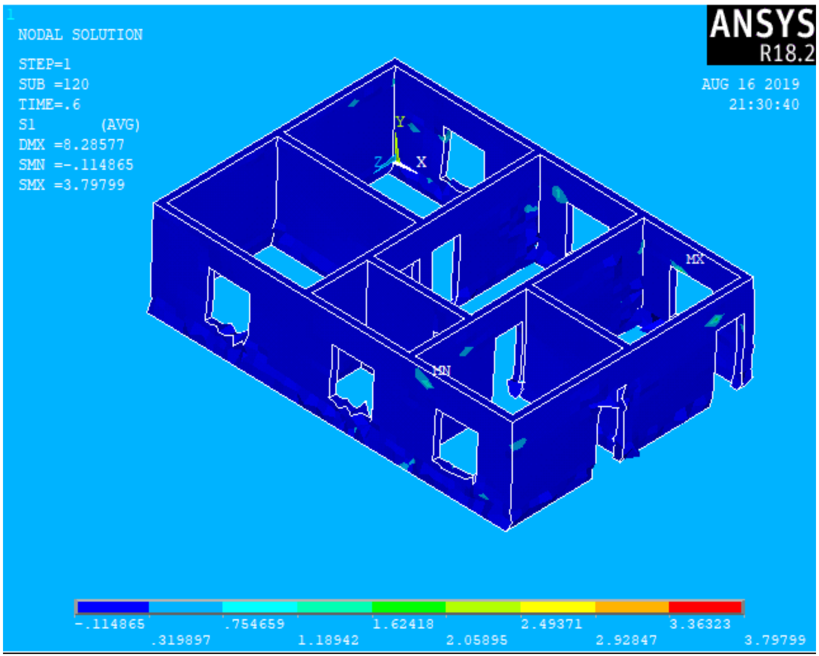

Figure (5.61) 1st principal stress in walls of Model No.2

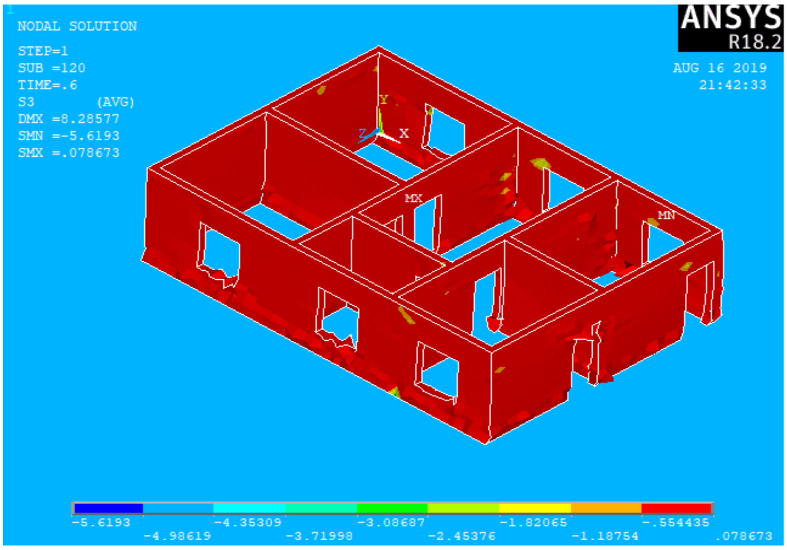

Figure (5.62) 3rd principal stress in walls of Model No. 2.

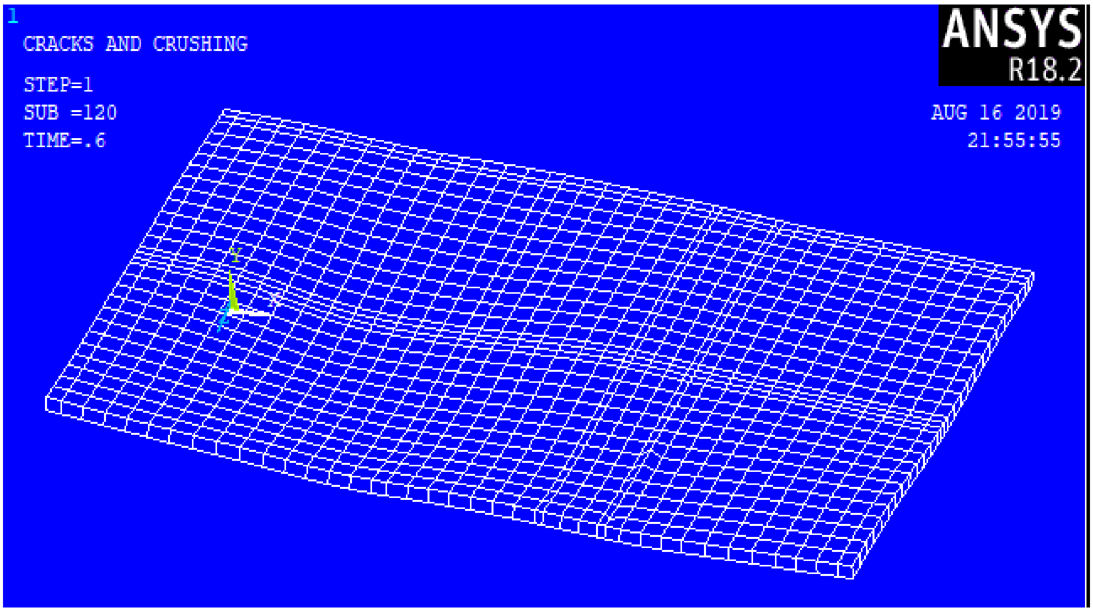

Figure (5.63) Cracks in concrete slab of Model No. 2.

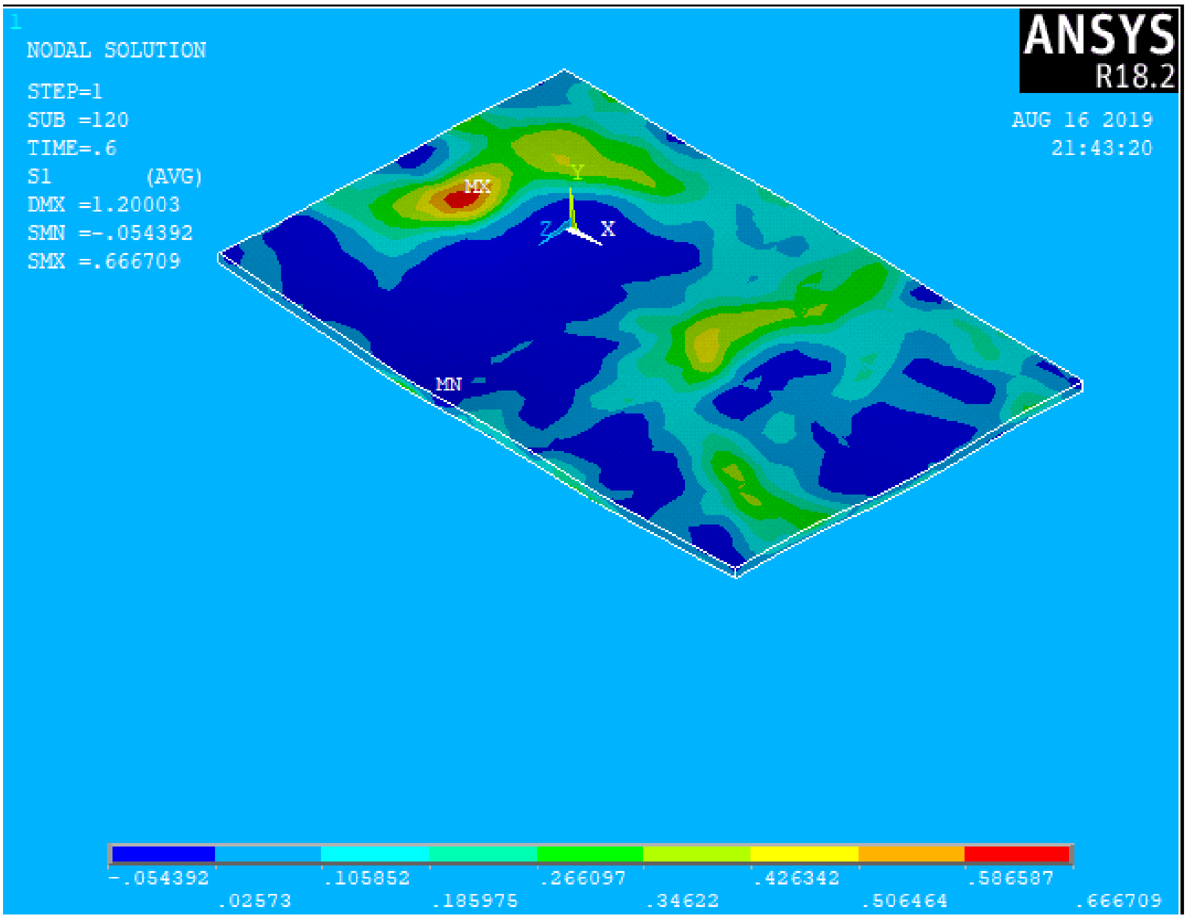

Figure (5.64) 1st principal stress in concrete slab of Model No.2.

The mesh was refined to check the acceptance of the element size and thus the length of the element edge was set to b 150 mm. The responses at roof level in z-direction before and after mesh refinement are as shown in Fig. (5.65).

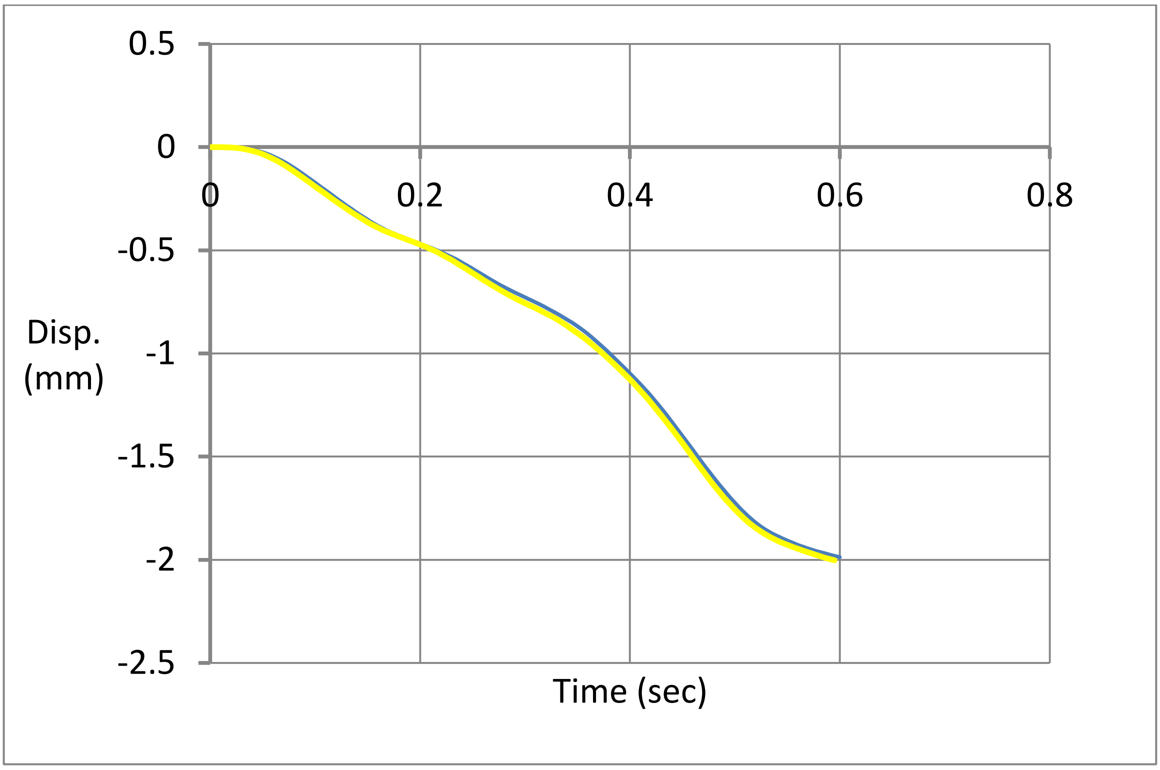

Figure (5.65) Responses at roof level in z-direction before and after mesh refinement for Model. 2.

It was found that a slight variance occurred in the displacement u_z^t and imperceptible variance occurred in the structure response u_x. Therefore, the element size of 200 mm edge length has been accepted.

The modal analysis results indicate the significant effect of openings on the building stiffness that the effective mass in the 1st mode is largest in x-direction (length of building) not in the width direction which is attributed to the existence of many and large windows reducing the stiffness in x-direction.

Figure (5.60) shows crack pattern at the end of solution in which severe damages are observed. The regions with multi-color cracks are regions where first cracks occur. Figures (5.61) and (5.62) show that the high stresses in the walls occur at the base of the structure and near openings. The 3rd principal stress values, shown in Fig.(5.62), reveal that no crushing occurred in masonry walls and all the observed cracks are tensile cracks attributed to the low tensile strength of masonry. The first principal stress values, shown in Fig. (5.64), illustrate that the stresses are still below the tensile strength of concrete which was used as 3.5 MPa. Therefore, no cracks occurred in the slab as it can be observed in Fig. (5.63).

The analysis was repeated for the one-story house model with the modeling of damping and with increasing the tensile strength of masonry from 0.15 MPa to 0.25. As mentioned before, the Rayleigh coefficients (α and β) were evaluated assuming a constant damping ratio of 3% and depending on the first two modes, but the mass-proportional damping results in undesired results when relatively a huge exists. In many practical structural problems, alpha damping (or mass-proportional damping) may be ignored ($\alpha = 0$) [50]. Since the diaphragm of this model has a huge mass, only beta damping was incorporated in the repeated analysis. The analysis went on more time, as can be observed in Fig. (5.66) that shows the structural response at the level of the roof in x-direction.

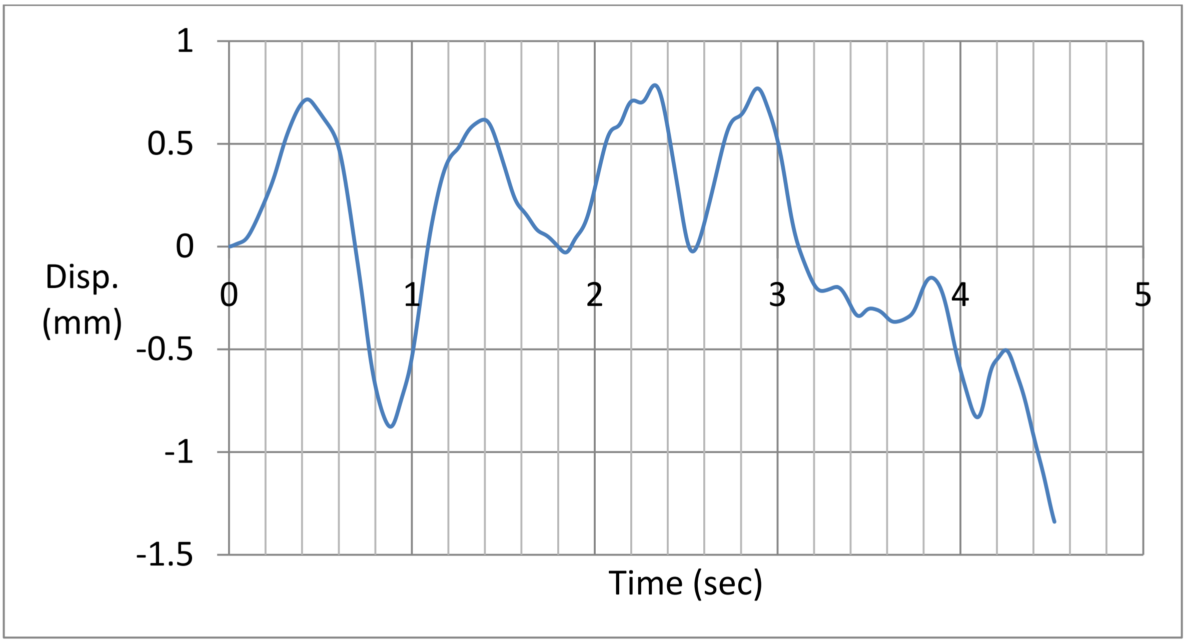

Figure (5.66) Damped response (u_x) of Model No.2

5.9 Model No. 3

This model is a two-storey building with a repeated plan of a single room at each floor. The plan is shown in Fig. (5.67). A value of 200 mm was used for the element size, and thus the FE model shown in Fig. (5.68) is built up of 5780 elements having 9261 nodes.

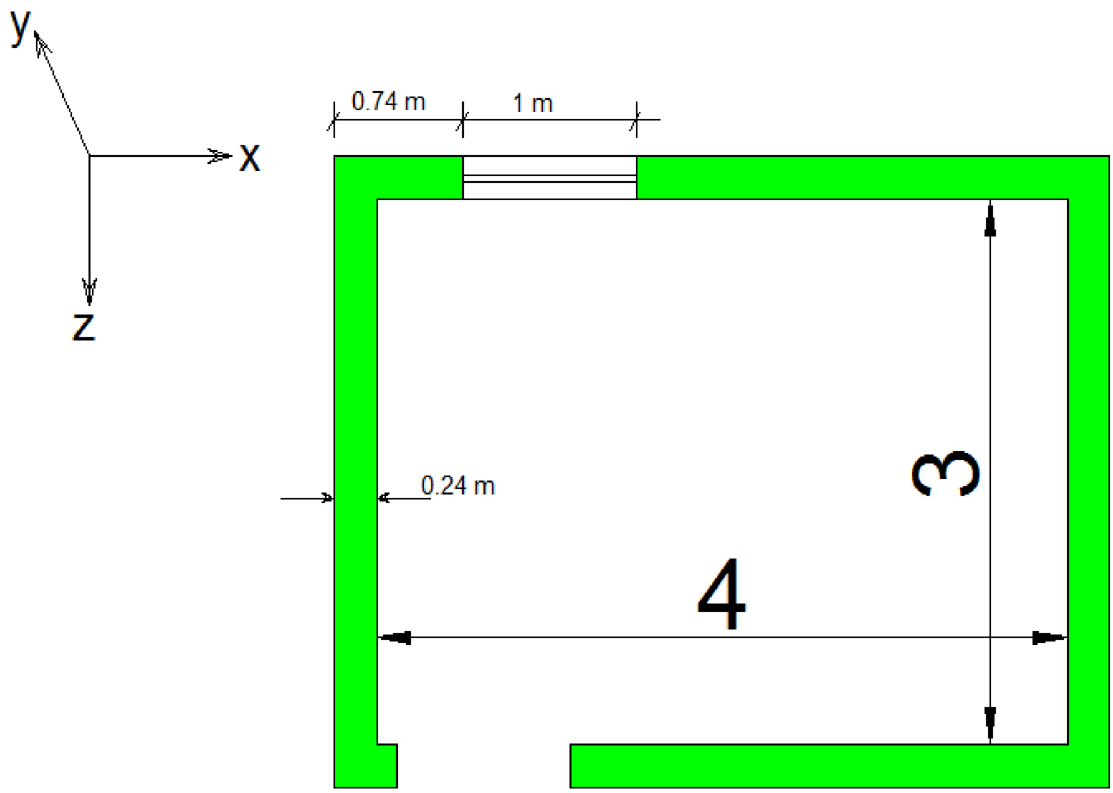

Figure (5.67) Plan of Model No. 3.

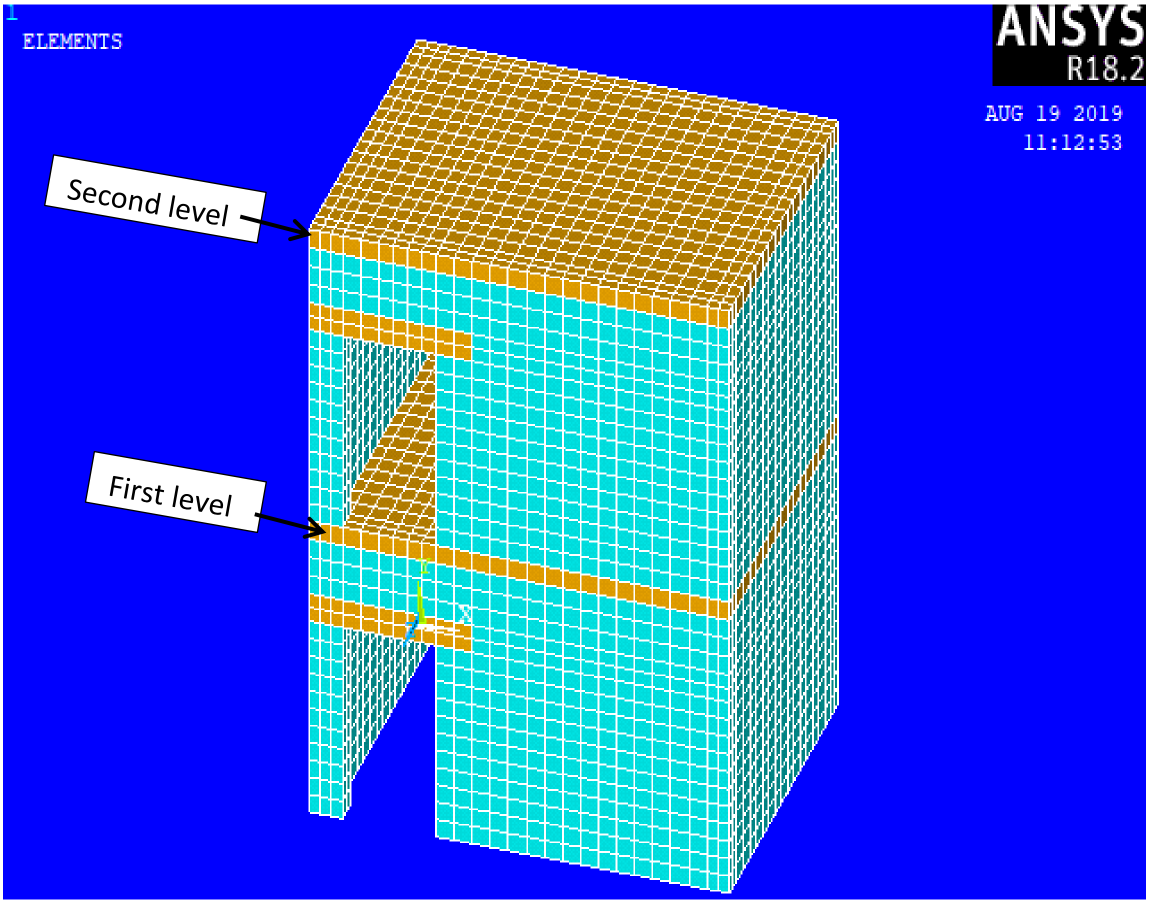

Figure (5.68) FE Model No. 3.

The modal analysis results are illustrated in Figures (5.69) to (5.72) as follows:

Mechanical APDL 18.2 Output Window

***** PARTICIPATION FACTOR CALCULATION ***** X DIRECTION

MODE	FREQUENCY	PERIOD	PARTIC.FACTOR	RATIO	EFFECTIVE MASS	CUMULATIVE MASS FRACTION	RATIO EFF.MASS TO TOTAL MASS
1	0.356101	2.8082	50.135	0.266457	2513.50	0.661852E-01	0.496419E-01
2	0.377175	2.6513	188.15	1.000000	35401.9	0.998382	0.699189
3	0.673695	1.4844	7.8377	0.041656	61.4297	1.00000	0.121324E-02
sum					37976.8		0.750045

***** PARTICIPATION FACTOR CALCULATION ***** Y DIRECTION

MODE	FREQUENCY	PERIOD	PARTIC.FACTOR	RATIO	EFFECTIVE MASS	CUMULATIVE MASS FRACTION	RATIO EFF.MASS TO TOTAL MASS
1	0.356101	2.8082	1.6787	0.296933	2.81787	0.787193E-01	0.556531E-04
2	0.377175	2.6513	5.6533	1.000000	31.9598	0.971541	0.631209E-03
3	0.673695	1.4844	-1.0093	0.178537	1.01873	1.00000	0.201200E-04
sum					35.7964		0.706982E-03

***** PARTICIPATION FACTOR CALCULATION ***** Z DIRECTION

MODE	FREQUENCY	PERIOD	PARTIC.FACTOR	RATIO	EFFECTIVE MASS	CUMULATIVE MASS FRACTION	RATIO EFF.MASS TO TOTAL MASS
1	0.356101	2.8082	183.65	1.000000	33726.0	0.926171	0.666092
2	0.377175	2.6513	-49.009	0.266868	2401.92	0.992132	0.474381E-01
3	0.673695	1.4844	16.927	0.092171	286.521	1.00000	0.565882E-02
sum					36414.5		0.719189

Figure (5.69) ANSYS report for Model No.3.

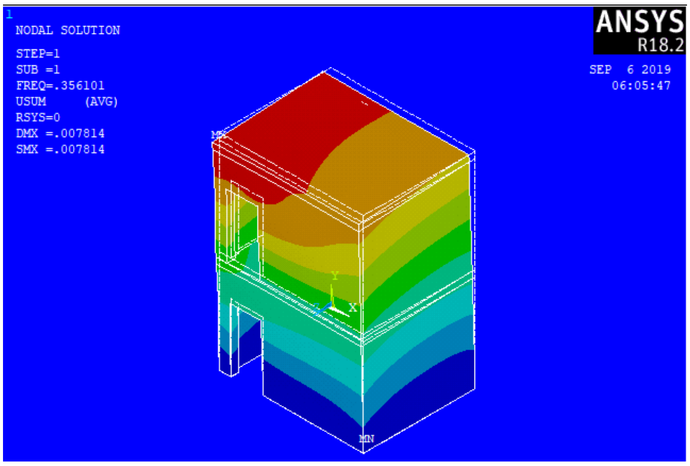

Figure (5.70) 1st mode of Model No.3.

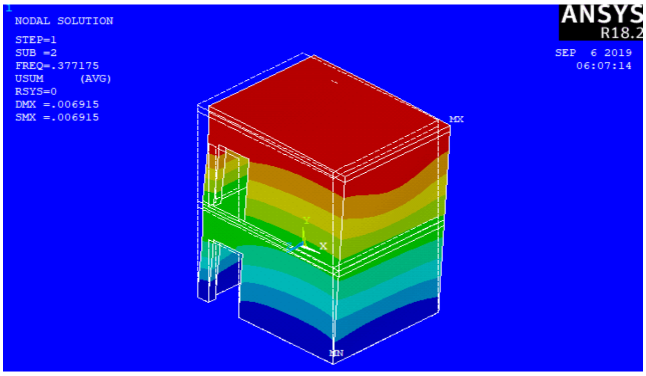

Figure (5.71) 2nd mode of Model No.3.

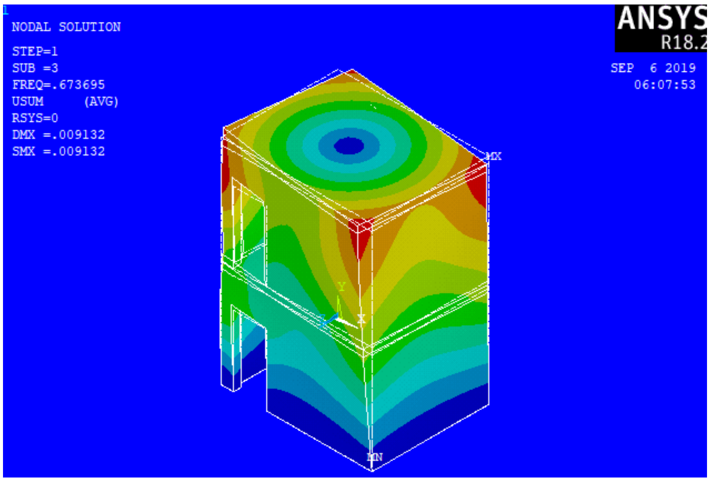

Figure (5.72) 3rd mode of Model No.3.

The seismic loading is the same loading applied to Model No.1 neglecting the effect of damping and adopting the value of 0.15 MPa for the tensile strength of masonry, which was obtained from the experimental work in this study. The responses at base level, first level, and second level are shown in Figures (5.73) to (5.76). Figure (5.77) shows the regions of the building where the first cracks appear, while Fig. (5.78) shows crack pattern at end of solution. Figures (5.79) and (5.80) show the first principal stress in masonry walls and Von misses stresses in the concrete slab and lintels, respectively.

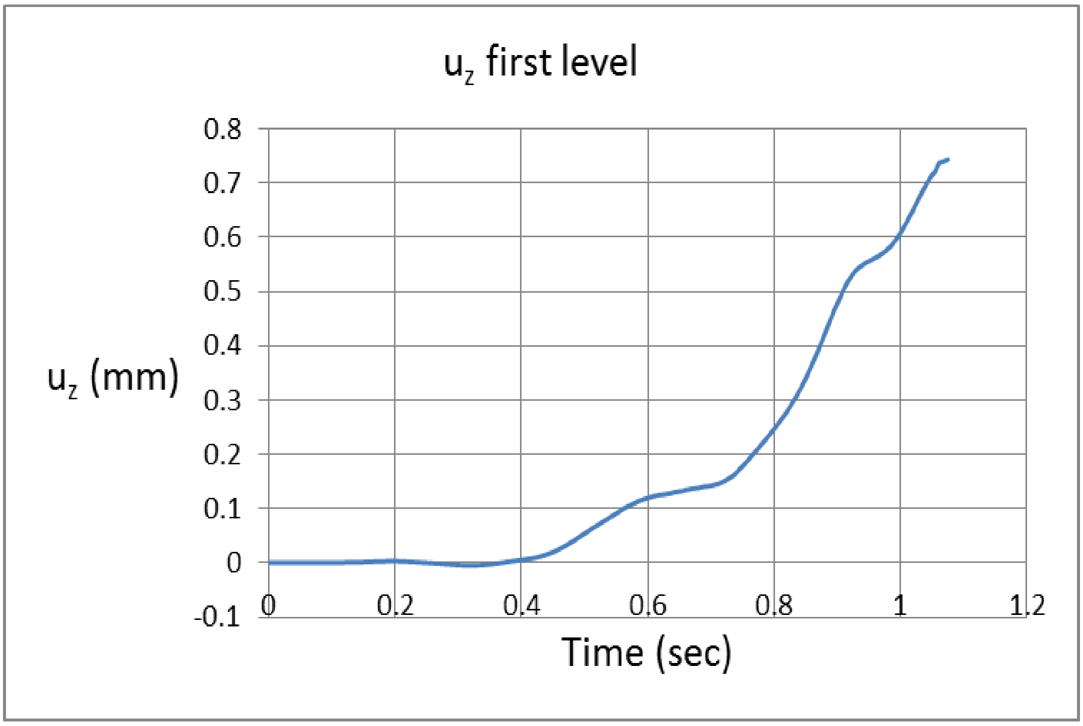

Figure (5.73) u_z at first level of Model No. 3.

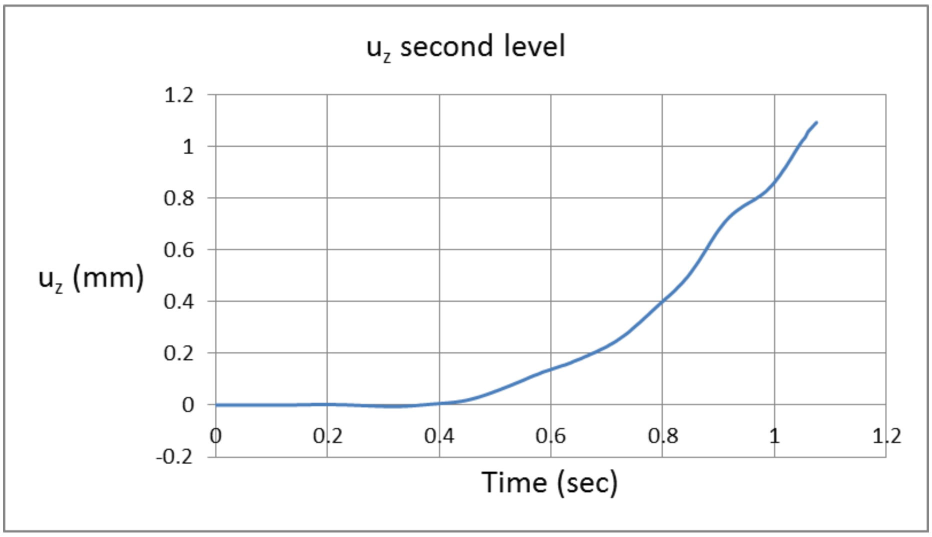

Figure (5.74) u_z at second level of Model No. 3.

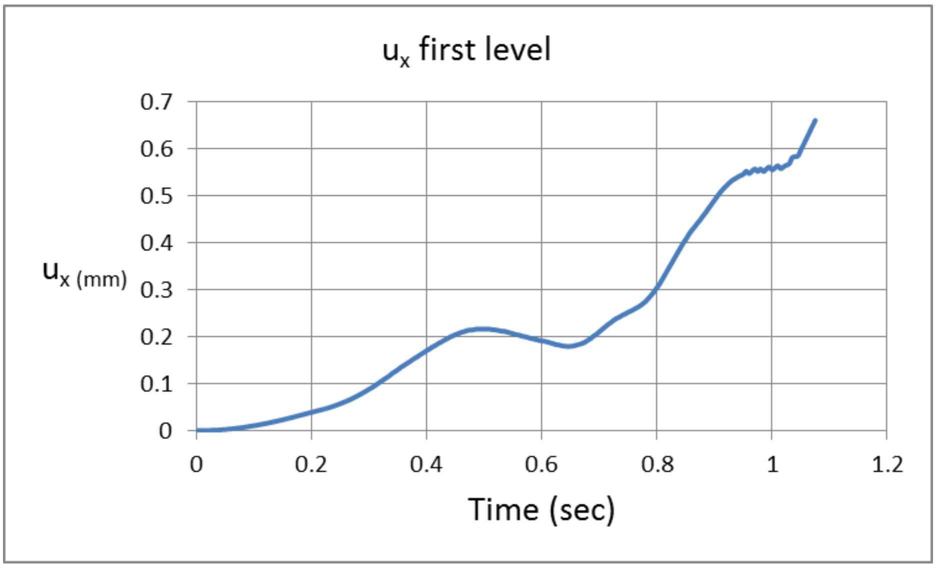

Figure (5.75) u_x at first level of Model No. 3.

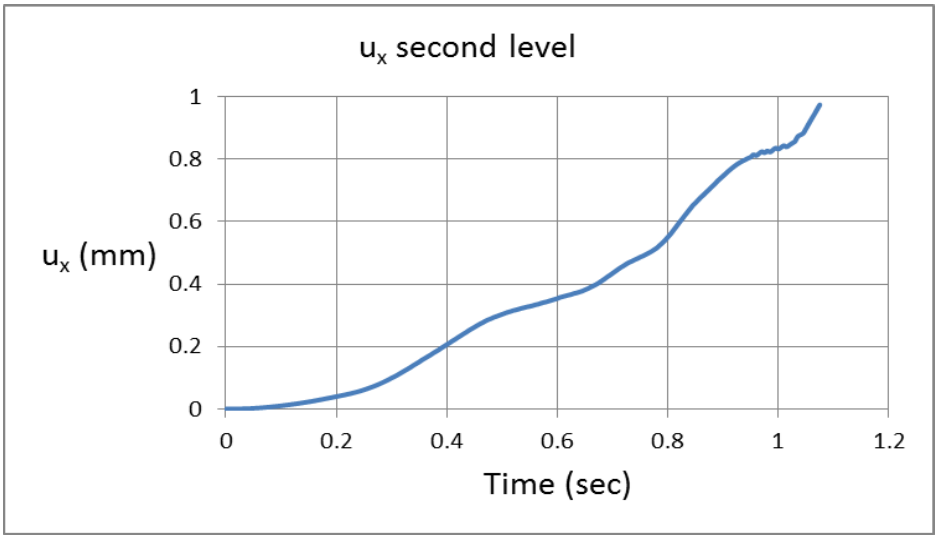

Figure (5.76) u_x at roof level of Model No. 3.

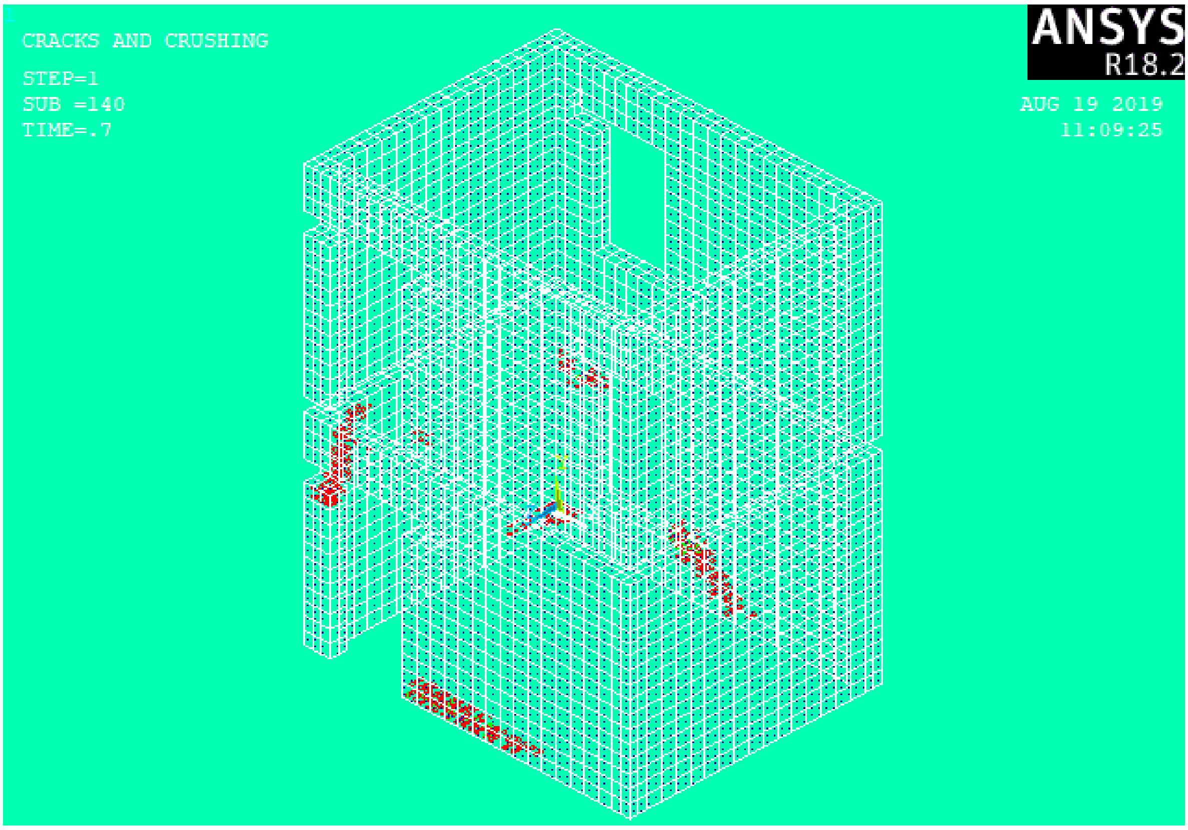

Figure (5.77) First cracks in Model No. 3.

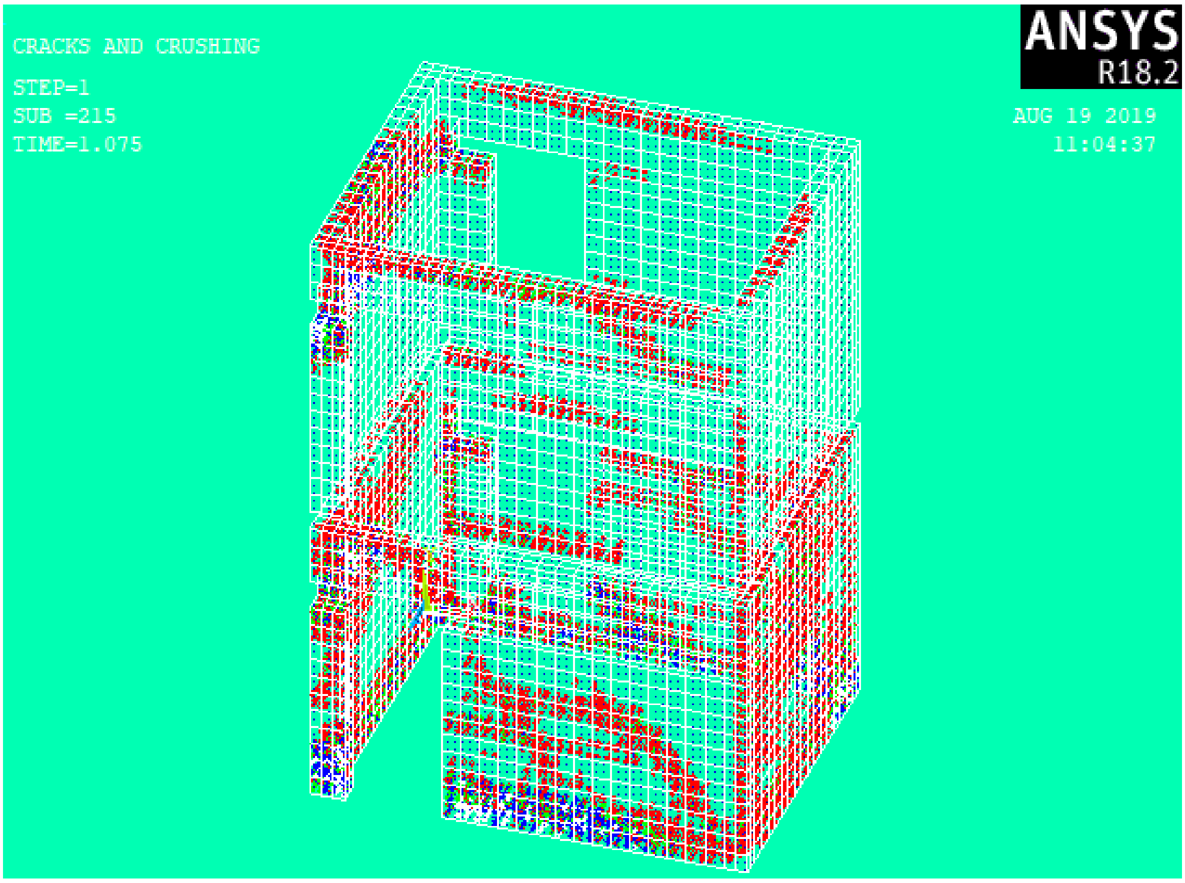

Figure (5.78) Crack pattern in Model No. 3.

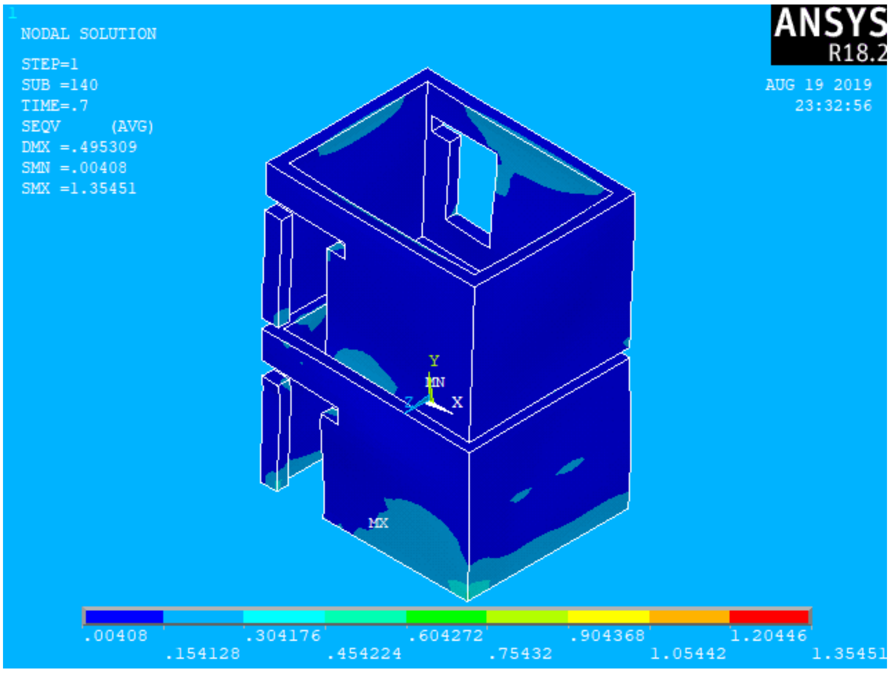

Figure (5.79) 1st principal stress in walls of Model No.3.

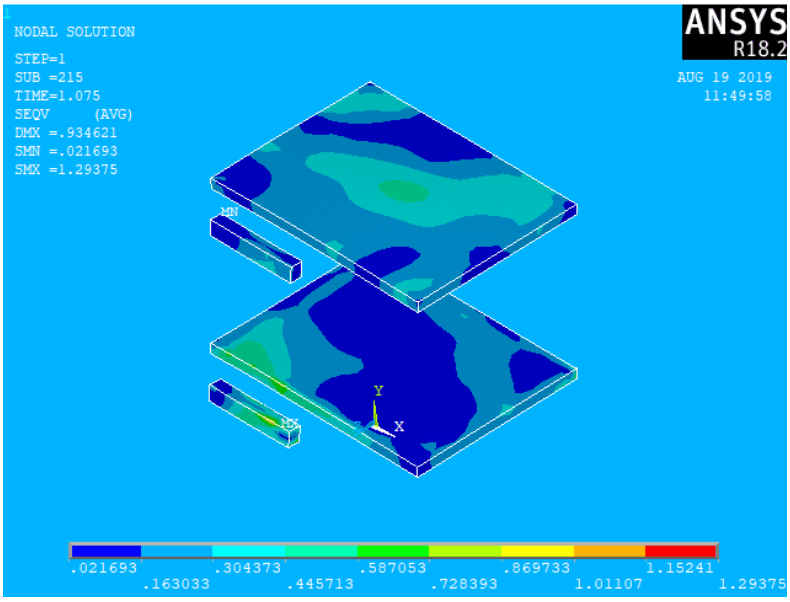

Figure (5.80) Von misses stress in concrete slabs and lintels.

The reduction in natural frequencies compared to Model No.1 is axiomatic since the mass is doubled while the stiffness is still the same. Fig. (5.77) shows that first cracks occur at the base of ground floor near the door opening and in diagonal paths towards the corners of windows and doors. The crack pattern shown in Fig. (5.78) denotes that severe damages occur at ground floor before the first one. The values of the first principal stress in masonry walls shown in Fig. (5.79) reveal that the highest stresses mainly occur at base of building and near the openings, while the Von misses stresses in concrete slab and lintels are maximum at the lintel over the door opening in ground floor.

5.10 Model No. 4

The model is a confined masonry room having the same plan and dimensions as those of Model No.1. The vertical confining components (tie columns) have a cross-section of (240*240) mm. They are reinforced with 4 Ø 12 mm longitudinal bars and Ø 6 mm @ 200 mm ties. The mechanical properties of concrete and reinforcement steel are as in Table (5.5).

Table (5.5) Mechanical properties of concrete and reinforcement steel.

property / material	Compressive Strength MPa	Tensile strength MPa	Modulus of elasticity MPa	Poisson's ratio
Concrete	25	3.5	24000	0.2
Steel	-----	400	200,000	0.3
masonry	5.5	0.15	2750	0.2

The FE model, shown in Fig. (5.81), is composed of 32728 solid elements and 6637 beam elements with 39072 nodes. The FE simulation of columns reinforcement is shown in Fig. (5.82). The seismic loading is the same loading used in Model No.1.

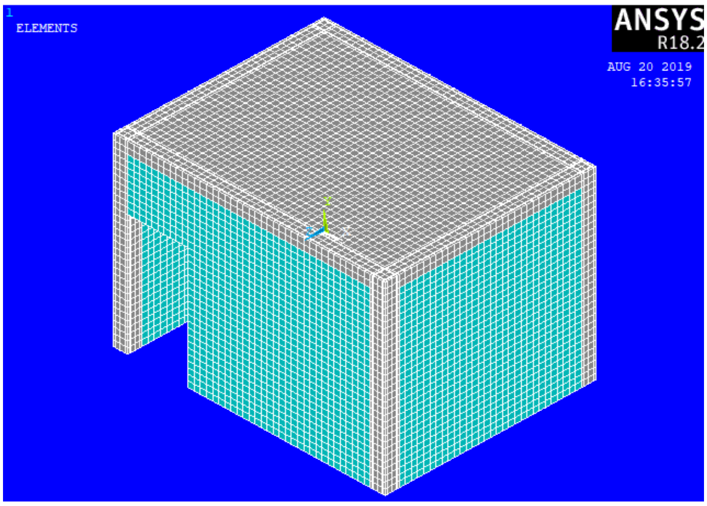

Figure (5.81) FE Model No.4.

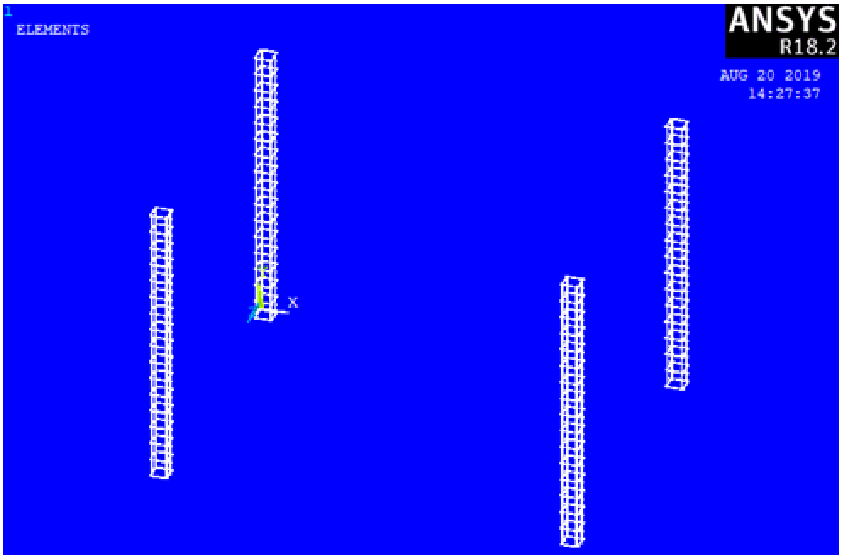

Figure (5.82) FE simulation of the reinforcement of confining columns of Model No.4.

The modal analysis results are illustrated in Figures (5.83) to (5.56) as follows:

Mechanical APDL 18.2 Output Window

***** PARTICIPATION FACTOR CALCULATION ***** X DIRECTION

MODE	FREQUENCY	PERIOD	PARTIC.FACTOR	RATIO	EFFECTIVE MASS	CUMULATIVE MASS FRACTION	RATIO EFF.MASS TO TOTAL MASS
1	0.859559	1.1634	138.35	1.000000	19141.6	0.944221	0.743909
2	0.911223	1.0974	-32.967	0.238279	1086.80	0.997831	0.422368E-01
3	1.13071	0.88440	6.6315	0.047932	43.9771	1.00000	0.170910E-02
sum					20272.4		0.787855

***** PARTICIPATION FACTOR CALCULATION ***** Y DIRECTION

MODE	FREQUENCY	PERIOD	PARTIC.FACTOR	RATIO	EFFECTIVE MASS	CUMULATIVE MASS FRACTION	RATIO EFF.MASS TO TOTAL MASS
1	0.859559	1.1634	6.2436	0.200085	38.9830	0.380744E-01	0.151501E-02
2	0.911223	1.0974	-3.3365	0.106922	11.1322	0.489472E-01	0.432637E-03
3	1.13071	0.88440	-31.205	1.000000	973.748	1.00000	0.378433E-01
sum					1023.86		0.397909E-01

***** PARTICIPATION FACTOR CALCULATION ***** Z DIRECTION

MODE	FREQUENCY	PERIOD	PARTIC.FACTOR	RATIO	EFFECTIVE MASS	CUMULATIVE MASS FRACTION	RATIO EFF.MASS TO TOTAL MASS
1	0.859559	1.1634	32.870	0.241792	1080.46	0.537814E-01	0.419904E-01
2	0.911223	1.0974	135.94	1.000000	18480.9	0.973696	0.718234
3	1.13071	0.88440	-22.988	0.169097	528.439	1.00000	0.205370E-01
sum					20089.8		0.780761

Figure (5.83) ANSYS report for modal analysis of Model No.4.

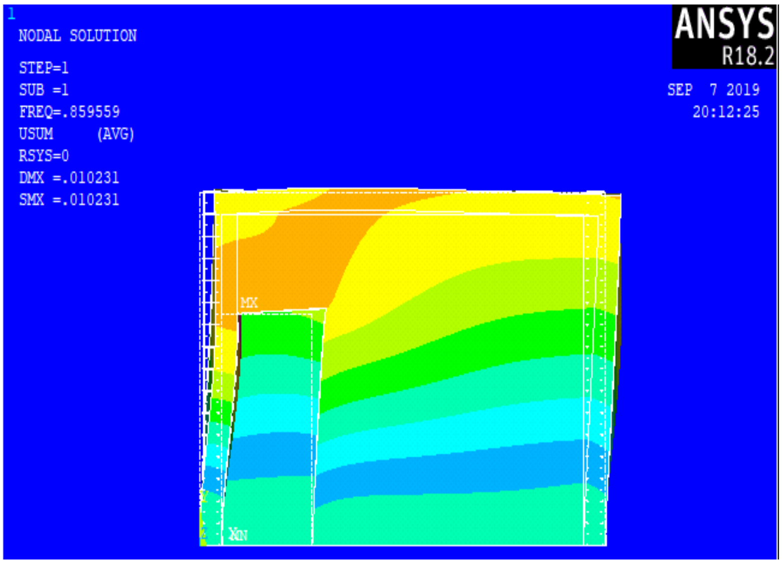

Figure (5.84) 1st mode of Model No.4.

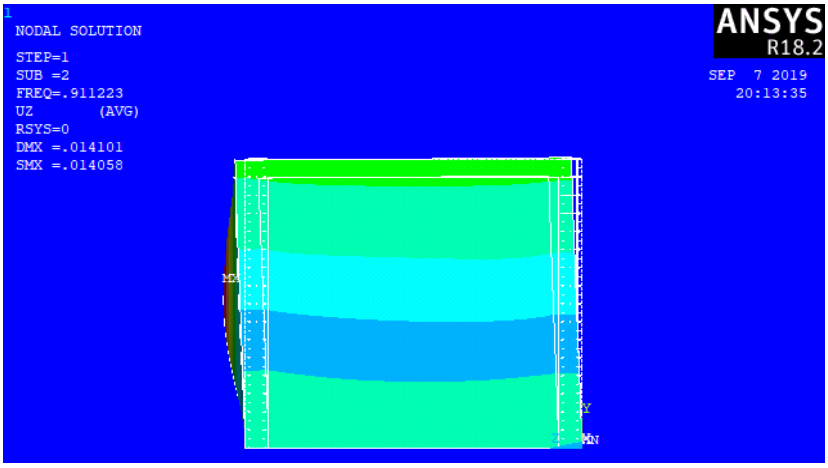

Figure (5.85) 2nd mode of Model No.4.

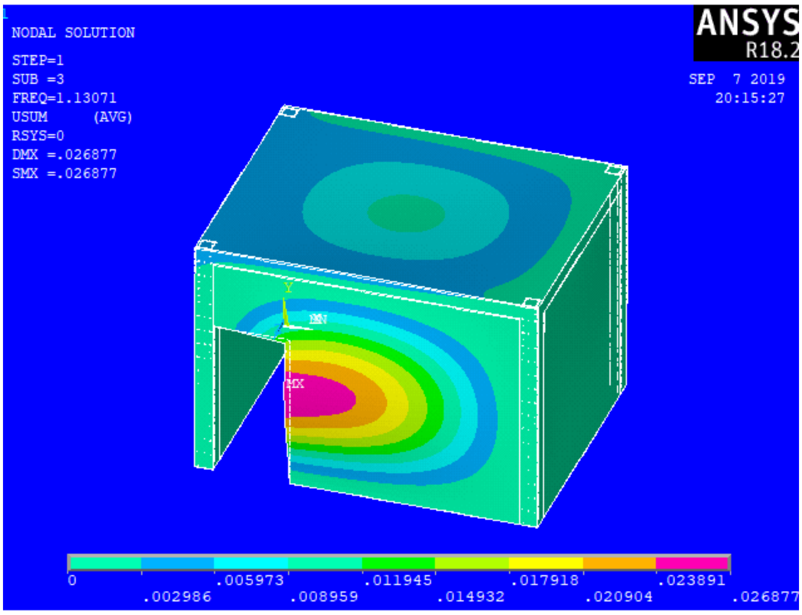

Figure (5.86) 3rd mode of Model No.4.

The responses u_z and u_x at roof level are shown in Figures (5.87) and (5.88), respectively.

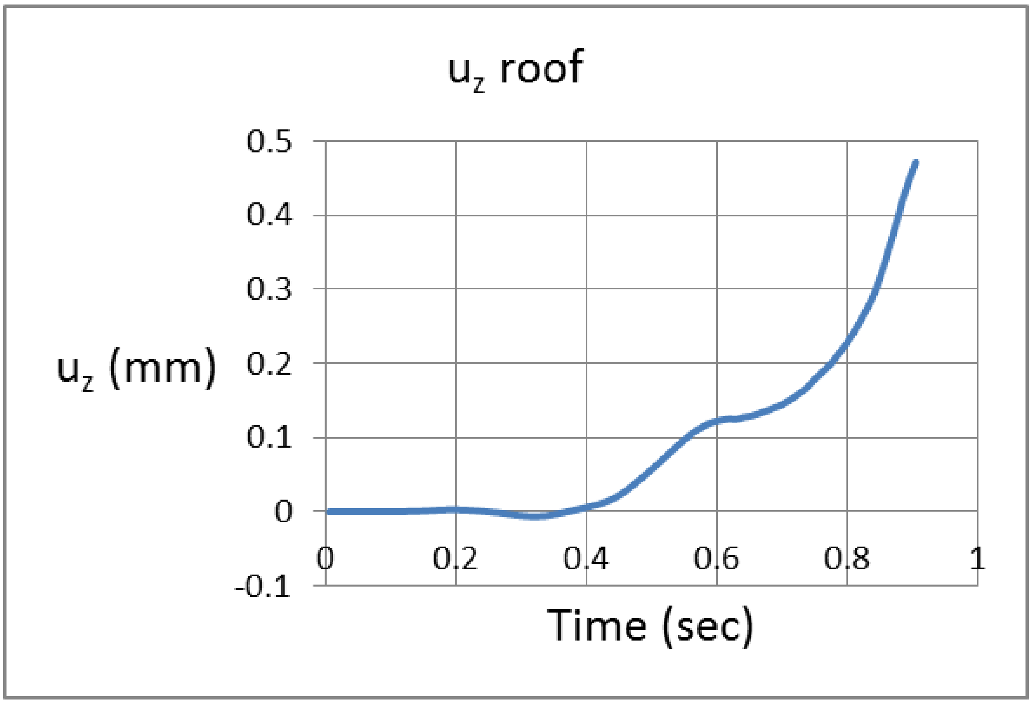

Figure (5.87) u_z at roof level of Model No.4.

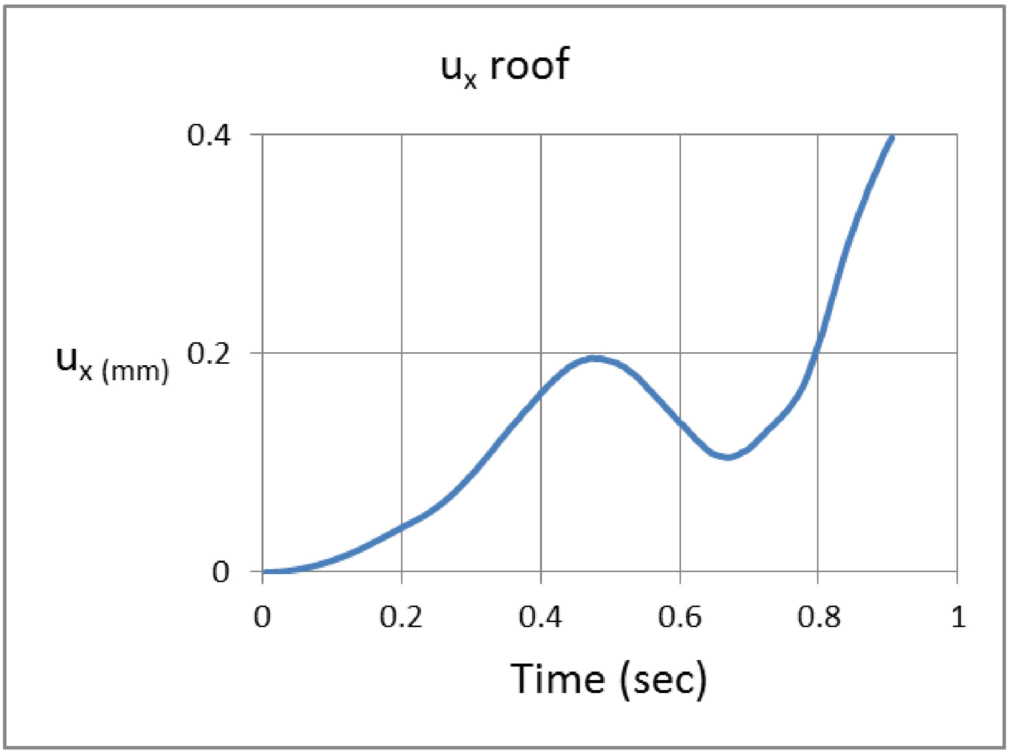

Figure (5.88) u_x at roof level of Model No.4.

Figures (5.89) and (5.90) show the crack pattern in masonry walls and in concrete frame (slab and confining tie columns), respectively.

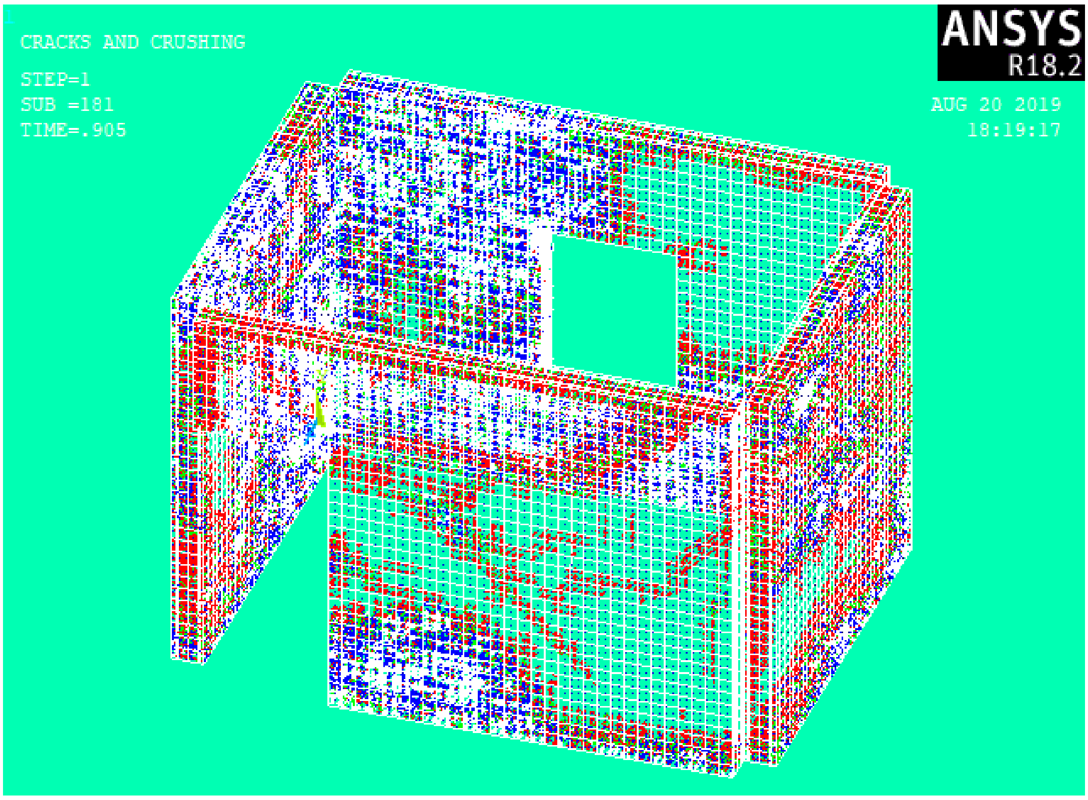

Figure (5.89) Crack pattern in masonry walls of Model No.4.

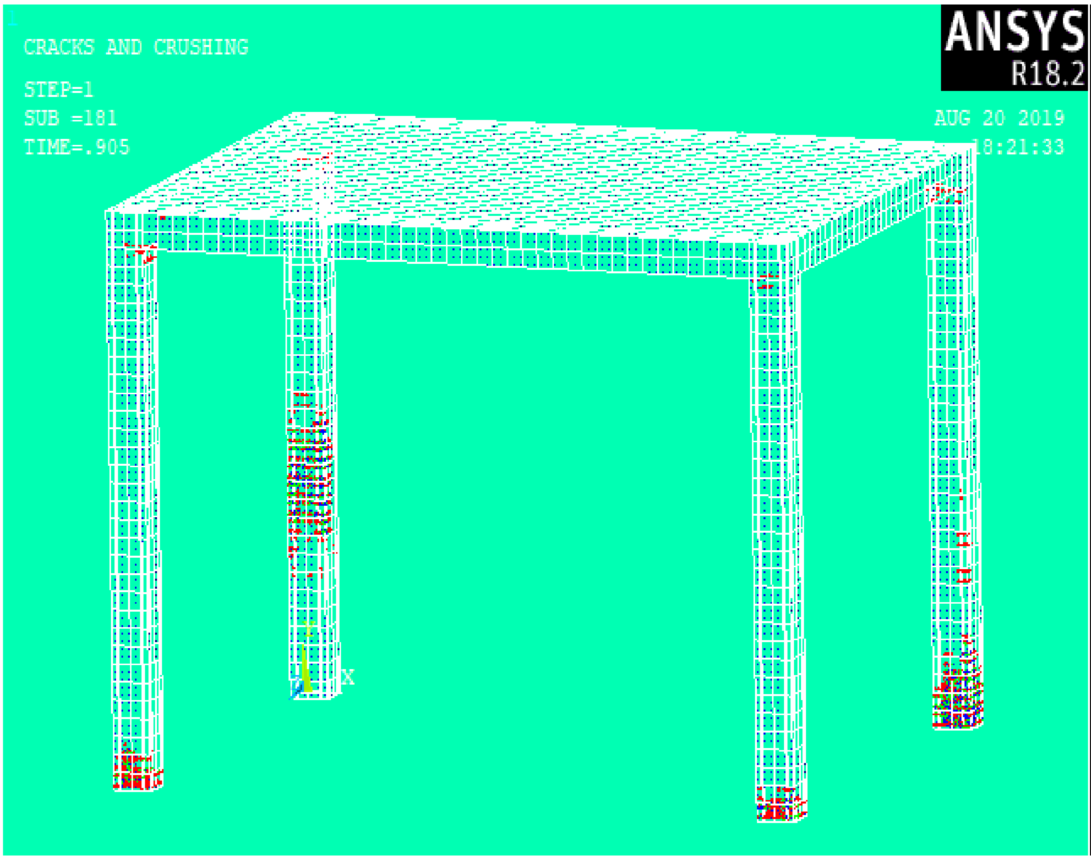

Figure (5.90) Crack pattern in concrete frame of Model No.4.

The stress in steel reinforcement is shown in Fig. (5.91) as follows:

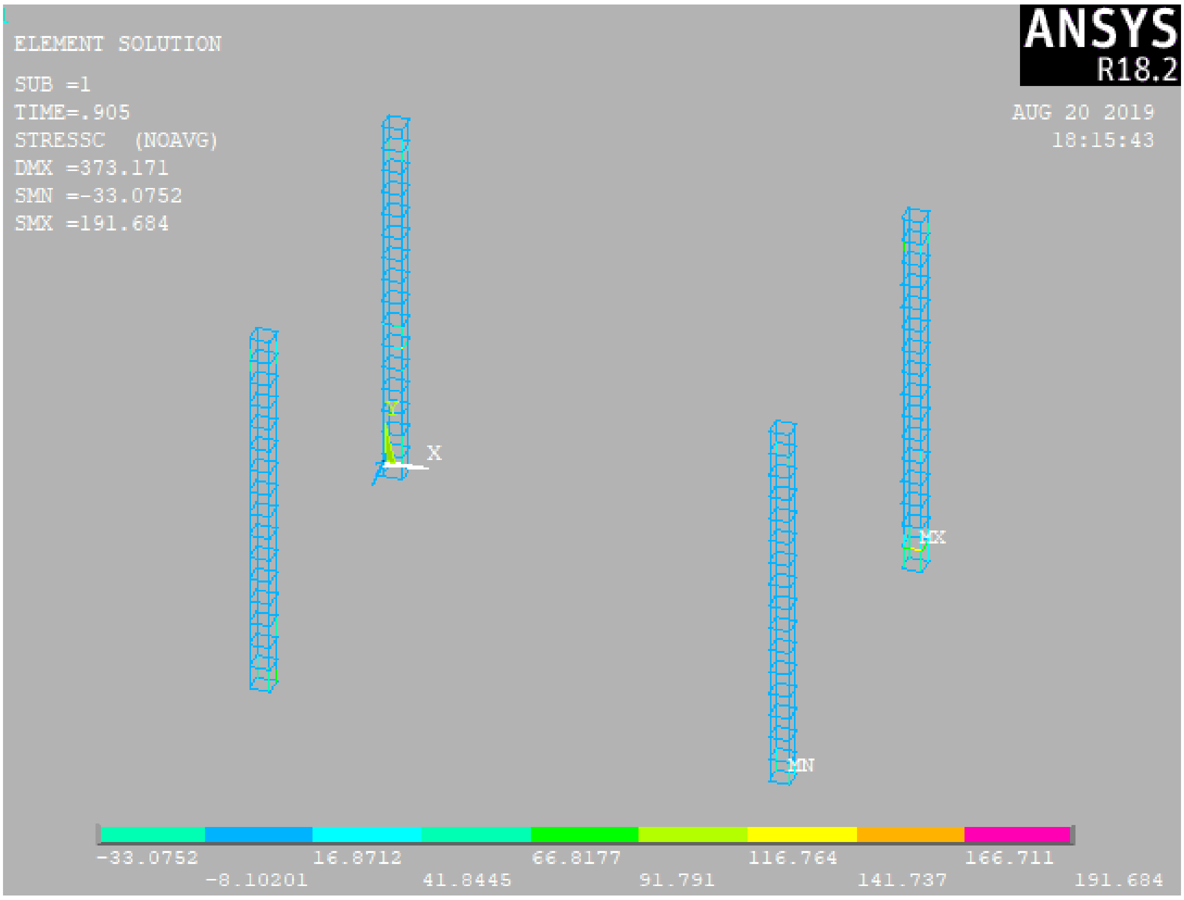

Figure (5.91) Stress in steel reinforcement of columns in Model No.4.

The increase in natural frequencies for the calculated modes compared to the corresponding ones of Model No.1 indicate the enhancing of stiffness provided by the existence of the four confining columns. The few cracks that appeared in the concrete frame compared to the severe cracks in masonry walls and the relatively low tensile stresses in reinforcement give good indication for the ability of the confinement to prevent the disintegration of damaged masonry walls during an earthquake.

5.11 Model No.5

The model is the same as Model No.4 but retrofitted with two plaster layers reinforced with steel wire mesh of 6 mm diameter for bars and (15*15) cm openings. The yield stress of steel mesh is taken as (fy =300 MPa) from previous tests. For simplicity in modeling, only the vertical bars were modeled. The FE model shown in Fig. (5.92) is built up of 26048 solid element and 7760 beam elements with 23256 nodes.

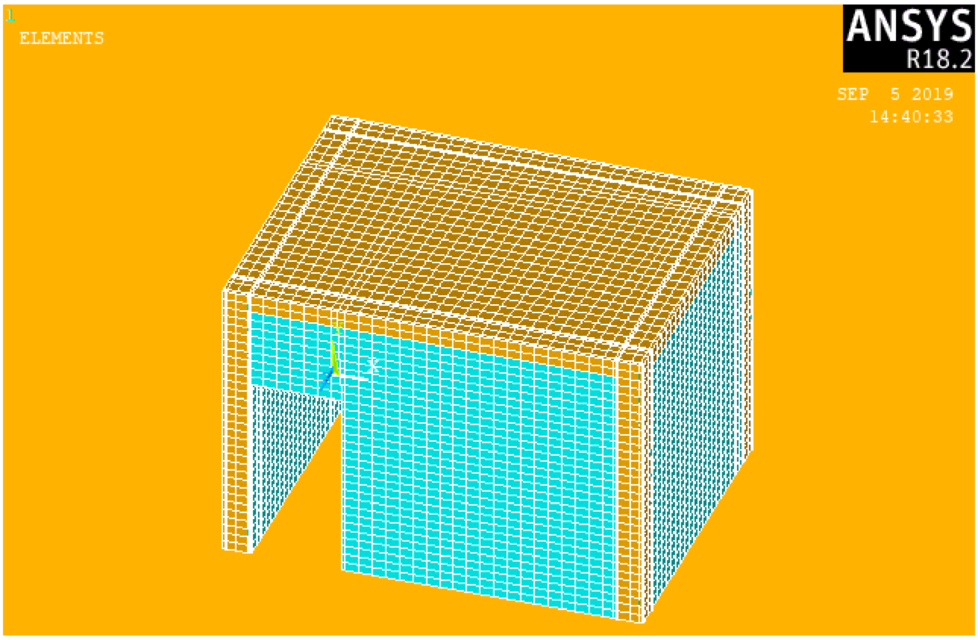

Figure (5.92) FE Model No.5.

The modal analysis results are illustrated in Figures (5.93) to (5.96) that follow:

Mechanical APDL 18.2 Output Window

***** PARTICIPATION FACTOR CALCULATION ***** X DIRECTION

MODE	FREQUENCY	PERIOD	PARTIC.FACTOR	RATIO	EFFECTIVE MASS	CUMULATIVE MASS FRACTION	RATIO EFF.MASS TO TOTAL MASS
1	1.18319	0.84517	156.45	1.000000	24477.4	0.929145	0.712090
2	1.26347	0.79147	-41.877	0.267663	1753.65	0.995712	0.510168E-01
3	1.65286	0.60501	-10.628	0.067933	112.961	1.00000	0.328622E-02
sum					26344.0		0.766393

***** PARTICIPATION FACTOR CALCULATION ***** Y DIRECTION

MODE	FREQUENCY	PERIOD	PARTIC.FACTOR	RATIO	EFFECTIVE MASS	CUMULATIVE MASS FRACTION	RATIO EFF.MASS TO TOTAL MASS
1	1.18319	0.84517	6.4611	0.096009	41.7455	0.912671E-02	0.121445E-02
2	1.26347	0.79147	-1.8535	0.027543	3.43561	0.987782E-02	0.999479E-04
3	1.65286	0.60501	67.296	1.000000	4528.81	1.00000	0.131751
sum					4573.99		0.133065

***** PARTICIPATION FACTOR CALCULATION ***** Z DIRECTION

MODE	FREQUENCY	PERIOD	PARTIC.FACTOR	RATIO	EFFECTIVE MASS	CUMULATIVE MASS FRACTION	RATIO EFF.MASS TO TOTAL MASS
1	1.18319	0.84517	41.577	0.266379	1728.66	0.662516E-01	0.502896E-01
2	1.26347	0.79147	156.08	1.000000	24361.9	0.999931	0.708728
3	1.65286	0.60501	1.3437	0.008609	1.80543	1.00000	0.525231E-04
sum					26092.3		0.759070

Figure (5.93) ANSYS report for modal analysis of Model No.5

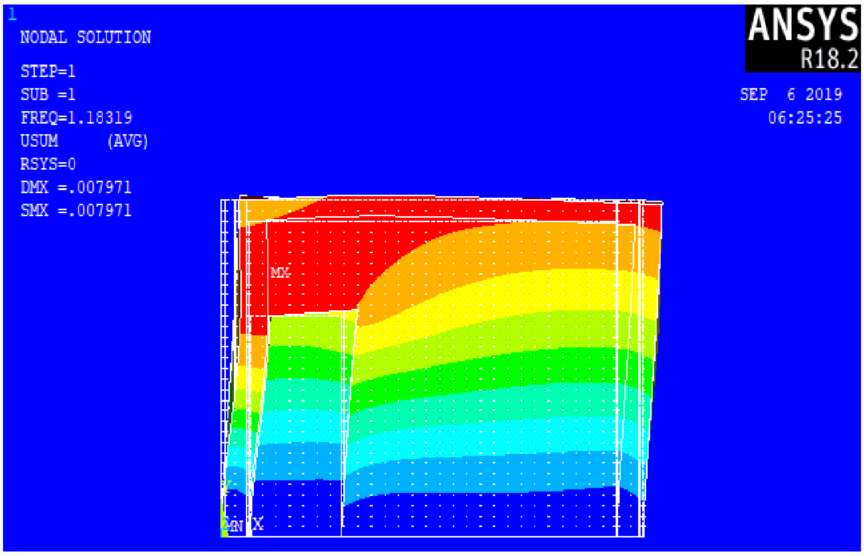

Figure (5.94) 1st mode of Model No.5.

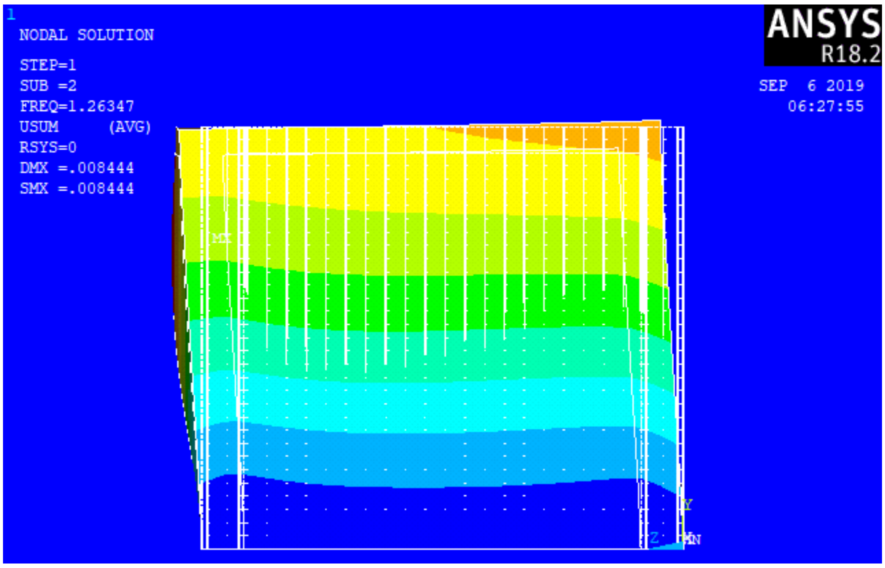

Figure (5.95) 2nd mode of Model No.5.

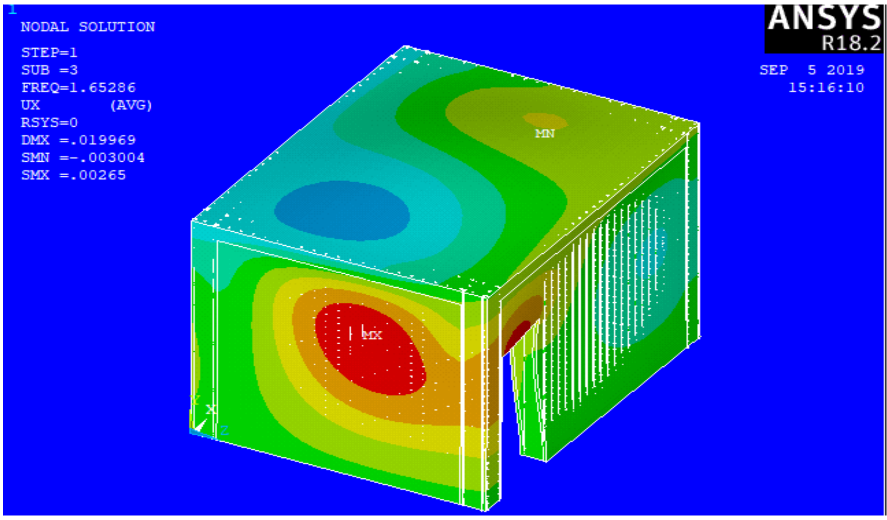

Figure (5.96) 3rd mode of Model No.5.

The seismic loading applied to the model is the earthquake described in Table (5.6) that follows:

Table (5.6) Description of the seismic records applied to Model No. 5

Event name	Year	station	M_w	PGA g	V_{s30} m/sec.
Mammoth Lake-01	1980	Mammoth Lakes H.S.	6.06	0.324	346.82

The accelerograms of the earthquake mentioned above are shown in Figures (5.97) to (5.99) as follows:

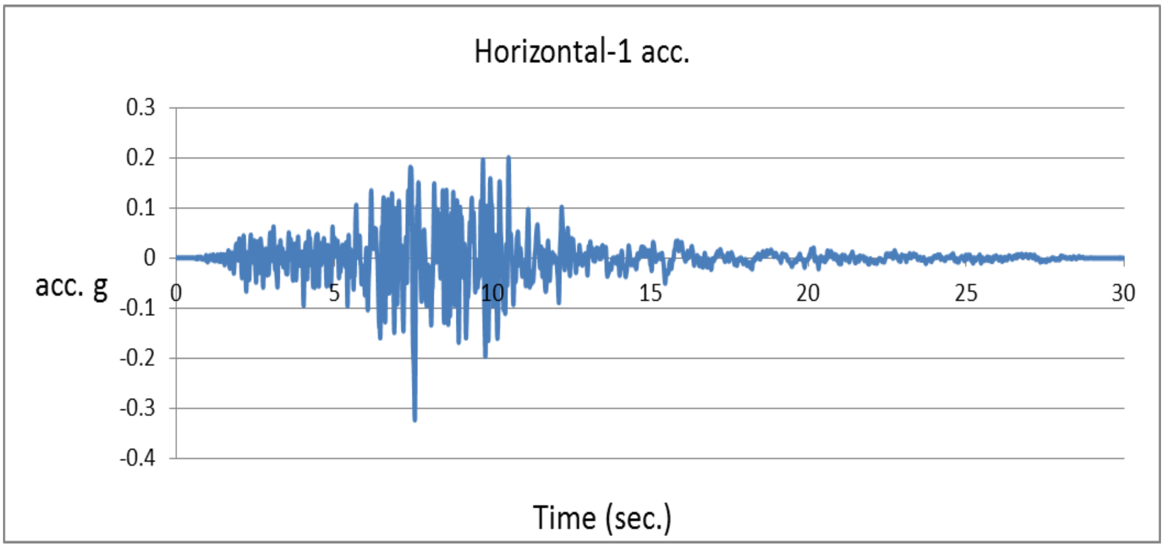

Figure (5.97) H -1 component of $\ddot{u}_g$ of Mammoth, 1980 event.

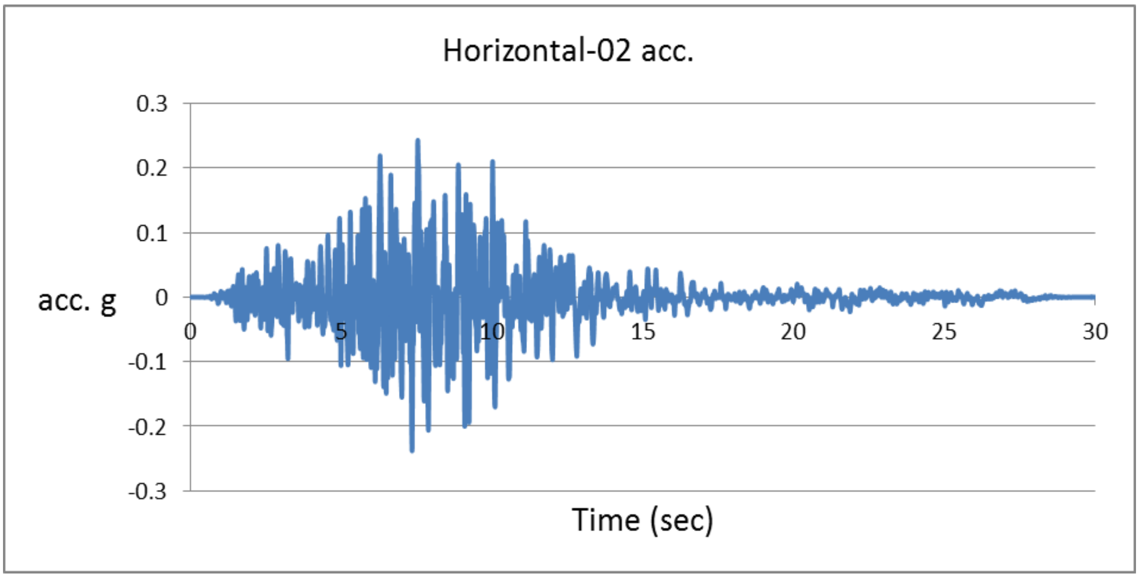

Figure (5.98) H-2 component of $\ddot{u}_g$ of Mammoth, 1980 event.

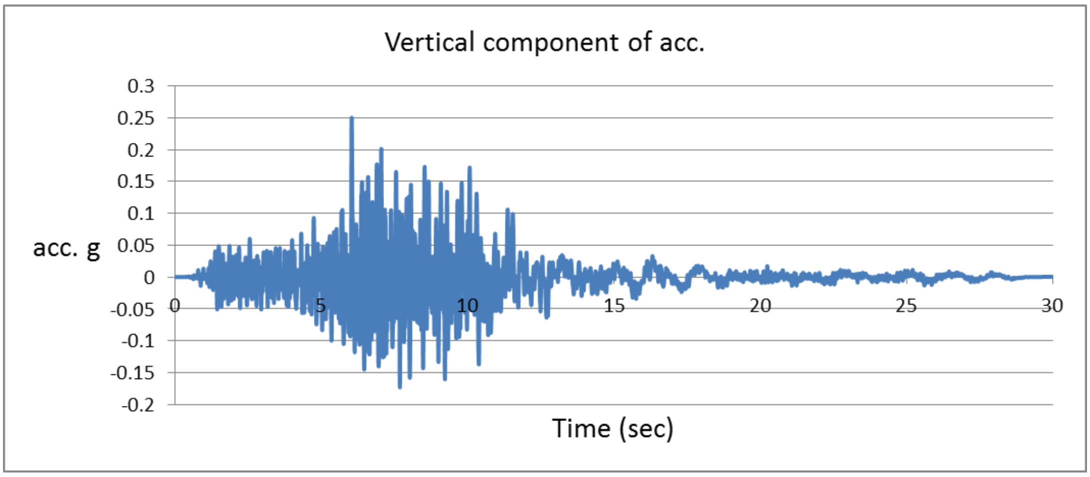

Figure (5.99) vertical component of $\ddot{u}_g$ of Mammoth, 1980 event.

The total displacements in z-direction at base level is as shown in Fig. (5.100), For verification purpose the ground displacement applied at the same direction is as shown in Fig. (5.101). It can be obviously seen that the two displacement are the same. The structural responses in z- and x-direction are shown in Figures (5.102) and (5.103). The crack patterns in masonry walls, concrete frame, and plaster retrofitting layers are shown in Figures (5.104) to (5.106). The stresses in steel reinforcement are shown in Fig. (5.107).

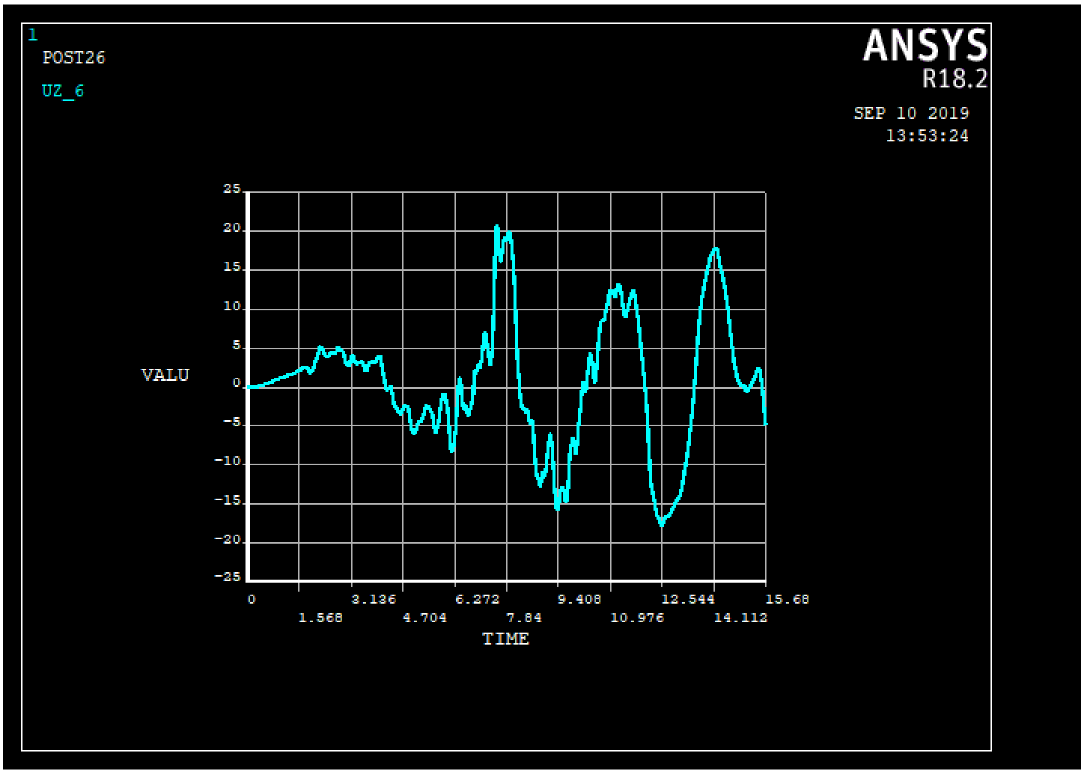

Figure (5.100) u_z^t at base level of Model No.5 (mm).

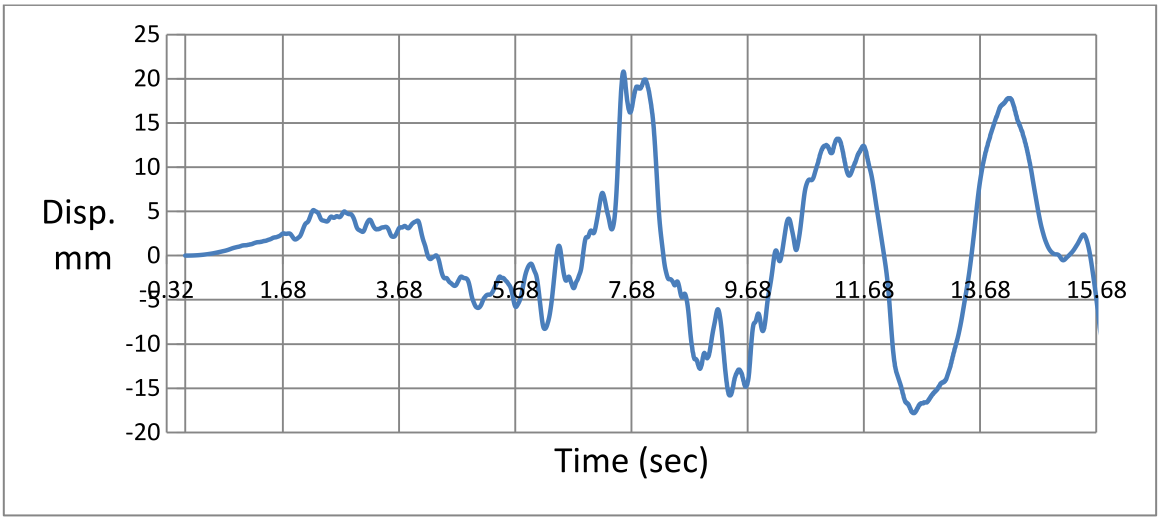

Figure (5.101) H -1 component of u_g of Mammoth, 1980 event.

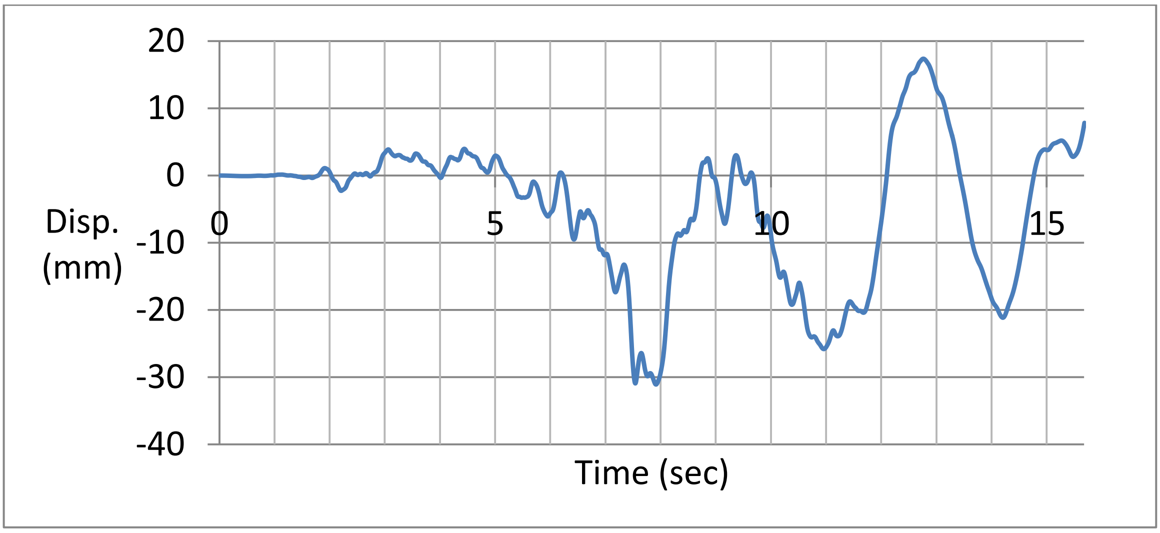

Figure (5.102) Response u_z at roof level of Mode No.5

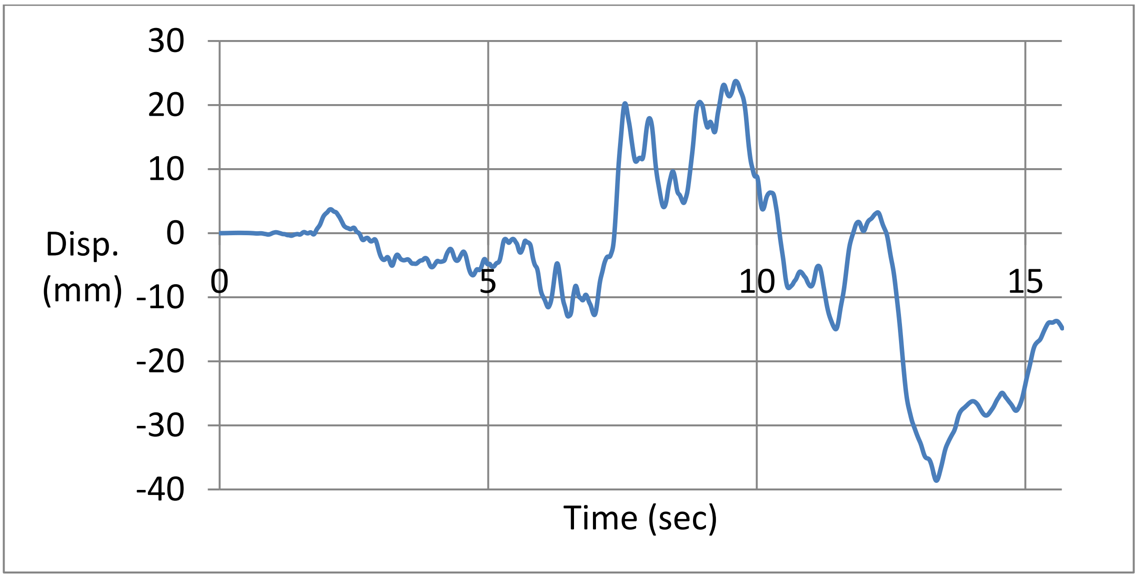

Figure (5.103) Response u_x at roof level of Mode No.5

In Fig. (5.102), the maximum displacement (u_z) is 31.08 mm, which corresponds a drift of (31.08/3000 = 1.036%). The maximum displacement in x-direction is 38.68 mm, as shown in Fig. (5.102). This displacements corresponds a draft of (38.68/3000 = 1.289%). This value of the drift is higher than the ultimate one of the wall tested by Naseer which was (12/995 = 1.2%). This represents a significant structural benefit of the existence of the retrofitting.

` From Figures (5.97) to (5.99), it can be seen that the ground acceleration components approximately vanish beyond the time 15 seconds. Therefore, the analysis was stopped at time 15,68 seconds to avoid excessive cost in time of computer running.

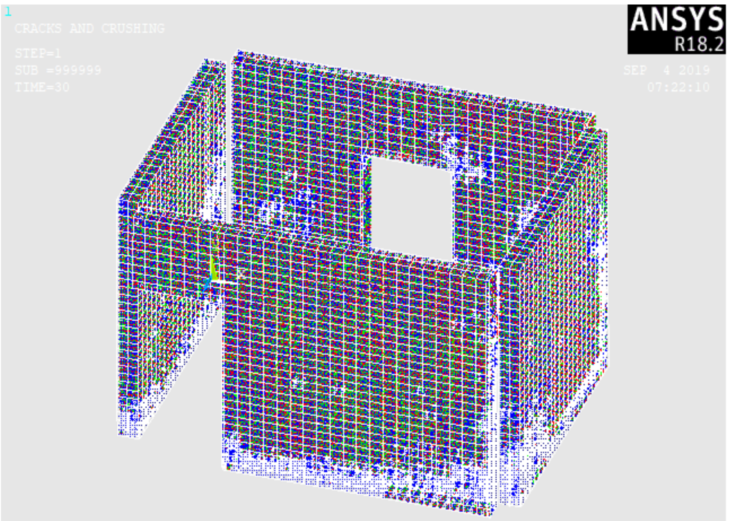

Figure (5.104) Crack pattern in masonry walls of Model No.5.

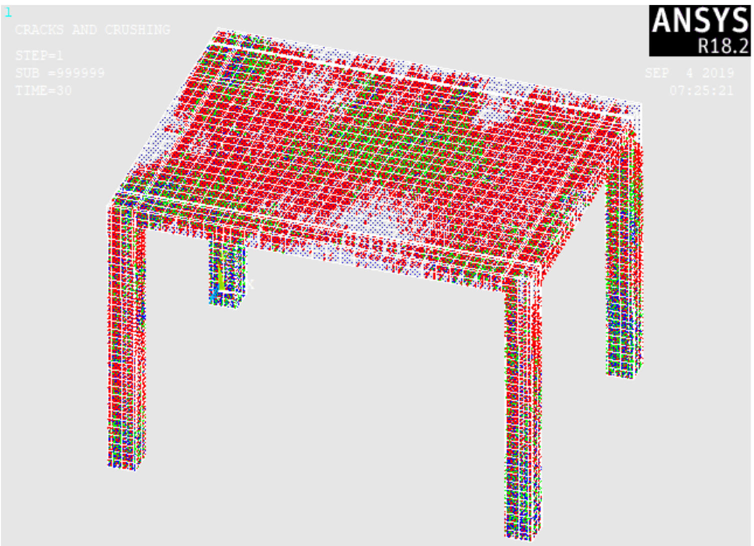

Figure (5.105) Crack pattern in concrete frame of Model No.5.

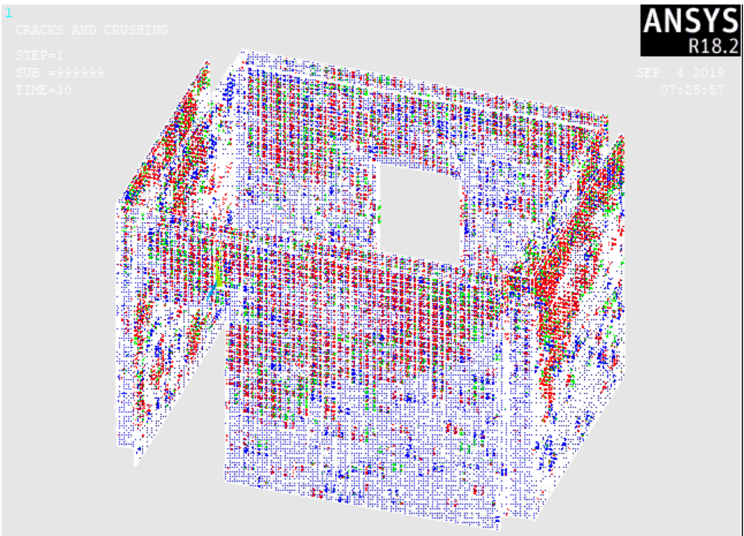

Figure (5.106) Crack pattern in retrofitting layers of Model No.5.

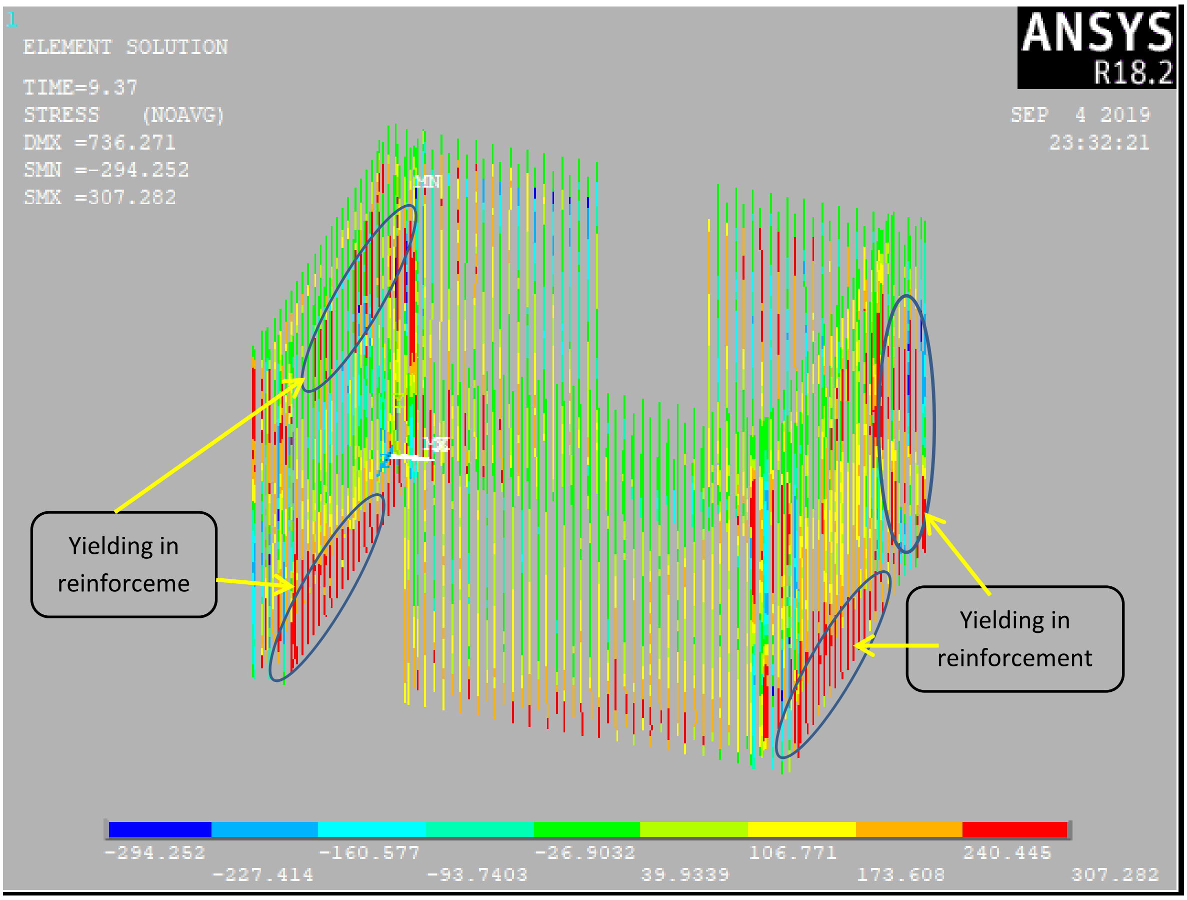

Figure (5.107) Stress in steel reinforcement of Model No.5.

Through the modal analysis results, it can be observed that a significant enhancing in lateral stiffness of the building is obtained after the application of the retrofitting; the significant increase in natural frequencies denote the considerable increase in stiffness. The crack patterns and the yielding of reinforcement indicate that the retrofitting together with the confinement cannot prevent masonry damages, but it prevents the disintegration of damaged masonry walls. From Fig. (5.102), it can be observed that severe cracks occurred in the diaphragm (the concrete slab). This is a reasonable matter since significant deformation occurred. However, the simulation of the reinforcement of the concrete slab is out of the objectives of the study.

5.12 Model No.6

The model is the same as Model No. 3 but retrofitted with two plaster layers simulated with reinforced Solid65 element. The smeared reinforcement was calculated to be equivalent to the use of steel wire mesh of the same properties mentioned in Model No.5. Both vertical and horizontal bars were smeared in the plastering layers. The FE model is shown in Fig. (5.108) as follows:

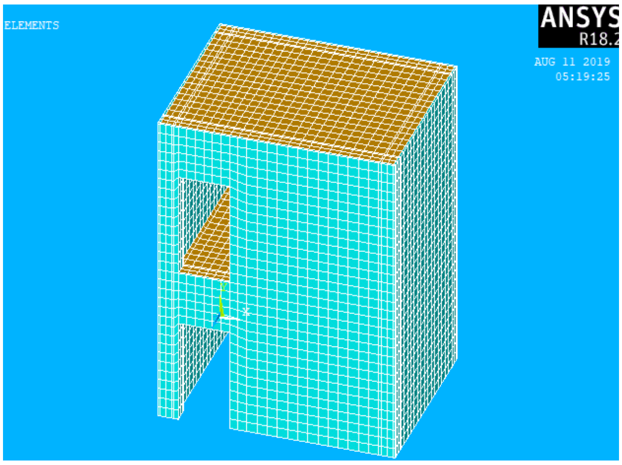

Figure (5.108) FE Model No.6.

The modal analysis outputs are illustrated in Figures (5.109) to (5.112) as follows:

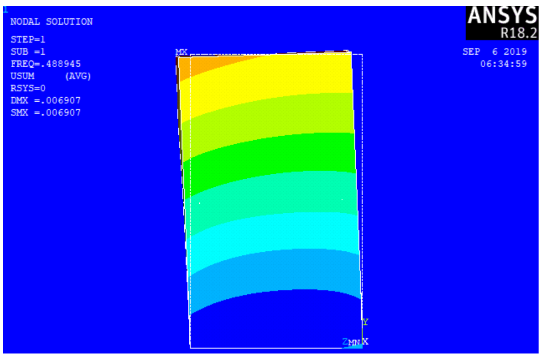

Figure (5.109) 1^{st} mode of Model No.6.

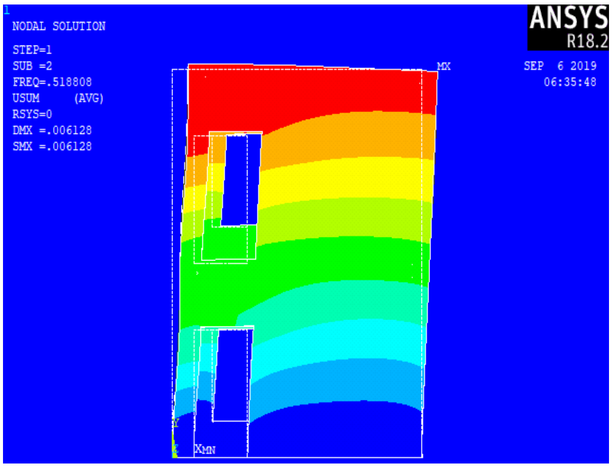

Figure (5.110) 2nd mode of Model No.6.

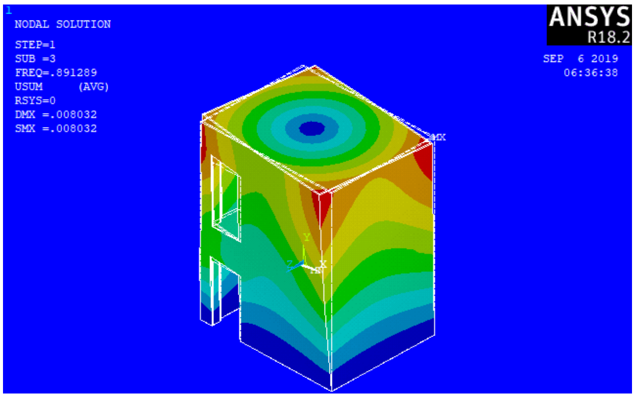

Figure (5.111) 3rd mode of Model No.6.

Mechanical APDL 18.2 Output Window

***** PARTICIPATION FACTOR CALCULATION ***** X DIRECTION

MODE	FREQUENCY	PERIOD	PARTIC.FACTOR	RATIO	EFFECTIVE MASS	CUMULATIVE MASS FRACTION	RATIO EFF.MASS TO TOTAL MASS
1	0.488945	2.0452	54.227	0.250939	2940.58	0.591396E-01	0.436419E-01
2	0.518808	1.9275	216.10	1.000000	46697.9	0.998306	0.693055
3	0.891289	1.1220	9.1785	0.042474	84.2447	1.00000	0.125030E-02
sum					49722.7		0.737947

***** PARTICIPATION FACTOR CALCULATION ***** Y DIRECTION

MODE	FREQUENCY	PERIOD	PARTIC.FACTOR	RATIO	EFFECTIVE MASS	CUMULATIVE MASS FRACTION	RATIO EFF.MASS TO TOTAL MASS
1	0.488945	2.0452	1.5735	0.270795	2.47595	0.674486E-01	0.367462E-04
2	0.518808	1.9275	5.8107	1.000000	33.7645	0.987245	0.501107E-03
3	0.891289	1.1220	-0.68427	0.117760	0.468223	1.00000	0.694901E-05
sum					36.7087		0.544802E-03

***** PARTICIPATION FACTOR CALCULATION ***** Z DIRECTION

MODE	FREQUENCY	PERIOD	PARTIC.FACTOR	RATIO	EFFECTIVE MASS	CUMULATIVE MASS FRACTION	RATIO EFF.MASS TO TOTAL MASS
1	0.488945	2.0452	210.69	1.000000	44388.6	0.931325	0.658782
2	0.518808	1.9275	-53.132	0.252185	2822.99	0.990555	0.418966E-01
3	0.891289	1.1220	21.218	0.100707	450.186	1.00000	0.668131E-02
sum					47661.8		0.707360

Figure (5.112) ANSYS report for modal analysis of Model No.6

The seismic loading is the same loading in Model No.2 neglecting the damping and taking the tensile strength of masonry with a value of 0.15 MPa. The crack patterns in masonry walls and retrofitting layers are shown in Figures (5.113) and (5.114), respectively.

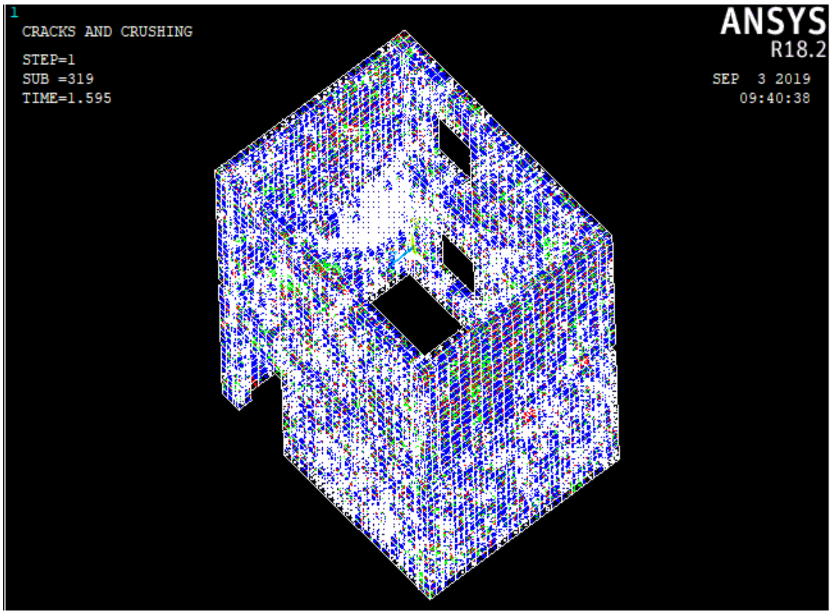

Figure (5.113) Crack pattern in masonry walls of Model No.6.

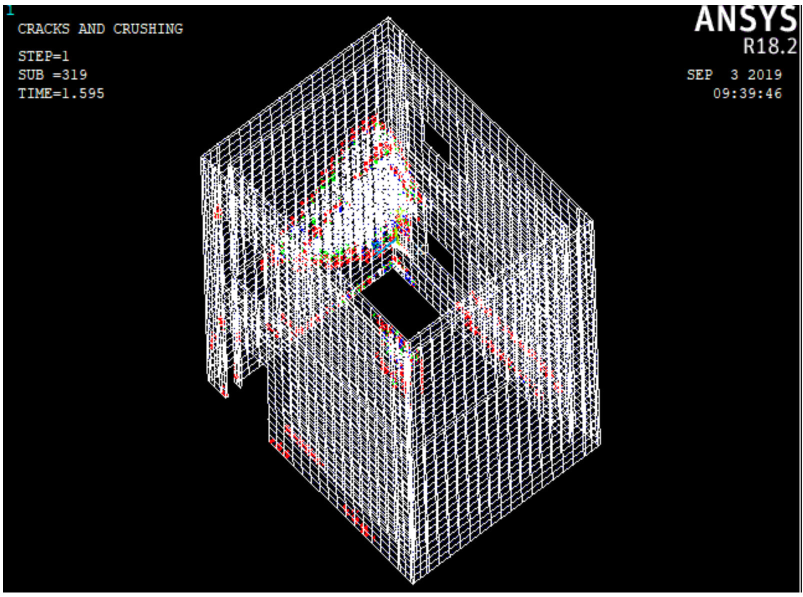

Figure (5.114) Crack pattern in retrofitting layers of Model No.6.

Increases in natural frequencies can be noted for the model compared to the URM building with the same dimensions (Model No.3). The crack patterns show that the reinforced plaster layers are still having few cracks while masonry is approximately damaged.

5.13 Model No.7

The model is an URM Wall of an aspect ratio equals 1 (height = length = 3 m) and the thickness is 0.24 m. A static load is applied in z-direction (out-of-plane direction). A constant overburden pressure of 0.1 MPa was applied at the top of the wall. 100 mm length was used for the element size, and thus the FE model, shown in Fig. (5.115), is built up of 2700 elements with 3844 nodes. The deflected shape in z-direction is shown in Fig. (5.116).

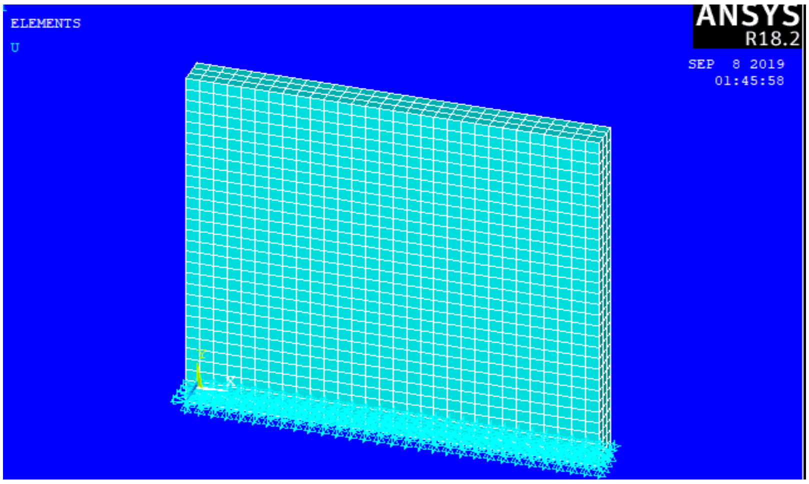

Figure (5.115) FE Model No.7.

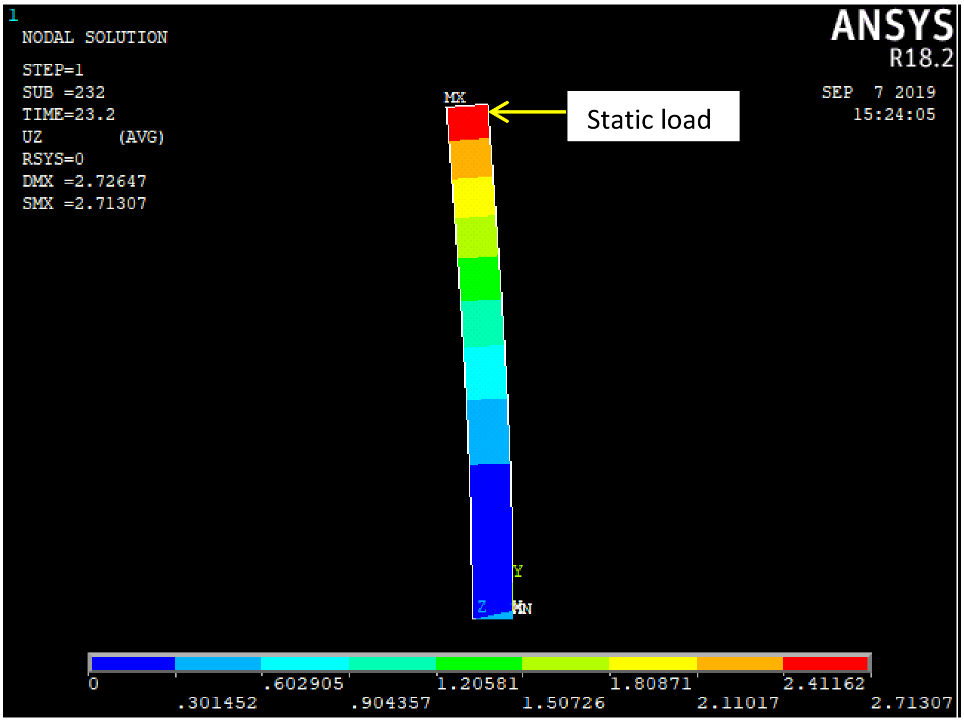

Figure (5.116) Deflected shape of Model No.7.

The lateral load capacity is 2.923 KN as shown in Fig. (5.117) that follows:

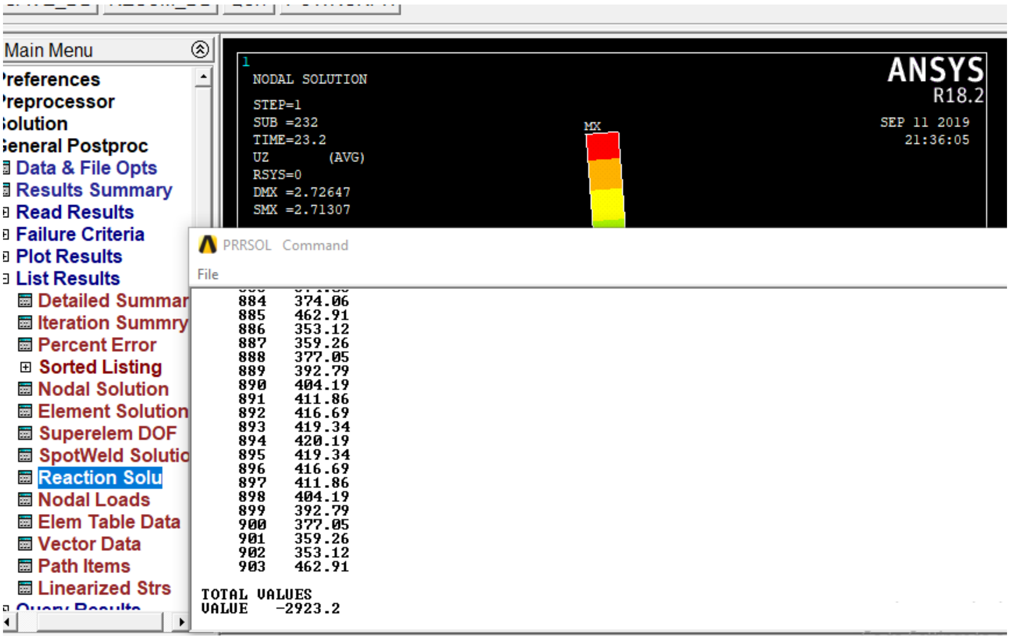

Figure (5.117) Reaction in z-direction for Model No.7.

The wall was analyzed under the effect of a static in-plane load with the same overburden pressure and the same tensile strength of masonry, which is 0.15 MPa. The load at which the solution terminated is 41 KN, as shown in Fig. (5.118).

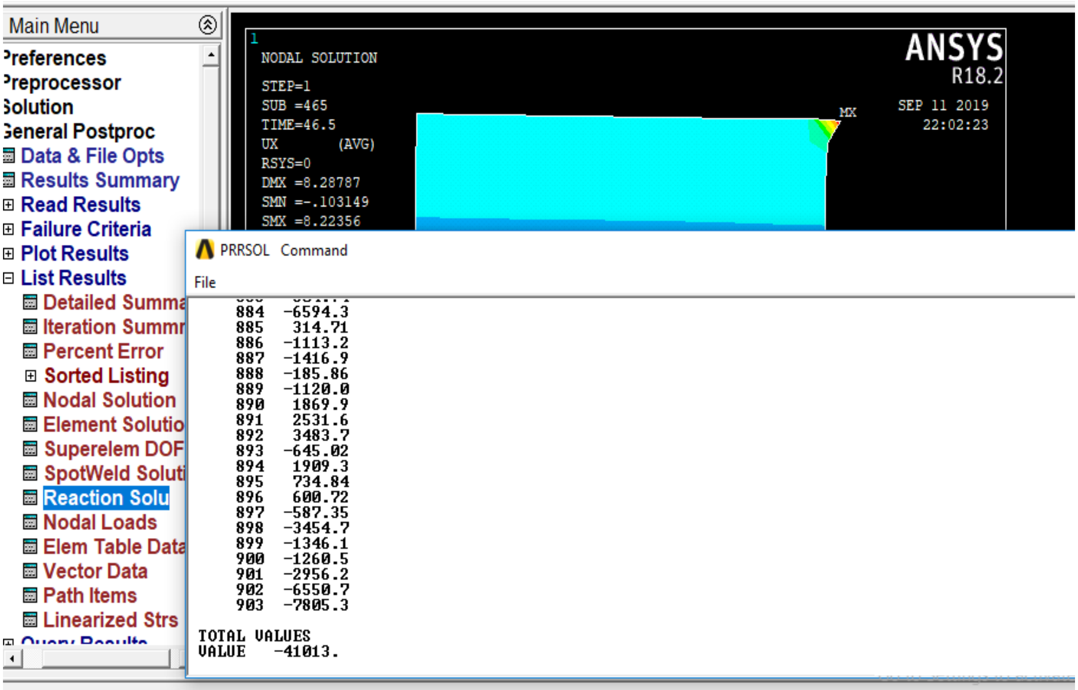

Figure (5.118) Ultimate in-plane load for Model No.7 having f_t= 0.15 MPa.

The compressive strength was increased from 5.5 MPa to 10 MPa keeping other properties and conditions unchanged, and the analysis was repeated. It was observed that the solution did not converge and terminated at the same load of the case before increasing the CS. This means that the in-plane load capacity does not increase with the increase of CS of masonry if the so low tensile strength of it is still not increased. The tensile strength was increased from 0.15 MPa to 0.3 MPa and the analysis was repeated using the CS unchanged (5.5 MPa). A notable increase in the in-plane load capacity was observed as the solution terminated at a load of 57.834 KN, as shown in Fig. (5.119).

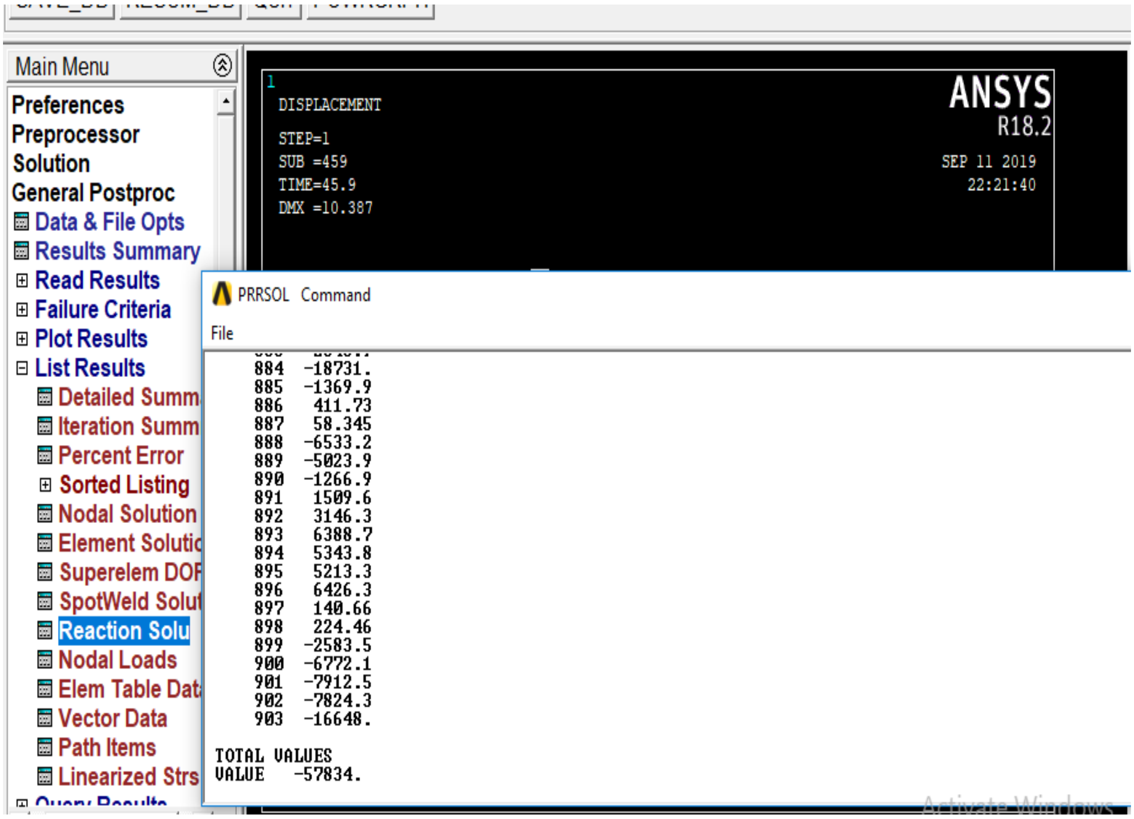

Figure (5.119) Ultimate in-plane load for Model No.7 having f_t= 0.3 MPa.

5.14 Model No.8

The model is the same as Model No.7 but retrofitted with tow plaster layers reinforced as in Model No.4. The FE model shown in Fig. (5.120) is composed of 20520 solid elements and 2520 beam elements with 22326 nodes. The tensile strength of masonry was used as 0.15 MPa. As that used in Model No.7, the overburden pressure of 0.1 MPa was applied. A static out-of-plane load was applied. The deflected shape and the ultimate out-of-plane load are shown in Figures (5.121) and (5.122). The ultimate in-plane load is shown in Fig. (5.123).

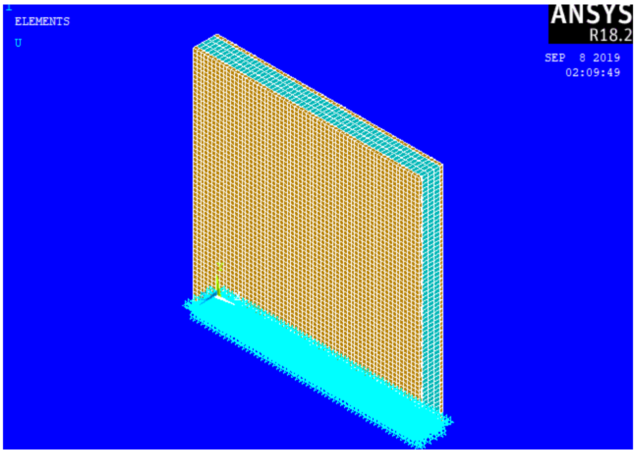

Figure (5.120) FE Model No.8.

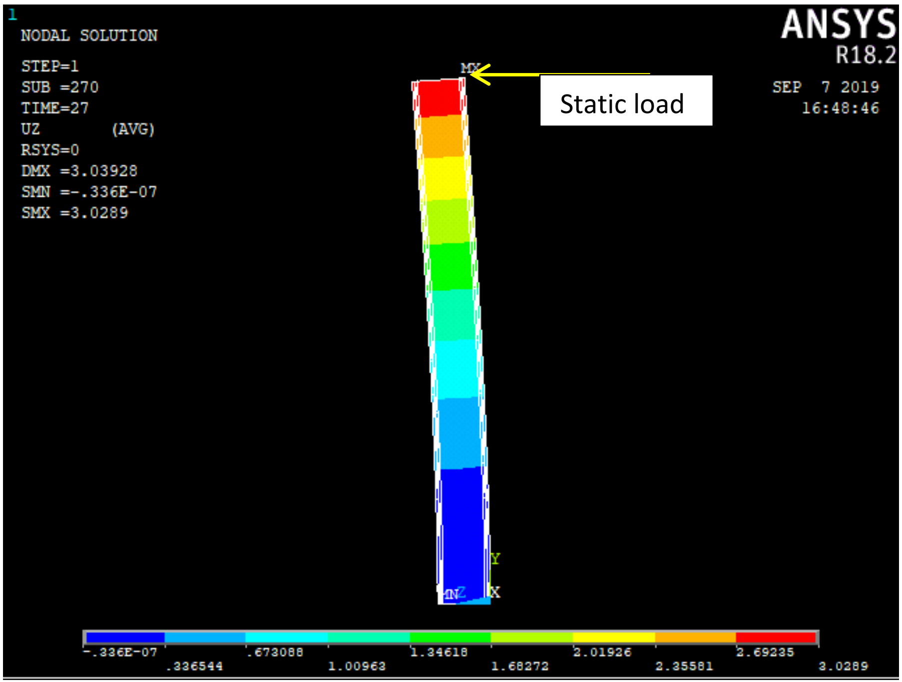

Figure (5.121) Deflected shape of Model No.8.

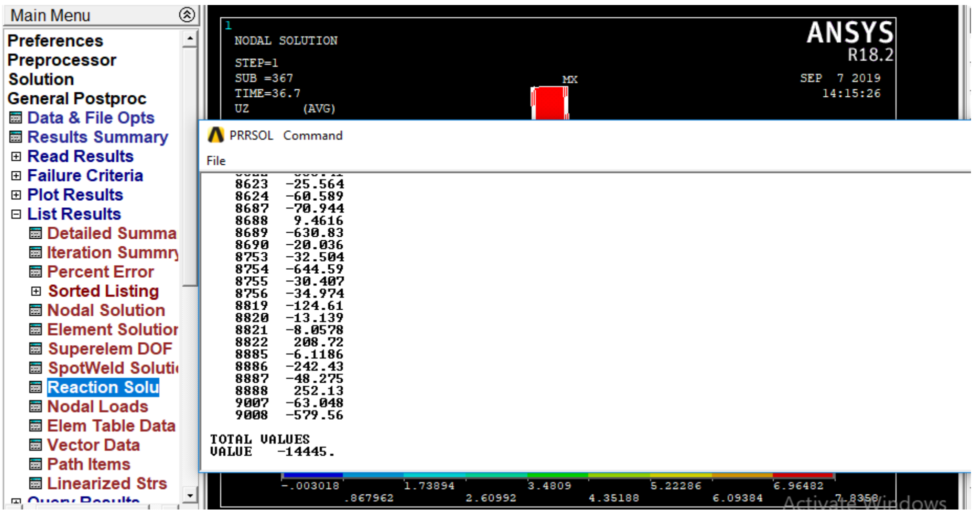

Figure (5.122) The out-of-plane load at end of solution for Model No.8

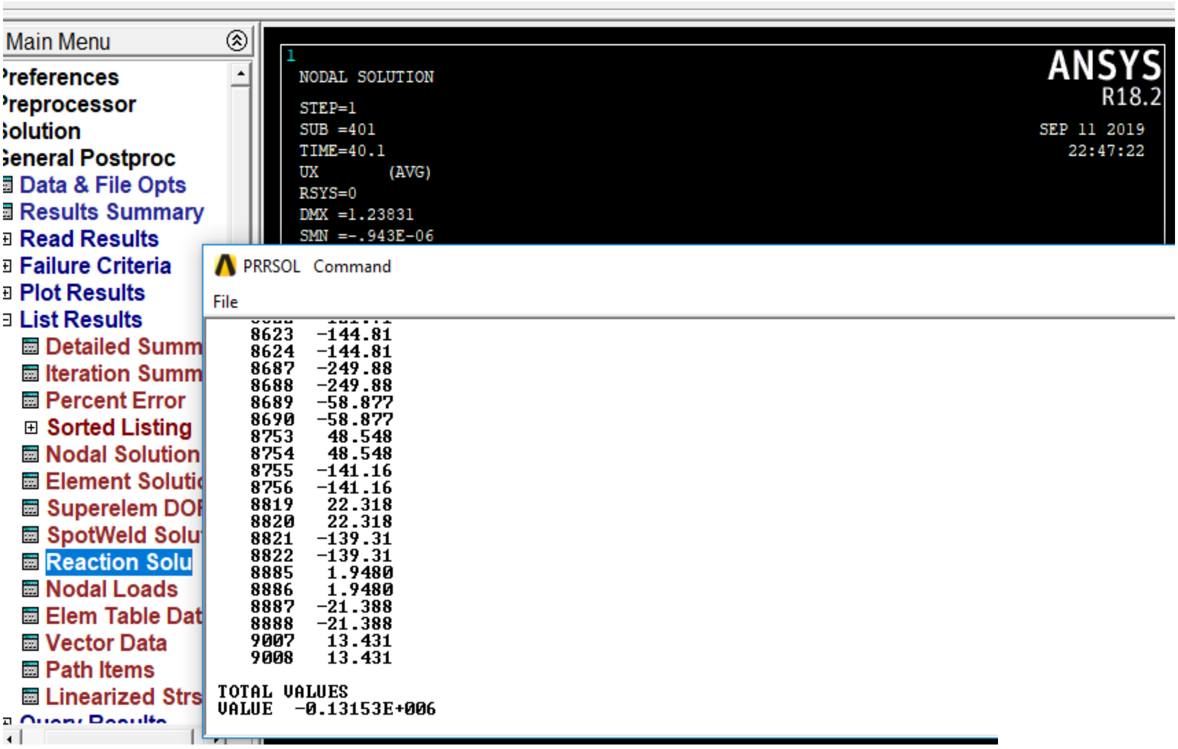

Figure (5.123) The in-plane load at end of solution for Model No.8

5.15 General Discussion

The solution of nonlinear equations, as mentioned in Chapter four, is accomplished in ANSYS using Newton-Raphson method. The Newton-Raphson equation used for the nonlinear solution can be written as in Eq. (5.4) that follows[49]:

$$[K_i^T].\{\Delta U_i\} = \{F^a\} - \{F_i^{nr}\} \qquad (5.4)$$

Where: $[K_i^T]$: tangential stiffness matrix, $\{\Delta U_i\}$: displacement increments, $\{F^a\}$: applied loads vector, and $\{F_i^{nr}\}$: the vector of element internal loads. In transient analysis, $\{F_i^{nr}\}$ includes the effective inertia and damping forces. The main criterion adopted in the study to assess the seismic performance of a studied structures is whether it resists and overrides the applied seismic waves or not.

All the URM models could not overcome the applied seismic loadings. Here, it should be interpreted, according to Eq. (5.4), what does it mean if the convergence is not satisfied. It means that the right hand side of the equation does not equal the left hand side within the limited tolerance. This inequality is attributed to the reduction in the stiffness matrix, which is caused by the missing stiffness of cracked elements. Consequently, the structure no longer has the required stiffness to resist the applied forces.

The combination of responses and crack patterns arouses the inquiry of how these significant cracks occur with small deformations. The answer for this inquiry requires the determination of yield displacement of URM walls in terms of the parameters governing it. As mentioned in Chapter two, Aldemir A. [28] has proposed the following relation for the yield displacement of URM walls:

$$\delta_y = 0.587\, p^{0.543} . e^{0.0949 f_m} . \lambda^{1.426} . L \qquad (5.4)$$

Where: δ, y, p, e, f_m, λ, and L are: yield displacement in mm, overburden pressure in MPa, the natural exponent, compressive strength of masonry in MPa, aspect ratio, and wall length in m, respectively. The overburden pressure on the top of the masonry wall has an essential effect on its structural behavior. Therefore, the gravity load highly affects the stability of URM structures subjected to lateral loads.

Taking Model No.1 as an example with an overburden pressure of 0.03 MPa, the yield displacement in z-direction is 0.41 mm. Comparing this calculated value to the response shown in Figure (5.41) reveals that the two masonry walls in z-direction yielded with deformations less than those estimated by Eq. (4). However, Eq. (4) has been formulated depending on a statistical process, and is not very strict. Another drawback in the proposed relation is missing an important independent parameter which is the tensile strength of masonry. However, there is no consensus within researchers regarding the displacement capacity of URM walls [57].

Finally, it is not strict enough to estimate the failure of the simulated buildings depending on the results of the numerical analyses, but it can be said that the seismic performance of such structures are questionable when subjected to moderate earthquakes.

The results of the study showed the high effect of the tensile strength of masonry on both the in-plane load capacity of masonry walls and then on the seismic performance of masonry buildings. Due to the low tensile strength of masonry, the overburden pressure applied on masonry walls and caused by gravity load is a so important parameter governing the stability of masonry buildings. To show the effect of the two parameters, Mohr's circle for the state of stress at an arbitrary point within the wall shown in Fig. (5.124-b).

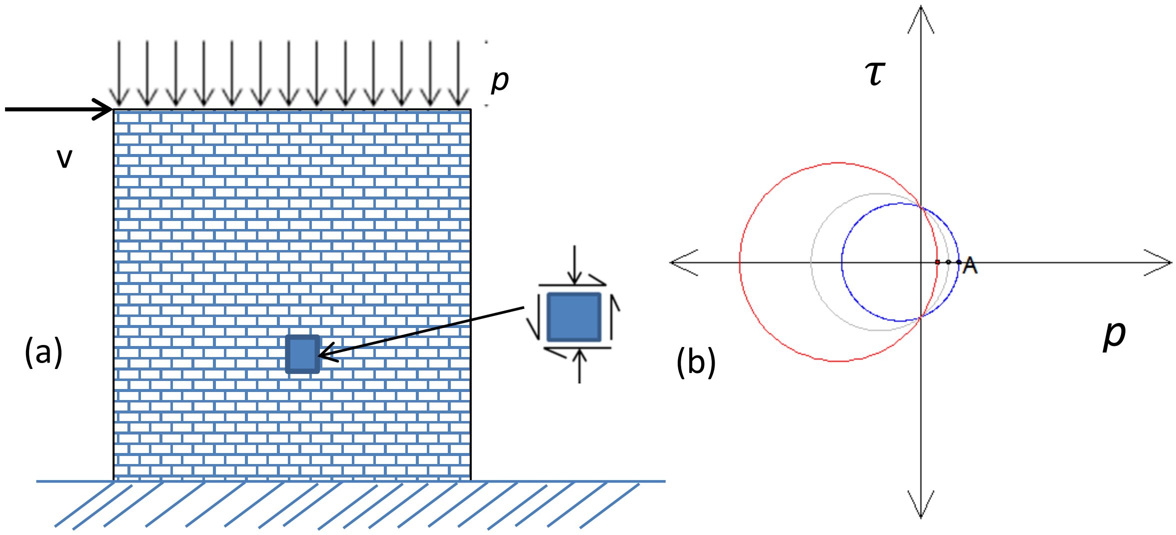

Figure (5.124) Effect of overburden pressure on the in-plane load capacity of URM walls: (a) in-plane loaded masonry wall, and (b) An exaggerated point and Mohr' circles for the states of stress.

From Fig. (5.124), it can be seen that the ordinate of point A, which is the maximum tensile stress within the studied point, decreases when the absolute value of the stress (p) increases with the value of the in-plane loading (v) remaining constant. This is how the value of gravity load affects the stability of URM structures. Therefore, the light weight diagrams are not the best choice for such structures, but the huge masses are also not suitable due the high inertial forces they cause during earthquakes. Consequently, the weight of the diaphragms must be chosen to compromise between the two cases.

Returning to Fig. (5.124-a), if the in-plane load (v) increases while the pressure (p) is remaining constant, the shearing stress (τ) increases and then the ordinate of point A becomes greater exceeding the low tensile strength of masonry. Fig. (5.125) also shows why diagonal cracks occur in the wall shown in Fig. (5.124) and how the tensile strength of the wall governs its load capacity.

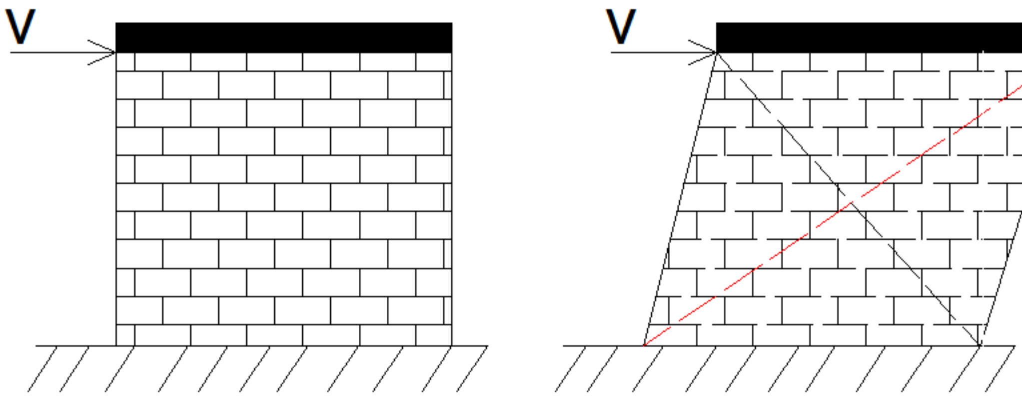

Figure (5.125) Effect of tensile strength on the in-plane load capacity of URM walls.

As the in-plane loading (v) shown in Fig. (5.125) applied, the red-colored diagonal increases in length as the wall deforms. Consequently, tensile stresses develop parallel to this diagonal. It the material has low tensile strength, such as masonry, tensile cracks will develop along the other perpendicular diagonal. This interprets the increase in the in-plane load capacity of Model No.7.

Compared to the undamped responses, the damped ones reveal the high effect of damping on the structural response. It is still a challenge to incorporate the damping correctly in the dynamic analysis. Concerning the Rayleigh damping which is formed of the mass-proportional damping and stiffness-proportional damping, A. K. Chopra says: “Neither of the two damping models are appropriate for practical applications”[51]. Therefore, including the damping in the nonlinear dynamic analysis needs further comprehensive investigations and discussions in future studies.

Chapter Six

Conclusions

and

Recommendations

CHAPTER SIX

CONCLUSIONS AND RECOMMENDATIONS

6.1 Conclusions

Depending on the study results, the following conclusions can be introduced:

1- The compressive strength, tensile strength, modulus of elasticity of the tested masonry specimens are 5.5 MPa, 0.15 MPa, and 2723 MPa, respectively.

2- The results of ANSYS simulations for masonry structures subjected to compressive loadings are more conservative in macro-modeling than in micro-modeling. This can be deduced from the values of the numerical results of simulating the prism test in the two cases. The failure load in macro-modeling was 83.6% of the experimental average result, and 98% in micro-modeling.

3- The one-story URM buildings having mechanical properties as mentioned above can override ground motions having PGAs of 0.011 g or less, such as the seismic waves recorded at Abadan station during the 7.3 M_w earthquake that hit the Iraq-Iran border on 12 November 2017.

4- Under the effect of the same seismic waves, increasing the tensile strength of masonry notably affects the seismic response of URM buildings and increases its time. For the URM single room that studied, increasing the tensile strength from 0.15 to 0.25 MPa increased the time of the response 14%.

5- Increasing the CS of masonry does not affect the seismic response of URM buildings nor the in-plane load capacity of URM walls if the low value of the tensile strength is still not increased.

6- For the studied one-story house, increasing the tensile strength from 0.15 MPa to 0.25 MPa and considering damping in the analysis increased the time of the structural response under the applied seismic waves from 0.6 to 4.5 seconds. This reveals the high effect of both damping and tensile strength of masonry on the seismic response.

7- The first cracks in masonry buildings during an effective earthquake occur in diagonal paths from base towards corners of doors and windows. Also they appear at bases of buildings.

8- The URM buildings are not safe during moderate or severe earthquakes having the probable PGAs.

9- The retrofitting with reinforced plaster layers enhances the seismic response of URM buildings significantly. For the one-story room, the model overrode an earthquake having a PGA of 0.324 g. The model exhibited a drift of 1.036% in z-direction and 1.289% in x-direction. The greater drift in the long direction indicates the effect of the openings in this direction. Also, the effect of the openings can be noticed through mode shapes that the first mode of the model has the greatest effective mass in the long direction.

10- The retrofitting mentioned above is sufficient to prevent the disintegration of collapsed masonry walls during an earthquake.

11- For the URM walls having aspect ratios about unity, increasing the tensile strength from 0.15 MPa to 0.3 MPa increases the in-plane load capacity 41% under the same vertical load.

12- The retrofitting with reinforced plaster layers increased the out-of-plane load capacity 494% and the in-plane load capacity 319.5%, and it increased the out-of-plane displacement 11.4%.

6.2 Recommendations

6.2.1 Practical Recommendations

Based on the results of the study, the following recommendations can be introduced for the practice:

1- It is so important to increase the bond between the joint mortar and units as highly as possible to enhance the tensile strength of masonry. Any economical and practical additives should be used for this purpose. Also, the surfaces of masonry units should be wet and free of dust during construction.

2- Providing suitable reinforced concrete confinements inside the openings of the doors and windows is necessary for the seismic performance. The confinemement must be along the inside perimeter of the opening.

3- For more safe seismic performance of URM buildings, the steel wire meshes can be used within the layers of the mortar plaster. The wire meshes should be fixed well to the foundations at the bottom and to the diaphragm at the top.

6.2.2 Recommendations for Future Studies

It is recommended to:

1- Simulate a single masonry room with micro-modeling and compare its structural behavior with a macro model under the same loading.

2- Perform shaking table tests for scaled and full scale models and verify the adequate value of the nonlinear convergence tolerance in ANSYS that makes the numerical solution as close as possible to the experimental response to propose its adequate value.

3- Investigate the nonlinear dynamic response of masonry buildings in both ANSYS and ABAQUS to compare their results to the experimental shaking table tests mentioned above. This comparison is necessary to know which one of the two simulation tools has more accuracy and adequacy.

4- Study the effect of mortar type on the structural performance of masonry construction.

5- Study the mechanical properties and seismic performance of concrete block construction.

6- Perform an experimental program to evaluate the out-of-plane and in-plane behavior of URM and retrofitted walls under lateral loading.

7- Investigate with shaking table tests or cyclic loadings the seismic behavior of confined masonry.

8- Analyze URM and CM buildings using seismic records obtained from the Iraqi strong motion stations.

9- Investigate the damping ratio of masonry structures experimentally and what the more appropriate values of Rayleigh damping coefficients that lead to more accurate results of the numerical simulations.

References

[1] T. Zimmermann and A. Strauss, "Masonry and Earthquakes: Material properties, Experimental testing and Design approaches," in Earthquake-Resistant Structures-Design, Assessment and Rehabilitation, ed: IntechOpen, 2012.

[2] J.-P. Kurtz, Dictionary of civil engineering: English-French: Springer Science & Business Media, 2004.

[3] I. INTERNATIONAL CODE COUNCIL, "2015 IBC INTERNATIONAL Building Code," May 30,2014 ed. THE U.S.A: IHS under licence with ICC, 2014.

[4] ساكو زهير و آرتين ليفون (1986): إنشاء المباني ،دار الحكمة للنشر و الترجمة و التوزيع، الطبعة الثانية، العراق، بغداد.

[5] H. B. Kaushik, D. C. Rai, and S. K. Jain, "Stress-strain characteristics of clay brick masonry under uniaxial compression," Journal of materials in Civil Engineering, vol. 19, pp. 728-739, 2007.

[6] M. R. Lindeburg and K. M. McMullin, Seismic design of building structures: a professional's introduction to earthquake forces and design details: Professional Publications, Inc., 2014.

[7] M. Gallonelli, "Dynamic response of masonry buildings with rigid or flexible floors," Master Thesis, Rose School, 2007.

[8] N. Abd, H. Mahdi, H. Al-Shukri, A. Catakli, H. Chlaib, and M. Su, "Induced Seismicity of Central Arkansas," in Istanbul 2012-International Geophysical Conference and Oil & Gas Exhibition, 2012, pp. 1-4.

[9] A. S. Elnashai and L. Di Sarno, Fundamentals of earthquake engineering: Wiley New York, 2008.

[10] M. R. Degg, "Earthquake hazard in the Middle East: an evaluation for insurance and reinsurance purposes," University of Nottingham, 1988.

[11] T. Onur, R. Gok, W. Abdulnaby, A. M. Shakir, H. Mahdi, N. Numan, et al., "Probabilistic seismic hazard assessment for Iraq," Lawrence Livermore National Lab.(LLNL), Livermore, CA (United States)2016.

[12] V. K. Sissakian, A. D. A. Ahad, and A. T. Hamid, "Geological hazards in Iraq, classification and geographical distribution," Iraqi Bulletin of Geology and mining, vol. 7, pp. 1-28, 2011.

[13] S. Brzev, Earthquake-resistant confined masonry construction: NICEE, National Information Center of Earthquake Engineering, Indian ..., 2007.

[14] R. Marques and P. B. Lourenço, "Unreinforced and confined masonry buildings in seismic regions: Validation of macro-element models and cost analysis," Engineering Structures, vol. 64, pp. 52-67, 2014.

[15] S. Hak, P. Morandi, G. Magenes, and T. J. Sullivan, "Damage control for clay masonry infills in the design of RC frame structures," Journal of Earthquake Engineering, vol. 16, pp. 1-35, 2012.

[16] M. ElGawady, P. Lestuzzi, and M. Badoux, "A review of conventional seismic retrofitting techniques for URM," in 13th international brick and block masonry conference, 2004, pp. 1-10.

[17] C. Murty, R. Goswami, A. Vijayanarayanan, and V. V. Mehta, "Some concepts in earthquake behaviour of buildings," Gujarat State Disaster Management Authority, Government of Gujarat, 2012.

[18] A. S. o. C. Engineers, "Prestandard and commentary for the seismic rehabilitation of buildings," FEMA, 2000.

[19] M. Lopes, "Evaluation of the seismic performance of an old masonry building in Lisbon," in Proceedings of the 11th World Conference in Earthquake Engineering, paper, 1996.

[20] J. Paquette and M. Bruneau, "Seismic resistance of full-scale single story brick masonry building specimen," in 8th North American Masonry Conference, Austin, Texas, USA, 1999.

[21] S. Franklin, J. Lynch, and D. P. Abrams, "Performance of Rehabilitated URM Shear Walls: Felxural Behavior of Piers," Mid-America Earthquake Center CD Release 03-03, 2003.

[22] R. Cardoso, M. Lopes, and R. Bento, "Seismic evaluation of old masonry buildings. Part I: Method description and application to a case-study," Engineering Structures, vol. 27, pp. 2024-2035, 2005.

[23] R. Bento, M. Lopes, and R. Cardoso, "Seismic evaluation of old masonry buildings. Part II: Analysis of strengthening solutions for a case study," Engineering structures, vol. 27, pp. 2014-2023, 2005.

[24] A. Carpinteri, S. Invernizzi, and G. Lacidogna, "In situ damage assessment and nonlinear modelling of a historical masonry tower," Engineering Structures, vol. 27, pp. 387-395, 2005.

[25] H. Mahmood, A. Russell, and J. Ingham, "Monotonic testing of unreinforced and FRP-retrofitted masonry walls prone to shear failure in an earthquake," in The 14th World Conference on Earthquake Engineering, Beijing, China, 2008.

[26] N. Mendes and P. B. Lourenço, "Seismic assessment of masonry “Gaioleiro” buildings in Lisbon, Portugal," Journal of Earthquake Engineering, vol. 14, pp. 80-101, 2009.

[27] A. Naseer, "Performance behavior of confined brick masonry buildings under seismic demand," NW. FP University of Engineering and Technology, Peshawar, Pakistan, 2009.

[28] A. Aldemir, "A Simple Seismic Performance Assessment Technique for Unreinforced Brick Masonry Structures," Master's Thesis, Middle East Technical

University Civil Engineering Department, Ankara, Turkey.[Google Scholar], 2010.

[29] I. O. Demirel, "A nonlinear equivalent frame model for displacement based analysis of unreinforced brick masonry buildings," Master's Thesis, Middle East Technical University Civil Engineering Department, Ankara, Turkey.[Google Scholar], 2010.

[30] A. A. M. G. d. Costa, "Seismic assessment of the out-of-plane performance of traditional stone masonry walls," 2012.

[31] S. Lagomarsino, A. Penna, A. Galasco, and S. Cattari, "TREMURI program: an equivalent frame model for the nonlinear seismic analysis of masonry buildings," Engineering Structures, vol. 56, pp. 1787-1799, 2013.

[32] F. Parisi and N. Augenti, "Seismic capacity of irregular unreinforced masonry walls with openings," Earthquake Engineering & Structural Dynamics, vol. 42, pp. 101-121, 2013.

[33] A. A. Yaseen, "Seismic Fragility Assessment of Masonry Buildings in the Kurdistan Region," University of Portsmouth, 2015.

[34] A. H. Abd, "SEISMIC EFFECTS ON MEDIUM AND LOW RISE MASONRY STRUCTURES," Ph.D Ph.D Thesis, Ph.D Thesis, University Of Basrah, Iraq, 2015.

[35] K. F. Abdulla, L. S. Cunningham, and M. Gillie, "Simulating masonry wall behaviour using a simplified micro-model approach," Engineering Structures, vol. 151, pp. 349-365, 2017.

[36] M. H. Saeed, "ANALYSIS OF MASONRY BUILDINGS EXPOSED TO EARHQUAKES WITHIN IRAQI ZONES," M.Sc. M.Sc. Thesis, University of Diyala, 2017.

[37] S. Kallioras, G. Guerrini, U. Tomassetti, B. Marchesi, A. Penna, F. Graziotti, et al., "Experimental seismic performance of a full-scale unreinforced

clay-masonry building with flexible timber diaphragms," Engineering Structures, vol. 161, pp. 231-249, 2018.

[38] B. Shakarami, M. Kabir, and R. Sistani Nezhad, "Parametric Study on Confined Masonry Walls Subjected to In-plane Cyclic Loading Through Numerical Modeling," AUT Journal of Civil Engineering, vol. 2, pp. 49-58, 2018.

[39] M. A. Erberik, C. Citiloglu, and G. Erkoseoglu, "Seismic performance assessment of confined masonry construction at component and structure levels," Bulletin of Earthquake Engineering, vol. 17, pp. 867-889, 2019.

[40] N. Ismail and N. Khattak, "Observed failure modes of unreinforced masonry buildings during the 2015 Hindu Kush earthquake," Earthquake Engineering and Engineering Vibration, vol. 18, pp. 301-314, 2019.

[41] L. Sorrentino, S. Cattari, F. da Porto, G. Magenes, and A. Penna, "Seismic behaviour of ordinary masonry buildings during the 2016 central Italy earthquakes," Bulletin of Earthquake Engineering, vol. 17, pp. 5583-5607, 2019.

[42] G. K. Al-Chaar, S. C. Sweeney, J. C. Trovillion, O. S. Marshall, and B. Danielson, "Pseudo Dynamic Testing and Seismic Rehabilitation of Iraqi Brick, Bearing and Shear Walls," ARMY ENGINEER DISTRICT LOS ANGELES CA2008.

[43] M. S. J. Committee, Building Code Requirements and Specification for Masonry Structures: Containing Building Code Requirements for Masonry Structures (TMS 402-08/ACI 530-08/ASCE 5-08), Specification for Masonry Structures (TMS 602-08/ACI 530.1-08/ASCE 6-08) and Companion Commentaries: Masonry Society, 2008.

[44] B. Standard, "Eurocode 6—Design of masonry structures—," British Standard Institution, London, 2005.

[45] D. Hutton, Fundamentals of Finite Element Analysis: McGraw-Hill, 2004.

[46] S. S. Rao, The Finite Element Method in Engineering: Elsevier, 2010.

[47] E. M. Alawadhi, Finite Element Simulations Using ANSYS: CRC Press, 2015.

[48] I. ANSYS, "Mechanical APDL Element Reference," ed: ANSYS Canonsburg, PA, 2013.

[49] P. Kohnke, "ANSYS mechanical APDL Theory Reference," Canonsburg, PA, USA: ANSYS Inc, 2013.

[50] I. ANSYS, "ANSYS Mechanical APDL Structural Analysis Guide, Release 15.0," ed, 2013.

[51] A. K. Chopra, Dynamics of Structures: theory and applications to earthquake engineering: Prentice-Hall, 2001.

[52] PEER Ground Motion Database [Online]. Available: https://ngawest2.berkeley.edu/

[53] Iran Strong Motion Network http://ismn.bhrc.ac.ir/en [Online].

[54] Q. S. a. A.-D. Mohammed and M. A. Abdulrassol, "Database of dynamic soil properties for most Iraq soils," American Scientific Research Journal for Engineering, Technology, and Sciences (ASRJETS), vol. 37, pp. 230-254, 2017.

[55] A. ASCE, "Minimum Design Loads for Buildings and Other Structures," ed: Reston, VA, 2010.

[56] S. Narayanan and M. Sirajuddin, "Properties of Brick Masonry for FE Modeling," American Journal of Engineering Research (AJER), vol. 1, pp. 6-11, 2013.

[57] A. H. Salmanpour, "Displacement Capacity of Structural Masonry," ETH Zurich, 2017.

Appendix –A-

To use Seismosignal program, follow the following basic steps:

Step -1-

Download the acceleration file from source.

Step -2-

Open the compressed file including the acceleration file and save the aimed acceleration file in a new location as shown below:

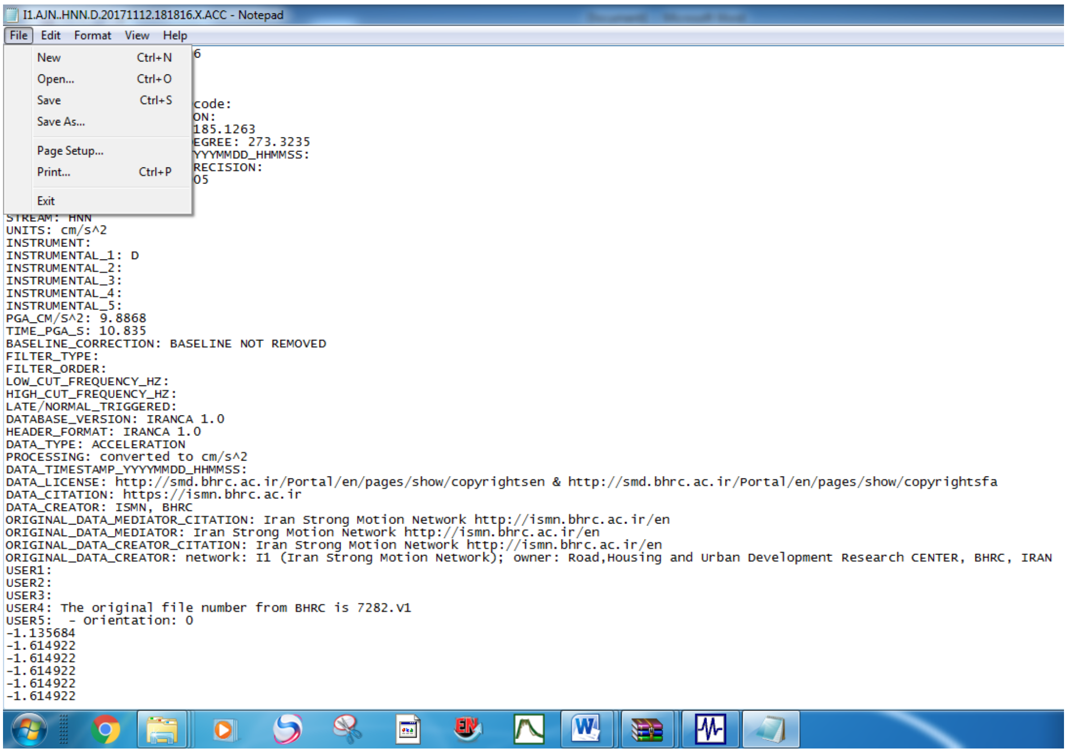

Step -3-

Open the acceleration file through Seismosignal as shown below:

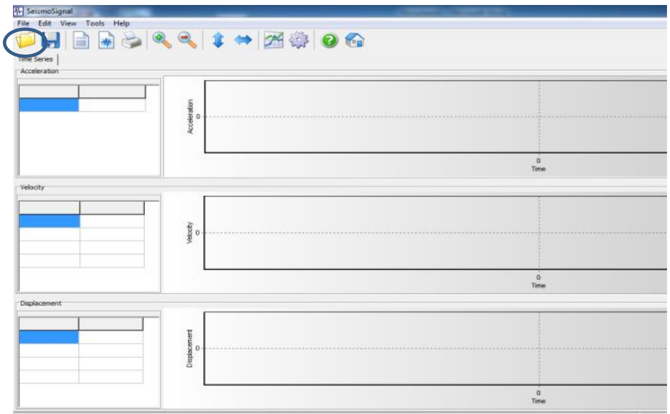

Step-4-

Enter correctly the file information in the setting window shown below:

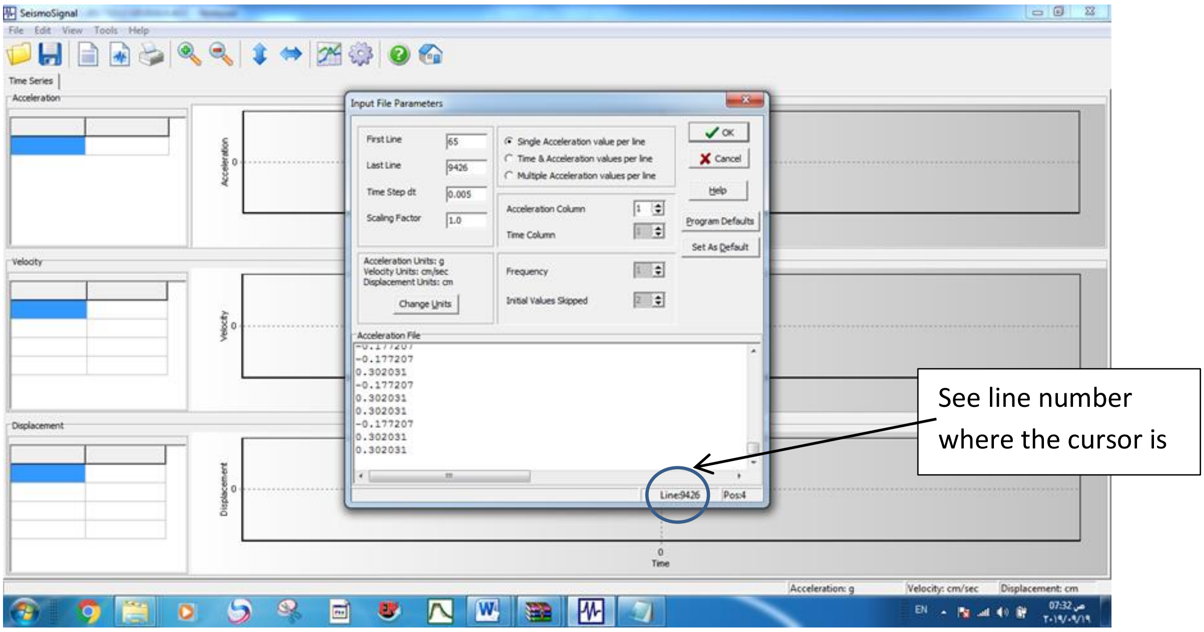

To know the first line number, move the cursor to the first acceleration value and see the line number that automatically appears. The same method can be done to know the last line number by moving the cursor to the last acceleration value. After clicking ok, the following window is opened:

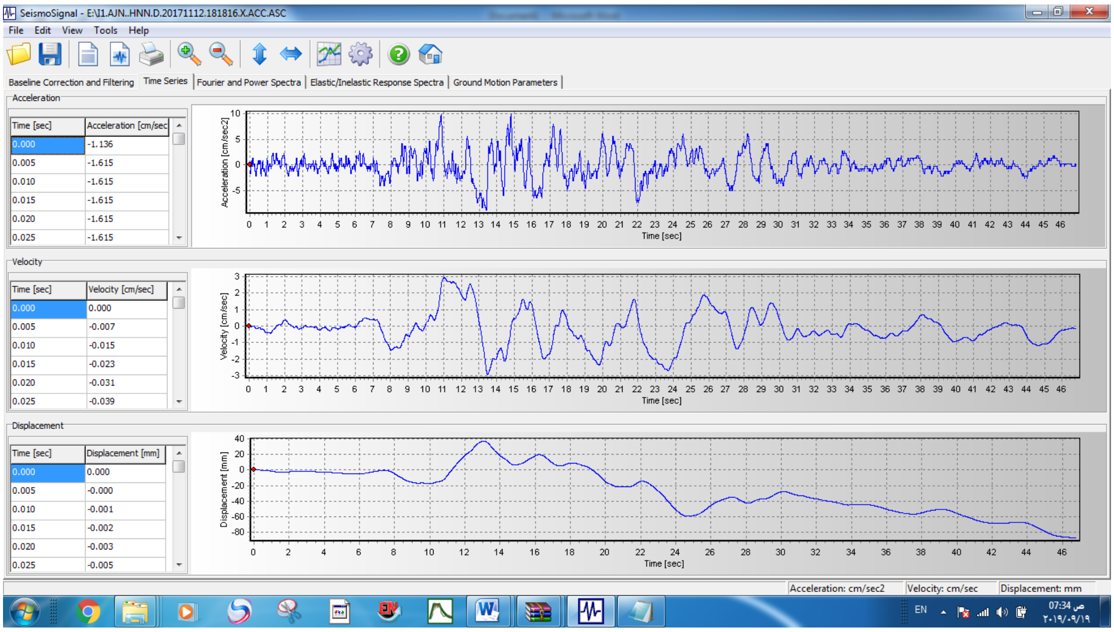

Step -5-

Do the filtering and baseline correction as follows:

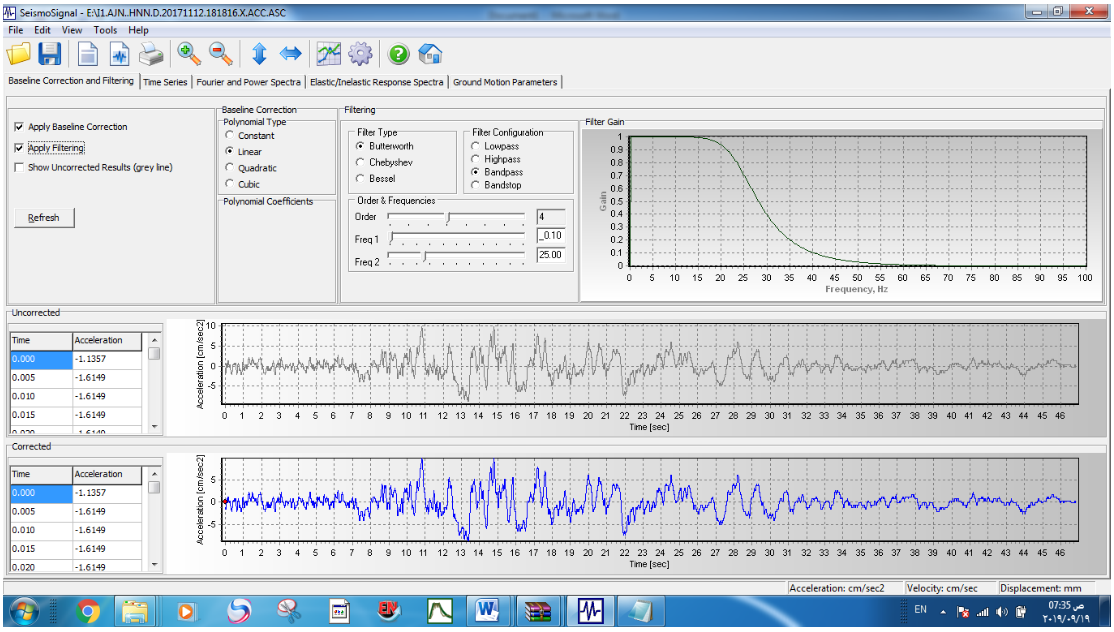

Choose polynomial type (linear is chosen in the example above). Then, click on Apply Baseline Correction and Apply Filtering.

Click Refresh.

Now the time series are corrected and you can return to them by clicking on Time Series. In the current example the corrected series are as follows:

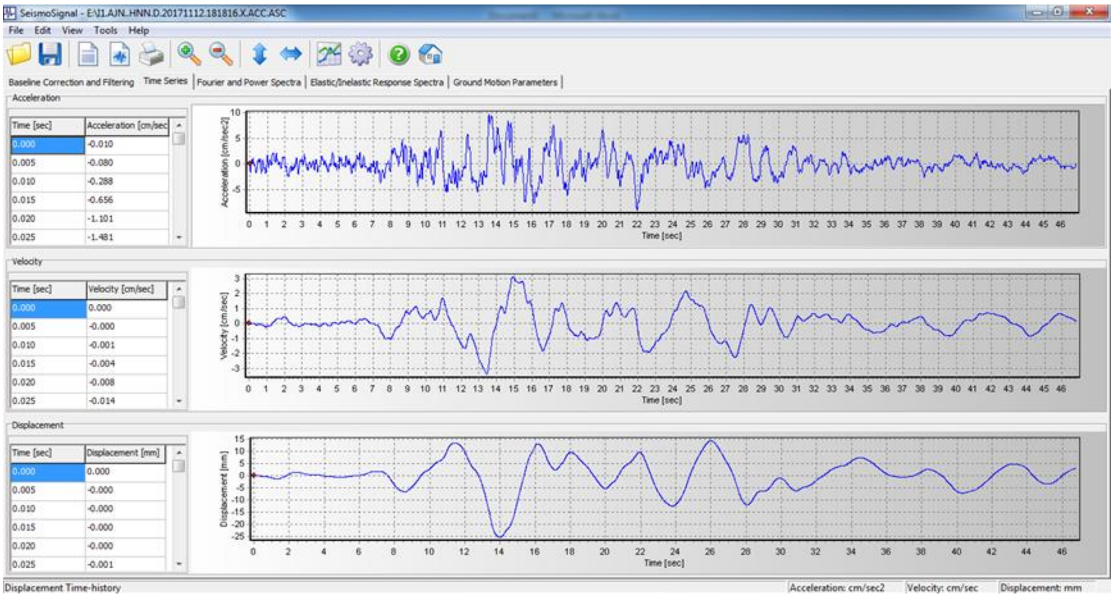

The difference can be obviously observed between displacement after correction and displacement before correction.

Step-6-

Save obtained time series as follows:

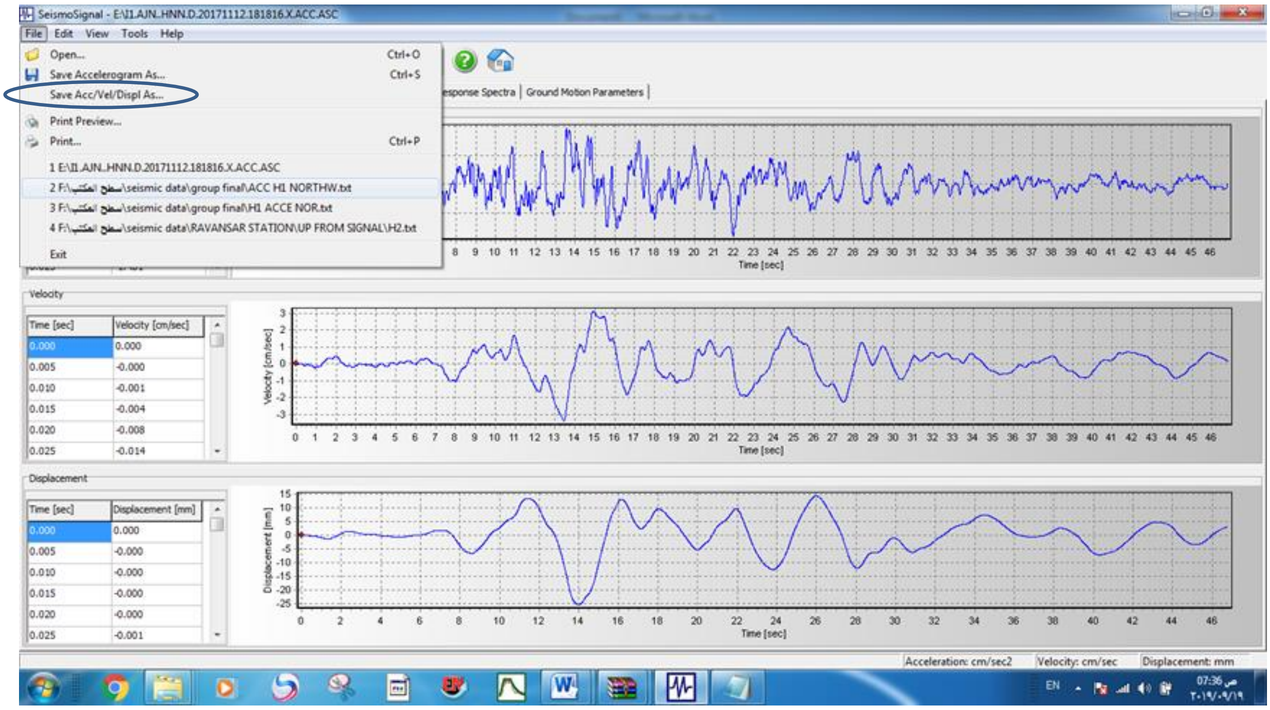

Appendix –B-

To create a contact between two bodies into ANSYS. program, follow the steps below:

Step-1-

Mesh the two volumes as shown below:

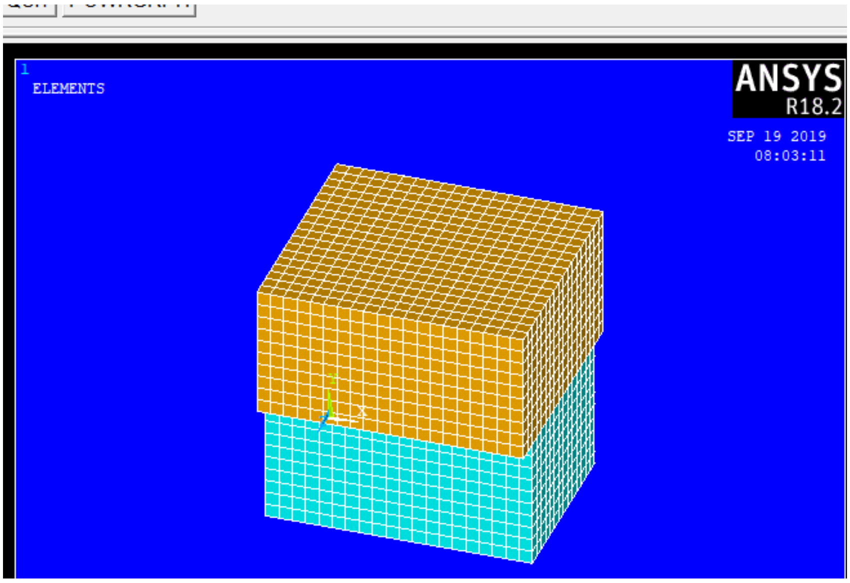

Step-2-

Move one of the volumes so that you can choose the needed area easily. The path of orders is as follows:

Modeling>Move>Volumes> pick the volume

Step-3-

Follow the coming path:

Modeling> create> contact pair

The contact wizard will be opened.

Step-4-

Click on new contact pair

Step-5-

Choose the target surface as shown below:

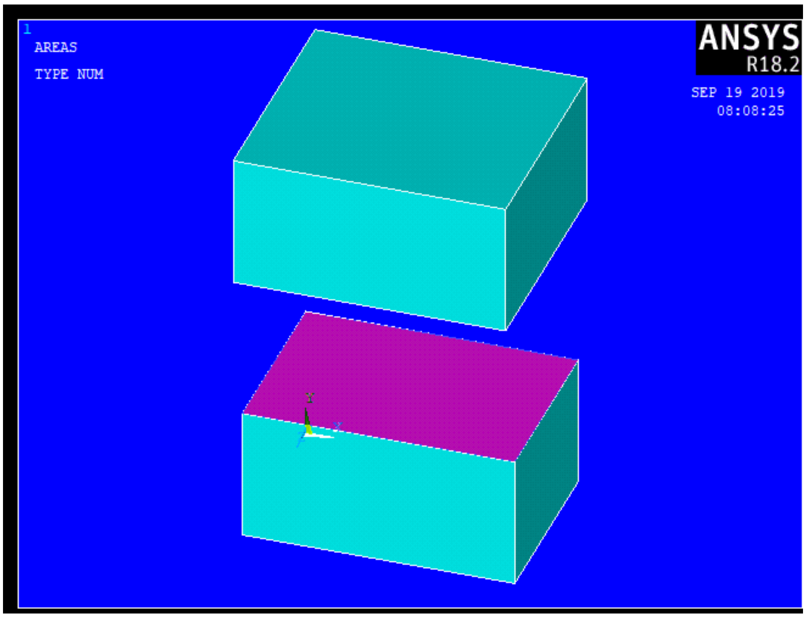

Step-6-

Choose the contact surface as below:

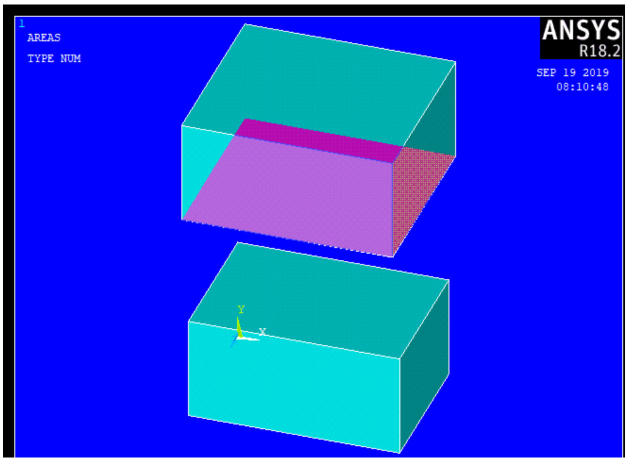

Step-7-

Setup the contact properties as follows:

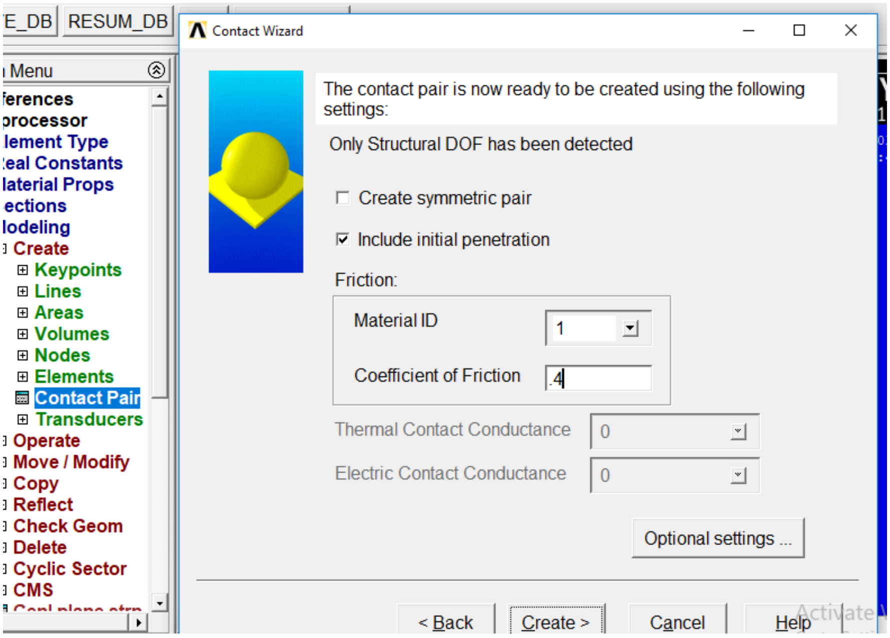

The zero pressure adhesion between the two surfaces can be entered as follows:

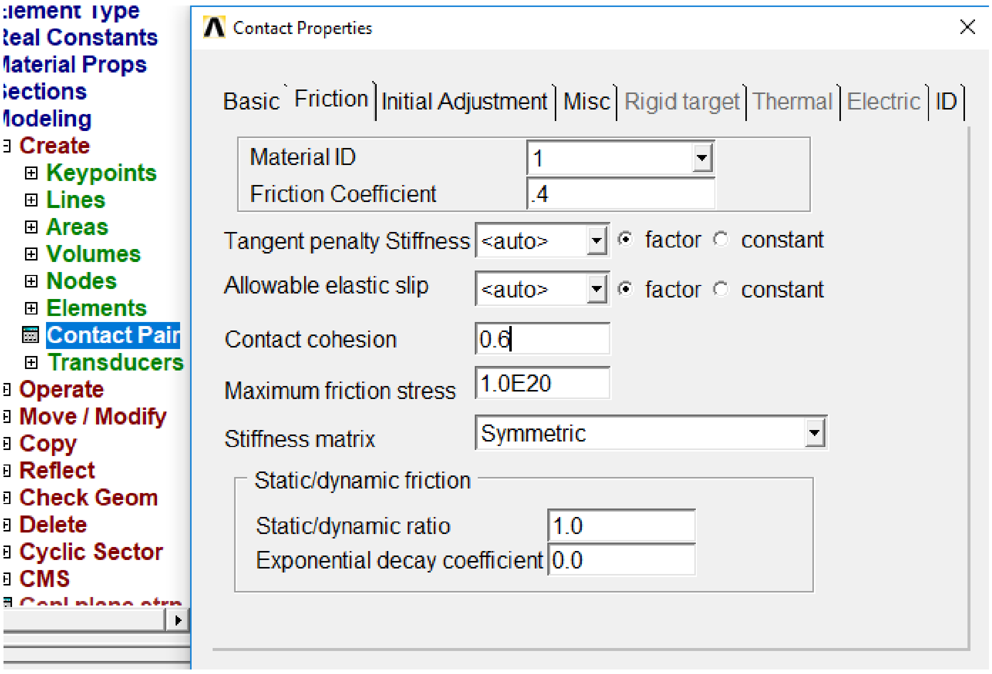

Click Create then click Finish

Return the moved volume to its original location.

الخلاصة

البناء بالطابوق من اقدم انواع البناء و ما زال يستعمل في العراق و في مختلف بلدان العالم، مقاومة الشد للجدران الطابوقية ضعيفة جدا ما يجعل البناء الطابوقي اضعف المنشآت تحت تأثير الاحمال الجانبية كالحمل الزلزالي. ان وجود الخطر الزلزالي في العراق يستدعي المزيد من الدراسات لتقييم الاداء الزلزالي للأبنية الطابوقية. هذه الدراسة تهدف الى تقييم الخواص الميكانيكية لبناء الطابوق الطيني و من ثم دراسة الاستجابة الديناميكية اللاخطية للابنية الطابوقية تحت تاثير الزلازل. مقامة الانضغاط بناء الطابوق الطيني ، و مقاومة الشد ، و معامل المرونة وجدت قيمها 5.5 ميكاباسكال، 0.15 ميكاباسكال، 2723 ميكاباسكال، على التوالي. كذلك تم تقييم الخواص الميكانيكية لمكونات البناء الطابوقي (وحدات الطابوق و مونة السمنت و الرمل).

تم استعمال برنامج أنسس (.ANSYS) اصدار 18.2 لاجراء التحليل اللاخطي لنماذج الابنية المدروسة، و في البدء تم التحقق من نتائج البرنامج من خلال دراسة جدارين سبق أن تم فحصهما عملياً من قبل باحثَينِ سابقَينِ ، و قد بينت نتائج المحاكاة بعد مقارنتها مع النتائج العملية مقبولية جيدة لنتائج التحليل العددي ببرنامج الأنسس. كذلك تم عمل المحاكاة لنموذج لفحص انضغاط البناء الطابوقي الذي تم تنفيذه في الجزء العملي من هذه الدراسة و قد تمت النمذجة بطريقتين : طريقة النذجة التفصيلية التي يميز فيها بين وحدات البناء و بين المونة و طريقة النمذجة المتجانسة التي يعتبر فيها البناء مادةً واحدةً متجانسة ، و قد لوحظ ان الطريقة التفصيلة أكثر دقةً من الطريقة المتجانسة حيث لوحظ ان حمل الفشل في النموذج الرقمي بالطريقة التفصيلية يساوي 98% من معدل حمل الفشل في الفحص العملي بينما كانت قيمته حسب التحليل بالطريقة المتجانسة تعادل 83.6% من معدل حمل الفشل التجريبي، و هذا ما يؤشر الى ان نتائج التحليل للابنية الطابوقية بطريقة النمذجة المتجانسة أكثر تحفظاً من التحليل بالنمذجة التفصيلية حين يكون الفشل تحت تاثير احمال انضغاطية. في الدراسة الحالية تمت نمذجة الابنية المدروسة بالطريقة المتجانسة و تم تمثيل حالة الفشل باستعمال معيار الفشل المعروف بمعيار (Willam-Warnke) الذي يتنبأ حالة الفشل للمواد الخرسانية و التي يقصد بها المواد الهشة أو غير المطيلية التي تتشقق باجهادات الشد التي تتجاوز مقاومتها للشد و تتهشم باجهادات الضغط التي تتجاوز مقاومة انضغاطها القصوى.

البيانات الزلزالية تم تحميلها من موقع PEER الالكتروني و تم اختيارها بطريقة كي تكون قدر الامكان ممثلةً للنشاط الزلزالي في المنطقة المدروسة من حيث قيم التعجيل القصوى المحتملة و من حيث خواص التربة. كذلك تم استعمال برنامج Seismosignal للحصول على السرعة و الازاحة الارضية من خلال بيانات التسارع للحركة الارضية للهزة ذات المقدار M_w=7.3 التي ضربت الحدود العراقية

الايرانية (بالقرب من مدينة حلبجه) بتأريخ 12 تشرين الثاني 2017 ، و بيانات التسارع المستعملة تم تسجيلها في احدى محطات الرصد الزالزالي الإيرنية. تتراوح قيم التعجيل القصوى للبيانات التي تم استعمالها في التحليل العددي من 0.1 g الى 0.324 g .

نتائج التحليل كشفت اداءً انشائياً رديئاً للأبنية الطابوقية تحت تأثير الهزات الارضية ذات القيم القصوى للتعجيل المحتمل، نتائج التحليل بينت ان زيادة مقاومة الانضغاط للبناء مع بقاء مقاومة الشد الضعيفة جدا على حالها لا تحسن مقاومة الجدران للاحمال المسلطة بمستوي الجدار و بالتالي لا تحسن الاداء الزلزالي للابنية الطابوقية غير المسلحة، بينما لوحظ ان زيادة مقاومة الشد تزيد من مقاومة الجدار الطابوقي للاحمال المسلطة في مستويه و تحسن الاستجابة الديناميكية للمنشا الطابوقي ، اظهرت نتائج التحليل ان تحمل الجدار للقوة قد ازداد بنسبة 41% عنما زيدت مقاومة الشد لنموذج الجدار الطابوقي غير المسلح من 0.15 ميكاباسكال الى 0.3 ميكاباسكال.

الدراسة تضمنت تقييم تأثير تقوية البنايات الطابوقية بطبقات لبخ مسلحة بمشبك حديدي و قد لوحظ ان الابنية التي تمت تقويتها حصلت زيادةٌ ملحوظةٌ في تردداتها الطبيعية بعد التقوية و هذا يدلل على زيادة جساءة تلك الابنية ضد الاحمال العرضية نتيجة التقوية ، كما نموذج الغرفة المنفردة الذي تمت تقويته قد تغلب على هزة ارضية ذات تعجيل اقصى قدره g0.324 و بانحراف جانبي قدره 1.036% باتجاه المحورz و بانحراف 1.289% باتجاه المحور x . ان نمط التشققات في طبقات التقوية مقارنة مع نمط التشققات في الجدران الطابوقية يدلل على فعالية تلك التقوية على الاحتفاظ باجزاء الجدار المحطم مما يقلل الاصابات البشرية و يزيد مطيلية الجداران الطابوقية. ان تاثير التقوية بطبقات اللبخ المسلحة تبين ايضا من خلال التحليل السكوني (الستاتيكي) لجدار طابوقي قبل و بعد التقوية و المقارنة بين الحالتين ، حيث تم تحميل الجدار حيث لوحظ ان التقوية زادت من تحمل الجدار للقوة باتجاه عمودي عليه بمقدار 494% و زادت الازاحة الجانبية بهذا الاتجاه 11.4%. كما زادت مقاومة الجدار للقوة المسلطة بمستويه بمقدار 319.5%.

جمهورية العراق
وزارة التعليم العالي و البحث العلمي
جامعة ميسان / كلية الهندسة
قسم الهندسة المدنية

الأداء الزلزالي لبناء الطابوق الطيني
في العراق

رسالة
مقدمة الى كلية الهندسة في جامعة ميسان كجزء من متطلبات
نيل شهادة الماجستير في علوم الهندسة المدنية / إنشاءات

من قبل
جبار عبدالعالي كاظم
(بكالوريوس هندسة مدنية 2003)

باشراف
ا.م. د عباس عوده داوود

محرم 1441 هـ أيلول 2019